ON THE LOCAL DYNAMICS OF CURRENTS IN THE ESTUARINE MARSDIEP BASIN

Jurre de Vries

Jurre de Vries
Royal Netherlands Institute for Sea Research (NIOZ)
Department of Physical Oceanography
PO box 59, 1790 AB Den Burg, Netherlands

2015

jurrej@hotmail@com

ISBN: 978-94-6228-679-5
Printing: Ridderprint BV

ON THE LOCAL DYNAMICS OF CURRENTS IN THE ESTUARINE MARSDIEP BASIN

De lokale dynamiek van de stroming in het estuarine Marsdiep

(met een samenvatting in het Nederlands)

Proefschrift

ter verkrijging van de graad van doctor aan de Universiteit Utrecht op gezag van de rector magnificus, prof.dr. G.J. van der Zwaan, ingevolge het besluit van het college voor promoties in het openbaar te verdedigen op vrijdag 28 augustus 2015 des middags te 12.45 uur

door

JURRE DE VRIES

geboren op 22 september 1986
te Groningen

PROMOTOR: Prof. dr. L.R.M. Maas
COPROMOTOR: Dr. H.M. van Aken

This research was funded by the Kansen voor West (KvW-EFRO) project 'Ontwikkeling grootschalige inzet offshore getijstroomenergie', No.21N.010

CONTENTS

LIST OF FIGURES

LIST OF TABLES

SUMMARY

The estuarine dynamics of the periodically-stratified Marsdiep basin are investigated through a broad range of observations and numerical model simulations. Spatial surveys and long-term point measurements of velocity, salinity, temperature, density and turbulence production and dissipation are complemented with a 1-D water column model (GOTM) and simulations of the western Dutch Wadden Sea (GETM/GOTM). This thesis aims at providing a better understanding of the factors and mechanisms that determine the vertical structure of velocity in the Marsdiep basin.

The spatial surveys show that the amplitude of the tidal currents in the Marsdiep basin is characterized by a great spatial variability as a result of the large variations in water depth. The tidal amplitude is proportional to the water depth, if smaller than approximately 15 m, due to the effect of bed friction on the flow. The tidal amplitude remains relatively uniform for greater water depths, but the fortnightly modulation is markedly greater for these water depths. Therefore, the lateral shears in along-stream velocity increase from neap to spring tide, and hence differential advection increases.

In the Marsdiep basin, the tidal wave is distorted as a result of the tide-bathymetry interaction. In the ebb-dominant section of the Marsdiep basin, where most measurements are conducted, the tidal wave is characterized by greater peak ebb than flood currents. Furthermore, the late flood phase consists of a long period of small currents, whereas the late ebb remains subject to large currents. The ebb current increases from neap to spring tide, whereas the flood current remains relatively constant. The tidal distortion has a considerable impact on the estuarine hydrodynamics.

The vertical structure of the along-stream current in the main tidal channel, the Texelstroom, is modified by the ebb-flood asymmetry in bed friction and by vertical stratification, which produce vertical profiles uncommon for standard periodically-stratified estuaries. Generally, the superposition of the barotropic and baroclinic pressure gradients creates vertical profiles with the near-bed (near-surface) vertical shears in along-stream velocity greatest during flood (ebb). In the Texelstroom, the near-bed shears are greatest during ebb due to the presence of asymmetric drag induced by the surrounding bathymetry. The large spatial variations in water depth and the variable distribution of bedforms implies that large spatial differences in drag coefficient are present in the Marsdiep basin. A uniform profile is present in the upper part of the water column during ebb, because the large ebb currents inhibit the generation of

vertical stratification by classical tidal straining, which generally enhances the vertical shears in the upper part of the water column.

On the contrary, vertical stratification is observed during late flood, generated by cross-stream tidal straining and differential advection. The vertical stratification during late flood persists because the small currents are not able to destroy the stratification. The vertical stratification dampens the vertical exchange of momentum, which creates a mid-depth maximum in along-stream velocity. The mid-depth velocity maximum is characterized by negative vertical shears in along-stream velocity in the upper part of the water column, which produce internally-generated turbulence.

A classical estuarine circulation is observed despite the absence of the classical tidal straining circulation and the occurrence of flood vertical stratification, scaling well with the Simpson number. The observed estuarine circulation is characterized by great seasonal variability and is superimposed on a depth-averaged residual current. The latter is forced by tide-bathymetry interaction and by remote wind effect. The strength of the estuarine circulation is primarily determined by the magnitude of the baroclinic pressure gradient and is less dependent on tidal amplitude. The increase in tidal amplitude, and associated maximum vertical mixing, from neap to spring tide is less important for the stability of the water column, because well-mixed conditions are already present during peak ebb and flood of neap tide. The data suggest that the estuarine circulation is primarily generated by a non-steady gravitational circulation during the long period of small currents from late flood to slack before ebb, which is further enhanced by increased shears related to the presence of vertical stratification. The estuarine circulation increases with increased tidal mixing, i.e. from neap to spring tide, which contrasts typical tidal straining estuaries. The increase in cross-stream tidal straining and differential advection towards spring tide promotes the generation of vertical stratification during late flood, which enhances the strength of the estuarine circulation during spring tide.

Furthermore, an ebb-dominant asymmetry in lateral advection is observed in the Marsdiep basin, which acts to reduce the strength of the estuarine circulation for along-stream salinity gradients greater than $2.5*10^{-4}$ psu/m. The observations suggest that the strength of the classical estuarine circulation in the periodically-stratified Marsdiep basin is primarily determined by the duration of the period of weak vertical mixing during late flood, the flood stratification and the strength of the baroclinic pressure gradient.

Turbulence dynamics in the Marsdiep basin varies on an intra- and inter-tidal timescale and influences the estuarine dynamics in a variety of ways. The magnitude of bed-generated turbulence is proportional to the strength of the tidal current. Therefore, the largest turbulence production is observed during peak ebb. Consequently, the bottom boundary layer persists over the entire water column during most of ebb, whereas it only covers the lower 8 to 12 m of the

water column during late flood, only covering the entire water column during peak flood. Surprisingly, bed-generated turbulence is not the only source of turbulence. Internal shears in cross-stream velocity during late flood and peak ebb contribute between 30 and 50 percent to the total turbulent kinetic energy production. The total production approximately balances turbulent kinetic energy dissipation, but only when the cross-stream component is included.

The presence of vertical stratification during late flood and early ebb creates a hysteresis effect in total production: values are smaller during late flood and early ebb, when the water column is weakly-stratified, than during the opposite phases of the tide, when the water column is well-mixed. Therefore, flood stratification during late flood acts as a sink for turbulent energy, which is commonly only observed during ebb. However, vertical stratification indirectly stimulates internal turbulence production by creating a mid-depth maximum in along-stream velocity, which enhances the vertical shears in the water column.

Summarizing, the Marsdiep basin is an estuary where a wide variety of estuarine processes occur, which all contribute to the vertical structure of velocity. The estuarine circulation is characterized by a highly non-steady behavior as a result of the great temporal variability in current speed and in vertical stratification. The tidal current strength, bed friction and the density gradients remain the most important underlying factors that drive the hydrodynamics in the periodically-stratified Marsdiep basin, despite the plentiful deviations from standard textbook estuaries.

SAMENVATTING

Een studie naar de estuariene dynamiek van het periodiek-gestratificeerde Marsdiep is uitgevoerd met behulp van een breed scala aan metingen en enkele numerieke model simulaties. Ruimtelijke karteringen en (lange-termijn) metingen van de snelheid, saliniteit, temperatuur, dichtheid, turbulentie productie en turbulentie dissipatie zijn aangevuld met 1-D waterkolom modelleringen met GOTM en model simulaties van de westelijke Wadden Zee met GETM/GOTM. Het doel van dit proefschrift is om een beter inzicht te verkrijgen in de factoren en mechanismen die de vertikale structuur van de stroomsnelheid in het Marsdiep bepalen.

De ruimtelijke karteringen laten zien dat de amplitude van de getijstroming in het Marsdiep wordt gekenmerkt door een grote ruimtelijke variabiliteit veroorzaakt door de sterke variaties in waterdiepte. De getij-amplitude is proportioneel aan de waterdiepte als gevolg van de toenemende remmende effecten van bodemwrijving op de stroming, wanneer deze kleiner is dan 15 m. De getij-amplitude blijft ongeveer constant voor grotere waterdieptes, maar is daarentegen gekenmerkt door een sterke spring-doodtij variatie. Deze diepteafhankelijke variaties in getij-amplitude leiden tot een toename in laterale schering van de langsstroming van dood- naar springtij, waardoor differentiële advectie ook toeneemt.

Karakteristiek voor de getijgolf in het Marsdiep is een vervorming door de interactie van het getij met de bathymetrie. In het eb-dominante gedeelte van het Marsdiep, waar de meeste metingen verricht zijn, is de getijgolf gekenmerkt door grotere piek (maximale) eb dan vloed stroomsnelheden. Bovendien is de late vloed fase gekenmerkt door een lange periode van kleine stroomsnelheden, terwijl de late eb fase onderhevig is aan hoge stroomsnelheden. Verder neemt de ebstroom sterk toe van dood- naar springtij, terwijl de vloedstroom relatief constant blijft. De vervorming van het getij heeft een grote impact op de estuariene hydrodynamica.

De vertikale structuur van de langsstroming in de hoofdgeul van het Marsdiep, de Texelstroom, wordt beinvloed door een eb-vloed asymmetrie in bodemwrijving en door de vertikale stratificatie, die resulteren in vertikale profielen atypisch voor standaard periodiek-gestratificeerde estuaria. In het algemeen leidt de superpositie van de barotrope en barocliene drukgradienten tot een vertikaal profiel met de grootste schering bij de bodem (wateroppervlakte) tijdens vloed (eb). De grootste schering nabij de bodem in de Texelstroom is waargenomen tijdens eb als gevolg van de asymmetrische bodemweerstand, geïndu-

ceerd door de complexe bathymetrie. De grote ruimtelijke variaties in waterdiepte en de ruimtelijke distributie van bedvormen in het Marsdiep impliceren dat een grote ruimtelijke variabiliteit in bodemwrijving en bodemweerstand te verwachten is. Verder is de schering in het bovenste gedeelte van de waterkolom tijdens eb minimaal en wordt het profiel gekenmerkt door een uniforme vorm: de sterke ebstroming verhindert het onstaan van vertikale stratificatie door klassieke getijschering (classical tidal straining) die normaal gesproken de gangbare toename in schering verklaart in het bovenste gedeelte van de waterkolom.

Vertikale stratificatie wordt daarentegen vooral waargenomen tijdens laat vloed, waar het ontstaat uit dwars-getijschering (cross-stream tidal straining) en differentiële advectie. De vertikale stratificatie blijft behouden tijdens laat vloed, omdat de zwakke stroomsnelheden niet in staat zijn de stratificatie te vernietigen. De vertikale stratificatie dempt de vertikale uitwisseling van impuls waardoor een mid-diepte maximum in de langsstroming onstaat. Het middiepte maximum is gekenmerkt door negatieve vertikale schering in de langsstroomrichting in het bovenste gedeelte van de waterkolom, die intern turbulentie genereert.

Een klassieke estuariene circulatie is waargenomen in het Marsdiep ondanks de af- en aanwezigheid van respectievelijk klassieke getijschering circulatie en vloed stratificatie. De estuariene circulatie is bovendien gecorreleerd aan het Simpson getal. De geobserveerde estuariene circulatie is gekenmerkt door een grote seizoensvariabiliteit en is gesuperponeerd op een diepte-gemiddelde residuele stroming. De laatstgenoemde wordt voornamelijk gedreven door de getij-bathymetrie interactie en door verre wind effecten gerelateerd aan grootschalige atmosferische drukverschillen. De grootte van de estuariene circulatie wordt voornamelijk bepaald door de grootte van de barocliene drukgradient en is minder afhankelijk van de getij-amplitude. De toename in getij-amplitude, en gerelateerde maximale vertikale menging, van dood- naar springtij is minder belangrijk voor de stabiliteit van de waterkolom, omdat goed-gemengde omstandigheden al voorkomen tijdens piek eb en vloed voor doodtij condities. De data suggereren dat de estuariene circulatie gegenereerd wordt door een onregelmatige gravitationele circulatie die voornamelijk belangrijk is gedurende de lange periode van kleine stroomsnelheden van laat vloed tot de kentering voor eb en die verder versterkt wordt door de toename in vertikale schering gerelateerd aan de aanwezigheid van vloed stratificatie. De estuariene circulatie intensiveert met toenemende vertikale mixing, namelijk van dood- naar springtij, wat afwijkt van typische getijschering-gedomineerde estuaria. De toename in dwars-getijschering en differentiële advectie richting springtij bespoedigt de formatie van vertikale stratificatie tijdens laat vloed wat de ontwikkeling van de estuariene circulatie bevordert tijdens springtij.

Daarnaast is een eb-dominante asymmetrie in laterale advectie aanwezig in het Marsdiep voor langs-saliniteitsgradienten groter dan $2.5*10^{-4}$ psu/m, die een afname in de sterkte van de estuariene circulatie veroorzaakt. De waarnemingen suggereren dat de sterkte van de estuariene circulatie in het periodiek-gestratificeerde Marsdiep voornamelijk bepaald is door de duur van de periode met zwakke vertikale menging tijdens laat vloed, de vloed stratificatie en de grootte van de barocliene drukgradient.

De dynamiek van de turbulentie in the Marsdiep varieert op een intra- en inter-getijde tijdschaal en beinvloedt de estuariene dynamica op verschillende manieren. Nabij de bodem gegenereerde turbulentie verhoudt zich evenredig met de sterkte van de getijstroming. De grootste turbulentie productie vindt daarom plaats tijdens piek eb. Dienentegevolge beslaat de bodemgrenslaag de gehele waterkolom tijdens het merendeel van eb, terwijl het gelimiteerd blijft tot de onderste 8 tot 12 m tijdens laat vloed, en beslaat alleen de gehele waterkolom tijdens piek vloed. Bijzonder is de observatie dat bodem-gegenereerde turbulentie niet de enige bron van turbulentie is in het Marsdiep. Interne schering in de dwarsstroming tijdens laat vloed en piek eb dragen tussen de 30 en 50 procent bij aan de totale turbulente kinetische energie productie. De totale productie is ongeveer in evenwicht met de turbulente kinetische energie dissipatie, maar alleen wanneer de dwars component daarbij is inbegrepen.

Verder creëert de aanwezigheid van vertikale stratificatie tijdens laat vloed en vroeg eb een hysterese effect in turbulentie productie: waardes zijn kleiner tijdens laat vloed en vroeg eb, wanneer de waterkolom licht-gestratificeerd is, dan tijdens de tegenovergestelde fases van het getij, wanneer de waterkolom goed gemengd is. Vloed stratificatie dient daarom als een put voor turbulente kinetische energie, wat over het algemeen voornamelijk wordt waargenomen tijdens eb. Echter, vloed stratificatie stimuleert indirect de ontwikkeling van intern-gegenereerde turbulentie door het creëren van een mid-diepte maximum in de langsstroom richting die de vertikale schering, en de turbulentie productie, in de waterkolom bevordert.

Samenvattend, het Marsdiep is een estuarium waar een breed scala aan estuariene processen plaats vinden, die alle bijdragen aan de vertikale structuur van de stroming. De estuariene circulatie wordt gekenmerkt door een zeer variabele dynamiek als gevolg van de grote temporele variabiliteit in stroomsnelheden en vertikale stratificatie. De stroomsnelheid, bodemwrijving en de dichtheidsgradienten behoren tot de belangrijkste onderliggende factoren die de hydrodynamica in het periodiek-gestratificeerde Marsdiep aansturen, ondanks de overvloed aan afwijkingen van standaard tekstboek estuaria.

To learning something new every day

1

INTRODUCTION

1.1 MOTIVATION

A renewed interest in the tidal dynamics of the Marsdiep basin has emerged from the sustainable energy sector, which has inspired and stimulated the research presented in this thesis. The sustainable energy sector aims at utilizing tidal energy as an alternative for fossil energy and thereby contributing to a broadening of the potential of renewable energy sources. However, tidal energy extraction is presently still in an early stage of development. Several test sites exist worldwide in e.g. the Orkney Islands (`http://www.emec.org.uk/`) and the Netherlands (`http://www.tidaltesting.nl/`). For tidal energy extraction with a submerged turbine to be feasible and profitable, an optimization strategy is required, which is achieved through, amongst others, a profound understanding of the hydrodynamics at the turbine site.

Several aspects of the hydrodynamics can impact the tidal energy extraction. First, energy production from the tidal current scales with the current velocity cubed, implying that small variations in current speed have great consequences for the energy yield of a turbine. Second, rotor blades of a turbine range between 5 and 15 m, thereby covering a substantial surface area. Spatial gradients in velocity, called shears, over this surface area reduce the power production. Third, the velocity shears produce differential forces acting on the structure of the tidal energy plant, which impacts its stability. Finally, the ambient turbulence partly determines the size of the wake of a turbine, which is an important consideration for the spatial-planning strategy of tidal energy farms. Therefore, a detailed knowledge of the vertical and spatial structure of velocity aids in several ways to optimize tidal energy extraction.

As part of the development of tidal energy extraction into a robust source of sustainable energy, a test floating platform with submerged turbines and rotor blades of 10 m in diameter will be allocated in the Marsdiep basin in spring 2015, creating the need for a comprehensive study of the hydrodynamics at the study site. In addition, insight into the hydrodynamic conditions may serve as

a reference case for possible (abiotic) impact studies of tidal energy extraction on the ambient environment.

Besides the immediate cause described above, a better understanding of the hydrodynamics benefits our understanding of the entire system. The Wadden Sea was named a UNESCO World Heritage Site in 2009, highlighting its uniqueness as one of the largest natural intra-tidal ecosystems around the globe, characterized by a broad range of natural habitats. The hydrodynamic conditions are an essential boundary condition for these biotic environments, and contribute to its uniqueness. For the Wadden Sea to remain extraordinary when facing present-day and future challenges as pollution and climate change, it is crucial to have a detailed understanding of the hydrodynamics of the system.

Zimmerman [1976b] and Ridderinkhof [1989] showed that the complex bathymetry in the Marsdiep basin impacts the depth-averaged tidal currents in the Marsdiep basin and creates horizontal circulation cells. Furthermore, recent studies [Buijsman and Ridderinkhof, 2007b; Duran-Matute et al., 2014; Nauw et al., 2014] have demonstrated the effect of wind on the depth-averaged residual currents and transport in the Wadden Sea. However, the vertical structure of the currents in the Marsdiep basin and the feedbacks between tides and density gradients have received less attention. To bridge this gap in knowledge, this thesis focuses on the vertical structure of currents, density and turbulence in the estuarine Marsdiep basin.

This introductory chapter presents an overview of the hydrodynamic processes and mechanisms that play an essential role in estuaries, with a focus on partially- and periodically-stratified estuaries similar to the Marsdiep basin. An outline of these fundamental characteristics of estuaries is followed by a short description of the study area: the western Dutch Wadden Sea and the Marsdiep basin in particular. The chapter ends with an overview of the objectives, research questions and research outline of the thesis.

1.2 ESTUARIES

Worldwide, estuaries are present in many different sorts, shapes and sizes. Generally, an estuary is defined as ”a semi-enclosed and coastal body of water, with free communication to the ocean, and within which ocean water is diluted by freshwater derived from land” [Cameron and Pritchard, 1963 in Valle-Levinson, 2010]. This definition incorporates estuaries like e.g. the Hudson Estuary [Geyer et al., 2000], the San Francisco Bay area [Lacy and Monismith, 2001], the Merrimack River Estuary [Ralston et al., 2010], the Wadden Sea [Becherer et al., 2011], the Baltic Sea [Burchard et al., 2005], the Yangtze/Yellow River [Jiang et al., 2012], fjords [Valle-Levinson et al., 2014] and many other systems into one single concept. However, the characteristics of these

estuaries vary greatly. To more adequately distinguish between these systems, several classifications have been suggested based on geomorphology, vertical distribution of salinity and/or hydrodynamics [Valle-Levinson, 2010].

A classification based on the vertical profile of salinity enables a separation of estuaries into well-mixed, partially- or periodically-stratified, strongly-stratified and salt-wedge estuaries, where fjords and bays fall within separate categories, and each category is characterized by its own dynamics [Geyer and MacCready, 2013, review on estuarine circulation]. Commonly, estuaries shift between regimes on a spring-neap to seasonal timescale [Jay and Smith, 1990a; Valle-Levinson et al., 1998; McLaughlin et al., 2003; Ralston et al., 2008; Li and Zhong, 2009]. The different states represent different hydrodynamic conditions and principally depend on the freshwater discharge and the magnitude of the currents. The estuary type is indicative of the processes that are important, as discussed below. The Marsdiep basin is located in the well-mixed and periodically-stratified regimes and the focus of this overview of the estuarine processes is therefore on these types of estuaries. But first, relevant tidal processes in estuaries are discussed.

1.3 TIDES, BATHYMETRY AND WIND

1.3.1 *Tides*

Tidal currents are driven by horizontal pressure gradients, originating from the orbital movements of the Sun and Moon [e.g. van Rijn, 2011]: the barotropic tide. The height of the sea surface elevation and the strength of the tidal current not only vary over a tidal cycle, but also vary between tidal cycles: the intra- and inter-tidal variability, respectively. The latter is mainly a function of the orientation of the Earth's axis with respect to the Moon (the diurnal inequality) and the respective positions of the Earth, Sun and Moon (the spring-neap tidal cycle). All the different components that contribute on different timescales to the shape of the tidal wave are named tidal constituents. The most important astronomic constituents are the diurnal and semi-diurnal tidal constituents of the Moon, O1 and M2, and of the Sun, K1 and S2, but many more exist [e.g. Cartwright, 2000]. The superposition of all these constituents produces a large intra- and inter-tidal variability in tidal current amplitude. It creates a highly dynamic environment characterized by temporally-varying hydrodynamic conditions.

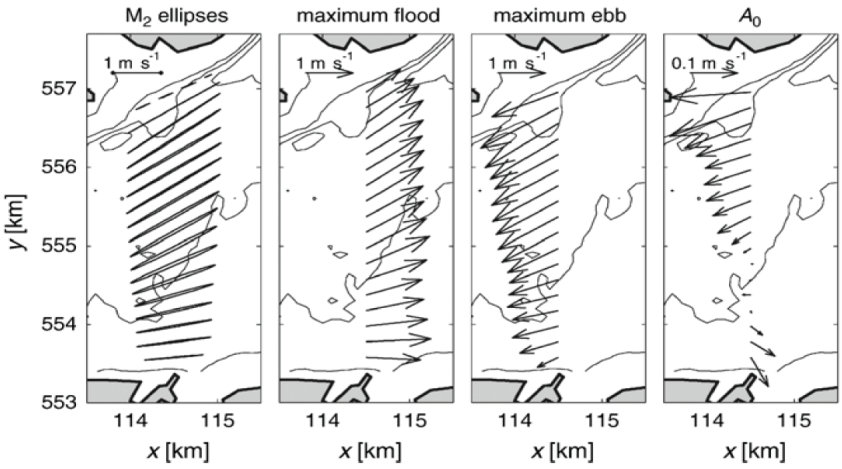

Figure 1.1: Spatial variability of depth-averaged tidal currents at Marsdiep tidal inlet (from Buijsman and Ridderinkhof [2007a]). From left to right: the M2 ellipses indicate the magnitude and direction of the M2 tidal constituent, the arrows indicate the magnitude of the maximum flood and ebb current and A_0 indicates the depth- and tidally-averaged residual current.

1.3.2 *Bathymetry*

In the open ocean, the tidal wave is characterized by a sinusoidal temporal variation. When the tide enters the shallower water depths of shallow seas and estuaries, the tidal wave is distorted by non-linear effects in response to bed friction, the large-scale geometry of tidal basins and the complex bathymetry, creating asymmetries in the tidal elevations and currents, i.e. differences in magnitude and duration of the ebb and flood phase [Dronkers, 1986].

Several authors have linked the shape of the estuarine basin, the hypsometry, to the tidal distortion [Boon and Byrne, 1981; Friedrichs and Aubrey, 1988; Maas, 1997; Stanev and Wolff, 2003]. They found that the ratio between the area of the channel and the area of the shoals is a paramount feature of the hypsometry, which creates horizontal exchange patterns with inflow in the channel and outflow over the shoals, or vice versa, depending on the ratio. Furthermore, Li and O'Donnell [2005] showed that the residual exchange patterns in an inlet depend on the length of the estuary.

The tidal distortion is characterized by great spatial variability. Bed friction dampens the tidal wave by extracting tidal energy, resulting in a modification of the tidal distortion along its propagation direction [Blanton et al., 2002]. Furthermore, bed friction, channel geometry and the length of an estuary determine if a tidal wave is progressive, standing or intermediate, which also impacts the tidal distortion [Dronkers, 1964; Winterwerp et al., 2013; Winterwerp and Wang, 2013]. Last but not least, estuaries generally consist of channels and shoals, which represent spatial variations in water depth and create three-dimensional circulation patterns, characterized by distorted shapes of the tidal wave. An example of the tidal distortion at the Marsdiep inlet is given in Figure 1.1. It shows the spatial variability in peak flood and ebb currents at the inlet, which produces a residual horizontal circulation cell, A_0 [Buijsman and Ridderinkhof, 2007a].

In a simplified situation, the distortion of a tidal wave at one location in a channel can be physically explained by the variations in phase speed of the tidal wave as a consequence of temporal (and spatial) variations in water depth. There is a proportional relationship between both: the wave celerity increases with water depth. Therefore, ebb-flood variations in water depth produce the largest celerities during flood, especially when the ratio between the amplitude of the surface tide is relatively large compared to the total water depth. To respect continuity, the greater water depth during flood is compensated by a stronger current during ebb, producing a mean or residual current, also called the Stokes drift [Valle-Levinson, 2010, and references therein].

Aubrey and Speer [1985] and Speer and Aubrey [1985] demonstrated that the strength of the tidal distortion can be expressed as the ratio between the magnitude of the most important astronomical constituent, commonly M2, and its first overtide, M4. An overtide is generated by the non-linear interactions of the tide with the seabed, the basin geometry and by advection driven by spatial variations in water depth. The wave period of a first-order overtide is half the tidal period of the original constituent (named first-order higher harmonic or quarter-diurnal constituent). In addition, the shape of the tidal distortion is expressed by the phase difference between both constituents. Depending on the phase difference, the tidal currents are either flood- or ebb-dominant, i.e. greater currents occur during flood or ebb, respectively. The variations in current speed as a result of the tidal distortion can have important ramifications for sediment transport, because the latter is related to the velocity to the power of 3 to 5 [e.g. van Rijn, 1993, and references therein]. Furthermore, these abovementioned studies illustrate that bed friction, water depth variations and basin geometry are important for the residual circulation patterns and transport of water and suspended matter.

1.3.3 *Wind*

The wind influences hydrodynamics in estuaries in a variety of ways, depending on its strength and direction with respect to the orientation of the basin geometry and the direction of the tidal current [Geyer, 1997; Guo and Valle-Levinson, 2008]. Furthermore, weak winds generally modify the upper part of the water column, whereas stronger winds impact the structure of the entire water column. In shallower intertidal areas like mudflats, wind-induced waves have a considerable impact on the sedimentation-erosion processes [Le Hir et al., 2000; Verney et al., 2007]. Besides these local wind effects, winds create additional large-scale pressure gradients, which drive residual currents: the remote wind effects.

Local wind forcing either mixes (the upper section of) the water column [Goodrich et al., 1987; Li et al., 2006b], if the forcing is sufficient, or modifies the vertical structure of the water column through wind straining [Scully et al., 2005; Chen and Sanford, 2009]. Wind straining either enhances or reduces vertical stratification, depending on the direction of the wind with respect to the direction of the tidal current. Remote wind effects primarily modify the depth-averaged residual current.

1.4 DENSITY GRADIENTS AND THE ESTUARINE CIRCULATION

The residual currents generated by (barotropic) tide-bathymetry interaction and wind are mainly a depth-averaged phenomenon. A fundamental feature of estuaries is the presence of horizontal density gradients, predominantly originating from spatial differences in salinity, which produce additional, so-called baroclinic, pressure gradients. These horizontal (and related vertical) density gradients radically modify the vertical structure of the instantaneous and residual currents in estuaries. Therefore, the vertical structure of the residual current, the estuarine circulation, is a major topic of estuarine research.

1.4.1 *1-dimensional perspective (vertical structure)*

Freshwater discharge from rivers or sluices into coastal seas creates density gradients in three dimensions, i.e. in along-stream (or along-channel), cross-stream (cross-channel) and vertical direction, which all vary over time. The magnitude of these density gradients, and their associated horizontal and vertical stratification, is partly determined by the freshwater discharge rate and plays an essential role in a variety of estuarine processes. Generally, the horizontal density gradient and the vertical mixing by the tidal current determines the type of estuary, as expressed by the Simpson number, which represents the

ratio between the stabilizing and de-stabilizing forces on the water column, defined as [Geyer and MacCready, 2013]:

$$Si = \frac{\beta g \frac{\partial s}{\partial x} H^2}{u_*^2}, \tag{1.1}$$

where β is the saline contraction coefficient ($\sim 7^{*}10^{-4}$), g is the gravitational acceleration, H is the water depth, $\frac{\partial s}{\partial x}$ is the along-stream salinity gradient and u_* is the friction velocity, the latter being a measure for vertical mixing by the tidal currents. Well-mixed and periodically- or weakly-stratified estuaries are defined as Si numbers smaller than 0.2 or between 0.2 and 1, respectively, indicating that tidal mixing is relatively important during most of the tidal period. As a result of tidal mixing, the water column is either continuously well-mixed for Si smaller than 0.2 or weakly vertically-stratified during a limited period of the tidal cycle for Si between 0.2 and 1. Strongly-stratified estuaries occur when Si is greater than 1, indicating that the along-stream density gradient is relatively important: the water column is vertically-stratified during the entire tidal cycle. The different types of estuaries are indicative of the different processes that are important for the vertical structure of the (residual) current.

The Simpson number explains the stability of the water column based merely on one-dimensional dynamics, neglecting for example the contribution of the cross-stream current and the cross-stream density gradient. Cross-stream variations in width and water depth and the Coriolis forcing are also important, as is discussed in more detail in the next section. Valle-Levinson [2008] proposed a classification for the estuarine exchange flow patterns incorporating these effects. All these classifications have in common that they provide insight into the structure of residual circulation in estuaries.

In essence, the vertical structure of the residual current in estuaries is determined by the difference in shape of the vertical profiles of the along-stream ebb and flood currents. This intra-tidal difference is caused by several estuarine processes related to the presence of the density gradients in the system. Before turning to these processes and their impact on the estuarine circulation, typical profiles of instantaneous along-stream ebb and flood currents in estuaries are depicted in Figure 1.2 [MacCready and Geyer, 2010]. It shows that the barotropic semi-diurnal tide produces identical shapes of the ebb and flood profiles of velocity ($-A$ and $+A$, respectively). The superposition of the barotropic tide and baroclinic effects creates increased (decreased) shears in velocity in the lower part of the water column during flood, U_f (ebb, U_e), as indicated by the difference between U and A, d, being greater than zero. In the upper part of the water column, the opposite occurs and d is smaller than zero. The difference

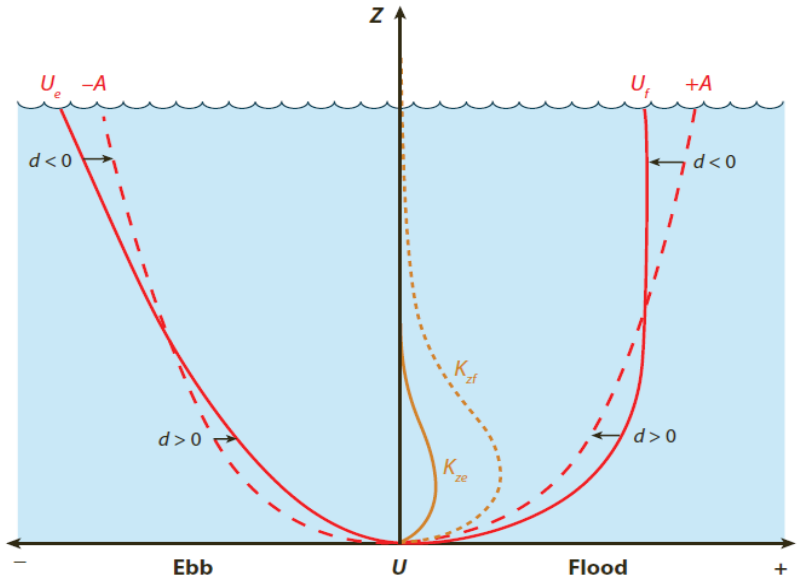

Figure 1.2: Standard vertical profiles (U, solid red lines) of ebb (e) and flood (f) currents and its deviation from the semi-diurnal velocity structure excluding the baroclinic tide (-A is ebb and +A is flood, dashed red lines). The profiles of the eddy mixing coefficients (K_z, yellow lines for ebb (e, solid line) and flood (f, dashed line)) are also given. The difference between A and U is indicated by d (from review on Advances in Estuarine Physics, MacCready and Geyer [2010]).

between the ebb and flood profiles as a result of the superposition of the barotropic tide and baroclinic effects generates the classical estuarine circulation.

Pritchard [1956] and Hansen and Rattray [1966] were the first to establish a research framework for estuarine circulation dynamics. They showed that the typical estuarine circulation is characterized by inflow near the bottom and outflow near the surface, resulting from the interplay between the barotropic and baroclinic pressure gradients and constant vertical mixing, as described above, which is called the classical gravitational circulation (classical U_G, Figure 1.3). This type of classical estuarine circulation is observed in most estuaries [Geyer and MacCready, 2013, and references therein], but the assumption of constant vertical mixing to model mixing in the classical estuarine circulation has been proven to be invalid. Later research has shown that the strength of the estuarine circulation is determined by several circulation mechanisms, which complicates the estuarine dynamics (Figure 1.3). The baroclinic pressure gradient drives a gravitational circulation (U_G), but is also responsible for another type of cir-

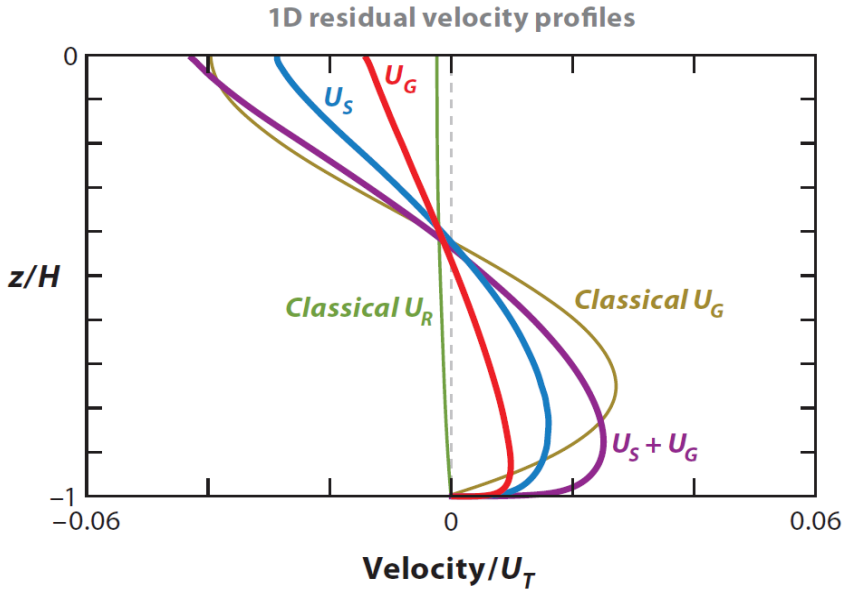

Figure 1.3: Components of estuarine circulation (from review on estuarine circulation, Geyer and MacCready [2013]), consisting of the classical gravitational circulation (classical U_G), the tidal straining circulation (U_S) and the classical river runoff (classical U_R). The magnitude of the residual current displayed on the x-axis is normalized by the tidal amplitude, U_T. Positive (negative) values indicate up-estuary (down-estuary) residual currents.

culation, namely tidal straining circulation (U_S), which is related to intra-tidal asymmetries in vertical stratification and vertical mixing.

Asymmetries in vertical mixing arise from the alternation between well-mixed and vertically-stratified conditions over the tidal cycle. Classical tidal straining is the principal mechanism that explains the (de-)stratification of the water column, as first described by de Ruijter [1983] and van Aken [1986], which was applied to estuarine conditions by Simpson et al. [1990]. They observed that the direction of the tidal current, which differs between ebb and flood, with respect to the steady direction of the along-stream density gradient determines if the water column becomes either well-mixed or vertically-stratified (Figure 1.4). During flood, the greater current velocities near the surface transport denser water from the sea into the estuary. The denser water sinks down, producing a well-mixed water column. During ebb, the greater currents near the surface transport fresher water over denser water towards the sea, creating vertical stratification. Classical tidal straining is a mere one-dimensional process. Jay

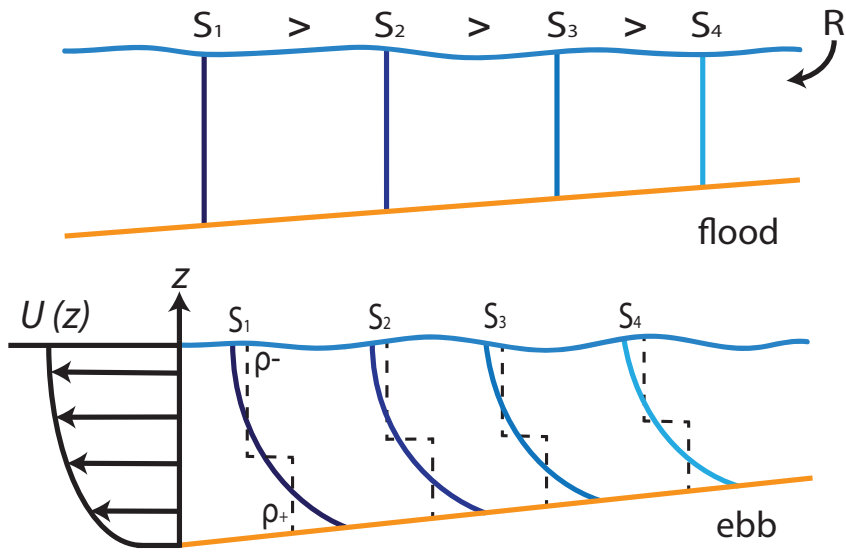

Figure 1.4: Principle of tidal straining adapted from Simpson et al. [1990]. The S indicates the isohalines during late flood and late ebb (upper and lower row, respectively). Relative small and large densities are indicated by $\rho-$ and ρ_+, respectively

and Musiak [1996] were the first to realize that tidal straining creates asymmetries in vertical mixing due to the alternation from well-mixed to vertically-stratified conditions (Figure 1.2 and 1.4). They hypothesized that these asymmetries could modify the vertical structure of the currents and thereby the magnitude of the estuarine circulation: the so-called tidal straining circulation (Figure 1.3, U_S). Several studies [Burchard and Hofmeister, 2008; Burchard, 2009; Burchard et al., 2011] have shown that tidal straining circulation has the same shape as the gravitational circulation. The former can contribute up to two-thirds to the total estuarine circulation in periodically-stratified estuaries [Burchard and Hetland, 2010].

1.4.2 *2-dimensional perspective (addition of cross-stream processes)*

Thus far, the forcing mechanisms of the estuarine circulation are mainly ascribed to along-stream processes, neglecting the influence of cross-stream dynamics. However, reality is more complex. Differential advection is an important two-

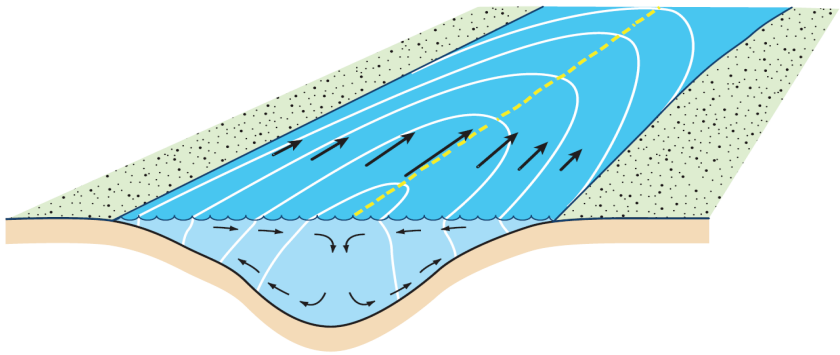

Figure 1.5: Principle of differential advection (from review Advances in Estuarine Physics, MacCready and Geyer [2010]). White lines indicate the isohalines and the arrows show the strength and direction of the currents.

dimensional process that contributes to, and complicates, estuarine dynamics [Nunes and Simpson, 1985, Figure 1.5]. Differences in water depth along a cross-section of a channel result in differences in current speed, generally with the largest currents located in the center, or the deepest part of the channel. The largest currents transport the most saline water from the sea during flood, creating cross-stream density differences. The baroclinic pressure gradient generates two cross-stream circulation cells with near-bed currents directed towards the side of the channel and near-surface currents directed towards the center of the channel (Figure 1.5). The cross-stream currents distribute salinity and momentum laterally, complicating estuarine dynamics. A certain amount of time is required for the cross-stream baroclinic pressure gradient to develop. Therefore, differential advection becomes most important during late flood. During ebb, the cross-stream circulation cells are reversed. Cross-stream circulation patterns are modified by curvature and Coriolis effects, vertical stratification and asymmetric cross-stream bathymetry, which impact differential advection [Lacy and Monismith, 2001; Buijsman and Ridderinkhof, 2008c].

Differential advection, and the other factors that drive cross-stream currents, re-distribute momentum and density. The re-distribution of salt and momentum

is divided into two processes, namely cross-stream tidal straining and lateral advection, respectively, which also influence the along-stream estuarine circulation.

Cross-stream tidal straining is a process that can generate vertical stratification during flood, creating ebb-flood asymmetries in vertical stratification and thereby modifying the estuarine circulation. Recently, evidence of flood stratification as a common phenomenon in estuaries has been reported [Scully and Geyer, 2012; Aristizábal and Chant, 2014, this thesis], which might impact the estuarine circulation. Stacey et al. [2008] showed that the timing of vertical stratification in periodically-stratified estuaries determines the strength and direction of the estuarine circulation. They showed that late flood stratification produces a reversed estuarine, tidal straining circulation, thereby neglecting any superimposed effect of the baroclinic pressure gradient and the gravitational circulation. Cheng et al. [2011, 2010] and Burchard and Schuttelaars [2012] demonstrated the importance of cross-stream straining for the strength of the estuarine circulation using idealized models.

Lateral advection also modifies the estuarine circulation by re-distributing momentum. Lerczak and Geyer [2004] modelled the intra-tidal variability of lateral advection in a straight estuarine channel and found a flood-dominant abundance of lateral advection. Lower momentum water is transported from the side to the upper part of the water column during flood, whereas higher momentum water is transported downward, enhancing the estuarine circulation. Vertical stratification during ebb due to classical tidal straining reduces the strength of the cross-stream circulation cell and is therefore not able to mitigate the lateral re-distribution of momentum from the flood phase. The asymmetry in lateral advection between ebb and flood generally enhances the estuarine circulation.

1.4.3 *3-dimensional perspective (including along-stream variability)*

Estuaries are generally not characterized by straight symmetric channels, as assumed above, but rather by curved bends and great along-stream variations in width and depth. Also, the tidal distortion varies spatially. Along-stream variations in estuarine circulation have been observed as a result of the complex bathymetry [Jay and Smith, 1990a; Martin and MacCready, 2011; Geyer and MacCready, 2013, and references therein]. These studies highlight the highly three-dimensional character of the estuarine circulation patterns in estuaries and remain an area of ongoing research.

Summarizing, all the discussed processes influence the vertical structure of the instantaneous and residual currents. However, in essence, most processes are directly or indirectly related to two factors: density gradients and vertical

mixing by tidal currents. The next section shows how tidal currents and density gradients are intricately intertwined by turbulence.

1.5 TURBULENCE AND MIXING

As has already become obvious in the previous sections, tidally-induced turbulence and vertical mixing are important for the vertical structure of velocity. Furthermore, turbulence determines the vertical distribution of suspended matter and re-distributes heat, salt and momentum. Therefore, it plays an essential role in natural systems.

Turbulence has several positive and negative feedbacks on currents and density gradients, augmenting the complexity of the estuarine system [Stacey et al., 2011, and references therein]. In addition, high-resolution and cost-efficient measurements of turbulence have only become possible since the last decades [Lohrmann et al., 1990; van Haren et al., 1994; Stacey et al., 1999b]. Therefore, the topic of estuarine turbulence is still an area of ongoing research. Recently, turbulence has been investigated in a wide variety of estuaries, ranging from well-mixed, weakly- and periodically-stratified, to strongly-stratified estuaries [Lu et al., 2000; Kay and Jay, 2003; Stacey and Ralston, 2005; Geyer et al., 2008; Ralston et al., 2010; Scully et al., 2011].

In well-mixed and periodically-stratified estuaries, bed-generated turbulence is generally the main source of turbulence production [Peters and Bokhorst, 2000, 2001; Rippeth et al., 2001; Becherer et al., 2011], where the shears near the seabed generate turbulence, which extends upwards over the water column. Turbulence partly determines vertical stratification and shears in velocity over the water column, but is also influenced itself by the other two factors [Stacey et al., 2001, 2008, 2011]. Turbulence decreases vertical stratification and shears in velocity, whereas vertical shears itself generate turbulence and decrease vertical stratification. On the other hand, vertical stratification dampens turbulence but increases the shears. The three-way interactions illustrate the positive and negative feedback mechanisms that exist between the actors. In periodically- and weakly-stratified estuaries, classical tidal straining generally results in vertical stratification during ebb, which dampens turbulence production during ebb and creates intra-tidal asymmetries in vertical mixing [Rippeth et al., 2001; Simpson et al., 2005; Verspecht et al., 2009], which in turn impact the total estuarine circulation. However, recent observations of vertical stratification during flood suggest stratification-mixing dynamics are more complex than the classical one-dimensional tidal straining dynamics [Scully and Geyer, 2012].

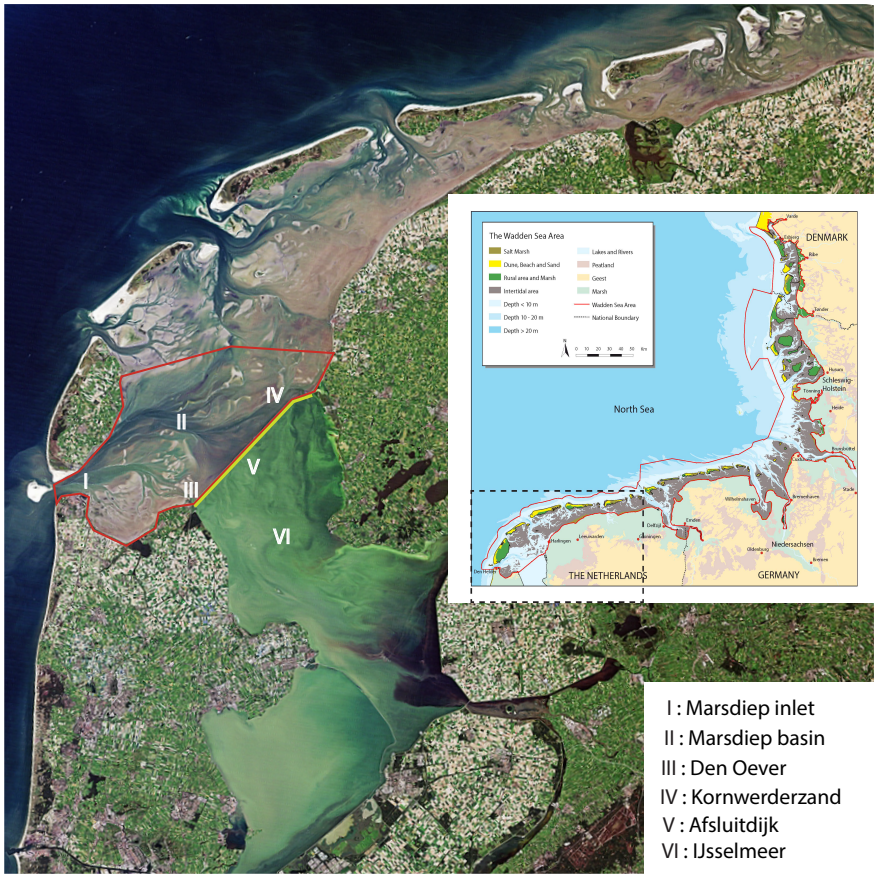

Figure 1.6: Landsat image of the Dutch part of the Wadden Sea (courtesy ESA) and a smaller overview map of the entire Wadden Sea area (courtesy Wadden Sea secretariat, http://www.waddensea-secretariat.org/). Roman numbers indicate different geographic locations as given in the legend and mentioned in the text. The yellow line (V) indicates the Afsluitdijk, which is approximately 30 km long. The red line delineates the borders of the Marsdiep basin (II).

1.6 MARSDIEP BASIN

The Marsdiep basin is the westernmost basin of the Wadden Sea, characterized by meandering channels and an extensive inter-tidal flat area (Figure 1.6). Prior to the closure of the Afsluitdijk (enclosure dyke) in 1932, the Marsdiep basin belonged to the larger Zuiderzee basin, together with the adjacent Vlie basin and the present-day freshwater lake, the IJsselmeer. In the past, freshwater was discharged into the southeast corner of the Zuiderzee by the river IJssel. Presently, the freshwater discharge from the IJsselmeer into the Marsdiep basin is regulated through outlet sluices. The complex bathymetry of the Marsdiep basin is characterized by large variations in water depth on a small spatial scale. Furthermore, migrating sandwaves and other bedforms are ubiquitous in the basin [Buijsman and Ridderinkhof, 2008a,b]. In addition, the morphology of the Marsdiep basin is still adjusting to the closure of the Afsluitdijk [Dastgheib et al., 2008].

The most important astronomic constituents in the Marsdiep basin are the M2 tidal constituent and its solar counterpart, S2, the latter being approximately 27 percent of the former [Buijsman and Ridderinkhof, 2007a]. The diurnal constituents are small, but the compound and overtides, e.g. M4, contribute considerably to the strength of the tidal currents, highlighting the large tidal distortion in the Marsdiep basin. The overtides originate from tide-bathymetry interaction via differential advection of vorticity [Zimmerman, 1976b; Ridderinkhof, 1989], which results in depth-averaged horizontal residual circulation patterns (Figure 1.1): the southern two-thirds of the Marsdiep inlet are flood-dominant, whereas the northern one-third is ebb-dominant [Buijsman and Ridderinkhof, 2007a]. Wind drives residual currents, superimposed on the tide-bathymetry interaction, which determines the direction (and variability) of the throughflow between the Marsdiep and other basins of the Wadden Sea [Ridderinkhof, 1988; Buijsman and Ridderinkhof, 2007b; Duran-Matute et al., 2014; Nauw et al., 2014].

The main sources of freshwater are the outlet sluices at Den Oever and Kornwerderzand, which discharge freshwater from the IJsselmeer into the Marsdiep basin during low water only. Until recently, the high currents in the Marsdiep were assumed to mix the entire water column and, therefore, density-related processes were assumed to be negligible [e.g. Zimmerman, 1976a; Ridderinkhof, 1989]. However, Buijsman [2007] and Groeskamp et al. [2011] noted that the water column is weakly-stratified during several phases of the tide. (This had already been observed during oceanography courses since the 1970's). The contribution of the density gradients to the vertical structure of velocity in the Marsdiep system has not yet been investigated in detail.

The previous studies mainly focused on the large-scale hydrodynamics of the western Dutch Wadden Sea, adopting an analytical [Zimmerman, 1976a]

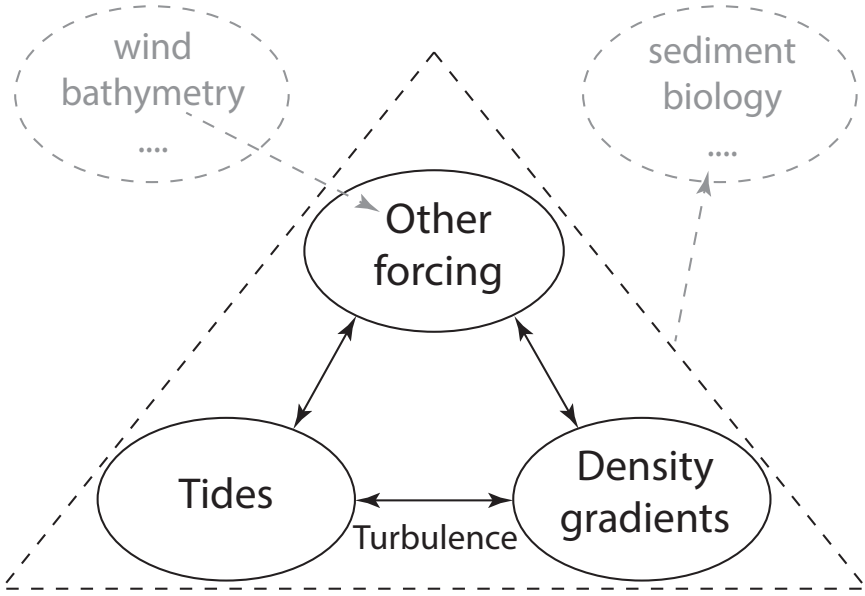

Figure 1.7: Simplified separation of the estuarine system into different compartments. The forcing of the hydrodynamics in estuaries is depicted within the triangle. Besides the tides and density gradients, wind and bathymetry (upper left corner) are other factors that force the hydrodynamics. The focus of this thesis is given in the triangle, separated into a tides, density gradients and turbulence component. The hydrodynamics force sediment transport and biological activity, as depicted in the upper right corner.

or numerical-modelling approach [Ridderinkhof, 1988; Duran-Matute et al., 2014]. The few observational studies in the Marsdiep basin primarily focused on the large-scale hydrodynamics through analysis of low-resolution ferry-based observations [Buijsman, 2007]. However, no detailed observational study of the small-scale spatial current characteristics has yet been conducted in the Marsdiep basin.

1.7 OBJECTIVE, RESEARCH QUESTIONS AND THESIS OUTLINE

The scarcity of detailed (small-scale) observational studies and the recent notion of vertical stratification warrant the necessity for more research on the small-scale estuarine hydrodynamics in the Marsdiep basin.

In this thesis, a wide variety of measurement techniques is combined in order to investigate the small-scale structure of the currents in the Marsdiep basin.

Spatial 13-hour surveys with the R.V. Navicula are conducted to measure vertical profiles of e.g. velocity, temperature and salinity which provide insight into the small-scale spatial dynamics. The vertical profiles of velocity are measured with an Acoustic Doppler Current Profiler (ADCP), whereas the conductivity, temperature and depth (CTD) are measured with a SeaBird CTD system. Also, separate moored 13-hour campaigns with the R.V. Navicula at one specific location, called anchor stations, illustrate the temporal evolution of the velocity and density field over a tidal cycle on a timescale of minutes to hours. Over ten anchor stations are conducted between 2011 and 2014, of which four are treated in this thesis. Long-term data (20 to 46 days) are obtained by deploying a bottom frame on multiple occasions, equipped with an ADCP and point-CTD (microCAT). At the bottom frame, vertical profiles of velocity and point measurements of temperature, salinity and depth are measured at 30 seconds intervals. The high-resolution long-term measurements provide a detailed overview of the vertical structure of velocity under a wide range of conditions from a minute to seasonal timescale. Furthermore, turbulence observations are collected with two different measurement techniques. A free-falling microstructure profiler (FLY) has been used to collect data every 20 minutes during several 13-hour anchor stations, whereas the ADCP measures turbulence every 12.5 minutes during spring and neap tide conditions for two individual bottom frame deployments (5 and 7 days, respectively). Most of the measurements have been collected near the site of the planned location of the test tidal energy plant. The diverse and comprehensive dataset provides the opportunity to investigate multiple aspects of the estuarine hydrodynamics in the Marsdiep basin.

Figure 1.7 presents an overview of the central topics considered in this thesis. The vertical structure of velocity in estuaries is predominantly determined by tides and density gradients, which are intricately intertwined by turbulence. These three aspects are the main focus of this thesis. Each aspect is influenced again by many other factors, such as wind, bathymetry, bed friction and benthic life forms. Bathymetry and wind are addressed in several chapters. The forcing of all components within the triangle, and their interactions, are essential for the distribution of suspended matter and the biological activity in the water column.

The following research questions are addressed to investigate the small-scale hydrodynamics in the Marsdiep basin:

1. *What is the spatial and temporal variability of the vertical structure of instantaneous along-stream tidal currents and density?*

2. *What determines the vertical structure of the residual currents, thereby focusing on the dynamics of the estuarine circulation?*

3. *What are the characteristics of turbulence during neap and spring tide conditions and how are these connected to the barotropic and baroclinic components of the tide?*

In Chapter 2, the spatial variability of the tidal currents and the density field is investigated through observations, providing an exploratory overview of the hydrodynamic conditions at the study site. Chapter 3 discusses the vertical structure of the tidal currents and their modification by the presence of density gradients. Spatial surveys and long-term moored observations are combined with simplified one-dimensional numerical water column modelling using GOTM. Both chapters address research question 1. Chapter 4 focuses on research question 2 and investigates the vertical structure of the residual currents by analyzing long-term mooring measurements. The observations are complemented with numerical model results from GETM/GOTM to highlight the spatial variability in vertical structure of the residual current. The role of turbulence is investigated in Chapter 5 by analyzing turbulence measurements collected during neap and spring tidal conditions, thereby addressing research question 3. In Chapter 6, an overview of the main results is given and an outlook to remaining gaps in our understanding of the estuarine dynamics in the Marsdiep basin is presented.

2

EXPLORATORY STUDY OF THE VARIABILITY OF CURRENTS AND DENSITY

Observational data of tidal currents and vertical stratification are presented in this chapter. The data were collected between 2010 and 2012 during multiple surveys in the Marsdiep basin. The aim of this chapter is to better understand the spatial variability of the tidal currents and the occurrence of vertical stratification in the Marsdiep basin. A harmonic analysis is applied to the depth-averaged velocity to obtain estimates of the tidal ellipse parameters of the M2 tidal constituent along the surveys. The spatial variation in magnitude of the tidal currents is complex but seems mainly related to water depth. This relationship varies in time on a daily to fortnightly timescale, which results in a variation of the lateral velocity shears over time. Furthermore, the tidally-averaged lateral density gradient is of the same order of magnitude as the longitudinal density gradient, implying that cross-stream processes are important in the Marsdiep basin. At some locations, vertical stratification is only observed during the flood phase which seems mainly driven by lateral processes. This pattern is inconsistent with the classical alongstream tidal straining mechanism, where vertical stratification develops during ebb and diminishes during flood. It is hypothesized that vertical stratification during flood increases from neap to spring tidal conditions due to increased differential advection. The strength and timing of vertical stratification is shown to be highly spatially variable in the Marsdiep basin, which might have implications for the residual circulation patterns.

This chapter is based on the following publication:
de Vries, J. J., Nauw, J. J., Ridderinkhof, H., and van Aken, H. M. (2014). An exploratory study of the variability of currents and density in the Marsdiep, *Cont. Shelf. Res.*, 84:70-83.

2.1 INTRODUCTION

Tides contain a copious source of kinetic energy and are therefore a dominant factor in advecting salt, heat, nutrients, pollutants, fish eggs, larvae, plankton and suspended particles in shelf seas and estuaries. In addition, buoyancy and wind forcing are other important factors, where their relative contribution depends on local conditions. Recently, tides are considered as a potential source of renewable energy, which resulted in a growing interest in the small-scale O(0.1-1 km) spatial variability of tidal currents. In the Marsdiep basin, a floating test tidal energy plant with a size of 100 x 30 m^2 is planned to be moored. Tidal energy production is related to flow speed cubed. It is therefore important to obtain a thorough understanding of the spatial variation in currents in order to find an optimal location for such a platform for optimizing tidal energy production.

In estuaries like the Marsdiep basin, the currents are influenced by bathymetry, wind and density gradients originating from freshwater inflow. Much research has already been conducted on the large-scale spatial variability of currents and on the residual circulation at the inlet of and in estuaries, e.g. the Chesapeake Bay [Valle-Levinson et al., 1998], Colombia River Estuary [Jay and Smith, 1990a,b,c] and the Marsdiep inlet [Buijsman and Ridderinkhof, 2007a]. The variation of tidal flow on a smaller spatial scale O(0.1-1km) has been another area of research. Murphy and Valle-Levinson [2008] investigated the spatial and temporal variability of currents on a smaller scale in the shallow (h<15 m), microtidal and subtropical Saint Andrew Bay system, Florida USA. Li [2002] covered the spatial variability at an axial convergence front system, whereas Li et al. [2006a] and Li et al. [2006b] investigated the small-scale variability of geometry-driven residual currents and eddies using observations and model simulations. In the Marsdiep basin, large depth variations are present on a small spatial scale, which makes it worthwhile to investigate the spatial variability of tidal currents. Furthermore, the temporal modulation of the spatial variability in currents has not yet been investigated in the Marsdiep basin. Variations in currents are important since the associated lateral shears are essential for horizontal mixing [Zimmerman, 1986] and the formation of fronts [Li, 2002]. In addition, they generate complicated flow patterns around complex bathymetry [Geyer, 1993]. Lateral velocity shears originating from differential advection have also been observed to drive secondary currents in a channel and to modify the density distribution [Nunes and Simpson, 1985].

The currents in the Marsdiep inlet itself are well described by Buijsman and Ridderinkhof [2007a] using measurements from the Den Helder-Texel ferry. However, less is known about the current field in the inner part of the Marsdiep basin. Groeskamp and Maas [2012] investigated the spatial variation in a small part of a tidal channel, the Malzwin, which has water depths between 5 and

15 m. At that location, they found a linear increase in flow strength with depth. They discussed two simple, but contradictory theories that predict tidal amplitude as a function of local water depth (inversely proportional) or as a function of friction (linearly/parabolically proportional) and they demonstrated that the latter was applicable to their research area. However, they did not cover the entire range of water depths in the Marsdiep which varies between 0 and 40 m. Furthermore, measurements were acquired during one single tidal cycle.

A fundamental characteristic of estuaries is the presence of longitudinal, lateral and vertical density gradients due to the (varying) influence of freshwater [Hansen and Rattray, 1966; Simpson et al., 1990; MacCready and Geyer, 2010, and references therein]. The density field in the Marsdiep basin has only been studied marginally [Zimmerman, 1976a,b; Buijsman and Ridderinkhof, 2008c], even though visible signs of their importance are a common feature in the Marsdiep basin such as frontal features, e.g. axial density lines which indicate the boundary of different water masses, and internal wave signatures [Groeskamp et al., 2011]. Generally, it is assumed that the gravitational estuarine circulation as well as tidal straining dominate the longitudinal exchange in narrow estuaries with inflow at the bottom and outflow at the surface. In wide estuaries however, rotational effects become more important. Valle-Levinson [2008] was able to semi-analytically express the density-driven exchange flow in terms of the Ekman and Kelvin number. Basdurak and Valle-Levinson [2012] demonstrated the great temporal variation in estuarine exchange patterns, i.e. horizontally versus vertically sheared, in a microtidal estuary. Recent studies have shown that lateral processes may influence the longitudinal exchange. Several model studies have shown that lateral advection is able to modify longitudinal exchange [Lerczak and Geyer, 2004; Cheng et al., 2009; Scully et al., 2009; Burchard and Schuttelaars, 2012], which has also been confirmed by an observational study in the microtidal James River Estuary [Basdurak and Valle-Levinson, 2012]. In the Marsdiep, Postma [1954], Zimmerman [1976a,b] and Ridderinkhof [1988, 1989] assumed the water column to be well-mixed as a result of the strong currents (up to 2 m/s). However, recent studies have shown that the Marsdiep is periodically-stratified during the flood and ebb phase [Buijsman and Ridderinkhof, 2008c; Groeskamp et al., 2011; de Vries et al., 2012]. Despite the observations in recent studies, the dynamics of the spatial density field and their effect on the residual circulation have not yet been investigated in detail in the Marsdiep basin.

Furthermore, the existence of an estuarine circulation in the Wadden Sea is still a topic of debate. Flöser et al. [2011] found indications of an estuarine circulation in the German Wadden Sea, in the Hörnum Deep near Sylt, by analyzing the vertical profile of the horizontal velocity during peak ebb and flood. However, Buijsman and Ridderinkhof [2007a] found contradictory vertical profiles of horizontal velocity in the Marsdiep inlet. They concluded that

the horizontal residual circulation pattern is explained by the advection of vorticity as described by Ridderinkhof [1989], which is determined by the complex bathymetry of the western Dutch Wadden Sea, but they did not analyze the vertical residual circulation. Flöser et al. [2013] presented suggestive indications of an estuarine residual circulation based on the vertical profiles of the horizontal velocity but they did not relate them to the strength of the longitudinal density gradients or any other baroclinic forcing. Therefore, the importance of tidal straining in the Wadden Sea is still a topic of debate.

Becherer et al. [2011] related the occurrence of vertical stratification in the German Wadden Sea during specific tidal phases to tidal straining and thereby indirectly suggest the presence of an estuarine circulation. The mechanism of tidal straining, first described by van Aken [1986] in a shelf sea and Simpson et al. [1990] in an estuary, explains the asymmetry in vertical stratification, in estuaries between ebb and flood, as a result of the interaction between tidal currents and the longitudinal density gradient. During the flood (ebb) phase of the tide, the longitudinal baroclinic pressure gradient opposes (enhances) the barotropic pressure gradient which decreases (increases) vertical stratification. Such a mechanism results in the strongest stratification during ebb and strongest mixing during flood. In this study, observations of vertical stratification are presented that deviate from those observed under the tidal straining mechanism. These patterns correspond to observations in other estuaries by Lacy et al. [2003], Scully and Friedrichs [2007], Scully and Geyer [2012] and Basdurak et al. [2013], and they illustrate that the formation of vertical stratification in the Marsdiep is not merely a one-dimensional process. Furthermore, the spatial variability in vertical stratification, presented in this study, may be large depending on the phase of the tide, which corresponds to other studies [Scully and Friedrichs, 2007; Cheng et al., 2009].

The aim of the research presented in this chapter is two-fold. Firstly, one aim is to obtain a better understanding of the variation of currents over a wide range of water depths. Secondly, due to its importance in estuarine dynamics, the spatial variability in occurrence and strength of vertical stratification in the Marsdiep is investigated. In section 2.2, the study site and material and methods are discussed. In section 2.3, the results are treated. In section 2.4, the results are discussed and in section 2.5 concluding remarks are given.

2.2 STUDY SITE, MATERIAL AND METHODS

2.2.1 *Study site*

The Marsdiep inlet forms the connection between the North Sea and the mesotidal Marsdiep basin. The Marsdiep basin is the westernmost tidal basin of the

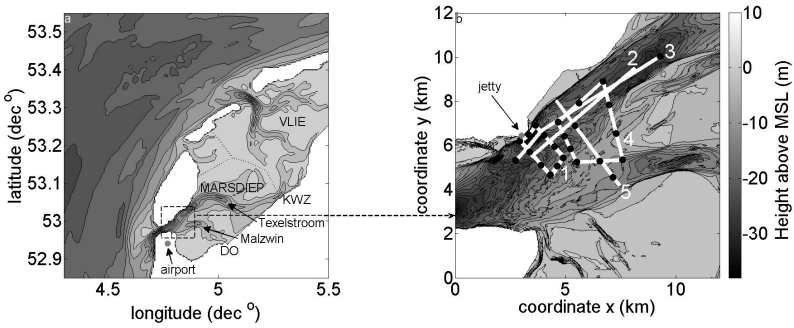

Figure 2.1: Bathymetric map of the western part of the Dutch Wadden Sea (a, reference mean sea level, MSL) and, in detail, the area where the observations were done (b) with the surveys (white lines) and CTD stations (black dots). The northern (southern) channel is the Texelstroom (Malzwin). To the east, these channels are separated by the tidal flat, Lutjeswaard. Numbers 1-5 indicate the survey number as used in table 2.1. DO (KWZ) indicates the freshwater sluices at Den Oever (Kornwerderzand). The grey dots indicate the location of the NIOZ jetty and the Den Helder airport. The coordinate frame in the zoom-in (b) is a Cartesian coordinate frame with the origin in the southwest corner.

Dutch Wadden Sea and the largest tidal inlet of the Netherlands (600 km^2, Figure 2.1a), almost twice as large as the Western and Eastern Scheldt (300 and 350 km^2, respectively). At the inlet, the Marsdiep consists of one channel. At the eastern, inner part of the inlet, the Marsdiep channel splits up into the Texelstroom channel (northern branch) and the smaller Malzwin channel (southern branch) which are separated by an intertidal shoal, named Lutjeswaard. The bathymetry of the Marsdiep basin varies strongly on different spatial scales. The intertidal flats and the channels are distinct morphological units with the channel being much deeper than the intertidal flats. Also within the channels, large depth variations are present. On larger spatial scales of O(10km), the channels become shallower further into the Wadden Sea. However over smaller scales of O(1km), depth variations in the main channels are in the order of 10-20 m, and are common at the seaward side of the basin, in the vicinity of the inlet, in along- and cross-stream direction. On a very small spatial scale (100-200 m), the depth in the main channels may vary by 2-3.5 m as a result of the occurrence of sandwaves. These have been observed in the tidal inlet using depth obser-

Survey	**Date**	**Wind**	**Wind**	**LC**	$\Delta\rho_{M2}$	$\Delta\rho_z$	**TR**
nr	dd-mm-yy	Bft	dir		kg/m^3	kg/m^3	m
Quad 1a	21-10-10	5-6	W-NW	2	4.0		1.5
Line 2	19-10-10	3-5	NW-N	4	5.3		1.4
Quad 4	19-10-11	4-6	NW	1	5.1	3.3	1.2
Quad 1b	20-10-11	3-4	NW-S	2	3.7	2.6	1.1
Line 3	11-03-12	2-3	NW	6	4.5	3.6	1.6
Line 5	03-05-12	3	S-N	3	6.2	4.0	1.5

Table 2.1: Wind conditions, tide, tidal density range, maximum vertical stratification and tidal range of each survey. The lunar cycle (LC) indicates the spring/neaptide modulation going from 1 (neaptide) to 7 (springtide). The $\Delta\rho_{M2}$ is the tidally-averaged density range at the surface. The $\Delta\rho_z$ is the maximum vertical density range during the survey, which was not measured during surveys 1a and 2. In the last column, the tidal range (TR) at the NIOZ jetty is given. Quadrangle (Quad) 1 was surveyed twice, named 1a and 1b.

vations from a ferry-mounted ADCP [Buijsman and Ridderinkhof, 2008a]. The main sources of freshwater are located at Den Oever (DO) and Kornwerderzand (KWZ), which are the outlet sluices of the freshwater lake IJsselmeer into the Marsdiep basin (Figure 2.1a). The sluices discharge only during low tide. The daily mean discharge at the DO and KWZ sluices for the period 1998-2004 is 333 m^3/s and 239 m^3/s, respectively. However, there is a great seasonal variability with on average high discharges in autumn and winter and low discharges in spring and summer [Buijsman and Ridderinkhof, 2008c]. All the freshwater from DO is assumed to be discharged through the Marsdiep basin via the Malzwin channel. Based on observed salinity distributions, it has been assumed that two-thirds of the freshwater from the sluices of KWZ are flushed into the North Sea via an adjacent tidal basin, the Vlie basin [Zimmerman, 1976a,b]; the other one-third originating from KWZ is assumed to be discharged through the Marsdiep basin, via the Texelstroom channel. Smaller sources of freshwater are water pumping stations, namely the Oostoever and Helsdeur pumping stations near Den Helder (7.8 m^3/s and 8.7 m^3/s) and the prins Hendrik pumping station on Texel (0.5 m^3/s) which further freshen the Malzwin and Texelstroom, respectively. Even though their contribution is small, their location close to the research area suggests a possible influence on the local density structure. The discharge of these pumping stations also displays a strong seasonal variability similar to that of the outlet sluices of the IJsselmeer.

2.2.2 *Data collection*

The data are collected during a series of surveys from 2010 to 2012. Repeated measurements during a semi-diurnal tidal cycle are carried out along different types of transects (Figure 2.1b and Table 2.1). Quadrangle 1 is surveyed twice (1a, 1b) on two distinct days and two (semi-) straight lines are surveyed along the Texelstroom (2, 3). Furthermore, once a quadrangle and once a line covering parts of both the Malzwin as well as the Texelstroom are surveyed (4, 5). Quadrangle 4 and 1b are surveyed with the lowest temporal resolution. During these surveys, 7 and 9 tracks are completed in 13 hours, respectively. Lines 3, 2, 5 and quadrangle 1a are surveyed 14, 19, 24 and 20 times, respectively. The variation in the number of repetitions of a specific survey is related to the different sizes of each transect and to the number of different types of measurements per survey.

Wind, density and tidal conditions of each survey are summarized in Table 2.1. The wind data was collected at Den Helder Airport, the Kooy (Figure 2.1a) and was provided by the Royal Dutch Meteorological Institute (`http://www.knmi.nl/klimatologie/uurgegevens/`). Henceforth, the surveys are referred to as quadrangles and lines combined with a survey number. The edges of each quadrangle have been indexed with roman numbers, as first shown in Figure 2.3.

2.2.3 *Instrumentation*

During the surveys, conductivity, temperature and depth (CTD-) and velocity measurements are performed. The current velocity profile is measured with a four-beam 1.2MHz RDI Workhorse Monitor ADCP attached to a pole at 1 m below the sea surface at the starboard side of the NIOZ R.V. Navicula. The ping rate of the ADCP is 1 Hz and ensembles are recorded every 2 s. The ADCP signal is corrected for the ship's pitch, roll and heading in real-time. The ship's velocity is measured by means of bottom tracking or by means of the ship's differential GPS (dGPS), if the former is unavailable. The bottom depth is estimated with 1 bottom ping per ensemble. The ship travelled at an average speed of 3 m/s (6 knots) during each survey.

A SeaBird SBE 911 plus CTD system is used to measure temperature, conductivity (for salinity) and pressure profiles at designated locations along the surveys, as indicated by the black dots in Figure 2.1b. Conductivity, temperature and pressure are recorded at 24 Hz and are used to compute temperature and density profiles with 0.5 m depth intervals. During quadrangle 1a and line 2, no CTD profiles are recorded. These early surveys only focused on the current velocity. During all other surveys, conductivity and temperature are also

recorded continuously at 1 m below the sea surface with a Seabird surface CT system, measuring with a frequency of 24 Hz.

At the NIOZ jetty (Figure 2.1b), the pressure is measured by a calibrated Keller 46 pressure sensor at 2.9 Hz. The pressure is converted real-time into sea surface elevation. Sea surface elevation is recorded every minute with an accuracy of 3 cm based on the median of 175 samples.

2.2.4 *Data processing*

During the post-processing, the water depth is retrieved from the bottom tracking echo. All data below the sea bed are removed as well as the first bin above the bottom, which contains unreliable data possibly due to side-lobe interference. Prior to each survey, calibration transects are carried out in order to estimate the angle between the ship's and the bottom-tracking velocities. The difference between the dominant direction of the ship's velocity and the bottom-tracking velocity is minimized to compensate for the ADCP compass offset. The ADCP compass offset is between 1-3 degrees for each survey, which corresponds to a correction in current velocity of maximum 2 cm/s. The sound velocity of the ADCP is not corrected for vertical variations in salinity since these variations are only in the order of 5 m/s, or 0.3 percent. This results in a vertical uncertainty of approximately 0.15 m, which is approximately three times smaller than the bin size.

Velocity outliers are identified as ensembles with a depth-averaged flow velocity higher than 2 m/s and these are removed. An additional quality control is performed based on the mean of the depth-averaged east-west and north-south velocity components of every 200 ensembles. Individual ensembles with a depth-averaged velocity deviation more than twice the standard deviation from the mean value are removed. Furthermore, an additional outlier removal is conducted after the flow field is rotated into an alongstream component, defined as the dominant velocity axis which coincides with the channels' orientation, and a cross-stream component, perpendicular to the dominant velocity axis. Two physical restrictions are imposed on the cross-stream velocity component. Ensembles with a depth-averaged cross-stream velocity higher than 0.5 m/s are removed because it would result in an unrealistic mass transfer in cross-stream direction. The difference between the maximum and minimum cross-stream velocity of an ensemble greater than 1.5 m/s represents an unrealistically strong circulation cell and these ensembles are also removed.

The CTD data are processed with the manufacturer's SBE Data Processing software (`http://www.seabird.com/software/`) in order to derive salinity (psu), potential density anomaly ($\sigma - \theta$, kg/m^3), temperature (ITS-90, °C) and depth (m). Outliers are removed and the data are low-pass filtered. Sub-

sequently, the data are averaged in bins of 0.5 m. The surface CT data are processed with Seasave (`http://www.seabird.com/software/SeasaveV7.htm`) and filtered with a running mean filter with a window of 2 seconds to remove spikes. At quadrangle 1a, an additional filtering is required due to the large amount of air bubbles from the high breaking waves present on that day. Outliers, or spikes, are characterized by a strong drop in salinity of 10 to 20 psu over a short time period. These spikes are believed unrealistic and are removed from the data by imposing a lower threshold on the potential density anomaly of 17.5 kg/m^3.

After the post-processing, gridpoints are defined at intervals of 100 m along each track. All velocity and surface CT data around a gridpoint are collected within a radius of 50 m. In the next section, the parameters computed after the data gridding are discussed.

2.2.5 *Data analysis*

2.2.5.1 *Harmonic analysis*

To present an estimate of the semi-diurnal tide with only 13 hours of data, the depth-averaged data from each gridpoint are fitted to an M2 tidal cycle. A least-squares harmonic analysis (LSHA) is performed with the frequency, $\omega = 1.4{*}10^{-4}$ rad/s, which is the frequency of the M2 tide with a period of 12.42 hours

$$a(t) = a_0 + a_{M2} cos(\omega t - \phi_{M2}) + \epsilon(t), \tag{2.1}$$

where a is the depth-averaged eastward, or northward current velocity component (u or v, resp. in m/s), a_{M2} is the amplitude of the M2 tidal constituent (m/s), t is the time (s), ϕ_{M2} is the phase (degrees), a_0 is the tidally averaged velocity (residual current, m/s) and ϵ is the unexplained part (m/s). The amplitude and phase lag between the east-west and north-south velocities are combined to compute the tidal ellipse parameters as described in Pawlowicz et al. [2002] (Figure 2.2). Because only 13 hours of data is available, other tidal constituents, which for example determine the spring-neap tidal modulation and the diurnal inequality, are implicitly included in resolving the amplitude, a_{M2}, and the unexplained part, ϵ. Therefore, the magnitude of a_{M2} and ϵ varies per survey.

The tidal ellipse parameters consist of a semi-major axis (SEMA), which is the maximum length of the speed axis of the tidal ellipse (m/s). The eccentricity (ECC) is the ratio between the length of the major and minor speed axis. Negative values indicate clockwise rotation and positive values anti-clockwise rotation of the velocity vector. The inclination (INC) is the angle between the

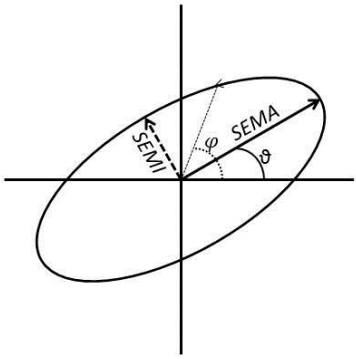

Figure 2.2: Example of a tidal ellipse consisting of a semi-major axis (SEMA), a semi-minor axis (SEMI), an inclination with respect to the positive x-axis (INC, θ). The eccentricity, ECC, is represented by the ratio between the SEMI and SEMA. An ECC greater (smaller) than 0 indicates counterclockwise (clockwise) rotation. The phase angle, ϕ, is the velocity at t=0.

SEMA and the eastward direction (in anti-clockwise direction). The phase reflects the moment (in degrees) at which the maximum current speed is reached. The phase lag (PHA, in degrees) is the difference between the phase of the sea surface elevation at the NIOZ jetty (reference) and the phase of the velocity data at each gridpoint. The tidal ellipses are used to gain insight into the spatial variability of the tidal currents in the Marsdiep.

2.2.5.2 *Density gradients and vertical stratification*

In Table 2.1, a density range over 1 tidal cycle ($\Delta\rho_{M2} = \rho_{max} - \rho_{min}$) is presented, based on the density of the continuously recorded surface CT data. The maximum vertical density range over 1 tidal cycle ($\Delta\rho_z$) is based on the density from the CTD data, as recorded on the CTD stations shown in Figure 2.1b. The maximum vertical density range is defined as the maximum difference in density of 1 profile between the surface and bottom over the tidal cycle.

The surface density records and the vertical density profiles are used to estimate the longitudinal, lateral and vertical density gradients on an intra-tidal and a tidally-averaged timescale. The tidally-averaged longitudinal and lateral density gradients of the quadrangles are computed as follows. Firstly, since the data are not synoptic, the surface density data are interpolated at half-hourly intervals at each gridpoint to ensure temporal uniformity at all gridpoints. Secondly, the surface density is tidally-averaged at each separate edge of a quadrangle. Finally, the longitudinal and lateral surface density gradients are computed by subtracting the tidally-averaged density of the opposing edges and dividing the result by the distance between the opposing edges. At the lines, the density gradient is computed based on the difference between the outer two, i.e. the first and last, gridpoints of each survey divided by the distance between them. The intra-tidal longitudinal and lateral surface density gradients are computed similarly, but without tidally-averaging the interpolated surface density data.

The vertical density gradient is computed at each separate CTD-station. Again, the density profiles are interpolated at half-hourly data intervals. Afterwards, the surface density is subtracted from the bottom density and divided by the water depth to obtain the vertical density gradient. The tidally-averaged and intra-tidal density gradients are used to investigate the importance of longitudinal, lateral and vertical stratification in the Marsdiep.

2.2.5.3 *Bottom boundary layer height*

To investigate the impact of bed friction on the water column and their possible impact on the dynamics of vertical stratification, the bottom boundary layer dynamics in the Marsdiep are analyzed. In tidal channels, the bed exerts friction on the flow which generates vertical shears up to a certain height above the bed. This layer subjected to bed friction is called the estuarine bottom boundary layer (BBL) and is well-mixed in partially or periodically stratified estuaries [Stacey and Ralston, 2005]. Stacey and Ralston [2005] observed that vertical stratification is only present above the BBL and that at the upper limit of the BBL, the gradient Richardson number is 0.25, which suggests a local dynamic balance between shear and stratification. In another study, Cudaback and Jay [2000] investigated the influence of bed friction on the height of the pycnocline and the height of the BBL. From a pragmatic point of view, this layer is considered to be represented well by a logarithmic fit [Lueck and Lu, 1997]. The question remains what the dynamics of the BBL are in the Marsdiep basin.

Stacey and Ralston [2005] proved that the height of the BBL, H_{BBL}, in a partially or periodically vertically-stratified estuary varies on an intra- and inter-

tidal timescale as a function of the local competition between shear production and density stratification as given by

$$H_{BBL} = h\sqrt{\frac{R_f}{Ri_x}}, \tag{2.2}$$

where R_f is the flux Richardson number (-), which is the ratio between the buoyancy production and the shear production of turbulent kinetic energy [Tennekes and Lumley, 1972] and Ri_x is the horizontal Richardson number (-) given by

$$Ri_x = \frac{gh^2}{\rho_0 u_*^2}\frac{\partial \rho}{\partial x}, \tag{2.3}$$

where g is the gravitational acceleration (9.81 m/s^2), $\frac{\partial \rho}{\partial x}$ is the longitudinal salinity gradient assumed to have a constant value of 10^{-4} kg/m^3/m, ρ_0 is a constant background density (1025 kg/m^3) and u_* is the friction velocity (m/s) which is retrieved from fitting measured velocity profiles to the logarithmic profile

$$u(z) = \frac{u_*}{\kappa} ln(\frac{z}{z_0}), \tag{2.4}$$

where $u(z)$ is the alongstream velocity (m/s) as a function of height z (m) above the bottom, κ is the von Karman constant (0.41) and z_0 is a roughness length (m). In this analysis, the effect of lateral density gradients in equation 2.3 is neglected. The R_f parameter is an important parameter which unfortunately can not be computed with the available data. In literature, a maximum value of R_f is between 0.15 and 0.2 based on oceanic turbulence measurements [Stacey and Ralston, 2005], but can be much lower for weakly stratified estuaries similar to the Marsdiep basin, such as the San Francisco Bay area, namely between 0.01-0.05 [Stacey et al., 1999b].

2.3 RESULTS

2.3.1 *Currents*

2.3.1.1 *Main features of the tidal ellipses*

The tidal ellipses of the depth-averaged currents for the four quadrangle surveys are depicted in Figure 2.3. The tidal ellipses of lines 2 and 3 are not shown since the surveys and the tidal ellipses are both in the direction of the Texelstroom channel resulting in overlapping ellipses from which no information can be detected. Parameters of the tidal ellipses of lines 2 and 3 are given in

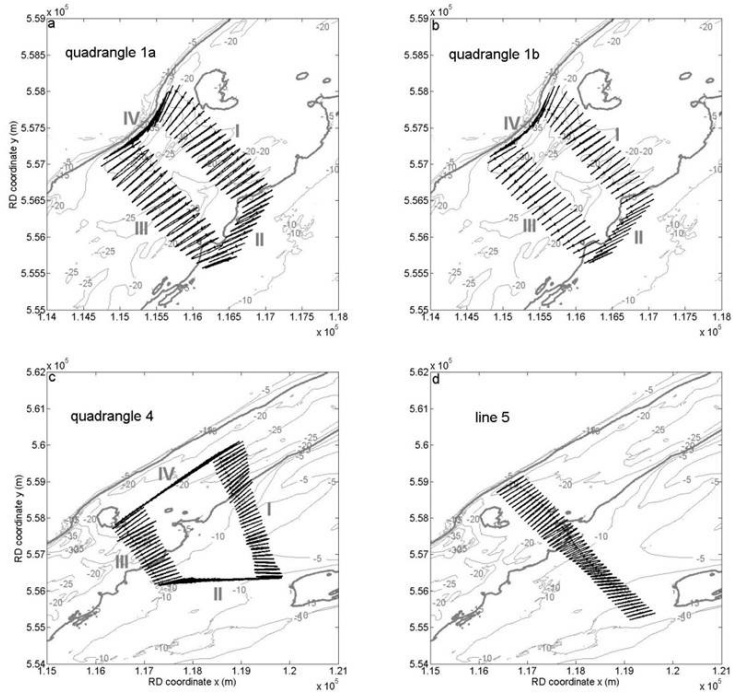

Figure 2.3: Tidal ellipses of the depth-averaged current at each gridpoint of a) quadrangle 1a, b) quadrangle 1b, c) quadrangle 4 and d) line 5. Roman numbers indicate the edges of each quadrangle. The 15 m isobath line is made bold.

the right column of Figure 2.5, which is discussed in more detail in section 3.1.2. Furthermore, alternative plots of the tidal ellipse parameters are given in Figures 2.4 and 2.5. Four major trends become evident. They illustrate the spatial complexity of the tidal currents in the Marsdiep:

- The magnitude of the SEMA depends on the local water depth and on the surrounding bathymetry (Figures 2.3, 2.4, and 2.5a,b,i,j). The depth-averaged SEMA increases with increasing local water depth for water depths up to 15 m, while it remains constant or even decreases slightly when the local water depth exceeds 15 m (Figures 2.4, 2.5a,b). The orientation of the tidal ellipses is aligned with the bathymetry of the Texelstroom channel where the water depth, h, is greater than 15 m (Figure 2.3). At the Lutjeswaard ($h < 15$ m), the orientation of the tidal ellipses crosses the isobaths at edge II of quadrangles 1a, 1b and at the southeastern part of line 5 (Figure 2.3a,b,d).

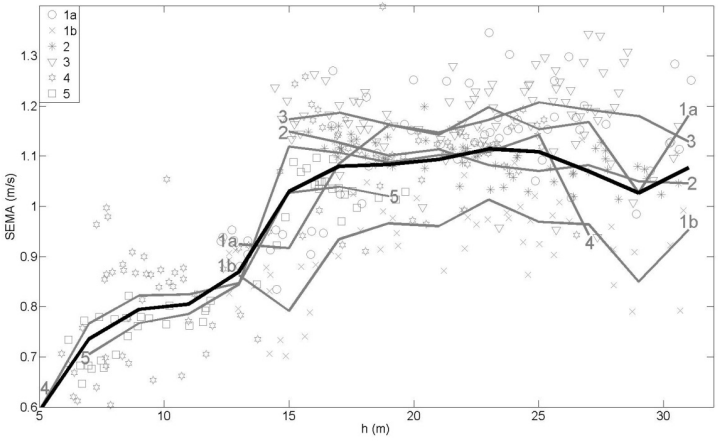

Figure 2.4: Depth-averaged SEMA as a function of local water depth, h. The icons indicate the independent gridpoints. The gray lines represent the averaged SEMA per individual survey. The black line represents the averaged SEMA of all surveys.

- The influence of the complex bathymetry (and the nearby coastline) on the flow is highlighted at edge IV of quadrangles 1a,b (Figure 2.3a,b, 2.5a). In this area, the magnitude and orientation of the flow varies strongly on a small spatial scale. The greatest water depths of quadrangles 1a and 1b, 32 m, are located at edge IV. Despite the great total water depths at this location, the SEMA is up to 0.3 m/s smaller than for total water depths between 20-25 m.

- The SEMA varies under different tidal forcing conditions. For line 2, the SEMA decreases slightly towards the Wadden Sea despite an increase in water depth, whereas for line 3, the SEMA increases towards the Wadden Sea. It suggests a temporal, fortnightly (i.e. spring-neap tidal) modulation of the SEMA.

- In general, the eccentricity of the tidal ellipse is small, indicating rectilinear currents. However, there are exceptions at the southern part of edge III of quadrangle 1a and at the middle part of line 5, indicated by a widening of the tidal ellipses. The variation in eccentricity for quadrangle 1a is most clearly visible in Figure 2.5g.

2.3.1.2 *Repeated surveys*

Since quadrangles 1a and 1b and lines 2 and 3 are repeated surveys of the same transect, it is possible to compare the tidal ellipse parameters of these similar

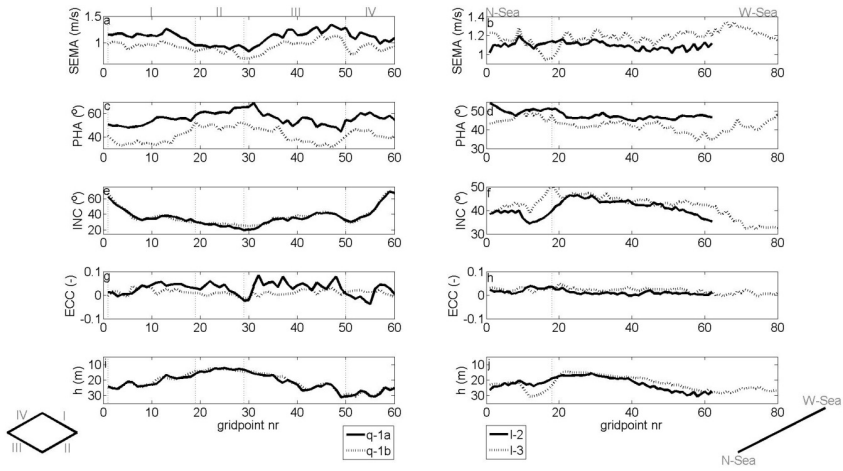

Figure 2.5: Tidal ellipse parameters consisting of the SEMA (a,b), PHA (c,d), INC (e,f) and ECC (g,h), and the water depth h(I,j) along repeatedly surveyed quadrangles 1a and 1b (left column, legend: q-1a, q-1b) and lines 2 and 3 (right column, legend: l-2, l-3). Roman numbering indicates the edges of the quadrangles. N-Sea and W-Sea indicate the seaward and landward end of the line surveys.

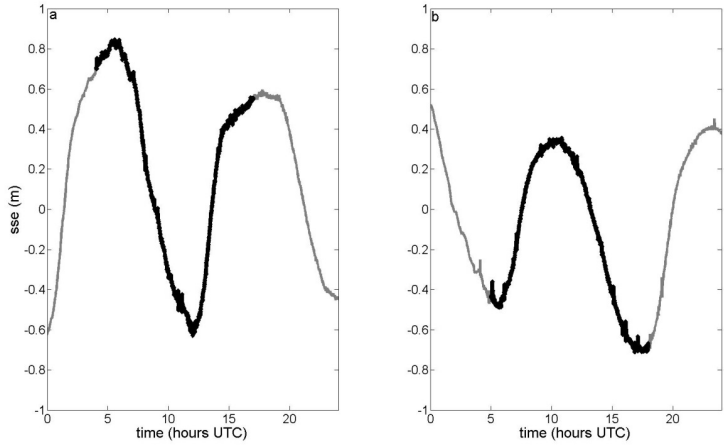

Figure 2.6: Sea surface elevation (gray line) at the NIOZ jetty on the days of quadrangles 1a (a) and 1b (b). The black part of the line indicates the time period that the surveys are conducted.

surveys under the different forcing conditions given in Table 2.1. Quadrangles 1a and 1b are conducted during the same phase of the spring-neap tidal cycle and under a similar tidally-averaged density range (Table 2.1). However, the tidal range (in sea surface elevation, Table 2.1 and Figure 2.6) varies as a result of the diurnal inequality. Lines 2 and 3 are measured at different phases of the spring-neap tidal cycle, which results in different tidal ranges (Table 2.1). An increase in tidal range implies an increase in horizontal barotropic pressure gradient, which results in higher flow velocities. The quadrangle and line surveys are used to indicate variations in tidal ellipse parameters in cross-stream and alongstream direction, respectively. The results suggest that the diurnal inequality is important in modifying the tidal dynamics in the Marsdiep and that lateral and longitudinal shears vary under different forcing conditions.

The difference in SEMA between both quadrangles is elucidated in Figures 2.5a and 2.7. The difference in SEMA increases for higher flow velocities, which occurs in the greater water depths (Figure 2.7). It suggests that an increase in the horizontal barotropic pressure gradient results in a non-uniform temporal modulation of the SEMA at different water depths. As a consequence, the depth-dependent temporal modulation of SEMA changes the magnitude of the lateral shears (Figure 2.5a, edges I and III). At the alongstream repeated surveys, i.e. at lines 2 and 3, a similar depth-dependent trend in SEMA is observed as at the quadrangles (Figure 2.5b). It suggests a temporal modulation of the longitudinal shears.

Also, the PHA differs between quadrangles 1a and 1b and lines 2 and 3 (Figure 2.5c,d). The phase difference between the maximum sea surface elevation of the jetty and the maximum flood current speed is higher for quadrangle 1a and line 3 than for quadrangle 1b and line 2. Furthermore, the difference between repeated surveys increases slightly for greater water depths. These trends suggest that greater current velocities produce a greater phase difference between slack tide and maximum flood velocity, which might possibly be explained by stronger inertial effects caused by stronger forcing.

Additionally, the eccentricity varies between quadrangles 1a and 1b (Figure 2.5g), whereas generally eccentricity is close to zero in the Marsdiep (e.g. Figure 2.5h). The tidal ellipses widen at edge III of quadrangle 1a as well as at the middle of line 5 on the slope of the channel (Figure 2.3a,d). A temporal variation in eccentricity has not yet been observed in the Marsdiep. In section 4.3, the temporal variation in eccentricity is examined in more detail.

The main point of section 2.3.1 is the observation of a temporal modulation of the SEMA, which depends on water depth and which changes the longitudinal and lateral shears. Its variability is determined by variations in tidal range from a daily to fortnightly timescale as a result of the diurnal inequality and the spring-neap tidal cycle, respectively.

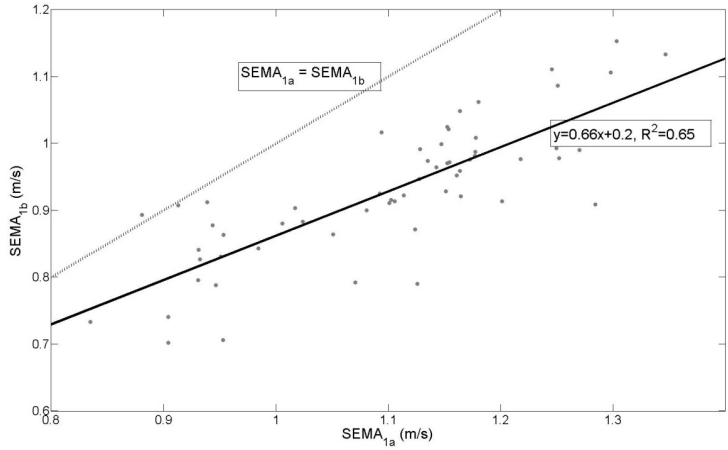

Figure 2.7: SEMA of quadrangle 1b relative to the SEMA of quadrangle 1a at each grid-point of the survey. The solid black line is the linear fit between the SEMA of both quadrangles. The dotted black line indicates where the SEMA of quadrangle 1b equals the SEMA of quadrangle 1a.

2.3.2 *Tidal variability of the density field*

2.3.2.1 *Density gradients*

The density distribution in the Marsdiep has not yet been investigated in detail despite its potential importance to the estuarine dynamics. Density gradients are indicative of the contribution of the baroclinic forcing to the system. The surface density field in the Marsdiep is characterized by lateral (across-channel), $[\frac{d\rho}{dy}]_{M2}$, and longitudinal (along-channel), $[\frac{d\rho}{dx}]_{M2}$, density gradients (Table 2.2). Here, ρ is the density, x and y are the longitudinal and lateral direction, respectively, which are positive in the direction of the North Sea and the island of Texel, and the subscript $M2$ indicates the tidal average. The gradients $[\frac{d\rho}{dx}]_{M2}$ and $[\frac{d\rho}{dy}]_{M2}$ of quadrangle 4 are not computed since the outline of the survey is not entirely in longitudinal and lateral direction of the channels, making the gradient somewhat ill-defined.

Table 2.2 shows that the longitudinal surface density gradient, $[\frac{d\rho}{dx}]_{M2}$, is of the same order of magnitude, i.e. 10^{-4} kg/m^3/m, for each survey. The tidally-averaged lateral surface density gradient, $[\frac{d\rho}{dy}]_{M2}$, can be greater than or equal to $[\frac{d\rho}{dx}]_{M2}$. The gradient $[\frac{d\rho}{dy}]_{M2}$ changes sign between quadrangle 1a and 1b. In estuaries, it is usually assumed that the longitudinal density gradient is the

	$[\frac{d\rho}{dx}]_{M2}$	$[\frac{d\rho}{dy}]_{M2}$
	$10^{-4}kg/m^3/m$	$10^{-4}kg/m^3/m$
Quadrangle 1a	1.08	3.78
Quadrangle 2b	1.57	-2.98
Line 2	1.78	-
Line 3	1.89	-
Line 5	-	2.28

Table 2.2: Along-stream, $[\frac{d\rho}{dx}]_{M2}$, and cross-stream, $[\frac{d\rho}{dy}]_{M2}$, tidally-averaged surface density gradients of each survey

dominant density gradient in driving the residual (estuarine) circulation, but these measured density gradients suggest that residual currents driven by a cross-stream density gradient may be of the same magnitude in the Marsdiep.

2.3.2.2 *Intra-tidal density dynamics*

To illustrate how the temporal variation in lateral shear influences the density field, the surface density along the cross-stream transects is depicted in Figure 2.8. The spatial density fields of the repeated surveys, quadrangle 1a and 1b, differ on a tidally-averaged and intra-tidal timescale. The surface density distribution at 1a-III contains much noise due to the strong wave-current interaction at that location and is therefore not depicted. However, the main patterns correspond well to the patterns along 1a-I. The surface density is highest during high water at the northern side of edge I of quadrangle 1a, whereas it is highest in the middle and southern part of edge I and III of quadrangle 1b (Figure 2.8). The variation in the lateral distribution of the longitudinal velocities and the corresponding variation in lateral velocity shear between quadrangle 1a and 1b (Figure 2.5a) is the most likely cause of these changes in the spatial density field. The higher longitudinal velocities at the northern side of quadrangle 1a transport the most saline water from the North Sea into the Marsdiep. Higher lateral velocity shear results in a greater lateral density gradient during flood. A variation in the lateral density distribution suggests a variation in cross-stream dynamics.

At quadrangle 1a during ebb, a plume with a lower density extends northwards, which is absent at quadrangle 1b. Variability in discharge at the Den Oever sluices most likely causes the decrease in density during ebb at the southern side of quadrangle 1a. Additionally, local small freshwater sources might

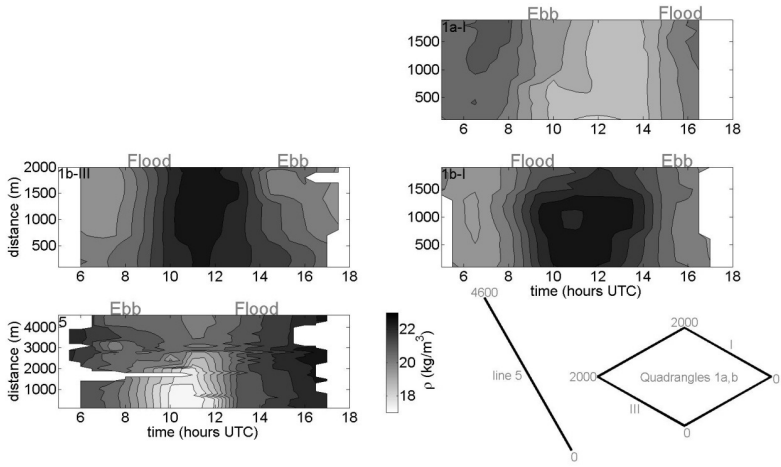

Figure 2.8: Surface density, ρ, as a function of cross-stream distance and time along several transect. Quadrangles 1a (1a-I) and 1b (1b-III and 1b-I) and line 5 (5) are depicted over a 10 to 12 hours time period. The cross-stream distance is relative to the southernmost point of a transect. Flood and ebb indicate the approximate time of peak flood and ebb currents.

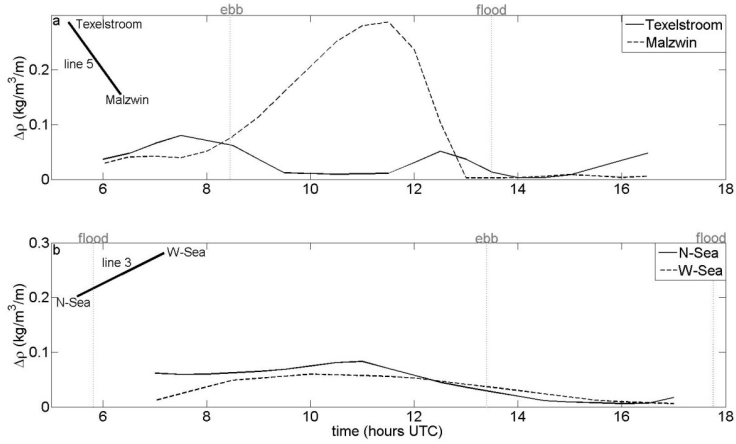

Figure 2.9: a) vertical stratification ($[\rho_{surface} - \rho_{bottom}]/h$) as a function of time at the middle of the Texelstroom and Malzwin channel along line 5 (running across the Texelstroom and Malzwin channel) and b) vertical stratification as a function of time at the seaward and landward end of line 3 (running along the Texelstroom channel). Flood and ebb indicate the approximate time of maximum flood and ebb currents, respectively.

change the surface density distribution. These will only additionally freshen the Malzwin channel and do therefore not modify the overall dynamics in the Marsdiep basin. The only local freshwater source on the Texel side is the small Prins Hendrik pumping station. The discharge was similar for both surveys (1a: 77504 m^3/day, 1b: 75879 m^3/day) and for the 3 days prior to both surveys (1a: 184274 m^3/3 days, 1b: 203965 m^3/ 3 days). The Prins Hendrik pumping station only discharges during low tide. The precipitation at the Den Helder Airport weather station was larger during survey 1b (3.7 mm to 0.7 mm), but all precipitation fell before the onset of the measurements (05:00 UTC). Precipitation during the 3 days prior of both surveys is similar (12 mm in total). Thus, the differences between quadrangle 1a and 1b cannot be ascribed to different discharge or precipitation rates. The spatial variations in current magnitude and related lateral shear are therefore the most likely mechanisms that explain the observed patterns.

An overall picture of the surface density distribution is provided by line 5, showing the surface density field along an entire cross-section of the Marsdiep (Figure 2.8-5). The cross-stream density distribution of line 5 also shows a large gradient between peak ebb and slack before flood as a result of brackish water outflow from the Malzwin channel at about 2300 m. Between peak flood and slack before ebb, the highest density is located in the middle of line 5, indicating that differential advection might play a role during this time period.

To evaluate the spatial variability in occurrence of vertical stratification and the relation to their potential generation mechanisms, the vertical stratification at different CTD stations is given in Figure 2.9. In the Malzwin channel, the tidal straining mechanism is applicable due to the high brackish water outflow during ebb (dashed line in Figure 2.9a, line 5). It results in a strong vertical stratification (0.3 kg/m^3/m) during the late ebb phase and during slack before flood. Less strong vertical stratification (0.05 kg/m^3/m) is present during the late flood phase in the Malzwin channel. During the same survey, no vertical stratification is observed in the Texelstroom during ebb. Here, the water column is only marginally stratified during the late flood phase. The pattern of strong vertical stratification during ebb and well-mixed conditions during flood due to tidal straining is not observed in the Texelstroom for line 3. Figure 2.9b shows clearly that the general tidal straining mechanism, as explained in section 1, does not apply to the Texelstroom since the strongest vertical stratification is observed during flood instead of during ebb. Vertical stratification is strongest during the late flood phase and slack before ebb, while vertical stratification decreases again during ebb. Differential advection, as implied by the lateral distribution of the surface density field, might be a possible mechanism that generates vertical stratification during flood, as already discussed by Lacy et al. [2003].

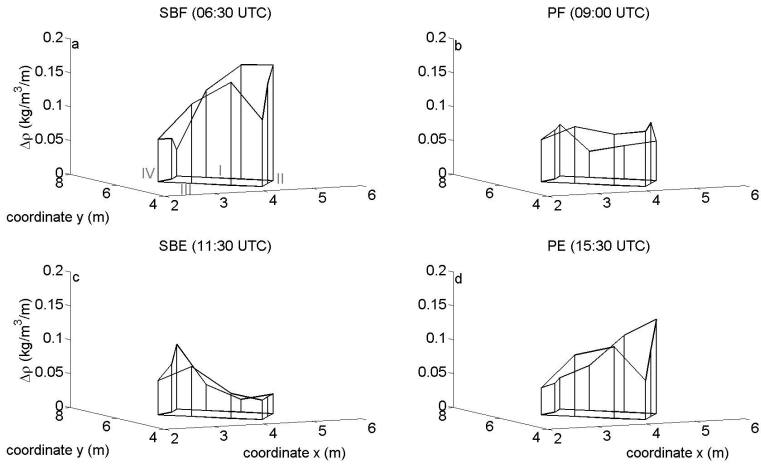

Figure 2.10: Vertical stratification, $(\rho_{surface} - \rho_{bottom})/h$, along the edges of quadrangle 1b during 4 phases of the tidal cycle: a) slack before flood (SBF), b) peak flood (PF), c) slack before ebb (SBE), and d) peak ebb (PE). The vertical black lines indicate the locations of the 10 CTD-stations and the height represents the strength of the vertical stratification.

2.3.2.3 *Spatial asymmetry in vertical stratification*

The previous section has shown large spatial variations in vertical stratification in the Marsdiep basin. To zoom in further on this subject, the vertical stratification during 4 distinct phases of the tidal cycle is depicted in Figure 10 for quadrangle 1b. The main lateral trend in the Marsdiep inlet is a decrease in flood vertical stratification from northwest to southeast across the channel and an increase in ebb vertical stratification in opposite direction. The vertical stratification is strongest during slack before flood (SBF, Figure 10a) but the magnitude differs by a factor 2 in the cross-stream direction, i.e. along edge I and III. During peak flood, vertical stratification is fairly uniform (PF, Figure 10b), whereas it is strongest at edge IV during slack before ebb (SBE, Figure 10c). During peak ebb, vertical stratification is strongest at edge II and decreases towards edge IV (PE, Figure 10d). So, the horizontal gradient in vertical stratification in the cross-stream direction changes sign between succeeding slack tide conditions during quadrangle 1b.

Vertical stratification during the flood phase is observed at multiple locations in the Texelstroom channel (Figures 2.9b and 2.10) and is therefore considered to be a common phenomenon. Buijsman and Ridderinkhof [2008c] described the ebb vertical stratification in the southern region and predicted an asym-

metry in vertical mixing. However, they did not observe vertical stratification during flood in the northern part of the inlet. An asymmetry in vertical stratification and vertical mixing might have important consequences for the nutrient and sediment distribution in the water column.

To summarize section 2.3.2, vertical stratification in the Marsdiep inlet is not necessarily generated by longitudinal processes only but may largely be driven by cross-stream processes. In parts of the Texelstroom channel, vertical stratification is stronger during flood than during ebb under certain conditions.

2.3.3 *Variations in the bottom boundary layer height*

In this section, the intra-tidal variations in bottom boundary layer height are described and it is shown that there is a spatial variability in H_{BBL}, which might have implications for the time period that vertical stratification is able to be generated. Furthermore, the asymmetry in friction velocity is less for smaller water depths, which implies that the mixing characteristics are spatially variable.

The temporal variability of currents and vertical stratification is depicted in Figure 2.11 for two CTD stations along edge III of quadrangle 1b. At station NW, the local water depth is 23 m and it represents the relatively deep conditions (Figure 2.11, left column), whereas at station SE the local water depth is 14 m which represents the shallower conditions in the southeast of the Texelstroom (Figure 2.11, right column). Flow velocities in alongstream, cross-stream and vertical direction are stronger in the deeper conditions. The peak alongstream velocities are more uniform in the upper part of the water column for deeper than for shallower water depths (Figure 2.11a,b). In addition, the tidal asymmetry becomes increasingly ebb-dominant in northwest direction.

To qualitatively evaluate the relationship between the H_{BBL} and the occurrence of vertical stratification, a visual comparison is made in Figure 2.11. The angle of the isohalines with respect to the horizontal is indicative for the presence and strength of vertical stratification. A small angle (i.e. horizontal) isohalines indicate there is vertical stratification, whereas the presence of vertical isohalines indicates well-mixed conditions.

Vertical stratification is present during early flood at both the deep and shallow station, which decreases during peak flood (Figure 2.11g,h). The isohalines become close to vertically-aligned at the shallow station, whereas at the deep station approximately the lower 15-20 m becomes well-mixed. During the late flood phase, vertical stratification is present at the deep station, whereas it remains well-mixed at the shallow station. During peak ebb, the reversed is observed: the isohalines are nearly vertical at the deep station and are at an angle of approximately 45 degrees at the shallow station.

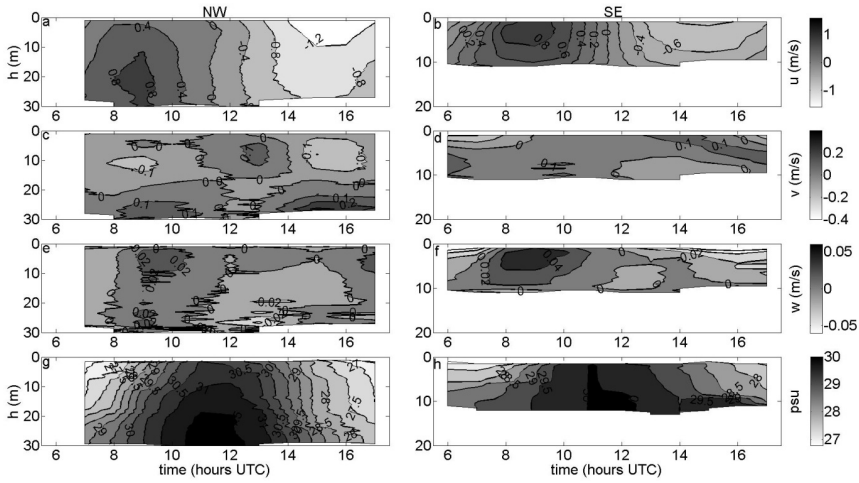

Figure 2.11: Alongstream (a,b) , cross-stream (c,d), vertical (e,f) velocities and salinity (g,h) as a function of time and depth for the deeper northwestern station, NW, (left column) and a shallower southeastern station, SE (right column) along edge III of quadrangle 1b.

These observations suggest that the *BBL* does not cover the entire water column during the full tidal cycle and that there is a relationship between the peak tidal currents, water depth and the occurrence of vertical stratification. Chant et al. [2007] observed that the top of the *BBL* in the Hudson river estuary coincides with a mid-depth (subsurface) velocity maximum. A mid-depth maximum has been observed by de Vries et al. [2012] in the Marsdiep during the flood phases of spring tidal conditions which is additional evidence that the *BBL* in the Marsdiep does not always cover the entire water column.

In Figure 2.12, the friction velocity and H_{BBL} are depicted for edge III of quadrangle 1b in an attempt to relate them to the occurrence of vertical stratification in Figure 2.11. Interestingly, the friction velocity is stronger during peak ebb than during peak flood (Figure 2.12b), contrary to the German Wadden Sea [Flöser et al., 2011]. The strong flow asymmetry is believed to be the main cause of this difference (Figure 2.11a,b and Figure 2.12a). In the southeastern shallow part of the survey, friction velocities are smaller than in the northwestern deeper part and the tidal asymmetry in the friction velocity is less. In the deeper part, the vertical stratification, present between 08:00 and 10:00 UTC, influences the vertical profile of the alongstream velocity which results in a lower friction velocity (Figure 2.11g,h and Figure 2.12b). After the vertical stratification has vanished, the friction velocity increases. Hence, there is a two-way interaction between the vertical stratification and the flow dynam-

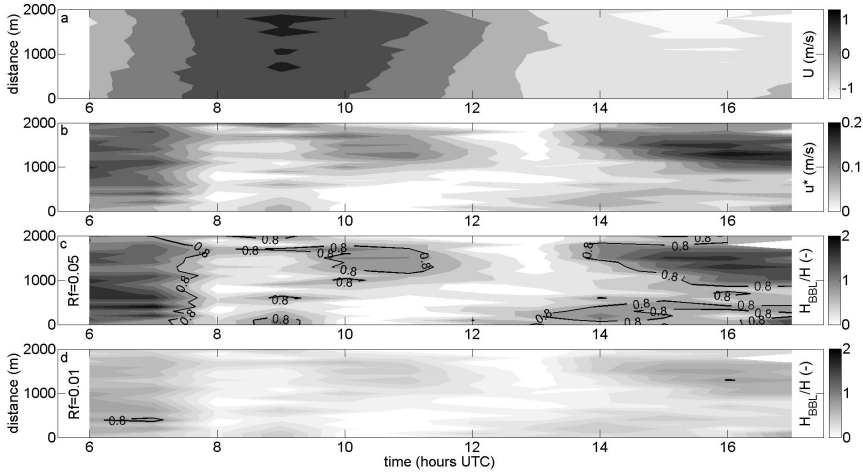

Figure 2.12: Depth-averaged alongstream velocity (a), friction velocity (b), the height of the bottom boundary layer with respect to the local water depth, H_{BBL}/h, for R_f=0.05 (c) and R_f=0.01 (d) along edge 3 of quadrangle 1b as a function of time and distance. In (c) and (d), the location and time where vertical stratification can form, approximated by $H_{BBL}/h = 0.8$, is indicated by the black lines.

ics. Longitudinal shear production and vertical stratification appear not always in equilibrium.

The H_{BBL} is depicted for different values of R_f, namely 0.05 and 0.01 (Figure 2.12c,d). Both parameter values display similar patterns in the dynamics of the H_{BBL}, only the ratio between the H_{BBL} and the total water depths varies. The black line indicates where the H_{BBL} covers 0.8 of the local water depth, and is assumed to represent the upper boundary below which vertical stratification is facilitated. The trends are best described using Figure 2.12c. The tidal asymmetry in flow velocity between ebb and flood results in an asymmetry in the duration when vertical stratification can be generated. It is hypothesized that this effect promotes the formation of vertical stratification during flood and undermines the generation of vertical stratification during ebb.

During the onset of the measurements, strong vertical stratification is observed (Figure 2.11g,h) while the H_{BBL} covers most of the water column. The vertical stratification during ebb is most likely related to fresher water from the Malzwin flowing over the denser Texelstroom water. During this time period, the assumption of a small R_f is not valid anymore since buoyancy fluxes are

expected to increase under strongly stratified conditions which lead to changes in the H_{BBL}.

2.4 DISCUSSION

2.4.1 *Bottom boundary layer dynamics*

The temporal variation in H_{BBL} illustrate that care should be taken when fitting logarithmic profiles to vertical profiles of velocity for greater water depths. Lueck and Lu [1997] already proposed an empirical relationship between the logarithmic layer height and the shear velocity. Furthermore, estimates in bed roughness might be influenced by variations in H_{BBL}. Li and Valle-Levinson [1999]; Li [2002]; Li et al. [2004] used a phase-matching method, which is valid for shallow water depths, to estimate the drag coefficient, C_D. They observed a logarithmically-shaped decrease in drag coefficient for greater water depths which is in agreement with the decreasing influence of bed friction with depth in this study. In addition, Li et al. [2004] observed a variation in drag coefficient between neap- and springtide conditions in the James River estuary.

A conceptual model is presented in Figure 2.13 which visualizes the potential impact of tidal asymmetries on the variation in H_{BBL} and the generation of vertical stratification. The H_{BBL} covers the entire water column during the stronger ebb currents, which mixes the entire water column and prevents the generation of vertical stratification (Figure 2.13, subpanel 1). During (late) flood conditions, the H_{BBL} covers only a part of the water column which facilitates the generation of vertical stratification due to cross-stream processes (Figure 2.13, subpanel 2). Model simulations are required to validate this conceptual theory but are outside the scope of this research. Furthermore, more research on the mixing mechanisms in the Marsdiep by bed-generated turbulence and internal shears (in longitudinal and lateral direction) is required in order to quantitatively investigate BBL dynamics in the Marsdiep.

Zooming out to a tidal timescale, the spatial variability in H_{BBL} with respect to the total water depth has the potential to modify the estuarine dynamics substantially. It is hypothesized that the spatially variable impact of bed friction on the vertical profile of horizontal velocity under variable tidal forcing conditions results in a temporal modulation of the depth-averaged current speed and forces the occurrence of vertical stratification. If the H_{BBL} is large compared to the total water depth, then the tidal current strength remains temporally-constant because the influence of bed friction is sufficiently strong to balance changes in barotropic forcing. A relatively small H_{BBL} results in a variable relationship in flow strength over time. Bed friction counter-balances the barotropic pressure gradient under all forcing conditions for relatively large BBL heights,

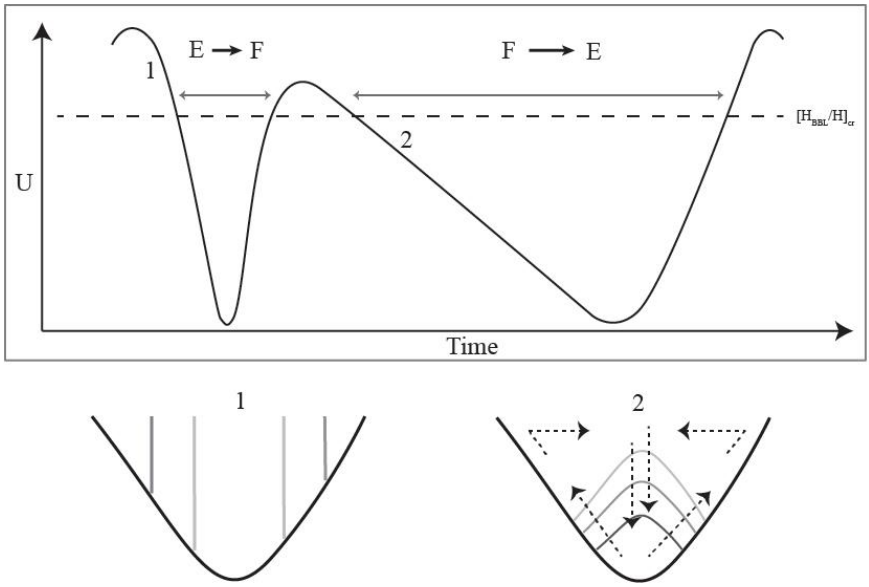

Figure 2.13: Simplified conceptual model of the impact of tidal asymmetries on the generation of vertical stratification. The absolute flow velocity is depicted as a function of time. E → F indicates the transition from ebb to flood and F → E vice versa. The dotted line indicates the threshold velocity below which vertical stratification is able to form ($[H_{BBL}/H]_{cr}$) due to a decrease in the height of the bottom boundary layer, H_{BBL}, with respect to the total water depth, H. Subpanel 1 depicts a cross-section of an idealized channel illustrating the well-mixed conditions during ebb, where the gray lines indicate the isohalines. Darker isholines represent greater densities. Subpanel 2 depicts a cross-section of an idealized channel illustrating the generation of vertical stratification by density-driven cross-stream processes. The dotted arrows indicate the flow patterns associated with differential advection as described by Nunes and Simpson [1985].

whereas for relatively small H_{BBL}, bed friction does not counter-balance the barotropic pressure gradient.

The depth-dependent temporal modulation of the tidal currents results in an oscillation of the lateral velocity shears on a diurnal and fortnightly timescale, which can modify the density field. The effect of diurnal inequality is strong. The difference in tidal range is in the order of 0.4 m, which is 37 percent of the tidal range of 1.07 m during neap tide conditions.

2.4.2 *Widening of the tidal ellipses*

Tidal currents in the Marsdiep are usually rectilinear which results in a negligible depth-averaged cross-stream component. However, under certain conditions the depth-averaged cross-stream component becomes more important, which results in a widening of the tidal ellipses. Li [2002] related an increase in eccentricity to the presence of divergence and convergence zones. The increase in ECC, i.e. the widening of the tidal ellipses, is a local phenomenon in an area with great depth variations. The locality and strong depth variations of this phenomenon are an indication that fronts and/or cross-stream driven flows are of importance. Observations by Maas and van Haren [1987] and Visser and Souza [1994] in the open North Sea showed that vertical stratification influences the clockwise and anti-clockwise rotating components of a tidal ellipse differently throughout the water column in areas with small variations in water depth. This variation is not observed in the measurements presented in this study (not depicted). Strong flow-topography interaction seems a more dominant factor in determining the shape of the tidal ellipses over the water column.

The strong lateral density gradients observed by Buijsman and Ridderinkhof [2008c], the large intra-tidal variability in cross-stream currents as described by de Vries et al. [2012] and the observations presented in this study, indicate the importance of lateral density gradients and cross-stream currents in changing the shape of the depth-averaged tidal ellipses. Strong cross-stream currents are generally observed during late flood, peak ebb and slack tides. The maximum and minimum of the surface density and of the cross-stream velocity (Figures 2.8 and 2.14) occur during the same tidal phase. During slack after flood (ebb), the depth-averaged cross-stream current is towards (away from) the Texelstroom channel (Figure 2.14).

The strong cross-stream currents and density gradients may lead to the presence of convergence-divergence areas and to front formation. Lateral density gradients and convergence-divergence areas can be created by three mechanisms. Nunes and Simpson [1985] observed a secondary circulation pattern induced by differential advection of density due to a lateral variation in the magnitude of the alongstream currents. Li and Valle-Levinson [1999]; Valle-

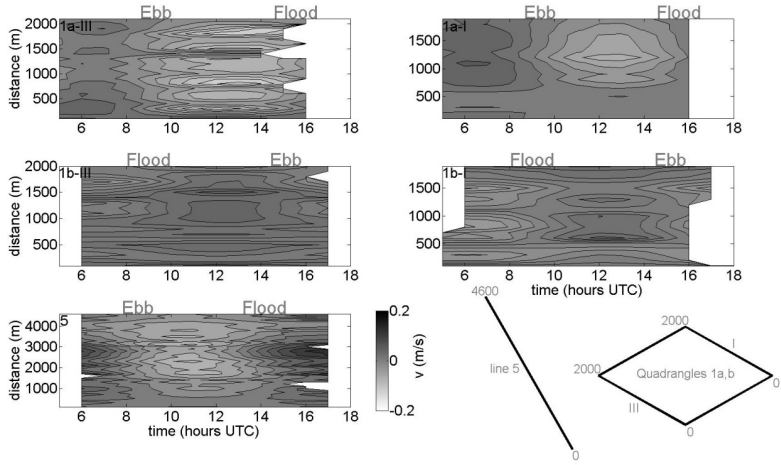

Figure 2.14: Depth-averaged cross-stream velocity, v, as a function of cross-stream distance and time. Edge III and I of quadrangles 1a (1a-III and 1a-I) and 1b (1b-III and 1b-I) and line 5 (5) are depicted over a 10 to 12 hours time period. The cross-stream distance is relative to the southernmost point of a transect. Flood and ebb indicate the approximate time of peak flood and ebb currents.

Levinson et al. [2000] explained convergence and divergence of the flow as a result of a frictional phase lag of tidal ellipses in varying water depths, named differential rotation. It results in small cross-stream currents in the middle of the channel and strong cross-stream currents on the edges of the channel slopes. Mied et al. [2000]; Handler et al. [2001] discussed vortex tilting as a third mechanism which was determined by the Coriolis force and water depth variations. Net tidal vorticity is advected towards the right of the alongstream flow direction which leads to convergence only at the right slope of a channel. Li [2002] observed that frontal features of convergence may also occur without the presence of a longitudinal density gradient.

In the Marsdiep, the tidal ellipses widen for large tidal ranges in sea surface elevation (Table 2.1) and the widening of the tidal ellipses occurs mainly on the slope of the channel (Figure 2.3a,d), where the cross-stream currents are strongest (Figure 2.14). The cross-stream currents are approximately 90 degrees out of phase with the alongstream currents. This pattern corresponds to the differential rotation mechanism of Li and Valle-Levinson [1999] and Li and Valle-Levinson [1999]; Valle-Levinson et al. [2000], and is an additional mechanism in the Marsdiep next to the density-driven cross-stream circulation. The phase lag between the velocity in the Marsdiep and sea surface elevation at

the jetty increases with increasing tidal amplitude which explains the absence of widened tidal ellipses during neap tide. It supports the results from Valle-Levinson et al. [2000] who showed that convergence zones are related to the tidal amplitude and steepness of the channel. Vortex tilting is believed to be of minor importance since frontal features were observed at the left side of the alongstream flow direction, whereas vortex tilting only results in convergence at the right side. Furthermore, convergence-divergence areas in the Marsdiep are strongest during the slack tides, whereas Handler et al. [2001] reported the presence of convergence-divergence areas over 80 percent of a tidal cycle. Differential advection is an additional mechanism in the Marsdiep which appears not to lead to a widening of the tidal ellipses, but is capable of driving cross-stream currents and indirectly generating vertical stratification. We suggest that density-driven cross-stream currents originating from higher lateral velocity shear and possibly differential rotation result in a widening of the ellipse during large tidal ranges. Other frontal features which do not modify the tidal ellipses seem to be driven by differential advection.

2.5 CONCLUSIONS

In this study, the spatial variability of currents and vertical stratification is investigated for multiple surveys in a periodically-stratified estuarine basin in the Western Dutch Wadden Sea. A harmonic analysis and an estimation of the bottom boundary layer height are used to analyze the tidal current dynamics and to evaluate their relationship with the occurrence of vertical stratification.

On a tidal timescale, the spatial variation in tidal currents in the Marsdiep is complex, but appears primarily a function of water depth. At locations where the total water depth is less than 15 m, the currents are strongly influenced by bed friction. At greater water depths, the tidal currents are less affected by bed friction and the bottom boundary layer does not cover the entire water column. The observations suggest that the variable impact of bed friction on the tidal currents produces a temporal modulation in lateral velocity shears, which is able to modify the density field on a daily to fortnightly timescale.

In addition, stronger tidal forcing generates stronger cross-stream currents on the slopes of the channel which results in a widening of the tidal ellipse, indicative of converging frontal systems [Li, 2002]. Our observations suggest that density-driven flow and possibly differential rotation are the driving mechanisms for convergence-divergence areas. Furthermore, differential advection plays a role at other locations.

On an intra-tidal timescale, the height of the bottom boundary layer with respect to the total water depth varies between ebb and flood due to the asymmetry in current magnitude and duration. It is hypothesized that these factors

inhibit the generation of vertical stratification during ebb and facilitate the generation of vertical stratification during flood by cross-stream processes in the ebb-dominant northern part of the Marsdiep basin, namely the Texelstroom channel.

The classic tidal straining, as indicated by the typically-observed patterns in vertical stratification, has not been observed in the northern part of the Marsdiep basin. At other locations, vertical stratification is observed both around slack before flood and slack before ebb. This contrasts with observations in the German Wadden Sea [Becherer et al., 2011; Flöser et al., 2011]. The broad width, the great depth gradients and high current velocities in the Marsdiep may most likely explain these differences. Furthermore, it is hypothesized that the strong increase in lateral velocity shear from neap to spring tide promotes the generation of flood stratification towards spring tide.

3

VARIABILITY OF THE VERTICAL CURRENT STRUCTURE

The vertical structure of the along-stream current in the main channel of the Marsdiep basin is investigated by combining long-term velocity measurements, collected during three different seasons, with a one-dimensional water column model. The observed vertical shears in the lowest part of the water column are greater during ebb than during flood due to an asymmetry in drag coefficient (i.e. bed friction), which is most likely determined by the surrounding complex bathymetry. This asymmetry is usually not incorporated in models. Furthermore, a mid-depth velocity maximum is observed and simulated during early and late flood which is generated by along-stream and cross-stream tidal straining, respectively. Negative shears are present in the upper part of the water column during flood, which correlate well with the along-stream salinity gradient. The mid-depth velocity maximum during late flood results in an early current reversal in the upper part of the water column. The elevated vertical shears during ebb are able to reduce vertical stratification induced by along-stream tidal straining, whereas cross-stream tidal straining during late flood promotes the generation of vertical stratification. The simulations suggest that these processes are most important during spring tide conditions. This study has demonstrated that an asymmetry in bed friction and the presence of density gradients both have a strong impact on the vertical structure of along-stream velocity in the Marsdiep basin.

This chapter is based on the following publication:
de Vries, J. J., Ridderinkhof, H., Maas, L. R. M., and van Aken, H. M. (2015). Intra- and inter-tidal variability of the vertical current structure in the Marsdiep basin, *Cont. Shelf. Res.*, 93:39-57.

3.1 INTRODUCTION

Currents in estuaries and coastal seas are the main transport agents of suspended matter. The net transport patterns of plankton, larvae, nutrients, pollutants and suspended sediment are partly determined by the residual current. The vertical distribution of suspended matter varies in the water column and therefore for understanding the vertical and horizontal exchange patterns in an estuary, it is important to also take the vertical profile of the current and salinity into account.

In estuaries, the shape of the vertical profile of along-stream velocity is determined by the interaction of the barotropic and baroclinic pressure gradients, which creates a difference in the shape of the vertical profiles between ebb and flood [Simpson et al., 1990; Jay and Musiak, 1996; Seim et al., 2002; MacCready and Geyer, 2010; Geyer and MacCready, 2013, and references therein]. During flood, the direction of the baroclinic force in the near-bottom layer coincides with the direction of the barotropic force, which in the absence of bed friction and vertical mixing would result in the strongest velocities near the seabed [Valle-Levinson and Wilson, 1994]. However, the seabed imposes a frictional drag on the tidal currents, which, in combination with the strong near-bed velocities during flood, results in greater near-bed shears, potentially generating a well-mixed water column [e.g. Jay and Musiak, 1996]. During ebb, the baroclinic and barotropic forces oppose each other near the bottom, generating smaller shears at the bottom and greater shears in the upper part of the water column. Furthermore, fresher water higher up in the water column is advected over saltier water during ebb which generates vertical stratification, a process called tidal straining [van Aken, 1986; Simpson et al., 1990]. Classical tidal straining only generates vertical stratification during ebb, because advection of salty water over less salty water during flood results in unstable stratification, which generates vertical mixing.

The steady baroclinic pressure gradient [Pritchard, 1956; Hansen and Rattray, 1966] and the strain-induced periodic stratification [Simpson et al., 1990; Jay and Musiak, 1996] modify the shape of the vertical profile in estuaries. Burchard and Hetland [2010] demonstrated with model simulations that tidal straining contributes approximately two-thirds to the total residual circulation, whereas the baroclinic tide itself contributes one-third in periodically-stratified estuaries. Both mechanisms are able to modify the shape of the vertical profile of along-stream velocity and thereby determine the vertical profile of residual circulation.

Commonly, the difference in shape of the vertical profiles between ebb and flood results in the classical residual estuarine circulation with inflow at the bottom and outflow at the surface [e.g. Geyer et al., 2000; Stacey et al., 2001, 2008; Seim et al., 2002; Murphy and Valle-Levinson, 2008]. There also exist

inverse estuaries, where the baroclinic force near the bottom is directed in the opposite direction (towards the sea), e.g. by strong evaporation within the estuary, which has an inverse effect on the vertical profiles of ebb and flood, producing an inverse estuarine circulation cell with the near-bed and near-surface residual currents directed down- and up-estuary, respectively [e.g Winant and Gutierrez de Velosco, 2003].

Additionally, the shape of the vertical profiles of velocity are strongly influenced by the impact of bed friction on the current. Generally, the drag coefficient is taken as a measure for bed friction and is in the order of 1 to $3*10^{-3}$ [Geyer et al., 2000; Seim et al., 2002; Li et al., 2004, e.g]. However, greater values have also been observed up to $1*10^{-2}$ [Cudaback and Jay, 2001; Fong et al., 2009]. In addition, the drag coefficient has been observed to vary from neap to spring tide, and from ebb to flood [Geyer et al., 2000; Li et al., 2004; Fong et al., 2009]. The drag imposed on the currents by the seabed is only transferred up into the water column to a certain height, called the bottom boundary layer. Stacey and Ralston [2005] demonstrated that the bottom boundary layer does not cover the entire water column during the entire tidal cycle in the northern San Francisco Bay, which has also been observed in the Marsdiep basin [de Vries et al., 2014, Chapter 2]. Also, several studies have shown that form drag is another important mechanism which is able to dissipate tidal energy [Chriss and Caldwell, 1982; Moum and Nash, 2000; Warner et al., 2013]. Form drag is the drag imposed on the fluid by pressure differences generated by currents traversing non-uniform bathymetry, which may be up to 10-50 times greater than drag generated by bed friction [Edwards et al., 2004; Warner et al., 2013]. Furthermore, Warner et al. [2013] showed that the presence of form drag produces elevated values of C_D, when it is estimated from the depth-averaged alongstream momentum balance.

In literature, less attention has been paid to understanding the shape of the vertical profiles of horizontal velocity during the remaining phases of the tide (namely during early and late ebb and flood). An interesting feature, described for several estuaries, is the occurrence of a mid-depth velocity maximum during flood [Jay and Smith, 1990a; Lacy and Monismith, 2001; Warner, 2005; Chant et al., 2007], which has also been observed in a modeling study of the Chesapeake Bay [Li and Zhong, 2009]. This velocity maximum occurs at the upper boundary of the bottom boundary layer [Chant et al., 2007]. Cudaback and Jay [2001] explained the occurrence of a mid-depth velocity maximum during early flood in the Colombia inlet, which is a strongly-stratified estuary, using a simple three-layer model based on the barotropic and baroclinic pressure gradients and bed friction. They concluded that bed friction and a strongly-stratified water column are crucial in driving a mid-depth jet. Similar observations in the stratified North Sea are explained by Maas and van Haren [1987] using a comparable model.

To complicate matters further, the shape of the vertical profiles of instantaneous and residual currents varies spatially due to bathymetric and nonlinear effects, as e.g. tidal asymmetry [Aubrey and Speer, 1985; Speer and Aubrey, 1985; Dronkers, 1986; Friedrichs and Aubrey, 1988]. Li and O'Donnell [1997] showed that a lateral gradient in water depth produces a tidally-driven horizontally-sheared exchange pattern, while Li and O'Donnell [2005] demonstrated that the length of an estuary determines the inflow and outflow patterns at the channel and shoals. Scully and Friedrichs [2007] observed lateral asymmetries in current magnitude and concluded that spatial asymmetries in mixing modify the duration of the ebb phase and change the residual circulation. In the Marsdiep basin, the tidal asymmetry is great and is spatially variable. Zimmerman [1976b], Ridderinkhof [1988] and Buijsman and Ridderinkhof [2007a] observed stronger flood currents, and inflow, at the shallower south side of the Marsdiep tidal inlet and stronger ebb currents, and outflow, at the deeper north side.

In the Dutch, German and Danish Wadden Sea, the mechanisms that contribute to the residual circulation are still a matter of debate [Zimmerman, 1986; Ridderinkhof, 1988; Buijsman and Ridderinkhof, 2007a; Burchard and Hetland, 2010; Becherer et al., 2011; Flöser et al., 2011]. The first three studies argue that tide-topography interaction is the major forcing of residual currents in the Wadden Sea, whereas the latter three argue that tidal straining, and the presence of an estuarine circulation, is the major forcing. Since the shape and variability of the vertical profiles of along-stream velocity are essential for estuarine dynamics, the aim of this chapter is to explain the structure (and variability) of the vertical profile of the horizontal velocity in the main channel of the Marsdiep basin. This study shows that the shape of the vertical profiles in the Marsdiep deviates in several ways from the standard estuarine profiles.

A bottom frame is deployed on three occasions in the main channel of the Marsdiep basin, equipped with an upward-looking Acoustic Doppler Current Profiler (ADCP) and temperature, conductivity and depth sensors (microCAT), providing over 100 days of current data from 3 different seasons. This dataset, in combination with simulations with the General Ocean Turbulence Model (GOTM), provides a better understanding of the factors that determine the shape of the vertical profiles of along-stream velocity in the Marsdiep. Hereby, we focus on the combined effects of bed friction and density-related processes, namely the baroclinic pressure gradients and vertical stratification, on the vertical profile of along-stream velocity over a tidal cycle. In addition, the mechanism behind the occurrence of a mid-depth along-stream velocity maximum during late flood is investigated. This phenomenon is related to the occurrence of vertical stratification during late flood, which is generated by cross-stream tidal straining and which the small currents are not able to destroy during this phase of the tide. We hypothesize that vertical stratification inhibits the vertical

momentum exchange in upward and downward direction, thereby producing the greatest current around the pycnocline: vertical stratification restricts bed-generated turbulence to the lower part of the water column limiting seabed-induced vertical mixing of momentum, whereas the superimposed effect of the barotropic and baroclinic components of the tide limits the increase in current speed with depth, as described earlier, to the part of the water column above the pycnocline.

This chapter is structured as follows. In section 3.2, more detailed information on the study area, the data handling as well as the model settings is presented. Sections 3.3 and 3.4 describe the observations and model simulations, respectively. In section 3.5, typical characteristics of the vertical current structure at the study site are discussed in more detail, and in section 3.6 the main findings of this chapter are summarized.

3.2 STUDY SITE, MATERIAL AND METHODS

3.2.1 *Study site description*

The study site is located in one of the main channels of the Western Dutch Wadden Sea, the Texelstroom channel (Figure 3.1b). The Western Dutch Wadden Sea is comprised of the Marsdiep and Vlie basins (Figure 3.1a) and there is only limited exchange between both basins [Zimmerman, 1976a,b; Buijsman and Ridderinkhof, 2007b]. The main channel, the Texelstroom, is located in the Marsdiep basin where a smaller channel, the Malzwin, is located to the southeast (Figure 3.1b). The Texelstroom channel is oriented in approximately westsouthwest-eastnortheast (along-channel) direction and the water depth varies between 10 and 35 meters (Figure 3.1b). At the study site, the bathymetry is characterized by a sloping seabed with shallower water depths in southwestward direction. The slope in this along-channel direction is approximately 0.013. In addition, the water depth decreases again up-estuary by approximately 20 m (Figure 3.1b). Sandwaves are a common feature in this area [Buijsman and Ridderinkhof, 2008a], but a multibeam survey of the study site showed that none are present at the location of the bottom frame (not depicted).

The tides along the Dutch coast and in the Marsdiep basin are semi-diurnal with a tidal range of approximately 1 and 1.5 m at the NIOZ jetty during neap and spring tide, respectively (Figure 3.3d-f). The vertically-averaged current amplitude varies between 1.2 and 1.8 m/s for neap and spring tide conditions, respectively (Figure 3.3a-c). The Marsdiep inlet is characterized by stronger peak ebb than peak flood currents at the southern side, whereas a reversed pattern is observed at the northern side of the inlet [Buijsman and Ridderinkhof,

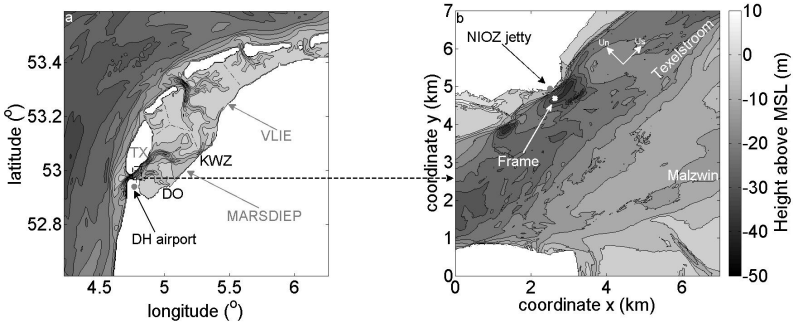

Figure 3.1: a) bathymetric map of the Western Dutch Wadden Sea (data source: Rijkswaterstaat, reference mean sea level, MSL) and, in detail, b) the study site with the location of the bottom frame. The northern (southern) channel is the Texelstroom (Malzwin). To the east, these channels are separated by the tidal flat, Lutjeswaard. DO (KWZ) indicates the location of the freshwater sluices at Den Oever (Kornwerderzand). The gray dots indicate the location of the NIOZ jetty and the Den Helder airport. The reference frame in the zoom-in (b) is a Cartesian coordinate reference frame with the origin in the southwest corner. The resolution of the zoom-in map of the study area is 20 m. The direction of the along-stream (Us) and cross-stream (Un) velocity components are indicated by the white arrows in (b).

2007a]. This tidal asymmetry results in a net inflow into the basin at the southern side and a net outflow at the northern side. Buijsman and Ridderinkhof [2007a] observed that the friction velocity, roughness length and drag coefficient during one single peak ebb and flood of a neap and spring tide, at the center of the Marsdiep inlet, displayed an ebb-flood asymmetry as well, but they did not explain these differences or their implications to the vertical current structure. They observed greater peak flood friction velocities, roughness lengths and drag coefficients, which suggests greater vertical mixing during flood.

The two major sources of freshwater in the Marsdiep basin are the outlet sluices at Den Oever (DO) and Kornwerderzand (KWZ), which only discharge freshwater from lake IJssel into the Wadden Sea during low water (Figures 3.1a and 3.2). The distance between the sluices at DO and KWZ and the NIOZ jetty is approximately 18 and 37 km. The discharge data is provided by the Dutch governmental agency for infrastructure, Rijkswaterstaat. For more information

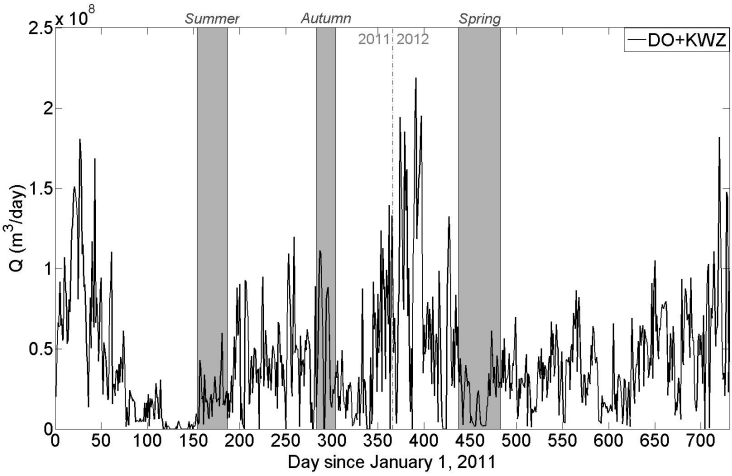

Figure 3.2: Sum of daily freshwater discharge at Den Oever and Kornwerderzand during 2011 and 2012. The two years are separated by the dotted gray vertical line. Day 1 represents January 1, 2011. The gray areas indicate the deployment periods, Summer, Autumn, Spring (data source: Rijkswaterstaat).

on the computation of the discharge rates and other minor freshwater sources is referred to Duran-Matute et al. [2014] and Chapter 2, respectively. Based on observed salinity distributions, it has been assumed that two-thirds of the freshwater from the sluices of KWZ are flushed into the North Sea via an adjacent tidal basin, the Vlie basin [Zimmerman, 1976a,b]; the other one-third originating from KWZ is assumed to be discharged through the Marsdiep basin, via the Texelstroom channel. All the freshwater from DO is assumed to be discharged through the Marsdiep basin via the Malzwin channel [Zimmerman, 1976a,b]. The discharge patterns of the outlet sluices display a strong seasonality with high discharges between October and April and low discharge between May and September (Figure 3.2). As a result, the water column is weakly-stratified up to 6 psu during slack tides, whereas it is well-mixed during peak currents [de Vries et al., 2012]. Interestingly, no modulation of the strength of vertical stratification by the spring neap tidal modulation is observed, as discussed by de Vries et al. [2012].

The Ekman ($Ek = A_z/(fH^2)$) and Kelvin ($Ke = B/R_i$) numbers indicate the importance of basin width, friction and Earth's rotation for the exchange flow patterns in estuaries [e.g. Valle-Levinson, 2008], where A_z (0.1 m^2/s) is the eddy viscosity, f ($1.16*10^{-4}$ s^{-1} at 53°N) the Coriolis frequency, H (25 m) the water depth, B (4 km) the width of the channel and R_i ($3*10^3$ to 10^4 m) the

internal Rossby radius ($R_i = \sqrt{g'H}/f$), g' being the reduced gravity. The latter indicates at which length scale rotation becomes important and is defined as the ratio between the internal wave speed and the local Coriolis frequency. Most values are obtained from Buijsman and Ridderinkhof [2008c] and Chapter 2. It results in conservative estimates of the Ekman and Kelvin numbers of 1.4 and 0.4 to 1.3 respectively, suggesting that the estuary is characterized by strong frictional effects and that the Earth's rotation is usually of minor importance for the exchange flow patterns at the inlet.

3.2.2 *Data collection and instrumentation*

A 1.25m-high bottom frame, equipped with an upward-looking Acoustic Doppler Current Profiler (ADCP) and a conductivity, temperature, depth sensor (microCAT), is deployed (and retrieved) at the north side of the Texelstroom channel on three occasions (Figure 3.1b). The bottom frame is placed on the seabed in approximately 32m water depth, and at a distance of approximately 200m from the Texel coast and approximately 300m southeast of the NIOZ jetty.

Characteristics of each deployment are given in Table 3.1. Each deployment is named after the season which covers the largest timespan of the deployment period, viz Summer, Autumn and Spring. The bottom frame is not equipped with a microCAT during the Summer deployment, because the survey only focused on measuring velocity. Besides the measurements from the bottom frame, 13-hours anchor station surveys with the R.V. Navicula are conducted next to the location of the frame, measuring amongst others current velocity, conductivity and temperature. This study focuses on the data measured at the bottom frame. The anchor station data from the R.V. Navicula provide an overview of the conditions at the study site since it contains information on the vertical profiles of salinity, which are not available for the bottom frame dataset. A detailed discussion on the instrumentation and data-processing of the shipboard data is already given in Chapter 2 and is therefore excluded from the present chapter.

To measure the flow velocity, the bottom frame is equipped with a four-beam 1.2MHz RDI Workhorse Monitor ADCP with a beam angle of 20 degrees relative to the vertical. The conductivity, temperature and depth (CTD) is measured with a Sea-Bird Electronics 37-SM MicroCAT. The top of the ADCP is located approximately 30 cm higher than the top of the microCAT sensor. The specific height of the frame is chosen to prevent the frame and sensors from being covered by sand as a result of the high bedload and bedform transport in the region.

The ping rate of the ADCP is set to 0.43 Hz and ensembles are recorded every 30 s containing 10 pings. The bin size is set to 0.5 meter, the number of bins to 79 and the blanking distance to 0.5 meter. Therefore, the ADCP can effectively

Name	**Start-End**	**Total**	**CTD**	$\langle \frac{\partial S}{\partial x} \rangle$	**AS**
	day	days		$10^{-4} psu/m$	date
Summer 2011	Jun. 3-Jul. 6	34.1	no	0.3	Jun. 22
Autumn 2011	Oct. 10-31	21.9	yes	2.3	Oct. 17
Spring 2012	Mar. 12-Apr. 27	47	yes	1.8	Mar. 10

Table 3.1: Characteristics of the Summer, Autumn and Spring deployment. In addition, the median of the tidally-averaged along-stream salinity gradient, $\langle \frac{\partial s}{\partial x} \rangle$, obtained from equation 3.1 and the date of the 13-hours anchor stations (AS), discussed in section 3.3.1, are given.

cover a range in water depths between 2 and 32 m above the bottom. The velocity data are stored in Earth coordinates (east-west, north-south velocities). In addition, the ADCP sends out one 'bottom' ping per ensemble to detect the echo of the water surface. The SBE 37-SM MicroCAT recorded one sample of conductivity, temperature and depth every 30 seconds.

At the NIOZ jetty (Figure 3.1b), the near-bottom pressure is measured at 2.9 Hz by a calibrated Keller 46 pressure sensor. The pressure is converted real-time into sea surface elevation. Sea surface elevation is recorded every minute with an accuracy of 3 cm based on the median of 175 samples. The surface conductivity and temperature are measured by a calibrated Aanderaa conductivity and temperature 3211 sensor. The data are recorded every 12 seconds by an Aanderaa 3634 datalogger. The salinity is computed using the Practical Salinity Scale 78 [PSS-78, Fofonoff, 1985].

3.2.3 *Data processing*

First, the erroneous velocity data of the ADCP above the water surface are excluded by removing all data above the height of the surface echo. Then, the data are rotated from east-west and north-south velocity components to an along-stream and cross-stream velocity component, defined as the direction of maximum and minimum variance of the depth-averaged horizontal velocity vector, respectively. The pitch and roll of the ADCP varied in time (on a timescale from days to weeks) due to morphological change of the seabed, but were almost always below 15 degrees. The only exception occurred between Day 7 and 15 of the Autumn deployment, when the pitch was 16 degrees. A visual inspection of the velocity data shows no anomalous small-scale velocity fluctuations, i.e. the vertical profiles resembled the classical law-of-the-wall profiles, and therefore the data is included in the analyses. However, the upper 5 meters of the

water column displays velocity variations due to strong orbital wave velocities. To exclude the instantaneous effect of waves on the current, the upper 6 meters are removed. Only the lower 27.25 meters of the water column are included in all analyses. Therefore, any side-lobe interference is implicitly excluded from the analyses.

The output data of the microCAT are already given in salinity (psu), potential density anomaly ($\sigma - \theta$, kg/m^3), temperature (ITS-90, °C) and depth (m), which is computed internally with the standard Seabird software.

In order to include only complete tidal cycles in the analysis, all data before and after the first and last slack tide are removed. The sea surface elevation (SSE), salinity and wind data are interpolated at 30 seconds intervals to produce a collection of synoptic datasets.

3.2.4 *Analyses*

3.2.4.1 *Data analysis*

First, characteristics of the vertical current structure are investigated by computing ensemble-averaged vertical profiles of along-stream velocity. Since the duration and shape of the vertical profiles differ per tidal cycle, the tidal phase (i.e. the timing of early, peak, late ebb and flood and slack tides) is better approximated by the depth-averaged velocity than by phase or time from a fixed moment of reference. Therefore, an average vertical profile of along-stream velocity is computed per averaging interval of 0.1 m/s of the vertically-averaged velocity, e.g. between 1.0 and 1.1 m/s, similar to Stacey [2003] and Stacey and Ralston [2005]. All the vertical profiles of along-stream velocity within each bin of 0.1 m/s of the depth-averaged current are selected and are averaged to obtain an average vertical profile. A 0.1 m/s interval of the vertically-averaged velocity produces both stable average vertical profiles and an adequate resolution of the tidal cycle. Within each bin, no profiles are excluded from the analysis. When an average profile is based on less than 20 profiles, it is considered not representative enough and is excluded from the analysis. This threshold results in the exclusion of 5 velocity bins at the outer limits of the velocity range. The number of velocity profiles varies between 24 and 8200 per bin with an average of 2300 velocity profiles. Differences between the deployments reflect temporal variations in forcing conditions. The analysis focuses on the vertical structure of the along-stream velocity.

This approach provides a clear picture of the first order variability of the vertical profile over one tidal cycle and between the seasons. However, the second order effects around slack tide as a result of the asymmetry of the tide are neglected, because the vertical profiles of the early and late ebb and flood phase fall within the same bin of the depth-averaged velocity. These effects are invest-

igated by computing average vertical profiles from peak ebb to peak flood and vice versa (EtoF and FtoE, respectively).

Second, the structure of the vertical profile under a varying salinity gradient is investigated in section 3.3.3 by analyzing the relationship between the vertical shear in along-stream velocity and the along-stream salinity gradient, $\langle \frac{\partial s}{\partial x} \rangle$ computed every two tidal cycles, as indicated by the brackets. The latter is approximated by a frozen field assumption [Stacey et al., 2010]

$$\langle \frac{\partial s}{\partial x} \rangle = 2\pi \frac{S_{rms}}{L}, \tag{3.1}$$

where S_{rms} is the root-mean-square of salinity and L $(= u_{rms} * T)$ is the tidal excursion length based on the root-mean-square of the depth-averaged along-stream velocity and the tidal period. The salinity is measured either at the bottom frame (Autumn and Spring) or, if the former is not available, at the NIOZ jetty (Summer). Stacey et al. [2010] mention that this method is more robust than the local advective calculation of the salinity gradient, because the latter is invalid in regions where lateral advection is important, as is the case in the Marsdiep basin, as this chapter will show. The computed values of $\langle \frac{\partial s}{\partial x} \rangle$ correspond well with the observed values discussed in Chapter 2 and provide a method to relate the variation in salinity gradient, i.e. density gradient, to the shape of the vertical current structure. The $\langle \frac{\partial s}{\partial x} \rangle$ ignores any information on the direction of the gradient.

Third, to investigate the impact of bed friction on the current structure, the drag coefficient can be computed using either direct stress estimates or logarithmic fits of vertical profiles of along-stream velocity. With the available data, only the latter approach is possible. This technique is discussed in more detail in e.g. Lueck and Lu [1997]. The logarithmic law-of-the-wall generally represents the lower part of the water column well, provided that the water column is well-mixed. In that case, an estimate of the friction velocity, u_* (m/s), and roughness length, z_0 (m), is obtained from fitting the logarithmic profile,

$$u(z) = \frac{u_*}{\kappa} ln(\frac{z}{z_0}), \tag{3.2}$$

to the observed current structure, where u is the along-stream velocity (m/s), z is the height above the bottom (m), κ is the von Karman constant (0.41). The lowest 10 m of the water column are used to obtain the roughness height and friction velocity through a least-squares fit of the vertical profiles. Up to this height above the bottom, the R^2 of the logarithmic fits are good, being greater than 0.95.

An estimate of C_D, based on u_*, is obtained using the bed shear stress, τ_b, given by

$$\tau_b = \rho u_*^2, \tag{3.3}$$

and the empirically-proven assumption that the shear stress in the lowest part of the water column (0.1H) is constant and equals the bed shear stress [van Rijn, 2011]. The drag coefficient is then computed by

$$C_D = \frac{u_*^2}{u_b^2}, \tag{3.4}$$

where u_b is a reference velocity, here at 2 m height above the bottom (hab). The drag coefficient represents the slope of a least-squares fit between the values of u_*^2 and u_b^2 [e.g. Geyer et al., 2000; Fong et al., 2009]. The u_* and u_b are computed every 10 minutes of each dataset based on the nearest 8 ensembles. A bootstrap, i.e. resampling method with 100 samples is used to compute the standard error and affirms the reliability of the computed drag coefficients. Other studies [Geyer et al., 2000; Fong et al., 2009] used a reference velocity at 1 m hab. Consequently, the values presented in this study underestimate with respect to previous studies, because the along-stream velocity is greater at 2 m hab.

3.2.4.2 *Numerical model set-up*

To understand the mechanisms that determine the shape of the vertical profiles of along-stream velocity, (semi-)idealized, and (highly-simplified) semi-realistic model simulations are run with the General Ocean Turbulence Model (GOTM, http://www.gotm.net/). An overview of the model runs is given in Table 3.2. The goal of the former is to identify the important (along-stream) hydrodynamic processes at the study site, assuming a sinusoidal tidal cycle, a constant salinity gradient and a constant bottom roughness. The goal of the latter is to determine and explain the observed shape of the vertical profiles at the study site by incorporating velocity data from the Spring deployment.

The numerical model GOTM is an open source state-of-the-art one dimensional water column model, which includes a variety of vertical mixing parameterizations [Burchard and Baumert, 1995; Burchard et al., 1998; Burchard and Bolding, 2001]. The one-dimensional dynamical horizontal momentum equations, neglecting advection, Coriolis and curvature terms are [Burchard, 2009; Burchard and Hetland, 2010]:

$$\frac{\partial u}{\partial t} - \frac{\partial}{\partial z}(A_z \frac{\partial u}{\partial z}) = -z\frac{\partial b}{\partial x} - p_g^x(t), \tag{3.5}$$

$$\frac{\partial v}{\partial t} - \frac{\partial}{\partial z}(A_z \frac{\partial v}{\partial z}) = -z\frac{\partial b}{\partial y} - p_g^y(t), \tag{3.6}$$

and the buoyancy equation, which includes advection is

$$\frac{\partial b}{\partial t} + u\frac{\partial b}{\partial x} + v\frac{\partial b}{\partial y} - \frac{\partial}{\partial z}(K_z\frac{\partial b}{\partial z}) = 0, \tag{3.7}$$

where x,y and z are the along-stream, cross-stream and vertical coordinate, respectively, and u, v, b, A_z and K_z are the along-stream velocity, cross-stream velocity, buoyancy, the eddy viscosity and eddy diffusivity. The along-stream and cross-stream barotropic pressure gradients are indicated by p_g^x and p_g^y. The second-order turbulence model of Canuto et al. [2001] is used. A comparative study of four turbulence closure models by Burchard and Bolding [2001] showed that this turbulence model performed best.

The first and second term on the right hand side of equations 3.5 and 3.6 represent the baroclinic and barotropic pressure gradients, respectively. The buoyancy is defined as

$$b = -g\frac{\rho - \rho_0}{\rho_0}, \tag{3.8}$$

where g is the gravitational acceleration, ρ is the density and ρ_0 is the constant reference density (1000 kg/m^3). The magnitude of the salinity gradient used as a model forcing is -2*10^{-4} psu/m, which is the same order of magnitude as the conditions in Autumn and Spring, and corresponds with observations in de Vries et al. [2014].

The barotropic pressure gradient function, p_g^x, is computed based on a simplification from the three-dimensional to the one-dimensional hydrostatic equations as described and validated in Burchard [1999] using information of the temporal derivative of velocity at one single point. It enables the computation of the barotropic pressure gradient based on a timeseries of velocity at one single location. For the idealized model simulations, the velocity is defined as a sinusoidal tidal wave with a period, T, of 12.5 hours

$$\bar{u}(t) = \frac{1}{H}\int_{-H}^{0} u(z,t)dz = Ucos(2\pi\frac{t}{T}). \tag{3.9}$$

The barotropic pressure gradients in the semi-realistic model scenarios are based on the velocity input from the Spring deployment. The technique to compute the barotropic and baroclinic pressure gradients assumes homogeneity along the x and y direction. Bathymetric variations are therefore not incorporated in the model. The incorporation of velocity data in the semi-realistic model implicitly includes environmental factors such as the bed slope.

All scenarios except run 3 are run in a water depth of 30 m, consisting of 100 layers. A time step of 10 seconds is chosen with an output resolution of 10 minutes. The results of the model output are insensitive to variations in time step. The bulk flow properties are the molecular viscosity and diffusivity and the formulation of the equation of state. The physical bottom roughness is set to 0.05 m. A relaxation time of 10800 s is specified (3 hours) for the bulk flow of salinity [e.g. Verspecht et al., 2009]. To keep the model stable, a relaxation time is imposed for when the bulk salinity deviates from the initial conditions. Verspecht et al. [2009] found that 3 hours provided stable model results. Since density variations are mainly determined by salinity, the temperature field is excluded. Advection of salinity is always permitted. The upper part of the water column, which is influenced by the intra-tidal in-situ water level fluctuations, and also the effect of wind stress are ignored, because these processes are considered of minor importance to the overall characteristics of the current structure.

The idealized scenarios (runs 1 to 3, Table 3.2) are characterized by a sinusoidal tidal velocity as described above, where the amplitude is varied between 0.8 and 1.2 m/s. In addition, the water depth is also varied. The salinity gradient is kept constant to $-2*10^{-4}$ psu/m.

The first four semi-realistic scenarios are forced by the measured along-stream velocity at 2 m above the bed from the Spring deployment (Runs 4 to 7, Z=2m in Table 3.2). Runs 4 to 7 are forced by an along-stream salinity gradient of $-2*10^{-4}$ psu/m and advection of salinity is permitted. An additional vertical stratification of 1 psu during the onset of flood is imposed for runs 5 and 7, which is allowed to develop over the tidal cycle. Runs 4 and 6 are characterized by well-mixed conditions of 28 psu, whereas the salinity profiles of runs 5 and 7 consist of 27 psu in the upper 10 m and 28 psu in the upper 10 m of the water column. In the middle 10 m, the water column is continuously-stratified. The well-mixed and weakly-stratified conditions correspond with the conditions observed at the study site as discussed in section 3.3.1.

The p_g^x is forced by the vertical profiles of along-stream velocity for run 8 and 9. So far, the cross-stream dimension of the barotropic and baroclinic terms has been neglected. In runs 8 and 9 of the semi-realistic model simulations, p_g^y is also forced by the observed vertical profiles of the cross-stream current. In addition, a constant lateral salinity gradient is imposed in order to investigate the effect of cross-stream processes on the generation of vertical stratification and on the shape of the vertical profile of along-stream velocity. The results of the model simulations are discussed in section 3.4.

Run nr	**Type** (-)	**(H)** (m)	Us (m/s)	$\frac{\partial S}{\partial x}$ $\mathbf{10^{-4}}$ (psu/m)	ΔS (psu)	Un (m/s)	$\frac{\partial S}{\partial y}$ $\mathbf{10^{-4}}$ (psu/m)
1	sine	30	1.2	-2	0	-	-
2	sine	30	0.8	-2	0	-	-
3	sine	15	0.8	-2	0	-	-
4	neap	30	Z=2m	-2	0	-	-
5	neap	30	Z=2m	-2	1	-	-
6	spring	30	Z=2m	-2	0	-	-
7	spring	30	Z=2m	-2	1	-	-
8	neap	30	VP	-2	0	VP	-2
9	spring	30	VP	-2	0	VP	-2

Table 3.2: Overview of the conditions of the numerical simulations (runs 1 to 9). The simplified and semi-realistic simulations are discussed in sections 3.4.1 and 3.4.2, respectively. The idealized runs are characterized by a sinusoidal tide. The type of the semi-realistic scenarios indicate neap or spring tide conditions. The other parameters are the water depth, H, the along-stream tidal current, Us, the along-stream salinity gradient, $\frac{\partial S}{\partial x}$, the top-to-bottom salinity difference, ΔS, the input of the cross-stream currents, Un, and the cross-stream salinity gradient, $\frac{\partial S}{\partial y}$. The semi-realistic runs (4 to 9) are fored by data input. The Z=2m indicates that the simulation is forced by the near-bed along-stream velocity. VP indicates that the model is forced by the entire observed vertical profiles of velocity.

3.3 RESULTS

3.3.1 *Current and salinity characteristics*

The temporal and vertical information of currents and salinity obtained from the bottom frame and 13-hours anchor station measurements provide us with an overview of the intra-tidal and seasonally variable conditions at the study site.

During the periods of data collection, the tidal amplitude (Uamp) and sea surface elevation (SSE) are mainly determined by the spring-neap tidal cycle and wind conditions (Figure 3.3a-f). In Summer, variations in Uamp and SSE component by the spring-neap tidal cycle are small but discernible (Figure 3.3a,d,j). The tidal amplitude is greater during spring tide than during neap tide. Between Day 290 and 293 of Autumn, a major storm event induced significant variations, which distorted the spring-neap tidal modulation (Figure 3.3b,e,k). In Spring,

wind-induced variations in SSE component are small (Figure 3.3c,f,l). A clear spring-neap tidal modulation is visible during the first 30 days, which is smaller from Day 465.

The low discharges at DO and KWZ the month prior to the Summer deployment (Figure 3.2) results in a high average salinity of around 32 psu during the first 27 days of the deployment (Figure 3.3g). Only small tidally-driven fluctuations are superimposed on the average salinity. The intra-tidal fluctuations increase during the last 6 days of the measurement period. On the last day, the salinity drops by 5 psu due to a northeasterly wind in combination with an increase in freshwater discharge from the sluices (Figure 3.3g,j). Similar events of decreases in salinity driven by (north)easterly winds occur between Day 286 to 289, 297 to 299 of Autumn and Day 457 to 462 of Spring, whereas southwesterly winds result in an average increase in salinity, e.g. between Day 291 to 293 of Autumn and Day 441 to 446 of Spring (Figure 3h,k,i,l). It suggests a considerable impact of wind dynamics on the flushing rates of the basin. The intra-tidal salinity fluctuations are greatest during Autumn and Spring (Figure 3.3h,i).

The salinity field (Figure 3.3g-i) is determined by the freshwater discharge rates prior to each deployment period (Figure 3.2). The freshwater discharge from the sluices during the Summer deployment is greater than in Spring (Figure 3.2). However, the mean salinity and the intra-tidal variations in salinity are smaller during Summer (Figure 3.3g-i). Our data indicate a lag effect of several weeks between the freshwater discharge of the sluices and the salinity variations at the inlet.

The anchor station data in Figure 3.4a-c, obtained with the moored R.V. Navicula, display a large intra-tidal difference in the strength and duration of the flood and ebb tide. The maximum flood current is reached rather abruptly and only occurs briefly. Generally, the short peak flood is followed by a longer period of weaker flood currents. The currents during ebb are greater than during flood. The variation in depth-averaged current between the anchor stations illustrates the great inter-tidal variability.

In Summer, the vertical profiles of along-stream velocity reach their maximum velocity near the surface. Deviations from the logarithmic velocity profile are observed in Autumn and Spring (Figure 3.4d vs 3.4e,f). Then, a mid-depth velocity maximum is observed during late flood, whereas during ebb the maximum velocities are still near the surface. The mid-depth velocity maximum coincides with the presence of a vertically-stratified water column (Figure 3.4j-l) and the occurrence of a cross-stream circulation cell (Figure 3.4g-i). In Summer, vertical stratification is negligible (< 1 psu). It is greater in Autumn and Spring, being up to 3 psu. Interestingly, the water column is well-mixed during

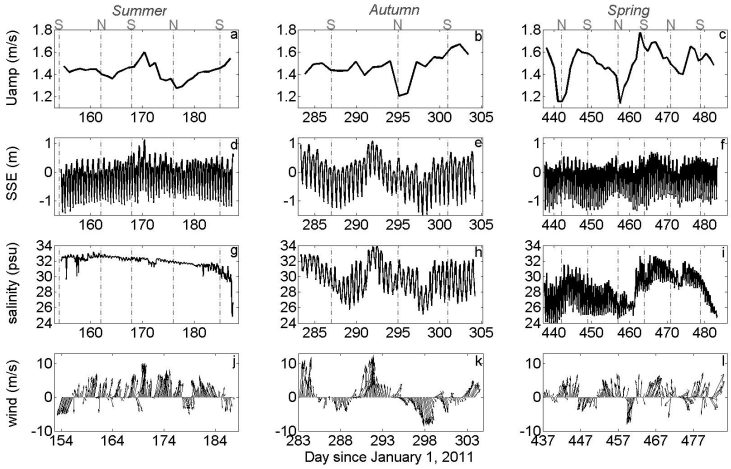

Figure 3.3: Depth-averaged tidal amplitude at the bottom frame (Uamp, 1st row), the sea surface elevation (SSE) and salinity at the NIOZ jetty (2nd and 3rd row, resp.) and wind vectors at Den Helder Airport (4th row) during Summer, Autumn and Spring (left, middle and right column, resp.). Uamp is a discrete value and is based on two tidal cycles to remove the diurnal inequality. It is defined as half of the range in depth-averaged current velocities. Wind vectors are oriented in down-wind direction. The spring-neap tidal cycle is indicated in gray by N and S at the top and by the dotted gray vertical lines in the panels, and is based on astronomical tidal charts. The time is given in Days since January 1, 2011.

ebb, indicating that classical tidal straining is not important at the study site, and the water column is most stratified during late flood and slack before ebb.

The strength of the cross-stream currents varies between and over the tidal cycles (Figure 3.4g-i). In Summer, the maximum cross-stream currents are only half the magnitude of those in Autumn and Spring, i.e. 0.15 and 0.30 m/s, respectively, most likely due to less freshwater discharge in the period preceding Summer (Figure 3.2). The greatest cross-stream currents are present during late flood and peak ebb. Cross-stream circulation cells are present between 6:00 to 10:00 (late flood) and 13:00 to 16:00 (peak ebb) hours UTC of Autumn and between 17:00 to 19:00 (late flood) and 12:00 to 14:00 (peak ebb) hours UTC of Spring. Buijsman and Ridderinkhof [2008c] showed that the cross-stream currents in the Marsdiep inlet are driven by centrifugal and Coriolis accelerations and by baroclinic pressure gradients. Furthermore, they conclude that differential advection is important during late flood because the densest flood water enters the Marsdiep basin in the middle of the channel, which creates

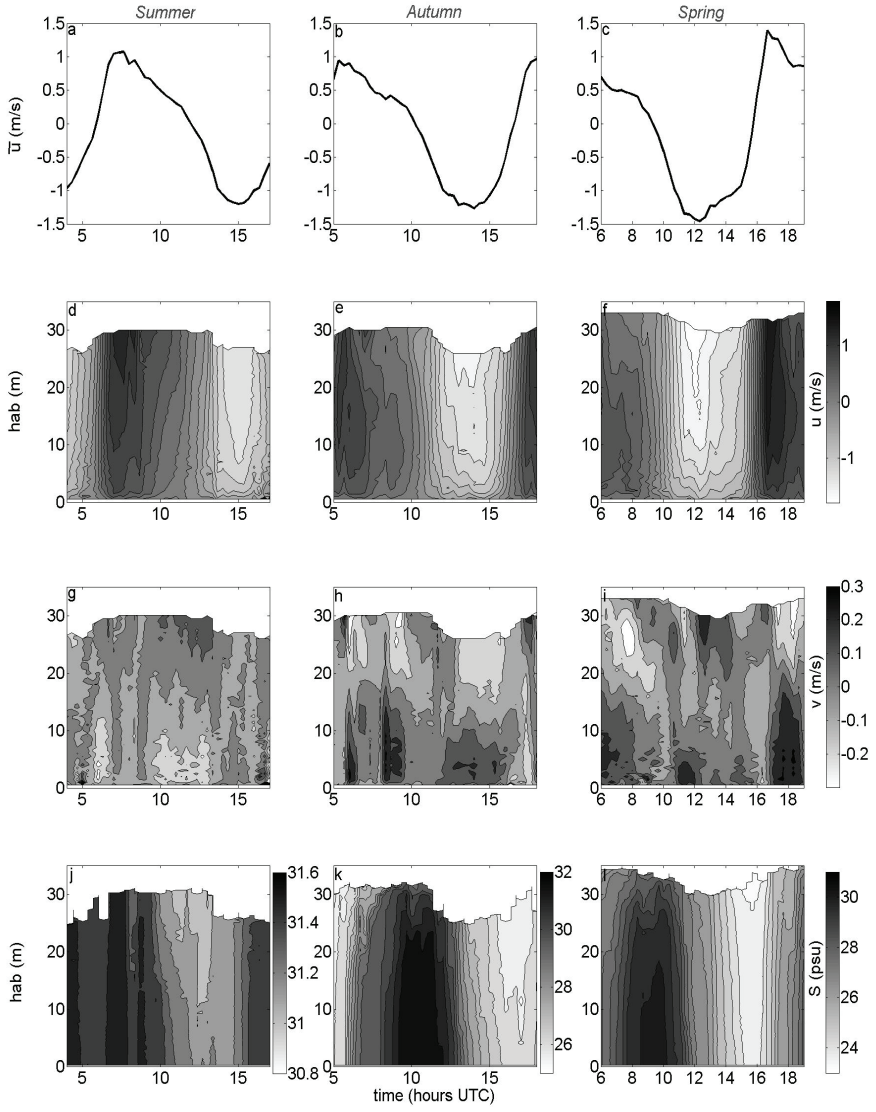

Figure 3.4: Overview of anchor station data collected during the three different deployment periods. The seasons are indicated at the top. The first row displays the depth-averaged along-stream velocity, the second and third row the vertical profiles of along- and cross-stream velocity, respectively, and the fourth row the vertical profiles of salinity.

a lateral density gradient and drives a cross-stream circulation cell. The differential advection mechanism is evident in the observed cross-stream circulation cell of Figure 3.4 and its seasonal variability. In the next section, the vertical structure of the along-stream velocity is treated in more detail using the data from the bottom frame deployments.

3.3.2 *Average vertical profiles of along-stream velocity*

The average vertical profiles of along-stream velocity as a function of the depth-averaged velocity are depicted in Figure 3.5. The x- and y-axis represent the velocity and height above the bottom, respectively. Each line represents an average vertical profile, as explained in section 3.2.4.

The vertical profiles of the strong (> 1 m/s) ebb and flood currents deviate substantially from each other (Figure 3.5). Strong ebb is characterized by greater vertical gradients in velocity, i.e. shears, in the lower part of the water column compared to strong flood (> 1 m/s). The velocity increases up to approximately 10 m above the seabed for strong ebb, whereas the vertical gradients in velocity are smaller in the lower part of the water column during strong flood. During flood, these vertical shears remain high up to 15-20 m above the seabed. In the upper part of the water column, the velocity profile is more uniform during strong ebb than during strong flood. These patterns contradict the standard estuarine vertical profiles as described by e.g. Jay and Musiak [1996].

Furthermore, the vertical profiles of the weak (< 1 m/s) flood and ebb currents differ from the strong currents. During weak ebb, the vertical gradients in velocity are more uniformly distributed over the water column (Figure 3.5). During weak flood, the shape of the vertical profiles changes greatly. A mid-depth velocity maximum is observed, modifying the vertical structure of the along-stream velocity during Autumn and Spring (Figure 3.5b,c). Also, the shape of the vertical profiles of the weak ebb and flood currents exhibits seasonal, inter-dataset, variability. The mid-depth velocity maximum during weak flood is better developed under the presence of fresher conditions in Autumn and Spring (Figure 3.3b,c): the mid-depth velocity maximum persists until higher depth-averaged velocities are reached. Higher depth-averaged velocities are characterized by a mid-depth maximum located higher up in the water column. It can be indicative of an intensification of the bottom-generated turbulence in the presence of vertical stratification, which is investigated in section 3.4.1 using numerical simulations. Weak ebb currents display an increase in vertical gradients of velocity in the upper part of the water column under the fresher conditions in Autumn and Spring, probably related to the dampening of turbulence by strain-induced vertical stratification as was observed for example

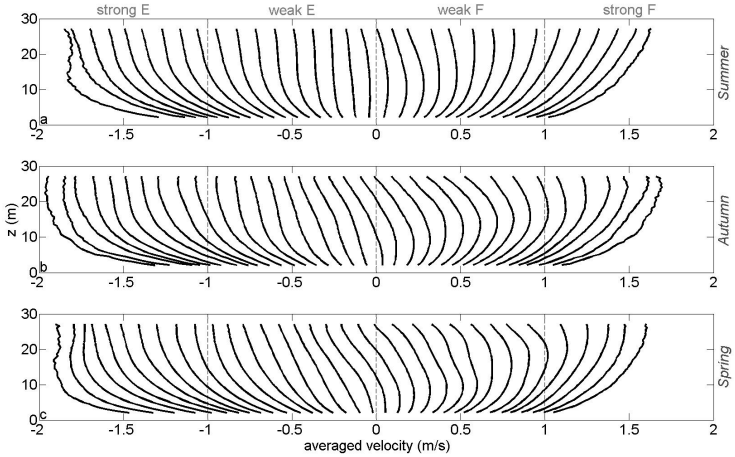

Figure 3.5: Average vertical profiles of along-stream velocity per bin of 0.1 m/s of the depth-averaged current for Summer, Autumn, Spring, as indicated at the right of each panel. The x- and y-axis show the velocity and height above the bed (Z), respectively. Each black line represents an averaged vertical profile as a function of the depth-averaged current as described in section 3.2.4. The vertical dashed lines indicate the transition from strong to weak ebb (E) and flood (F) currents and the location of the slack tide.

in the German Wadden Sea [Becherer et al., 2011] and the York River estuary [Scully and Friedrichs, 2007].

Around slack tide, the vertical profiles resemble a tidally-averaged profile of estuarine circulation during Autumn and Spring (Figure 3.5). Weak ebb and flood currents show landward flow at the bottom and seaward flow at the surface. The inter-tidal variability reflects the seasonal fluctuations in baroclinic forcing. In Summer, the vertical profiles near slack tide are uniform over almost the entire water column due to the absence of strong density gradients (Table 3.1 and Figure 3.5a), whereas in Autumn and Spring indications of an estuarine circulation are more apparent due to the presence of higher density gradients during these time periods caused by the elevated discharge at the sluices (Figure 3.5b,c). The higher baroclinic pressure gradients can modify the vertical profiles during slack tide by enhancing the vertical stratification and the related vertical shears in along-stream velocity in the water column. This could potentially enhance the residual circulation as discussed by Stacey et al. [2001].

To investigate the impact of asymmetric effects on the tide, a distinction is made between the vertical current structure from peak ebb to peak flood (EtoF) and its antagonistic phase (FtoE). The asymmetry in near-bed velocities and

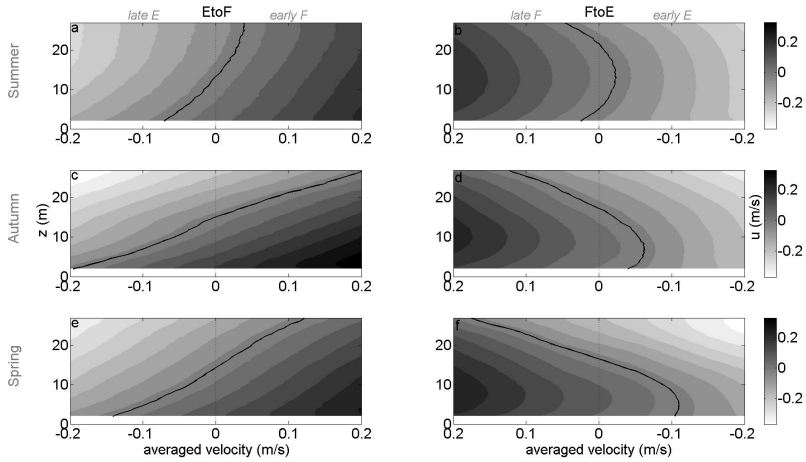

Figure 3.6: Vertical profiles of along-stream velocity for the Summer, Autumn and Spring deployment (upper to lower row, resp.) during the slack tides. The slack period from ebb (flood) to flood (ebb), named EtoF (FtoE), is depicted in the left (right) column. Early and late flood (F) and ebb (E) are indicated at the top in gray. Along-stream velocity is given as a function of the depth-averaged velocity (x-axis) and height above the bed (Z, y-axis). The solid black lines indicate the location where the velocity is 0 m/s, which is a measure for the reversal of the current.

vertical shear between ebb and flood are similar for EtoF and FtoE as well as the occurrence of a mid-depth velocity maximum during early and late flood (not depicted). However, the vertical profiles of EtoF and FtoE differ from one other around the slack tides (Figure 3.6). In Figure 3.6, the x-axis of FtoE is reversed in order to accurately represent the temporal propagation of the tide from late flood to early ebb. The onset of the flow reversal from EtoF starts near the seabed due to the effect of bed friction on the flow. Higher up in the water column, frictional effects are smaller and therefore inertial effects dominate and the current reverses later. From FtoE, the flow reversal patterns display entirely different characteristics. The flow reversal begins in the upper part of the water column and ends in the lower part of the water column. During late flood, there is another momentum sink, resulting in the earliest flow reversal in the upper part of the water column, which is greater than the frictional effects of the seabed. A cross-stream circulation cell during late flood, generated by differential advection as illustrated in Figure 3.4 and discussed in section 3.3.1, is a mechanism which can serve as an additional momentum sink.

Greater density gradients in Autumn and Spring are accompanied by an enhancement of the patterns described above (Figure 3.6c-f). The range of depth-averaged velocities over which the current reverses direction is greater than in Summer. The slower reversal from EtoF with respect to Summer might be indicative of the greater vertical stratification that is generated by the large density gradients, which dampens the vertical momentum exchange and delays the onset of the flood tide, as was already discussed by Scully and Friedrichs [2007].

The median duration of the slack tides, defined as the time period when the along-stream current is not unidirectional over the vertical profile, is much smaller from EtoF than from FtoE, being between 10-17 and 43-61 minutes, respectively (Figure 3.6). The duration increases from Summer to Autumn and Spring, which suggests that the vertical density gradients influence the duration of the current reversal, probably by limiting the vertical momentum exchange. The duration of the current reversal from EtoF is greater in Autumn than in Spring, whereas the duration from FtoE is greater in Spring than in Autumn.

Summarizing, the vertical gradients in along-stream velocity in the lower part of the water column are greater during ebb, whereas they are greater in the upper part of the water column during flood. These patterns deviate from the standard estuarine vertical profiles. The horizontal density gradient, by forcing the strength of the vertical stratification, has a considerable influence on the structure of the vertical profiles, amongst others reflected in the inter-seasonal variability. Around slack tide, the vertical profiles represent an estuarine circulation. The early and late phases of ebb and flood are characterized by similar vertical current structures, but the current reversal around high and low water slack differ markedly from one other.

3.3.3 *Impact of density field on the vertical current structure*

To further investigate the impact of the density field on the vertical current structure, the relationship between the calculated salinity gradient, $\langle \frac{\partial s}{\partial x} \rangle$, and the vertical shear in along-stream velocity is analyzed. The shear during different current strengths is compared by tidally-averaging over a range of the depth-averaged along-stream current as given in each panel of Figure 3.7. Also, the vertical shear at different heights above the bottom is depicted in each panel, as indicated by the different gray icons. The solid lines are the least-squares linear fits to the shears at each height above the bed. Negative (positive) shear during ebb (flood) signifies increasing current velocities with increasing height above the bed.

High current velocities during ebb and flood are characterized by the greatest shears, $|du/dz|$, close to the seabed (h2.5) for all salinity gradients (gray dotted line, Figure 3.7a,b). The vertical shears higher up the water column are small

(h15 and h25, dotted black and solid black lines). For all ebb velocities (Figure 3.7a,c,e), similar patterns are observed, which are characterized by high shears near the bed and small shears higher up in the water column. These patterns resemble the classical logarithmic profiles of along-stream velocity. Furthermore, there is no clear relationship between $\langle \frac{\partial s}{\partial x} \rangle$ and vertical shear, which indicates that the vertical profile is not substantially influenced by the along-stream salinity gradient.

In contrast, the shear of the flood currents does correlate with $\langle \frac{\partial s}{\partial x} \rangle$. Weak flood currents (0.3-0.7 and 0.8-1.2 m/s in Figure 3.7f and d, resp.) are characterized by a reversal of the sign of the vertical shear in the upper part of the water column. In Figure 3.7d, the R^2 is 0.37 and 0.55 for 15 and 25 m above the bed, respectively. In Figure 3.7f, the values are 0.3 and 0.66, respectively. This reversal in sign of the vertical shear corresponds with the presence of a mid-depth velocity maximum. It evidences a linear relationship between the strength of the salinity gradient and the magnitude of the negative vertical shear, which implies a relationship between the mid-depth velocity maximum and the baroclinic pressure gradient.

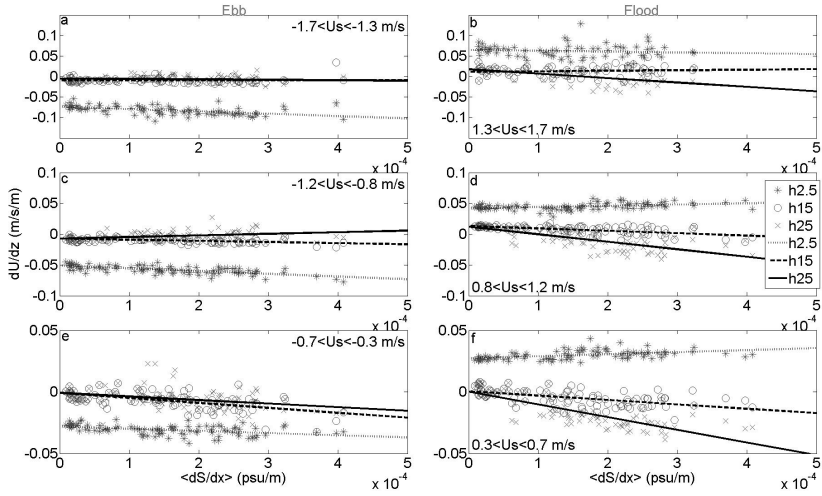

Figure 3.7: Vertical shear in along-stream velocity, dU/dz, during ebb and flood (left and right column, resp.) as a function of the along-stream salinity gradient, $\langle \frac{\partial s}{\partial x} \rangle$. The shear is computed for different current magnitudes, which are the averages of 1.3-1.7 (upper row), 0.8-1.2 (middle row) and 0.3-0.7 m/s (lower row). For each individual tidal cycle of all deployments, the vertical shear is computed at 2.5, 15 and 25 m above the bed (*, o and x, resp.) based on the closest 5 bins. The least-squares linear fits at each height above the bed are indicated in the legend.

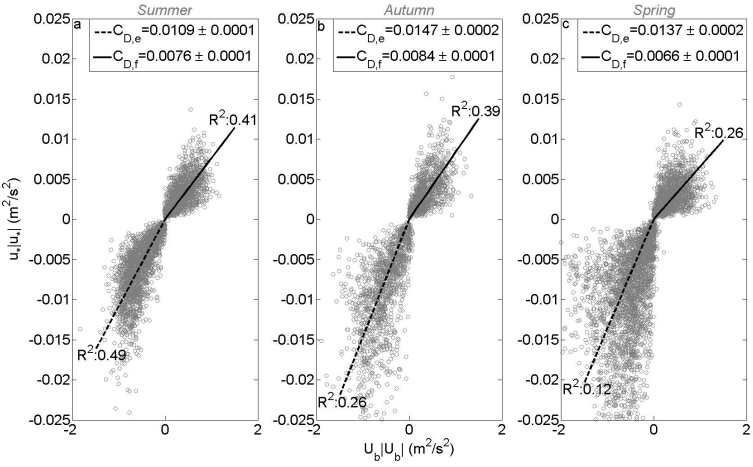

Figure 3.8: The relationship between friction velocity, u_*, squared and near-bed velocity, u_b, (at 2 m above the bed) squared for Summer, Autumn and Spring (left, middle and right column, resp.). The gray circles indicate the individual values of the 8-ensembles averages. The dashed and solid lines indicate the least-squares fit to the datapoints for ebb and flood, respectively. The slope represents the drag coefficient, C_D, as given in the legends. The R^2 is given in each panel.

3.3.4 *Drag coefficients*

The near-bed observed vertical shears in along-stream velocity can be explained by an asymmetry in drag coefficient. Evidence of an asymmetry is given in Figure 3.8, which shows the 4-minute averages of u_* and u_b squared as well as the estimates of the drag coefficient. An asymmetry in the drag coefficient between ebb and flood is observed for all deployments. The scatter increases considerably from Summer to Autumn and Spring which suggests that other processes influence the estimation of the drag coefficient under increased baroclinic forcing. The greater variability during Autumn and Spring (Figure 3.8b,c) might be driven by variations in vertical stratification and in cross-stream currents. It is striking that the asymmetry in drag coefficients is very similar for all seasons. The drag coefficient is between 1.5 and 2 times greater during ebb than during flood, which suggests a time-independent process, such as e.g. tide-bathymetry interaction by form drag. During peak ebb, the observations deviate from the linear fit with overestimated values of u_*^2, similarly to the observations of Geyer et al. [2000] in the Hudson estuary. Geyer et al. [2000] suggest that other mo-

mentum sinks or variations in the stress-velocity relationship might explain this deviation.

The persistent asymmetry in drag coefficient in Figure 3.8 is time-invariant under a wide range of conditions. Therefore the variable cross-stream currents and vertical stratification are unlikely factors to explain this asymmetry. The contribution of the cross-stream currents to the modification of the drag coefficient is investigated by removing all data points with near-bed cross-stream velocities greater than 0.1 m/s. It results in only minor variations in C_D and the asymmetry between ebb and flood remains similar (not shown). Vertical stratification is highly variable in the Marsdiep and might explain the great variability, but not the asymmetry itself. Possible explanations for the deviation in near-bed velocities from standard estuarine theory are considered in the discussion.

3.4 NUMERICAL MODEL RESULTS

To better understand what determines the vertical structure of along-stream velocity in the Marsdiep, several model scenarios are run with GOTM (Table 3.2). Idealized runs are used to identify the basic one-dimensional along-stream processes that shape the vertical structure under conditions similar to the study site. Furthermore, the importance of the strong currents and large water depths is evaluated. Dissimilarities between the observations and the idealized model runs indicate the possibility of other processes being important. Semi-realistic runs are then applied to understand these characteristic processes.

3.4.1 *Idealized scenarios*

To investigate the conditions that are required to generate a mid-depth velocity maximum, idealized scenarios are run. These runs show that the presence of vertical stratification can generate a mid-depth velocity maximum. Furthermore, they show that along-stream tidal straining can only explain a mid-depth velocity maximum during early flood since the peak flood currents mix the entire water column.

The tidal amplitude of 1.2 m/s in run 1 produces a well-mixed water column with maximum velocities near the surface during nearly the entire tidal cycle (Figure 3.9a,d,g). A small increase in vertical stratification is observed in the upper part of the water column during the early flood phase, which is driven by along-stream tidal straining. The weak stratification during early flood is already capable of generating a small mid-depth maximum (Figure 3.9a).

The smaller amplitude of run 2 results in the presence of a mid-depth velocity maximum during the entire flood phase (Figure 3.9b) because the peak currents lack sufficient kinetic energy to mix the entire water column. There-

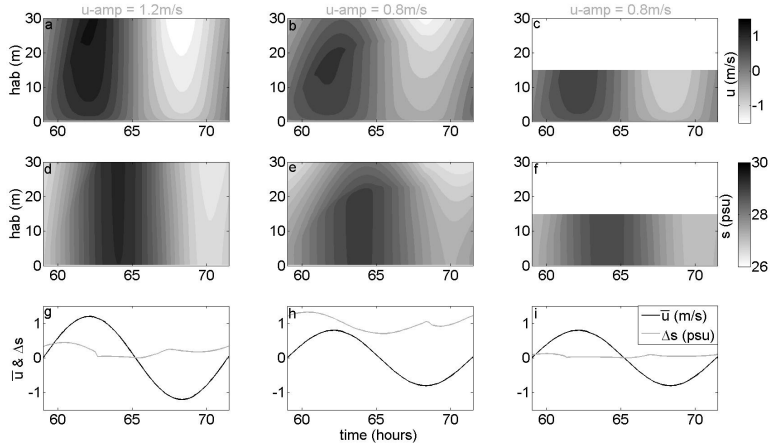

Figure 3.9: Model output of current velocities (upper row) and salinity (middle row) during 1 tidal cycle of the idealized model scenarios (runs 1 to 3). The x- and y-axis represent time and height above the bed, respectively. In the lower row, the depth-averaged current velocity ($\bar{u}$, black line) and the top-to-bottom salinity difference (Δs, gray line) are depicted as a function of time. The left, middle and right columns represent model runs with tidal amplitudes of 1.2, 0.8 and 0.8 m/s, resp.

fore, vertical stratification is generated at 15-20 m above the bed. Also, the average vertical stratification is greater during the entire tidal cycle (Figure 3.9h). Vertical stratification is greatest during late ebb and smallest during late flood, which is typical for the classical tidal straining mechanism. This process, therefore, mainly modifies the vertical current structure in one-dimensional, along-stream, direction (Figure 3.9e). These simulations only explain the mid-depth velocity maximum during the early flood phase, because the peak flood currents in the Marsdiep are generally able to mix the entire water column during peak flood. It is therefore implausible that vertical stratification during late flood is a relic from classical tidal straining generated during ebb.

Only the presence of a weakly-stratified water column is required to generate a mid-depth velocity maximum under such a high current regime. The transition from well-mixed to weakly-stratified conditions from peak to slack currents is exemplified in the left and middle column of Figure 3.9 and shows that the great water depth enables this shift. The right column of Figure 3.9 shows that smaller water depths experience well-mixed conditions under a smaller tidal forcing (run 3). A greater water depth creates a greater variation in vertical stratification over the tidal cycle (Figure 3.9h,i).

The stratifying dynamics are further investigated using the Simpson number. The Simpson number, Si, which was previously called the horizontal Richardson number, [e.g. Stacey et al., 2008, 2010], displays the (1-D) balance between the stratifying and de-stratifying forces in the water column as a function of the horizontal salinity gradient, $\langle \frac{\partial s}{\partial x} \rangle$ (psu/m), water depth, H (m), and the friction velocity, u_* (m/s), where the latter represents the kinetic energy of the currents

$$Si = \frac{g\beta \langle \frac{\partial s}{\partial x} \rangle H^2}{u_*^2}, \tag{3.10}$$

where g is the gravitational acceleration (9.81 m/s^2) and β is the haline contraction coefficient (7.7*10^{-4}). A Si value greater than 1 indicates that the potential energy is greater than the kinetic energy which implies that the water column remains vertically-stratified during the entire tidal cycle. Stacey and Ralston [2005] and Burchard et al. [2011] demonstrated that tidal straining is important for $Si > 0.2$. A small friction velocity of 0.05 m/s, approximately $\frac{1}{3}max(u_*)$, and a tidally-averaged $\langle \frac{\partial s}{\partial x} \rangle$ of 2*10^{-4} psu/m in a water depth of 30 m are representative values for the Marsdiep [de Vries et al., 2014, Chapter 2], and results in a Si of 0.54, sufficient to allow vertical stratification by tidal straining during weak currents. Peak currents are characterized by Si values of approximately 0.05 and imply well-mixed conditions.

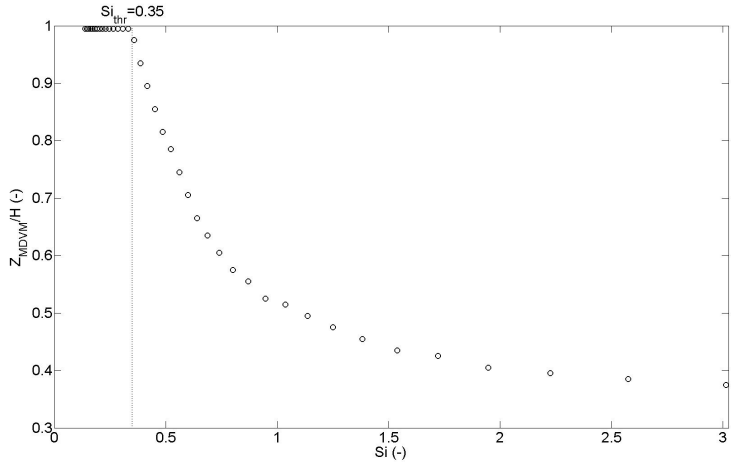

Figure 3.10: Relationship between the dimensionless height of the mid-depth velocity maximum (Z_{MDVM}/H) and the Simpson number based on 39 model simulations where the tidal amplitude is varied.

To evaluate under which Simpson numbers along-stream tidal straining generates a mid-depth velocity maximum during the entire flood tide, the height of the mid-depth velocity maximum during peak flood is assessed for a range of Simpson numbers. A total of 39 model simulations are run with varying tidal amplitudes (and therefore varying friction velocities), which produce a wide range of Simpson numbers. The values of H (30 m) and $\langle \frac{\partial s}{\partial x} \rangle$ (-2*10^{-4} psu/m) are kept constant. The height of the mid-depth velocity maximum is defined as the height above the bed where the along-stream velocity reaches its maximum value, normalized by the water depth (Z_{MDVM}/H). Figure 3.10 shows that Si values smaller than 0.35 are characterized by a near-surface velocity maximum. An increase in Si between 0.35 and 1 results in the generation and rapid lowering of a mid-depth velocity maximum due to along-stream tidal straining. For high Si values, the non-dimensional height of the mid-depth velocity maximum stabilizes to 0.35. Figure 3.10 shows that for Si values smaller than 0.35, other processes than along-stream tidal straining are responsible for the generation of a mid-depth velocity maximum during peak and late flood, which is discussed in more detail in section 3.4.2.

A comparison between the observations and model simulations highlight two main discrepancies. First, along-stream tidal straining only explains the vertical structure of salinity and velocity satisfactorily during early flood since the peak flood currents mix the entire water column. Furthermore, the interaction of the barotropic and baroclinic pressure gradients in GOTM results in the greatest near-bed velocities during flood, which creates the classical estuarine circulation pattern. However, observed near-bed velocities are stronger during ebb than during flood (Figure 3.5). This variation in near-bed currents may change the dynamics of vertical stratification and modify the vertical current structure. Semi-realistic scenarios are run to investigate the effect of the observed near-bed velocities on the vertical structure. In addition, the contribution of cross-stream advection of salinity on the generation of vertical stratification during late flood is investigated.

3.4.2 *Semi-realistic scenarios*

The asymmetry in near-bed velocities is incorporated using the observed near-bottom along-stream velocities (2 m above the bottom) of Spring as a model forcing for neap and spring tide conditions (runs 4-7, Table 3.2). Neap and spring tide conditions are simulated with a uniform salinity of 28 psu over the entire water column. Alternatively, the effect of vertical stratification generated by non-along-stream processes is incorporated by imposing a two-layer vertical stratification. In Figure 3.11, the scenarios are depicted for neap and spring tide conditions with and without a two-layer vertical stratification.

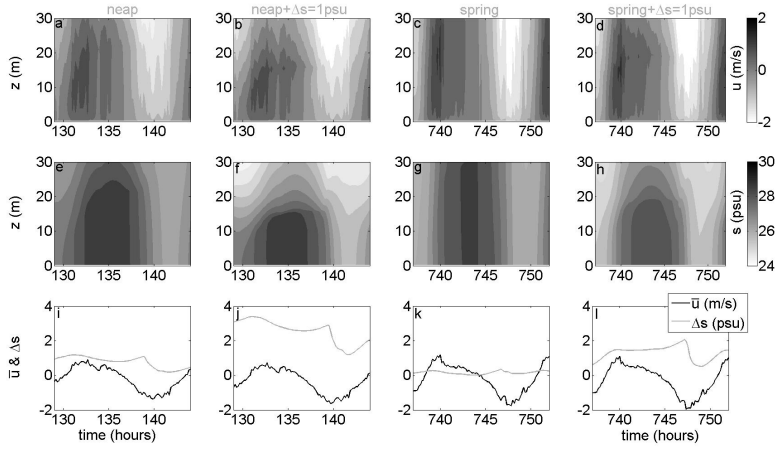

Figure 3.11: Same as Figure 3.9, but then for the semi-realistic model runs 4 to 7 in Table 3.2. Neap tide conditions are given in the first two columns (runs 4 and 5), where in the scenario of the 2nd column a vertical stratification of 1 psu is imposed on the water column. The 3rd and 4th column are organized similarly but then for spring tide conditions (runs 6 and 7).

Neap tide conditions are characterized by a mid-depth velocity maximum during the entire flood phase, driven merely by the along-stream advection of salinity (run 4, Figure 3.11a,e). The small two-layer vertical stratification increases the strength of the mid-depth velocity maximum (run 5, Figure 3.11a,b;e,f). Figure 3.11i-j shows that vertical stratification is strongest during slack before flood, around 131 hours, as a result of tidal straining. However, around 140 hours, the second slack before flood, a considerable decrease in vertical stratification is observed as a consequence of the high near-bed velocities during the late ebb phase. The greater near-bed velocities during ebb counteract tidal straining and decrease vertical stratification during the late ebb phase.

Spring tide conditions without a two-layer vertical stratification are characterized by a well-mixed water column during the complete tidal cycle (run 6, Figure 3.11c,g,k). It implies that vertical stratification during spring tide is not only generated by along-stream processes for an along-stream salinity gradient of $2*10^{-4}$ psu/m. Surprisingly, the superposition of vertical stratification results in the strongest vertical stratification during late flood, in combination with the occurrence of a mid-depth velocity maximum (run 7, Figure 3.11d,h,l). During ebb, the vertical stratification is destroyed (Figure 3.11l). The stronger ebb currents and the elevated vertical mixing rates both appear to contribute to the destruction of vertical stratification during ebb. This mechanism, and its

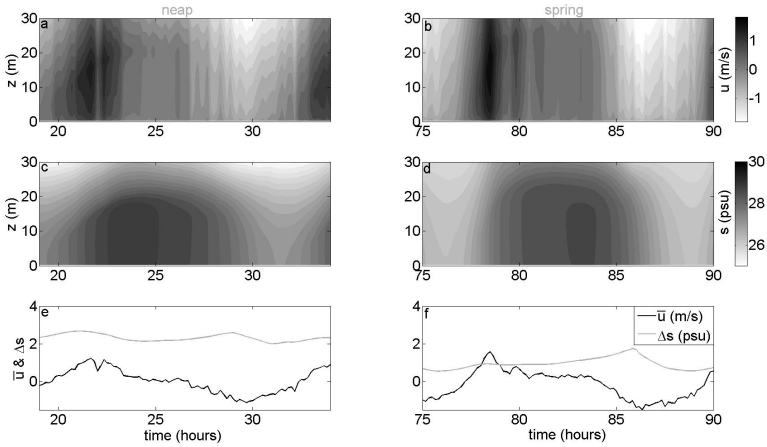

Figure 3.12: Same as Figure 3.9, but then for semi-realistic model runs 8 and 9 in Table 3.2. Model output of current velocities and salinity are given for 1 tidal cycle during neap- and springtide (left and right column, respectively). This simulation incorporates advection of salinity by cross-stream currents.

effect on the vertical current structure, are most pronounced during spring tide conditions. To investigate if cross-stream processes are able to generate vertical stratification during late flood, as already hypothesized by van Haren [2010] and de Vries et al. [2014], simulations 8 and 9 were run.

The velocity field of Spring in along-stream and cross-stream direction over the entire water column is used to force a neap and spring tide scenario with a constant salinity gradient of $2*10^{-4}$ psu/m in along-stream and cross-stream (x and y, resp.) direction. Figure 3.12 demonstrates that the addition of a cross-stream component has a minor impact on the vertical current structure during neap tide (run 8). However, it results in an increase of vertical stratification during the late flood of spring tide (run 9, Figure 3.12e,f). Apparently, the rate of salinity advection by cross-stream processes from neap to spring tide increases more strongly than the rate of vertical mixing, which results in an increase of vertical stratification from neap to spring tide conditions. It also explains the presence of a mid-depth velocity maximum during the late flood phase by cross-stream advection of salinity. It suggests a spring-neap tidal modulation, and asymmetry, in vertical stratification during late ebb and late flood.

Concluding, the asymmetry in drag coefficient and in near-bed velocities results in the destruction of vertical stratification during ebb, which counteracts the tidal straining mechanism. Cross-stream advection of salinity is important during the late flood phase, which creates vertical stratification and generates

a mid-depth velocity maximum. In our model runs, both processes appear to increase in importance from neap to spring tide.

3.5 DISCUSSION

3.5.1 *Near-bed dynamics*

Generally, the drag coefficient is assumed constant in the depth-averaged along-channel momentum balance. A constant drag coefficient or a constant eddy viscosity both represent constant vertical mixing rates, which enables a simplification of estuarine dynamics in order to compute the residual circulation by the solution proposed by Pritchard [1956] and Hansen and Rattray [1966]. However, several studies have observed asymmetries in the drag coefficient (and eddy viscosity), invalidating the assumption of a constant C_D under certain conditions.

Geyer et al. [2000] observed a constant bed roughness during most of the tidal cycle in the Hudson, an estuary characterized by a uniform bathymetry. However, their observations displayed small but persistent differences between neap and spring tide, also found in the James River estuary by Li et al. [2004]. Seim et al. [2002] observed variations in drag coefficients between $1.5*10^{-3}$ and $2.5*10^{-3}$ on the ebb phase, depending on the presence of vertical stratification generated by cross-stream currents. Fugate and Chant [2005] found variations in bed roughness between ebb and flood related to variations in vertical stratification. Fong et al. [2009] observed large variations in C_D not driven by asymmetries in cross-stream currents or vertical stratification but driven by asymmetric bedforms. The drag coefficient was found to be notably greater during flood than during ebb. All these studies relate differences in C_D to 1-D processes in the bottom boundary layer. In addition, at several locations on the continental shelf and in Puget Sound, studies have shown that form drag can contribute substantially to the magnitude of the drag coefficient [e.g. Edwards et al., 2004; Warner et al., 2013].

With the available data, it is impossible to isolate the different contributors to form drag. Empirically, many different parameterizations for bed roughness have been formulated, e.g. the Chézy and Manning coefficient, which incorporate pressure and frictional differences in the drag coefficient by inclusion of the slope of the seabed and/or a roughness length [van Rijn, 2011]. It is outside the scope of this research to investigate the factors that contribute to the magnitude of the drag coefficient. However, this study shows that the assumption of a constant drag coefficient is not valid in the Marsdiep basin and that the values are greater than the canonical value of $2.5*10^{-3}$. The latter implies that other processes, i.e. vertical stratification, cross-stream advection of

momentum and/or form drag influence the near-bed vertical shears. The persistent asymmetry under a wide range of conditions suggests that form drag is the dominant process.

It remains the question to what degree different spatial scales (sandwave-scale and channel-scale water depth variations) contribute to the drag. The seabed is sloping at the study site, which results in a decrease (increase) in water depth in downstream direction during ebb (flood) and creates a force opposing the ebb current. Furthermore, there is an upstream obstruction during ebb located approximately 1 km up-estuary, which is characterized by water depths 10 to 15 m smaller than at the study site (Figure 3.1b). This might be a source of form drag and could produce elevated values of C_D during ebb. Both characteristics of the bathymetry correspond with the observed asymmetry in C_D, and potentially explain the elevated values.

This study only treats observations at one location. However, the complicated bathymetry is certainly not atypical for the Marsdiep basin. Figure 3.1b shows that the channels in the Marsdiep and Vlie basins are characterized by great variations in water depth. It is therefore hypothesized that the magnitude, and asymmetry, of the drag coefficient is spatially highly variable. This hypothesis is supported by Buijsman and Ridderinkhof [2007a] who observed different values of the friction velocity and drag coefficient in the shallower center of the Marsdiep inlet with respect to the values presented in this study.

By modifying the intra-tidal vertical mixing characteristics, the asymmetric drag may have implications for the residual circulation. As a result, the residual circulation may therefore be highly spatially variable in complex bathymetries like the Marsdiep basin. Geyer and MacCready [2013] already propose in their review on the estuarine circulation that the along-stream variability of the estuarine circulation requires more research. Here, we suggest that more knowledge on the spatial variability of the drag coefficient, with particular emphasis on form drag, is important for a better understanding of the spatial variability in estuarine circulation for estuaries with a complex bathymetry. Furthermore, numerical models might benefit from the inclusion of a drag coefficient not only dependent on the grain size diameter, but which also depends on e.g. the spatial derivative of water depth.

3.5.2 *Mid-depth velocity maximum*

To the authors' knowledge, the observation of a mid-depth velocity maximum occurring separately during both early and late flood has not been made in previous studies. It is interesting that a mid-depth velocity maximum, characteristic of strongly-stratified estuaries, is important in a weakly- and periodically-stratified estuary as the Marsdiep basin. The simulations have shown that the

presence of vertical stratification is a requirement for the development of a mid-depth velocity maximum. In the Marsdiep, the peak current conditions are characterized by well-mixed conditions, whereas the early and late phase of the tide are influenced by density-driven processes. The alternation of these regimes results in different generation mechanisms of the mid-depth velocity maxima.

The model simulations imply that vertical stratification generated by tidal straining is sufficient to facilitate the occurrence of a mid-depth velocity maximum during early flood. Cudaback and Jay [2001] demonstrated that strong bed friction is required to decrease the current velocities close to the bed, which applies to the Marsdiep basin. The well-mixed conditions during peak flood inhibit the late flood mid-depth velocity maximum to originate from the classical tidal straining. The addition of a realistic cross-stream current and a salinity gradient in the model simulations show that cross-stream tidal straining is a likely candidate to explain vertical stratification generated during late flood.

To further substantiate the claim of the relevance of along- and cross-stream straining in the Marsdiep basin, a scaling of the tidal straining terms is obtained from the dynamic potential energy anomaly equation. For a detailed explanation of all the terms is referred to Burchard and Hofmeister [2008] and de Boer et al. [2008]. The along-stream (S_x) and cross-stream (S_y) tidal straining component are scaled by

$$S_x = \frac{g}{H}\int_{-H}^{\eta} \tilde{u}\frac{\partial \rho}{\partial x} z dz, \tag{3.11}$$

and

$$S_y = \frac{g}{H}\int_{-H}^{\eta} \tilde{v}\frac{\partial \rho}{\partial y} z dz, \tag{3.12}$$

where $\tilde{u} = u - \bar{u}$ and $\tilde{v} = v - \bar{v}$ denote the vertical deviation from the mean of the along-stream and cross-stream velocities, respectively. The values of velocity are based on the data of the anchor station depicted in Figure 3.4. The values of $\frac{\partial \rho}{\partial x}$ and $\frac{\partial \rho}{\partial y}$ are based on the salinity gradients in Table 3.1. de Vries et al. [2014] observed the tidally-averaged along- and cross-stream salinity gradients to be of the same order of magnitude in the Marsdiep basin for 2 distinct spatial surveys, being between 1 and $3*10^{-4}$ kg/m^3/m. Therefore, an along- and cross-stream salinity of the same magnitude ($2*10^{-4}$ kg/m^3/m) is used to evaluate the effects of S_x and S_y. This assumption neglects any intra-tidal variation in along- and cross-stream salinity gradients, but serves well to illustrate at which moments of the tidal cycle cross-stream straining is important. It is not possible to estimate the advective and nonlinear terms of tidal straining with the

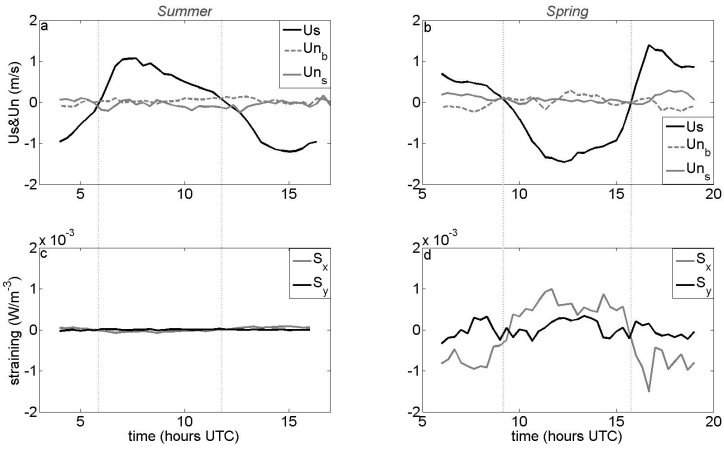

Figure 3.13: Along- and cross-stream tidal straining terms during the anchor stations measurements in Summer and Spring (left and right column, resp.). The upper row displays the depth-averaged along-stream current, $\bar{u}$, and the surface (v_s) and bottom (v_b) cross-stream currents. The lower row displays the along-stream, S_x, and cross-stream, S_y, tidal straining terms as given in equations 3.11 and 3.12. The vertical dotted lines indicate the moment of the slack tides.

available data. The goal here is to evaluate the potential role of along-stream and cross-stream tidal straining in the stratification dynamics and their relation to the occurrence of a mid-depth velocity maximum. Using model simulations, Burchard and Hofmeister [2008] and de Boer et al. [2008] showed that the tidal straining term is one of the main mechanisms in estuarine and downstream regions of freshwater influence (ROFI), but they stress that there are great spatial differences.

Figure 3.13 shows that along- and cross-stream tidal straining contribute during different phases of the tide, depending on the season. In Summer, tidal straining is negligible because of the small salinity gradients. However in Spring, along-stream tidal straining has a stratifying (mixing) impact on the water column during ebb (flood). Cross-stream tidal straining stratifies the water column during distinct phases of the tide. During late flood and late ebb, cross-stream tidal straining is important. The stratifying influence of tidal straining is opposed by vertical mixing. The observations and model simulations show that the water column is well-mixed during ebb because of the strong currents and corresponding mixing. Therefore, tidal straining during ebb is not able to stratify the water column. The weak currents during late flood enable the gen-

eration of vertical stratification by cross-stream tidal straining, which is similar to the differential advection described by Nunes and Simpson [1985] and Lacy et al. [2003].

Differential advection during late flood might be accompanied by advective transport of momentum, which might enhance the development of the along-stream mid-depth velocity maximum. Lower momentum water from the sides of the channel is transported upwards and migrates towards the center of the channel. Simultaneously, higher momentum water is transported downwards in the center of the channel and migrates sideways. Several studies have shown that advective processes contribute to the horizontal momentum balance and impact the strength of the estuarine circulation [Lerczak and Geyer, 2004; Cheng and Valle-Levinson, 2009; Scully et al., 2009; Burchard et al., 2011; Basdurak et al., 2013]. It is complicated to isolate the effects of cross-stream tidal straining and lateral advection of momentum, since they are both related to the strength of the density gradients. So, advection of salinity, and possibly momentum, might both contribute to the development of a mid-depth along-stream velocity maximum, and are both dependent on the density gradients. This study shows that the presence of weak vertical stratification by cross-stream tidal straining is already sufficient to create a mid-depth along-stream velocity maximum.

Stacey et al. [2008] found, based on idealized model simulations, that the timing of periodic vertical stratification is important for the development of vertical shears in velocity and for the strength of the estuarine circulation. Stratification imposed on the early flood or early ebb phase produces enhanced shears, which disappear quickly during the high current velocities. Vertical stratification imposed during late ebb or late flood has a longer lasting impact on the vertical shears. The shears can remain enhanced until after the succeeding slack tide. The generation of vertical stratification by cross-stream straining in the Marsdiep basin during late flood suggests that lateral processes can have a great effect on vertical shears and possibly the strength of the estuarine circulation. However, the enhanced vertical shears simulated by Stacey et al. [2008] contradict with the reversal in sign of the vertical shears in the upper part of the water column as presented in this study, most likely because Stacey et al. [2008] focused on the timing of vertical stratification and neglected the superimposed directional effect of the baroclinic pressure gradient.

The variable current dynamics discussed in this study illustrate the importance of two crucial components of the estuarine Marsdiep system. First, the presence or absence of vertical stratification plays an important role in modifying the vertical structure of along-stream velocity. Second, the strong bed friction, probably determined by the complex bathymetry of the sandy seabed, dissipates the tidal energy near the bed and is characterized by an unexpected asymmetry in ebb and flood drag coefficients.

3.6 CONCLUSIONS

Hundred days of current and salinity data and simulations with a 1-D water column model are combined to investigate the mechanisms and processes that determine the vertical profile of along-stream velocity in the periodically-stratified Marsdiep basin. The vertical current structure at the study site is characterized by strong bed friction, i.e. a large drag coefficient, which is at least 3 to 6 times greater than the canonical value of $2.5*10^{-3}$. In addition, the friction velocity and near-bed vertical shears are greater during ebb than during flood for the same current magnitude. In estuaries, the superposition of the barotropic and baroclinic tide predicts an opposite asymmetry in friction velocity and near-bed vertical shears. This asymmetry in friction velocity is caused by an asymmetry in bed roughness, which is most likely caused by the complex bathymetry. The simulations show that the asymmetry can result in increased mixing rates during ebb, which can destroy the vertical stratification generated by classical tidal straining. The importance of this mechanism increases from neap to spring tide.

Higher up in the water column, the vertical shears in along-stream velocity are greater during flood than during ebb. During early and late flood, a mid-depth velocity maximum in along-stream velocity is observed. Both phenomena are generated by different mechanisms. The strong drag coefficient in the area (flood: $7.7*10^{-3}$, ebb: $1.25*10^{-2}$) and the periodic stratification of the water column are the conditions required to create a mid-depth velocity maximum, as already suggested by Cudaback and Jay [2001] for a strongly-stratified estuary. Vertical stratification during early flood is a relic of tidal straining during late ebb, whereas vertical stratification during late flood is generated by advection of salinity by cross-stream straining. Vertical stratification during late flood inhibits the vertical momentum exchange and facilitates the generation of a mid-depth velocity maximum by the superimposed effect of the barotropic and baroclinic pressure gradients.

This study shows that the baroclinic pressure gradient and the asymmetry in bed friction are both important in shaping the vertical current structure in the Marsdiep basin. The measurements are collected at only one location, but similar complex bathymetry in the rest of the Marsdiep basin suggests a more ubiquitous applicability. The mechanisms that enable the destruction and formation of vertical stratification at the study site during ebb and flood, respectively, might have considerable effects on the residual circulation.

4

ON THE VERTICAL STRUCTURE OF THE RESIDUAL CURRENT

The vertical profile of the residual current is investigated by analyzing current data collected during three different seasons, with special attention being dedicated to the dynamics of the estuarine circulation. The wind and tidal asymmetries principally modify the depth-averaged residual current, whereas the strength of the estuarine circulation is controlled by variations in freshwater discharge. The magnitude of the estuarine circulation scales well with the solution proposed by Geyer et al. [2000] for a limited range of along-stream salinity gradients. For salinity gradients smaller than $1*10^{-4}$ psu/m, the solution under-predicts the surface-to-bottom difference in residual currents. It is suggested that barotropic processes mainly determine the residual profile under very weak salinity gradients. For salinity gradients greater than $2.5*10^{-4}$ psu/m, lateral advection contributes to the tidally- and depth-averaged momentum balance and modifies the estuarine circulation. Lateral advection is observed to be stronger during ebb than during flood for strong salinity gradients and acts to reduce the estuarine circulation. Interestingly, the creation of an estuarine circulation in the Marsdiep basin appears to be centered around the long period of weak currents from late flood to slack before ebb. The gravitational circulation and cross-stream total tidal straining are the most likely generation mechanisms. The absence of classical tidal straining is explained by the presence of strong currents during late ebb and the short duration of slack before flood. This study has demonstrated that a non-steady estuarine circulation is present in a deep, ebb-dominant part of the Marsdiep basin, which is occasionally modified by lateral advection. Model simulations indicate a reduction in estuarine circulation in the shallower, flood-dominant part of the Marsdiep basin. The observed non-steady behavior suggests that the duration of weak vertical mixing is more important at the study site than the strength of maximum vertical mixing.

This chapter is based on the following paper, currently under review as:
de Vries, J. J., Ridderinkhof, H., Duran-Matute, M., and van Aken, H. M. (under review). On the vertical structure of the residual current in the periodically-stratified Marsdiep basin, *Cont. Shelf. Res.*

4.1 INTRODUCTION

Estuaries are important as a source and stopover for nutrients and terrestrial sediments along their pathway from land to sea. The availability of sediments and nutrients is essential to the (a)biotic conditions of estuaries and coastal regions. To understand the net exchange patterns of these gate-ways, it is important to study the vertical structure of residual currents in estuaries since these partly determine the net transport of suspended matter.

Pritchard [1956] and Hansen and Rattray [1966] established the research framework on the vertical structure of residual currents by demonstrating that, in estuaries, the barotropic and baroclinic pressure gradients balance vertical mixing of momentum. Consequently, a tidally-averaged vertical profile of velocity in shallow and narrow estuaries is characterized by inflow near the bottom and outflow near the surface: the gravitational or classical estuarine circulation. A constant eddy viscosity, i.e. constant vertical mixing, is an important assumption of their model, which later research has shown to be invalid. Jay and Musiak [1996] hypothesized that the residual current structure is determined by an intra-tidal asymmetry in vertical mixing by the tidal straining of the density field, a mechanism first described by de Ruijter [1983], van Aken [1986] and Simpson et al. [1990]. Other research has supported this hypothesis [Burchard and Hetland, 2010; MacCready and Geyer, 2010; Geyer and MacCready, 2013, and references therein]. Model simulations by Burchard and Hetland [2010] suggest that under certain conditions tidal straining circulation might be more important than the gravitational circulation. Recently, several studies have shown that lateral cross-stream straining and lateral advection might also influence the residual circulation [Lerczak and Geyer, 2004; Scully et al., 2009; Burchard et al., 2011; Burchard and Schuttelaars, 2012; Basdurak et al., 2013].

Lerczak and Geyer [2004] were the first to show with idealized model simulations of a straight, stratified estuary that an ebb-flood asymmetry in lateral advection can modify the strength of the estuarine circulation. Lateral advection during flood transports high (low) momentum water to the lower (upper) part of the water column, which enhances the estuarine circulation. This process of momentum exchange is reversed during ebb. However, lateral advection during ebb is reduced by the presence of vertical stratification. This asymmetry in lateral advection enhances the estuarine circulation. Besides lateral advection, cross-stream tidal straining can also modify the estuarine circulation by altering the internal asymmetry in the eddy viscosity-vertical velocity shear covariance, as discussed by Burchard and Schuttelaars [2012]. These different cross-stream processes are difficult to isolate. Therefore, Burchard et al. [2011] expanded the definition of (total) tidal straining to all processes that contribute to the covariance of the eddy viscosity and vertical shear in velocity, thereby incorporating multiple processes into one single concept.

One of the main goals of estuarine research is to predict the estuarine exchange of salt, heat and suspended matter. Hansen and Rattray [1966] provided one of the first scalings of the estuarine circulation, which lacked the inclusion of important processes as tidal straining and lateral advection, but which predicted the strength of the estuarine circulation reasonably well using a constant eddy viscosity as a calibration parameter. Geyer et al. [2000] provided an alternative scaling, where the bottom friction replaced the constant eddy viscosity as a measure for vertical mixing. Seim et al. [2002]; Ralston et al. [2008] demonstrated that the assumption of bed-generated vertical mixing covering the entire water column is not always valid over an entire tidal cycle. Instead, they suggested an effective water depth based on a tidally-averaged height of the bottom boundary layer. All these scalings have in common that they include a measure for the strength of the baroclinic forcing and the strength of vertical mixing, and that they implicitly include processes as tidal straining and lateral advection. Scully et al. [2009] discussed the different feedbacks of the implicit processes on the strength of the predicted estuarine circulation.

These scalings assume that the estuarine circulation is best explained through a tidally-averaged approach. However, Nunes-Vaz et al. [1989] hypothesized that the gravitational circulation should increase during slack tides because of small vertical mixing. Stacey et al. [2001] observed an increased gravitational circulation around slack tides in a partially stratified estuary, confirming the hypothesis of Nunes-Vaz et al. [1989]. However, these pulses only occurred for periods with strong vertical stratification around slack before flood, where the horizontal Richardson number was greater than 3, indicating dampening of vertical mixing by tidal straining. The two studies indicate that the generation of estuarine circulation might be primarily a non-steady process.

Tide-bathymetry interaction and wind are two other important factors that contribute to the residual circulation in estuaries. On a basin scale, the tide-bathymetry interaction mainly drives depth-averaged residual currents and creates spatially-varying tidal asymmetries in velocity and duration [e.g. Aubrey and Speer, 1985; Speer and Aubrey, 1985; Friedrichs and Aubrey, 1988], which are determined by the hypsometry of the basin [Maas, 1997; Stanev and Wolff, 2003]. Furthermore, Li and O'Donnell [1997, 2005] theoretically showed that the depth-averaged inflow and outflow patterns in an estuary are dependent on the shape of the inlet and on the length of the basin, respectively.

Wind contributes to the net transport of water in a variety of ways. It can act as an additional source of kinetic energy which mixes the (upper layer of the) water column during high-energetic wind events [Goodrich et al., 1987; Li et al., 2006b]. However, wind can also modify the strength of the vertical stratification by wind straining, indirectly modifying the sub-tidal residual circulation, under moderate wind conditions [Scully et al., 2005; Chen and Sanford, 2009]. These studies mainly focused on local wind effects. Several studies have shown that

local and remote wind effects differ from one other [Wong, 1994; Wong and Moses-Hall, 1998; Wong and Valle-Levinson, 2002]. For example, Wong and Moses-Hall [1998] showed that remote wind effects influence sub-tidal water level fluctuations, whereas local wind effects influence the local currents.

The interaction between all these factors determines the vertical structure of the residual circulation in estuaries. Stacey et al. [2010] demonstrated that tidal asymmetries and baroclinic forcing have a superimposed effect on the residual current structure in the San Francisco Bay, whereas Guo and Valle-Levinson [2008] presented model simulations of the Chesapeake Bay, elucidating the impact of different wind directions on the density-driven circulation. Furthermore, Scully and Friedrichs [2007] demonstrated that barotropically-induced asymmetries in vertical mixing produce a spatial variation in vertical stratification which can modify the residual circulation. All these processes and feedback mechanisms make research on the estuarine circulation a complex matter.

Previous research in the Marsdiep basin has mainly focused on the basin-scale flushing rates and depth-averaged residual transport, which is mainly determined by bathymetry- and wind-driven currents [Zimmerman, 1976a; Ridderinkhof, 1988; Buijsman and Ridderinkhof, 2007a; Duran-Matute et al., 2014; Nauw et al., 2014]. The importance of tidal asymmetries, wind and density gradients to the vertical structure of the residual current has not yet been investigated in detail in the Marsdiep basin. Therefore, the objective of this study is to investigate the vertical structure of the residual currents in the Marsdiep, focusing on the estuarine circulation. A total of one hundred days of velocity observations distributed over three different seasons enables an investigation of the residual current structure under a wide variety of conditions.

Detailed information of the study site, the data collection and the analysis techniques is given in section 4.2. Section 4.3 discusses the observed contribution of tidal asymmetries, wind and especially density-related processes to the residual circulation. Section 4.4 discusses the estuarine dynamics in more detail. The main findings of this study are presented in section 4.5.

4.2 STUDY SITE, MATERIAL AND METHODS

4.2.1 *Study site*

The Marsdiep basin consists of two channels, the Texelstroom and the Malzwin channels, which are separated by an intertidal shoal (Figure 4.1b). The divergence and confluence points of these channels are located eastward of the Marsdiep inlet. A bottom frame is deployed in the Texelstroom channel as indicated in Figure 4.1b. The main sources of freshwater are the outlet sluices at Den Oever (DO) and Kornwerderzand (KWZ), which discharge freshwater from

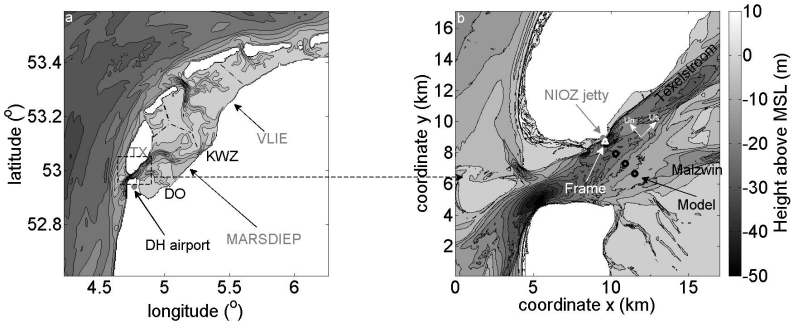

Figure 4.1: Bathymetric map of the Western Dutch Wadden Sea (a) and of the study site (b). The Marsdiep and Vlie basin are demarcated by the dashed-dotted black lines. Den Oever (DO) and Kornwerderzand (KWZ) are the freshwater outlet sluices of lake IJssel. The Marsdiep inlet is confined by the island of Texel (TX) to the north and by the city of Den Helder on the mainland to the south. The zoom-in on the study site shows the bifurcation of the Marsdiep channel into the Texelstroom and Malzwin channel. Also, the location of the bottom frame is indicated. Measurements of sea surface elevation and salinity are recorded at the NIOZ jetty. Wind conditions are recorded at Den Helder (DH) airport. A Cartesian reference frame is used in (b) with the origin to the southwest of the study site. The direction of the along-stream (Us) and cross-stream (Un) velocity components are indicated by the white arrows. The black circles in (b) indicate the location of the model output discussed in section 4.4.2.

lake IJssel during low water only. The water column is well-mixed during peak ebb and flood conditions and becomes weakly stratified around slack tide. For a more detailed description of the study site, the reader is referred to Chapter 3.

The depth-averaged horizontal circulation in the Marsdiep inlet is characterized by a net inflow at the shallower southern side and outflow at the deeper northern side [Buijsman and Ridderinkhof, 2007a]. The flood (ebb) currents are greater at the southern (northern) side of the inlet. The sub-tidal inlet-averaged transport through the Marsdiep inlet is determined by tidal stresses, freshwater discharge and wind stresses [Buijsman and Ridderinkhof, 2007b]. Duran-Matute et al. [2014] concluded from model simulations of the Western

Dutch Wadden Sea that the sub-tidal transport and flushing rates display varying patterns, depending on wind direction and strength. Nauw et al. [2014] observed a relationship between alongshore winds along the closed Dutch coast south of Den Helder and the sub-tidal transport in the Marsdiep inlet, suggesting that remote wind effects mainly determine the variation in sub-tidal transport. These studies focused on the inlet and basin-scale dynamics of flushing rates and sub-tidal transport. Thus far, the small-scale spatial variability has received little attention. A bottom frame is deployed in an ebb-dominant section, characterized by net outflow. Chapter 3 describes the vertical current structure at the same location using the same dataset and shows that density gradients modify the vertical shear in along-stream velocity in the upper part of the water column under weak currents. A mid-depth velocity maximum is observed during late flood. Vertical stratification during late flood is generated by cross-stream tidal straining and creates a mid-depth velocity maximum by dampening vertical momentum exchange. Furthermore, an asymmetry in near-bed vertical shear is observed with the greatest shear during ebb, which might have a negative feedback on strain-induced periodic stratification. The impact of these anomalies on (the variability of) the estuarine circulation in the Marsdiep basin has not yet been investigated. At the study site, the duration of slack before ebb (SBE) and slack before flood (SBF) differs strongly, being on average 52 and 14 minutes, respectively. Slack tide is here defined as the period around current reversal when the current is not uni-directional.

4.2.2 *Data collection and instrumentation*

The data collection and analysis of this paper are similar to Chapter 3, and therefore, parts of sections 4.2.2 and 4.2.3 are shortened versions of the former study. The dataset is collected on three occasions by deploying a 1.25m-high bottom frame at the north side of the Texelstroom channel (Figure 4.1b), equipped with an upward-looking four-beam 1.2MHz RDI Workhorse Monitor Acoustic Doppler Current Profiler (ADCP) and a conductivity, temperature, depth sensor (SBE 37-SM microCAT). The frame is placed on the seabed at a distance of approximately 200m from the Texel coast and approximately 300m southeast of the NIOZ jetty, in approximately 32m water depth. Each deployment is named after the season which covers the largest timespan of the deployment period, viz Summer, Autumn and Spring. The bottom frame is not equipped with a microCAT during the Summer deployment. Each deployment period has its own time reference (in UTC time), Day 0 being the day when the bottom frame is deployed.

The ping rate of the ADCP is set to 0.43 Hz and ensembles are recorded every 30 s containing 10 pings. The bin size is set to 0.5 meter, the number of bins to

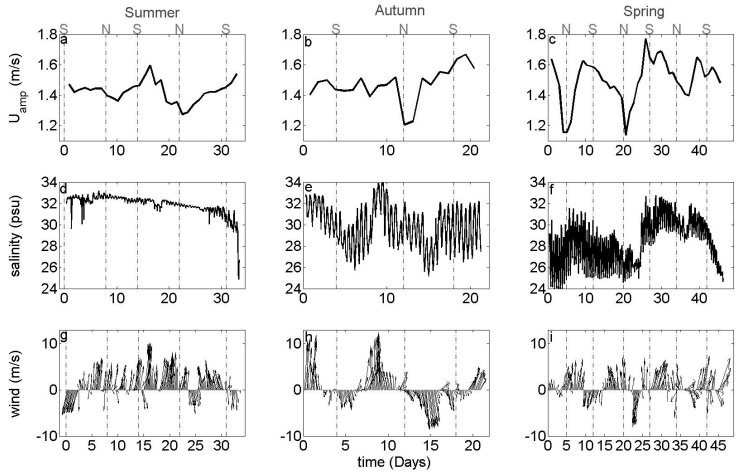

Figure 4.2: The current amplitude, the 10-minute averages of surface salinity at the NIOZ jetty and the wind vectors (upper to lower rows, resp.) for the Summer, Autumn and Spring deployments (left to right columns, resp.). The $Uamp$ is defined as half of the velocity range, recorded over 2 full tidal cycles. The spring (S) and neap (N) phases are indicated by the vertical dashed gray lines and are based on (astronomical) predictions of the sea surface elevation, i.e. two days after new/full Moon and two days after first and last quarter, respectively.

79 and the blanking distance to 0.5 meter. Therefore, the ADCP can effectively cover a range in water depths between 2 and 32 m above the bottom. The velocity data are stored in Earth coordinates (east-west, north-south velocities). The SBE 37-SM MicroCAT records one sample of conductivity, temperature and depth every 30 seconds.

At the NIOZ jetty (Figure 4.1b), the near-bottom pressure is measured at 2.9 Hz by a calibrated Keller 46 pressure sensor. The surface conductivity and temperature are measured by a calibrated Aanderaa conductivity and temperature 3211 sensor. The data are recorded every 12 seconds by an Aanderaa 3634 datalogger. The salinity is computed using the Practical Salinity Scale 78 [PSS-78, Fofonoff, 1985].

The tidal amplitude of the depth-averaged current velocity ($Uamp$), the salinity at the NIOZ jetty and the wind conditions at Den Helder Airport (Figure 4.1b, http://www.knmi.nl/klimatologie/uurgegevens/) in Figure 4.2 illustrate the conditions during the three measurement periods. Figure 4.2 shows a great temporal variability in salinity and wind conditions between the different seasons. Characteristics of Figure 4.2 are discussed in more detail in Chapter 3.

4.2.3 *Data processing*

First, the erroneous velocity data of the ADCP above the water surface are excluded by removing all data above the height of the surface echo. Then, the data are rotated from an east-west and north-south reference frame to an along-stream and cross-stream reference frame, defined as the dominant tidal velocity axis and the axis perpendicular to it, respectively, which results in an orientation as indicated in Figure 4.1b. The pitch and roll of the ADCP for each dataset varies in time due to morphological change of the seabed, but are almost always below 15 degrees. The only exception occurred between Day 7 and 15 of the Autumn deployment, when the pitch is 16 degrees. A visual inspection of the velocity data shows a coherent velocity structure and therefore the data is included in the analyses. However, the upper 5 meters of the water column displays velocity variations due to strong orbital wave velocities. To exclude the instantaneous effect of waves on the current, the upper 6 meters are removed. Only the lower 27.25 meters of the water column are included in further analyses. Therefore, any side-lobe interference is implicitly excluded from the analyses.

In order to include only complete tidal cycles in the analysis, all data before and after the first and last slack tide are removed. The data of the jetty and the wind data are interpolated at 30 seconds intervals to produce a collection of synoptic datasets.

4.2.4 *Data analyses*

Several aspects of the vertical structure of the residual currents are analyzed to investigate the role of wind, hypsometry and density gradients. First, to better understand the inter-tidal variability of the depth-averaged residual current, the asymmetry in magnitude and duration between ebb and flood is computed. Values are computed per two tidal cycles (approximately 24.84 hours) to remove any bias by the diurnal inequality. The start and end of the averaging period is taken at slack tide, which is defined as the moment that the depth-averaged current equals zero.

The asymmetry in magnitude of the tidal current, $MR_{F/E}$, is defined as the ratio between the peak flood (F) and ebb (E) currents. The asymmetry in current duration, $DR_{F/E}$, is quantified by the ratio between the fraction of time when the depth-averaged current is greater than (F) and smaller than (E) zero.

Second, the vertical profile of the residual current, $U_{res}(z,t)$, is investigated by time-averaging the vertical profiles of along-stream velocity over two tidal

cycles. The difference between the surface ($z = 27m$) and bottom ($z = 2.5m$) residual currents provides a measure for the observed estuarine circulation,

$$\Delta U_{res}(t) = U_{res}(27m,t) - U_{res}(2.5m,t). \tag{4.1}$$

The observed estuarine circulation in equation 4.1 is correlated with the Simpson number, Si, [e.g. Stacey et al., 2001]

$$Si = \frac{\beta g \frac{\partial s}{\partial x} H^2}{u^2_{*,amp}}, \tag{4.2}$$

where β is the saline contraction coefficient ($7.7{*}10^{-4}$), g is the gravitational acceleration (9.81 m/s^2), H is the water depth (m) and $\frac{\partial s}{\partial x}$ is the along-stream salinity gradient (psu/m) approximated by [Stacey et al., 2010]

$$\langle \frac{\partial s}{\partial x} \rangle = 2\pi \frac{S_{rms}}{L}, \tag{4.3}$$

where S_{rms} is the root-mean-square of salinity and L ($= u_{rms} * T$) is the tidal excursion length based on the root-mean-square of the depth-averaged along-stream velocity and the tidal period. The salinity is measured either at the bottom frame (Autumn and Spring) or, if the former is not available, at the NIOZ jetty (Summer). The computed values of $\frac{\partial s}{\partial x}$ correspond well with the values discussed in Chapter 2. The $u_{*,amp}$ in equation 4.2 is the mean of the peak ebb and flood friction velocities (m/s) and represents the amplitude of tidal mixing. Therefore, the value of Si primarily represents the hydrodynamic conditions during peak current conditions. The value of u_* is obtained from least-square fitting the law-of-the-wall equation to the vertical profiles of along-stream velocity as discussed by e.g. de Vries et al. [2015].

Third, ΔU_{res} is compared to the expected residual circulation, U_e, which is based on the solution by Geyer et al. [2000] who substituted the eddy viscosity by the drag coefficient, thereby enabling an easy and reliable way to compute the strength of the estuarine circulation [Scully et al., 2009; Valle-Levinson, 2010]

$$U_e = a_0 \frac{\beta g \frac{\partial s}{\partial x} H^2}{C_D U_{amp}}, \tag{4.4}$$

where a_0 is a calibration constant ($a_0 \sim 2.0$, here $a_0 = 2.5$) and C_D is a tidal average of the drag coefficient ($1{*}10^{-2}$; de Vries et al. [2015]). The constant a_0 is calibrated to match the conditions when the baroclinic and stress divergence terms in the tidally- and depth-averaged momentum balance each other (equation 4.8). Scully et al. [2009] found values of a_0 between 1.9 and 2.5 in their modelling study of the Hudson estuary, corresponding with the value for

the Marsdiep basin. Vertical mixing ($C_D U_{amp}$) in equation 4.4 is based on the tidal amplitude, implying that maximum mixing conditions are essential for the strength of the estuarine circulation. It is noted that the strength of U_e is only linearly related to vertical mixing, whereas for the Simpson number there is a squared relationship.

An alternative strength of the estuarine circulation, Ug_p, is computed following

$$Ug_p = \frac{\beta g \frac{\partial s}{\partial x} H^2}{|<u_*>|}, \tag{4.5}$$

where the friction velocity, $|<u_*>|$, is the absolute value of the mean friction velocity averaged over two tidal cycles. Here, vertical mixing is based on an estimate of the tidal average incorporating all tidal phases. Stacey et al. [2001] showed that the strength of the residual circulation during the time period that vertical mixing is negligible can be estimated assuming that the vertical mixing timescale is much shorter than the time scale over which the gravitational circulation develops (uT/H). The expected estuarine circulation, Ug_e, is then

$$Ug_e = \beta g \frac{\partial s}{\partial x} HT, \tag{4.6}$$

where T is the timescale over which the residual flow develops, i.e. the period of weak mixing. Equations 4.5 and 4.6 are used to investigate the dynamics around the slack tides. Furthermore, the observed shape of the residual current structure around the slack tides and the correlation to $\frac{\partial s}{\partial x}$ provide indications of the mechanisms that force the estuarine circulation.

Fourth, the processes that contribute to the residual circulation are investigated using the tidally-averaged along-stream momentum balance [Stacey et al., 2010]

$$\begin{aligned} 0 = &\underbrace{-g\langle\frac{\partial \eta}{\partial x}\rangle}_{(1)} \underbrace{-g\beta\langle\frac{\partial S}{\partial x}\rangle\frac{H}{2}}_{(2)} + \underbrace{\frac{<u_*|u_*|>}{H}}_{(3)} \underbrace{-\frac{\partial}{\partial y}[\langle\tilde{u}\tilde{v}\rangle]^z}_{(4)} \underbrace{-\frac{\partial}{\partial z}[\langle\tilde{u}\tilde{w}\rangle]^z}_{(5)} \\ &\underbrace{-\frac{1}{H^2}\langle\eta u_{*,s}|u_{*,s}|\rangle}_{(6)}, \end{aligned} \tag{4.7}$$

where η is the sea surface elevation, $\sim$ denotes the instantaneous along-stream (u), cross-stream (v) and vertical (w) velocity components, and $u_{*,s}$ is the surface-boundary wind-friction velocity. The angled brackets denote a tidally-averaged value and the straight brackets indicate integration over depth, z. The along-stream and cross-stream direction are indicated by x and y, respectively.

The terms on the right hand side represent the barotropic pressure gradient (1), the baroclinic pressure gradient (2), the vertical stress divergence (3), the lateral advection (4), the vertical advection (5) and the wind stress (6). Only the Spring deployment is discussed in detail because of the great range in salinity gradients during that period. The wind forcing was small during this period and therefore term 6 is excluded. Because of the small vertical velocities, it is difficult to reliably estimate the vertical advection term. For now, this term is assumed small and the results presented in section 4.3.4 seem to sustain this assumption. Excluding terms 5 and 6, the momentum balance is reduced to

$$0 = \underbrace{-g\langle\frac{\partial\eta}{\partial x}\rangle}_{(1)} \underbrace{-g\beta\langle\frac{\partial S}{\partial x}\rangle\frac{H}{2}}_{(2)} + \underbrace{\frac{<u_*|u_*|>}{H}}_{(3)} \underbrace{-\frac{\partial}{\partial y}[\langle\tilde{u}\tilde{v}\rangle]^z}_{(4)}. \tag{4.8}$$

The lateral advection term is estimated following Stacey et al. [2010]. They assumed that the tidal stress goes to zero near the boundary, so the lateral gradient can be estimated by dividing the lateral advection term by the distance from the boundary (200m). Unfortunately, no estimate of the barotropic term is available. The observations presented in section 4.3.4 show that only the last 3 terms in equation 4.8 are required to close the momentum balance of the residual current, suggesting that the tidally-averaged value of the barotropic term is small.

4.3 OBSERVATIONS

4.3.1 *Forcing of the depth-averaged residual current*

In essence, residual currents arise from the difference in strength and duration between the ebb and flood current. To understand the forcing mechanisms that explain this difference, it is useful to analyze the characteristics of the tidal asymmetries of the depth-averaged current. This section shows that tidal asymmetries in the Marsdiep basin are mainly influenced by the spring-neap tidal cycle and the wind.

Generally, the ratio between peak flood and peak ebb currents, $MR_{F/E}$, is smaller than one (Figure 4.3a-c). The gray lines in Figure 4.3a show that it is important to consider the effect of diurnal inequality by averaging over two tidal cycles. Furthermore, the duration asymmetry, $DR_{F/E}$, is also smaller than one (Figure 4.3d-f). So at the study site, currents are generally ebb-dominant in magnitude and duration, which corresponds well with the horizontal residual circulation cell described in section 4.2.1. Our observations suggest that the asymmetry in magnitude as well as the duration contribute to the characteristics of the horizontal circulation cell. Differential advection of vorticity

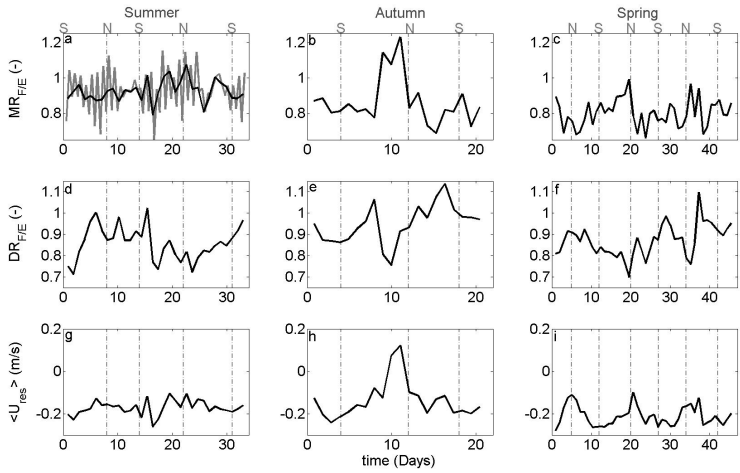

Figure 4.3: Asymmetry in strength, $MR_{F/E}$, and duration, $DR_{F/E}$, (1st and 2nd rows) and depth-averaged residual velocity, $\langle U_{res} \rangle$, (3rd row) for the Summer, Autumn and Spring deployments (left to right column, respectively). In (a), $MR_{F/E}$ is computed for one and two tidal cycles (gray and black line, respectively) to illustrate the effect of the diurnal inequality.

generated by the bathymetry has been suggested by Zimmerman [1976b], Ridderinkhof [1989] and Buijsman and Ridderinkhof [2007a] to drive the horizontal circulation cell.

The tidally-integrated and depth-averaged residual current, $\langle U_{res} \rangle$, displays a strong spring-neap tidal variability, which is obscured in the tidal asymmetries (Figure 4.3g-i). Generally, the residual current is in seaward direction and almost doubles from neap to spring tide conditions (Figure 4.3i). It shows a spring-neap tidal modulation of the horizontal circulation cell in the Marsdiep inlet due to tide-topography interactions. However, wind forcing also plays a role. During the major storm events around Day 10 in Autumn, there is inflow at the study site (Figure 4.3h). Furthermore, the strong winds in Summer obscure the tidal signal so clearly present in Spring.

The influence of wind on the tidal asymmetry is characterized by various patterns. Persistently weak southwesterly (up-estuary) winds correlate with an increase in duration asymmetry, as indicated by a gradual decrease in $DR_{F/E}$ from 1 to 0.72 between Day 6 and 22 in Summer, whereas $MR_{F/E}$ remains relatively constant. However, when the wind direction is more variable, as between Day 20 and 45 in Spring, the $DR_{F/E}$ increases. So, the response of both asym-

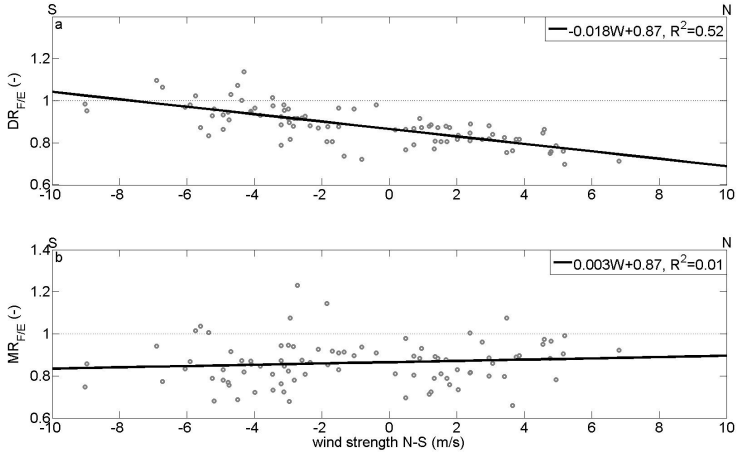

Figure 4.4: Ratio between flood and ebb duration, $DR_{F/E}$ in (a), and magnitude, $MR_{F/E}$ in (b), as a function of north (positive) and south (negative) winds. Wind is defined as the direction of origin. The gray icons indicate values of individual tidal cycles. The black lines are the linear fits, where the relationship and R^2 are indicated in the legend of each panel. The dotted horizontal gray lines indicate the transition from ebb- to flood-dominant asymmetric conditions.

metries varies as a function of wind strength, direction and duration, where a distinction can be made between moderate and major wind conditions.

The effect of moderate winds on tidal asymmetries is further highlighted in Figure 4.4. It displays the relationship between north-south winds and the tidal asymmetries. The wind direction indicates the wind origin. The relationship between along-stream winds and tidal asymmetry is also analyzed, but displayed a less significant relationship (not depicted). There is an evident relationship between the wind and the ratio of flood-ebb duration, $DR_{F/E}$, characterized by an increase in (ebb-dominant) duration asymmetry for winds from a northerly direction (Figure 4.4a), whereas it is insignificant for the ratio of current magnitude ($MR_{F/E}$, Figure 4.4b). Wind above 7.6 m/s (Beaufort 4) from the south changes the duration asymmetry from ebb-dominant to flood-dominant.

The good correlation of the duration asymmetry with the day-averaged north-south winds suggests that remote wind effects are important. The correlation between the duration asymmetry and day-averaged along-estuary winds is small (R^2=0.18), indicating that local atmospheric processes above the channel are less important. These trends suggest that the duration is mainly driven by atmo-

spheric processes above the North Sea, supporting the coastal current along the approximate North-South Dutch coastline, as was also discussed by Nauw et al. [2014]. So, the wind principally modifies the strength of the depth-averaged residual current by altering the duration asymmetry, which is predominantly a remote wind effect.

Strong winds from the southwest (major storm events) have a profound impact on the asymmetry. They are capable of reversing the magnitude and duration asymmetry during a short time period, which result in peak flood currents and flood duration being greater than during ebb (Autumn, Day 8-12, Figures 4.2h;4.3b). Furthermore, they have a longer-lasting impact on the asymmetry because asymmetries require several days to return to equilibrium (e.g. Autumn Day 8-12, Figure 4.3b,e). Also, high-energetic winds from the southwest in Summer and Autumn decrease or reverse the depth-averaged residual current.

4.3.2 *Vertical structure of the residual current*

While keeping the characteristics of the depth-averaged current in mind, the variability of the vertical structure of the residual current is presented in this section. The observations indicate that the vertical profiles of the along-stream residual current are mostly determined by the baroclinic pressure gradient. The tidal amplitude and wind mainly determine the strength of the depth-averaged residual current. Surprisingly, fortnightly variations in vertical mixing seem not to influence the strength of the residual circulation.

Figure 4.5 shows that the vertical profiles of U_{res} are characterized by a great inter-seasonal variability. The vertical variation in residual currents is smaller in Summer than in Autumn and Spring and the vertical structure is characterized by more uniform vertical profiles. The vertical variation scales well with the intra-tidal salinity excursion (figure 4.2d-f). In Figure 4.6a, the ΔU_{res} of all deployments shows a good correlation with the horizontal Richardson number, demonstrating that the baroclinic pressure gradient has a strong impact on the shape of the vertical profiles of U_{res}.

In Spring, a fortnightly modulation of U_{res} is apparent, which corresponds with the spring-neap tidal cycle. The near-bed residual currents are smaller or even landward-directed during neap tide (Day 5, 21 and 35, Figure 4.5e). Coincidentally, the near-surface residual currents are also smaller during neap tide. Figure 4.6b shows more clearly that for all deployments the magnitude of the depth-averaged residual current is a function of tidal amplitude, suggesting a spring-neap tidal variation in the depth-averaged residual current. It elucidates two important aspects of the residual currents in the Marsdiep basin. Firstly, the magnitude of the depth-averaged residual current oscillates on a fortnightly timescale (under a constant density forcing). Secondly, superimposed on the

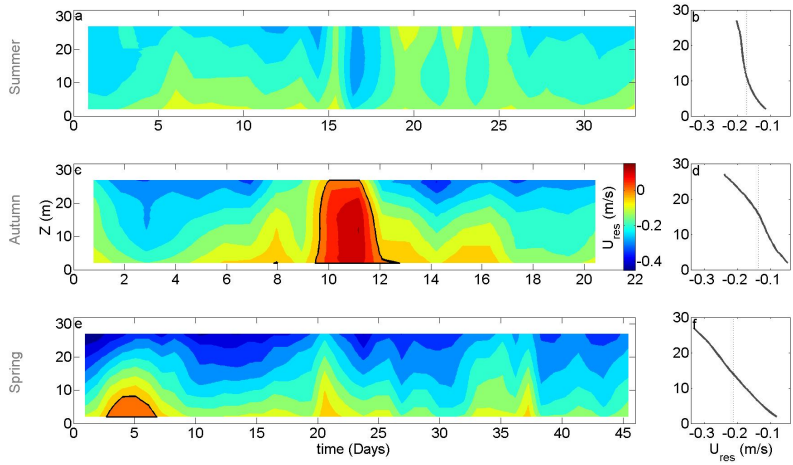

Figure 4.5: Vertical profiles of the residual currents, U_{res}, for Summer, Autumn and Spring as a function of time (first to third rows of left column, respectively). The y-axis represents the height above the bed (Z). The black line indicates U_{res} equals zero. The right column shows the averaged residual current structure for each dataset, where the vertical black dotted line indicates the depth-averaged residual current.

fortnightly oscillation of the depth-averaged current, ΔU_{res} remains fairly constant (Figure 4.5a,c,e). Variations in the tidal amplitude and associated vertical mixing only seem of minor importance in shaping ΔU_{res}. The spring-neap tidal modulation of the depth-averaged residual current might be crucial in determining the net flux of total suspended matter in the lower part of the water column. However, the strength of the estuarine circulation appears not to be influenced by the tidal amplitude and is mainly determined by the baroclinic pressure gradient.

Wind has multiple impacts on the shape of the residual circulation. First, persistent winds influence U_{res} in the upper part of the water column, as exemplified in Summer (Figure 4.2g;4.3a). Between Day 20 and 25, persistent southwesterly winds decrease the magnitude of outflow in the upper part of the water column. It corresponds with wind straining in up-estuary direction as described by Scully et al. [2005]. Second, storm events drive uni-directional currents, which are capable of reversing the typical outflow observed at the study site. A major storm event between Day 9 and 12 in Autumn from a south-southwestern direction drives landward-directed currents over the entire water column. The strongest landward-directed currents are located in the lower part

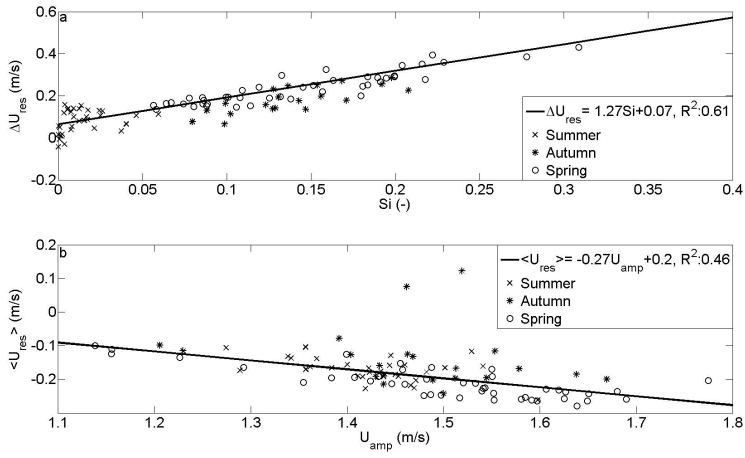

Figure 4.6: Relationship (a) between ΔU_{res} and Simpson number, Si, and (b) the depth-averaged residual current, $\langle U_{res} \rangle$, and the tidal amplitude, U_{amp}. The ΔU_{res} is based on the difference between the bottom and surface values at 2.5 and 27 m above the bed, respectively. The black lines indicate the linear fit with the individual data points, where the linear relation and R^2 are quantified in the legends.

of the water column, which suggests a superimposed effect of the density gradients on the wind-driven depth-averaged residual current. The first pattern most likely corresponds with local wind forcing, whereas the second is probably related to remote wind effects, which primarily influence the duration asymmetry.

The median vertical profiles of U_{res} summarize the contribution of the different forcing agents to the residual current structure. The depth-averaged residual, seaward currents are mainly driven by tidal asymmetries, which may decrease or even reverse during major southwesterly storms. The vertical shear of the residual current is principally driven by the baroclinic pressure gradient.

4.3.3 *Scaling of the estuarine circulation*

The relationship between the Simpson number and ΔU_{res} indicates the existence of an estuarine circulation in the Marsdiep basin, which is superimposed on the wind- and bathymetry-driven depth-averaged residual current. To further support these observations, the magnitude of the estuarine circulation is validated using equation 4.4, which considers the effects of baroclinic forcing

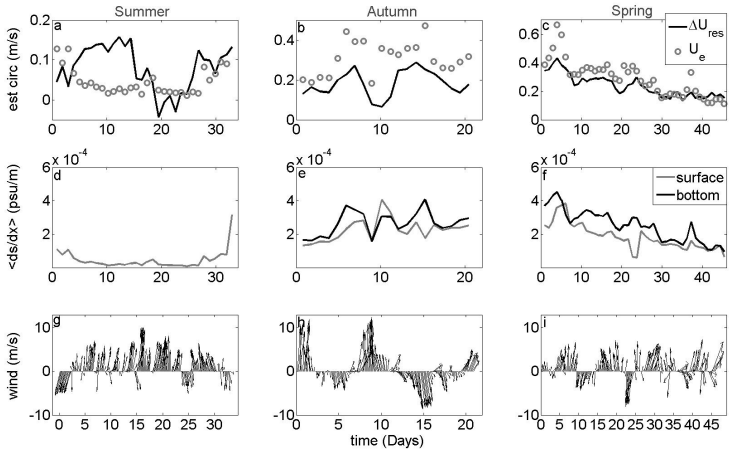

Figure 4.7: Time evolution of (first row:) the observed (ΔU_{res}, equation 4.1) and predicted (U_e, equation 4.4) estuarine circulation; of (second row:) the horizontal surface and bottom salinity gradient, $\langle \frac{\partial s}{\partial x} \rangle$; and (third row:) of the wind direction and magnitude for Summer, Autumn and Spring (left to right column, respectively). No bottom salinity is available in Summer (absence of black line in d).

and vertical mixing. The scaling predicts the strength of the estuarine circulation well for a limited range of salinity gradients.

Under very weak baroclinic forcing as in Summer (Figure 4.7a,d), the magnitude of the computed estuarine circulation, U_e, corresponds poorly to the magnitude of ΔU_{res}. The small salinity gradients ($\frac{\partial s}{\partial x}$<1*10^{-4} psu/m) are not sufficiently strong to drive a measureable estuarine circulation. Therefore, the observed residual circulation seems mainly determined by the barotropic tide and/or by the wind.

Under moderate and strong baroclinic forcing ($\frac{\partial s}{\partial x}$>1*10^{-4} psu/m), the scaling U_e matches reasonably well with the observations of ΔU_{res}, as is shown for Autumn and Spring (Figure 4.7b,c,e,f). Interestingly, there is no spring-neap tidal modulation discernable in Spring. The strength of the estuarine circulation seems mostly determined by the strength of $\frac{\partial s}{\partial x}$. The U_e overestimates for salinity gradients greater than approximately 2.5*10^{-4} psu/m, suggesting that other processes become increasingly important for stronger salinity gradients.

The effect of wind on the estuarine circulation varies as a function of its strength, direction and duration. The major southwesterly storm event around Day 10 of Autumn reduces the estuarine circulation as expected from the calculated salinity gradient (second column, Figure 4.7). The minor northwesterly

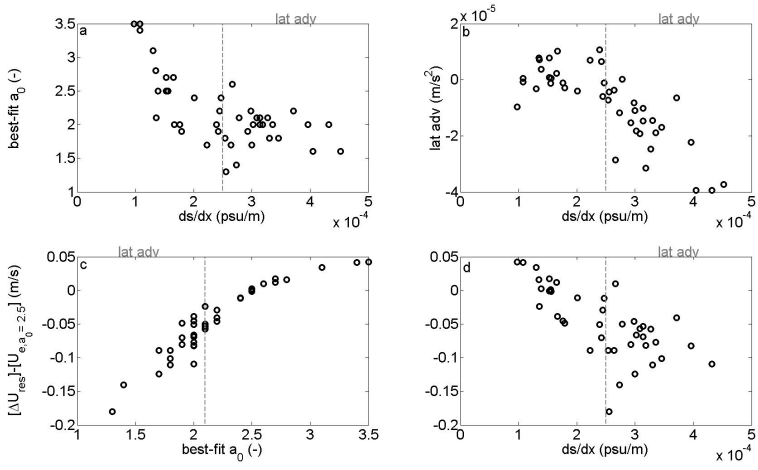

Figure 4.8: Dependency of the value a_0 in equation 4.4 on the strength of lateral advection and on the along-stream salinity gradient, $\frac{\partial s}{\partial x}$. The relationship between the best-fitted value of parameter a_0 and $\frac{\partial s}{\partial x}$, and between the lateral advection term in equation 4.8 and $\frac{\partial s}{\partial x}$ is given in a) and b), respectively. A bias in estimate of U_e is indicated by the difference in U_e,a_0=2.5 and ΔU_{res} as a function of the best-fitted value of parameter a_0 and $\frac{\partial s}{\partial x}$ as shown in c) and d), respectively.

storm on Day 15 of Autumn has a limited effect on the vertical structure in the sheltered Marsdiep basin. The modification of the residual current in the upper part of the water column between Day 15 and 25 of Summer by persistent along-channel winds appears not to have a significant impact on the overall strength of U_e and is mostly restricted to the upper 5 to 10 m of the water column (first column, Figure 4.7).

The role of a_0 in accurately predicting U_e under a range of salinity gradients and the relationship of a_0 with lateral advection is investigated in Figure 4.8. The best-fit value of a_0 decreases for greater salinity gradients (Figure 4.8a). The absolute value of the lateral advection term in 4.8 simultaneously increases for greater salinity gradients (Figure 4.8b), suggesting that lateral advection becomes increasingly important and that it generates a decrease in strength of the estuarine circulation. This lowering in ΔU_{res} is implicitly incorporated in a decrease in a_0. The overestimation by assuming a constant a_0 (2.5) is quantified by taking the difference between U_e,a_0=2.5 and ΔU_{res} as a function of the best-fit value of a_0 (Figure 4.8c). Best-fit values of a_0 smaller than 2.1 and $\frac{\partial s}{\partial x}$ greater than 2.5*10^{-4} psu/m show a large overestimation of U_e up to 0.2 m/s in the

period that lateral advection is important. In the absence of lateral advection, the estimation of U_e,a_0=2.5 is accurate (Figure 4.8c,d). In section 4.3.4, the contribution of lateral advection in the Marsdiep basin to the depth-averaged tidally-averaged momentum balance is investigated in more detail.

The scaling of the estuarine circulation applies reasonably well for a limited range of salinity gradients. Lateral advection and other incorporated processes in a_0 are able to modify the strength of the estuarine circulation and inhibit an understanding of the processes that drive the estuarine circulation in the Marsdiep. Scully et al. [2009] showed using model simulations of the Hudson Estuary that the predictive skill of several estuarine scalings decreases with increasing river discharge. They found that lateral advection increases the estuarine circulation, whereas the observations presented in this study show a decrease in estuarine circulation in a periodically-stratified estuary. To better understand the estuarine dynamics, the processes that contribute to the estuarine circulation are examined in more detail in the next section.

4.3.4 *Estuarine processes*

Processes such as total tidal straining circulation, gravitational circulation and lateral advection all contribute to the strength of the estuarine circulation. This section shows that the importance of classical tidal straining circulation at the study site is negligible, whereas the gravitational circulation, lateral advection and possibly other cross-stream processes play an important role in the estuarine dynamics of the Marsdiep.

Generally in estuaries, classical tidal straining circulation is created during (late) ebb and is characterized by the greatest difference between the surface and bottom currents around SBF, as is discussed for example in the review paper on the estuarine circulation by Geyer and MacCready [2013]. A time-average of the current reversal around SBF is expected to produce a vertical structure similar to the estuarine circulation, which should also scale with the baroclinic forcing. Around SBE, no correlation is expected because tidal straining is absent. The observations in the Marsdiep display the opposite pattern.

The bottom-to-surface difference averaged over SBE and SBF as a function of $\frac{\partial s}{\partial x}$ is depicted in Figure 4.9. The slack period is defined as the period that the current is not uni-directional. To exclude high-energetic wind effects and weak baroclinic forcing, only the Spring deployment is used. Interestingly, the difference around SBF is independent of $\frac{\partial s}{\partial x}$, which suggests that classical tidal straining is not important at the study site (Figure 4.9a). To the contrary, strong slack-averaged velocity differences are present around SBE and correlate positively with the strength of $\frac{\partial s}{\partial x}$ (Figure 4.9b). The magnitude of the slack-averaged vertical difference around SBE is of the same magnitude as ΔU_{res} in Figure 4.7c,

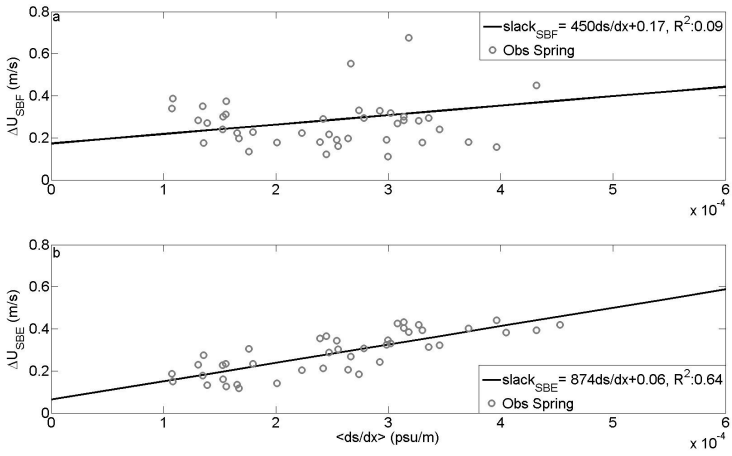

Figure 4.9: Bottom-to-surface difference, in slack-averaged currents as a function of $\langle \frac{\partial s}{\partial x} \rangle$ for all the tidal cycles of the Spring deployment (Obs Spring). The upper panel shows the relationship for slack before flood (SBF) and the lower panel for slack before ebb (SBE). Slack tide is defined as the period that the current is not uni-directional over the vertical.

which suggests that the estuarine circulation is for a large part generated during late flood and SBE. The well-mixed conditions, resulting from the strong currents during ebb are the most likely explanation for the absence of classical tidal straining circulation, as discussed in Chapters 2 and 3 and in more detail in section 4.4.1.

The correlation between the slack-averaged top-to-bottom difference and the Simpson number is also investigated but lacked good correlation. It indicates that vertical mixing is of minor importance for the generation of slack-residual vertical difference in velocity. The insignificance of vertical mixing to the strength of the estuarine circulation explains the absence of a spring-neap tidal modulation in estuarine circulation and suggests that the estuarine circulation is mainly generated under weak current conditions.

The top-to-bottom difference around SBE might be generated by the gravitational circulation and/or cross-stream straining during weak currents, and it is therefore worthwhile to zoom in further on this topic. The strength of the gravitational circulation is computed using equations 4.5 and 4.6 to investigate if gravitational circulation is able to generate slack-residual current profiles of this magnitude. A tidal average of the gravitational circulation is based on the strength of vertical mixing, here represented by $|<u_*>|$ (Figure 4.10a). The gravitational or baroclinic circulation, Ug_p, is negligible compared to ΔU_{res}

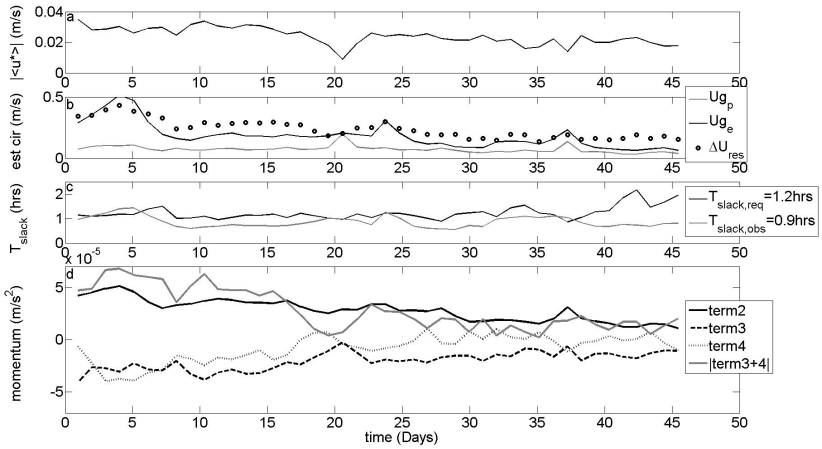

Figure 4.10: Scaling of gravitational circulation based on equations 4.5 and 4.6 and overview of the terms of the depth-averaged along-stream momentum balance as given in equation 4.8 for the Spring deployment. (a) shows the tidal average of u_*, (b) shows the observed (ΔU_{res}), expected (Ug_e) and predicted (Ug_p) gravitational circulation, (c) shows the time available around slack tide that Ug_e can develop, $T_{slack,obs}$, and the time required for Ug_e to develop, $T_{slack,req}$, and (d) shows the terms of the momentum balance as given in equation 4.8. Term 2, 3 and 4 are the baroclinic, stress divergence and lateral advection term, respectively.

(Figure 4.10b). Using a tidally-averaged approach, the gravitational circulation seems not to contribute to the estuarine circulation. However, if the strength of the gravitational circulation is computed based on the available time during which vertical mixing is negligible (Figure 4.10c), the strength of Ug_e corresponds well with the observations. It strengthens the hypothesis that the slack-residual currents around SBE are partly generated by the gravitational circulation.

To investigate the contribution of lateral advection in more detail, the tidally-averaged and intra-tidal momentum balances (equation 4.8) are analyzed. The tidally-averaged along-stream momentum balance shows that for higher freshwater discharge conditions, the baroclinic term is balanced by lateral advection and vertical stress divergence (Figure 4.10d). For smaller freshwater discharge conditions, the baroclinic term is only balanced by the vertical stress divergence term. The transition between both regimes is at approximately $2.5*10^{-4}$ psu/m (Figure 4.7f) or around Day 20 (Figure 4.10d). During the first 20 Days of

Term	2	3	4	1+ϵ
	10^{-5} m/s^{-2}	10^{-5} m/s^{-2}	10^{-5} m/s^{-2}	10^{-5} m/s^{-2}
Summer	0.5	-0.7	0.3	0.1
Autumn	3.0	-1.0	-0.5	1.5
Spring	2.8	-2.0	-0.8	0

Table 4.1: Terms in equation 4.8 computed for each lander deployment. Terms 2, 3 and 4 are the baroclinic, stress divergence and lateral advection terms, respectively. The barotropic term and unexplained part (1+ϵ) is given in the last column.

Spring, the lateral advection term is of the same magnitude or greater than the stress divergence term. The summation of both terms equals the magnitude of the baroclinic term. When the strength of the baroclinic term decreases, the lateral advection terms decreases by an order of magnitude, whereas the stress divergence term decreases to a constant value between 1-3*10^{-5} m/s ^{2}. The negative value of the lateral advection term corresponds with the overestimation of U_e as shown in Figure 4.7c. In Table 4.1, an overview of the momentum terms is given for each deployment, which shows that the momentum balance is closed by the baroclinic, stress divergence and lateral advection terms in Summer and Spring. The balance in Autumn is most likely disturbed due to the major storm event. An estimation of the wind term in equation 4.8 is troublesome because of the sheltering effect of the island of Texel. Based on the unexplained part of the terms in equation 4.8 for Autumn, the wind term is approximately -1.5*10^{-5} m/s^{2}.

So far, the observations indicate that classical tidal straining is negligible at the study site, whereas pulses of gravitational circulation and the occurrence of asymmetric lateral advection are important. To further investigate the importance of the cross-stream circulation and lateral advection during distinct phases of the tide, the near-bed and near-surface cross-stream currents and the lateral advection term of the intra-tidal momentum balance are depicted in Figure 4.11. Two spring tidal cycles of Spring were selected with different along-stream salinity gradients, named weak and strong baroclinicity. Estimates are based on 10-minute averages.

The intra-tidal variability during strong baroclinicity is characterized by an ebb-dominant asymmetry in lateral advection. A strong negative lateral advection is observed during peak ebb of the strong baroclinic conditions, whereas lateral advection is small during flood (Figure 4.11e). Strong cross-stream circulation cells are present during both ebb and flood which suggest that cross-stream tidal straining might be important (Figure 4.11c,d). The cross-stream

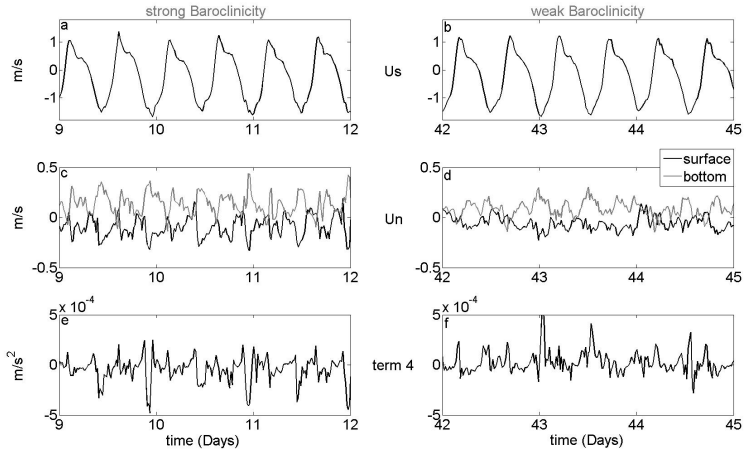

Figure 4.11: Overview of the depth-averaged along-stream current (a,b), of the near-bottom and near-surface cross-stream currents (c,d) and of the lateral advection term (e,f) of intra-tidal depth-averaged along-stream momentum balance in 4.8 for strong and weak baroclinicity (left and right column, resp.) as observed during Spring.

circulation cells are stronger during strong baroclinicity. de Vries et al. [2015] suggest that cross-stream tidal straining is important during late flood. Buijsman and Ridderinkhof [2008c] provide a thorough analysis of the mechanisms that drive the cross-stream currents in the Marsdiep inlet. The potential contribution of cross-stream straining is discussed in more detail in section 4.4.1.

4.4 DISCUSSION

4.4.1 *Estuarine dynamics*

Previous observations in Chapter 3 and de Vries et al. [2015] show great shifts in hydrodynamic conditions in the Marsdiep over one tidal cycle. Large currents occur during (late) ebb and the duration of slack before ebb is short. Both diminish the importance of the classical tidal straining mechanism. The well-mixed conditions during peak flood are followed by a long period of low current velocities during late flood, where vertical stratification is able to develop. The observations in this chapter suggest that the vertical profile of the residual current is mainly generated during late flood and slack before ebb. This period of weak currents is characterized by cross-stream tidal straining and by the presence of vertical stratification. In this section, the dynamics of the generation

mechanisms of the non-steady estuarine circulation during late flood are discussed and compared with literature.

A non-steady oscillation in strength of the estuarine circulation has already been described in literature as pulse-like behavior originating from decreased energetic conditions [Nunes-Vaz et al., 1989; Stacey et al., 2001]. Stacey et al. [2001] observed pulse-like behavior of the estuarine circulation during weak ebb for $Si > 3$, and they related these pulses to the interaction of the currents and strain-induced stratification. They hypothesized that strain-induced stratification is able to significantly dampen vertical mixing which in turn increases the vertical gradients in velocity for high Si values. Classical tidal straining is only expected to occur during late ebb, but cross-stream tidal straining might be able to modify the shape of the vertical profile of velocity during other phases of the tidal cycle.

The timing of vertical stratification is a crucial component for the strength and direction of the estuarine circulation, as already demonstrated by Stacey et al. [2008] using idealized model simulations. They implied that vertical stratification during late flood produces a reversed estuarine circulation, but neglected the directional influence of the baroclinic pressure gradient. Chapter 3 shows that vertical stratification develops during late flood and produces a reversal in sign of the vertical shears in velocity in the upper part of the water column as a result of the directional influence of the baroclinic pressure gradient, which is not present in the idealized simulations of Stacey et al. [2008]. This chapter shows that vertical stratification during late flood can generate a classical estuarine circulation, which is an unexpected feature based on typical estuarine stratification dynamics. If the internal tidal asymmetry in vertical stratification is not capable of explaining the observed estuarine circulation, the question arises which processes are responsible.

First, the gravitational circulation is able to drive an estuarine circulation of the observed magnitude because of the long duration of weak current conditions around slack before ebb as discussed in section 4.3.4. Second, cross-stream tidal straining and lateral advection might also modify the strength of the estuarine circulation as discussed by e.g. Burchard and Schuttelaars [2012]. With the available data, it is impossible to isolate the different processes because these processes are inter-connected and both depend on the cross-stream salinity gradient. However, inferences can be made.

An asymmetry in lateral advection modifies the strength of the estuarine circulation for salinity gradients greater than $2.5 * 10^{-4}$ psu/m. The ebb-dominant asymmetry is opposite to the flood-dominant asymmetry, first described by Lerczak and Geyer [2004], and it therefore results in a decrease in strength of the estuarine circulation. The opposite asymmetry observed at the Marsdiep study site might be determined by several conditions. Curvature effects are important in the Marsdiep inlet, which are stronger during the larger ebb currents. In

addition, the absence of vertical stratification during ebb due to the high currents inhibits the dampening of lateral advection by a stratified water column. More research is required to investigate the effect of tidal asymmetries and temporally-varying vertical stratification on the strength of lateral advection. Important in the discussion here is that the asymmetry in lateral advection decreases the strength of the estuarine circulation and therefore seems not to be important for the generation of the estuarine circulation during late flood.

Burchard and Schuttelaars [2012] showed that cross-stream straining and lateral momentum advection can significantly modify the covariance between the eddy viscosity and the vertical shear in velocity, which might also be important in the Marsdiep. The definition of total tidal straining, which includes all processes that modify the above-mentioned covariance, might therefore contribute to the generation of the estuarine circulation during late flood. However, it is not possible to isolate these processes with the available data. A future study will focus on the turbulence characteristics at the study site and can shed light on the covariance between eddy viscosity and vertical shear in velocity.

This study shows clearly that, under certain conditions, an estuarine circulation is present in the Marsdiep basin. The estuarine circulation is mainly generated during late flood and slack before ebb because of the long duration of weak current conditions. The strong current conditions during peak and late ebb diminish the contribution of tidal straining circulation. The estuarine circulation is generated predominantly under weak currents, which implies that the duration of the weak current conditions rather than the magnitude of the tidal amplitude is important for the strength of the gravitational circulation in the Marsdiep. This feature also explains the observed absence of a fortnightly modulation in estuarine circulation. Furthermore, it also suggests that the observed asymmetries in bed friction in Chapter 3 are of minor importance for scaling the strength of the estuarine circulation in periodically-stratified estuaries.

4.4.2 *Spatial variability - model simulations*

This study focuses on the observed dynamics of the estuarine circulation at one single location. However, the hydrodynamic conditions in the Marsdiep are characterized by a great spatial variability [Buijsman and Ridderinkhof, 2007a; de Vries et al., 2014]. Therefore, the strength of the estuarine circulation might vary spatially as a result of variations in water depth and tidal asymmetries, which is highlighted in this section.

Variations in water depth and in tidal asymmetries can modify the interaction between currents, stratification and vertical shear in velocity. The observations at the study site imply that the barotropic residual current is superimposed on

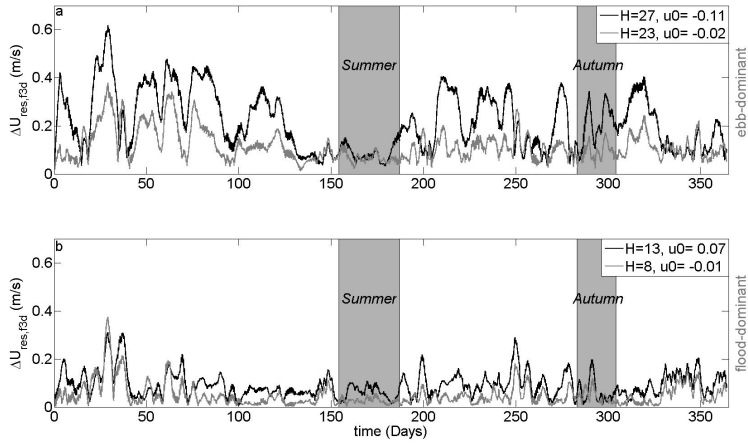

Figure 4.12: Modelled vertical difference in residual currents, $\Delta U_{res,f3d}$, for 2011 along a lateral transect in the Texelstroom channel. The $\Delta U_{res,f3d}$ is based on the top-to-bottom sub-tidal velocity difference computed with a 3-day low-pass filter. The upper and lower panel indicate the northern ebb- and southern flood-dominant section of the channel, respectively. Water depth (H) and the yearly residual of the depth-averaged current (u_0) are indicated in the legends. Day 0 is January 1, 2011. The two periods when the bottom frame is deployed are indicated by the filled gray areas.

the estuarine circulation. However, it is not known whether this also applies to shallower water depths.

The tidal currents are flood-dominant in the southern part, which is shallower by 5-10 m. Therefore, the transition from a well-mixed to a weakly-stratified state may occur during different moments of the tidal cycle. The unsteadiness (velocity) parameter, Un, proposed by Burchard et al. [2011] is defined as

$$Un = \frac{\omega H}{u_*}, \tag{4.9}$$

where ω is the tidal frequency, u_* is the friction velocity, H is the water depth and Un is a measure for bottom boundary layer mixing. The value of Un is expected to be smaller for the flood-dominant southern side of the Marsdiep and indicates that the water column will be well-mixed for a longer time period, as implied in Chapter 2.

Model simulations from the western Dutch Wadden Sea, described in detail by Duran-Matute et al. [2014], are used to illustrate the spatial variability of the estuarine circulation (Figure 4.12). The $\Delta U_{res,f3d}$, indicative of the estu-

arine circulation, is based on a top-to-bottom difference in sub-tidal velocity. The sub-tidal velocity is computed with a 3-day low-pass filter. The locations of the model output are indicated in Figure 4.1b. The estuarine circulation is characterized by a large lateral variability with the strongest sub-tidal residual circulation located in the ebb-dominant deeper northern part. The estuarine circulation decreases southward with decreasing water depth. So a spatial pattern is discernable, which is characterized by a decrease in estuarine circulation for smaller water depths and agrees with the expected pattern in Un. This spatial variability might have important implications for the transport pathways and residence times.

In the shallower flood-dominant southern part, the $\Delta U_{res,f3d}$ is small and the net transport of salt and suspended matter is most likely uniformly directed into the basin. In the deeper ebb-dominant northern part, the residual shear is large, resulting in enhanced outflow near the surface and diminished outflow, or even inflow, near the bed. The vertical distributions of salt and suspended matter seem therefore more important for the net transport pathways in the deeper part of the Texelstroom channel. It is hypothesized that in the deeper ebb-dominant part, the estuarine circulation might be the crucial component in determining if the net transport of near-bed suspended matter is directed into or away from the Wadden Sea.

4.5 CONCLUSIONS

One hundred days of current and salinity data obtained in Spring, Summer and Autumn are analyzed to investigate the vertical structure of the residual circulation. Bathymetry- and wind-driven residual currents primarily contribute to the strength and direction of the depth-averaged residual current. Remote wind effects modify the duration tidal asymmetry, whereas the magnitude tidal asymmetry is unaffected. In addition, wind straining has been observed to occur during persistent along up-estuary winds, modifying the vertical structure of the residual circulation in the upper 10 m of the water column.

The observations in this study clearly demonstrate that the estuarine circulation principally determines the vertical profile of the residual circulation for salinity gradients greater than $1*10^{-4}$ psu/m. At the study site, an ebb-dominant asymmetry in lateral advection acts to decrease the strength of the estuarine circulation for salinity gradients greater than $2.5*10^{-4}$ psu/m. The strong currents during ebb diminish the contribution of classical tidal straining to the generation of the estuarine circulation. The estuarine circulation appears mainly created from late flood to slack before ebb during a long period of weak currents. Furthermore, total tidal straining might be an additional mechanism that modifies the vertical shear in velocity. More research on the turbulence

characteristics is required to understand the dynamics between cross-stream tidal straining, vertical mixing and the vertical shear in velocity.

Model simulations of the Marsdiep basin suggest that the estuarine circulation is strongest in the deeper ebb-dominant part of the main channel and that it decreases southeastward towards the shallower flood-dominant part of the channel. It is hypothesized that spatial variations in tidal asymmetries and water depth have a strong influence on the strength of the estuarine circulation in the Marsdiep basin. This study shows that the creation of the estuarine circulation in the ebb-dominant part of the periodically-stratified Marsdiep basin is a non-steady process, which primarily occurs during the long weak energetic period from late flood to slack before ebb. Lateral advection and possibly total tidal straining significantly modify the strength of the estuarine circulation.

5

OBSERVATIONS OF TURBULENCE

The intra- and inter-tidal variability of turbulence are investigated by analyzing observations of turbulent kinetic energy production and dissipation during neap and spring tide conditions. The turbulence dynamics differ between ebb and flood due to the presence of tidal asymmetries in current strength, with the largest currents during ebb. As a result, the bottom boundary layer covers almost the entire water depth during the entire ebb phase, whereas it is restricted to the lower 8 to 12 m of the water column during most of the flood phase, only covering the total water depth during peak flood. It contrasts the classical pattern in weakly- and periodically-stratified estuaries. The well-mixed conditions during peak flood are followed by weakly-stratified conditions during the small currents of late flood (3-4 hours), which reduce the turbulent intensity. Consequently, a greater total production of turbulence is observed during late ebb and early flood than during late flood and early ebb: a hysteresis effect. Differences in spring-neap tidal variations of the ebb and flood currents produce a large disparity in the turbulence characteristics: a large fortnightly variation in turbulence production and dissipation is observed for the ebb phase, whereas the variability is relatively small for flood. The observations show that turbulent kinetic energy production approximately balances dissipation under most conditions, but only when the cross-stream component is taken into account. Cross-stream production of turbulence contributes between 30 and 50 percent to the total production, except near the bed, and originates from internal shears in cross-stream velocity. Furthermore, the occurrence of a mid-depth maximum in along-stream velocity, and the associated increase in internal vertical shears, during late flood are another source of internally-generated turbulence at mid-depth. Advection of turbulence during peak ebb and its temporal decay during slack tides illustrate the temporal evolution of turbulence. This chapter shows that turbulence production in the periodically-stratified Marsdiep basin is determined by bed-generated as well as (cross-stream) internally-generated turbulence with an approximate tidally-averaged balance present between production and dissipation. The long period of weak vertical mixing during late flood

facilitates the generation of an estuarine circulation, which increases from neap to spring tide due to increased vertical stratification.

This chapter is based on the following paper, currently under review as:
de Vries, J. J., Ridderinkhof, H., and van Aken, H. M. (under review). Observations of turbulence in the periodically-stratified Marsdiep basin, *J. Geophys. Res.*

5.1 INTRODUCTION

Turbulence and mixing are essential components of environmental systems because they redistribute salt, heat, momentum and suspended matter vertically and horizontally. In estuaries, large variations in turbulence occur over the water column during a single tidal cycle, which can have a profound impact on the strength of the estuarine circulation [e.g. Stacey et al., 2001, 2008; Cheng et al., 2011]. Also, horizontal mixing is important for the exchange of water properties and suspended matter between different water masses, occurring for example at the channel-shoal interface [Collignon and Stacey, 2012].

Cost-efficient and non-intrusive measurements of turbulence have become technologically feasible in the last decades [Lohrmann et al., 1990; van Haren et al., 1994; Stacey et al., 1999a; Fisher et al., 2002; Souza et al., 2008]. Tropea [1981] and Lohrmann et al. [1990] proposed a technique to measure the Reynolds stresses over the water column using a moored laser Doppler anemometer and pulse-to-pulse coherent sonar, respectively. This was further developed by van Haren et al. [1994] and Stacey et al. [1999a,b] for application to Acoustic Doppler Current Profilers (ADCP), named the variance method. Several studies investigated the reliability and validity of the variance method in estuaries and shelf seas [Rippeth et al., 2002, 2003; Williams and Simpson, 2004]. An ADCP measures the mean and fluctuating parts of the velocity field, enabling simultaneous computation of the Reynolds stresses and the vertical shear in velocity. From these, the turbulent kinetic energy production can be estimated. In addition, Wiles et al. [2006] developed a technique to measure the turbulent kinetic energy dissipation with an ADCP, named the structure function method. A combination of both techniques provides estimates of the turbulent kinetic energy production and dissipation using one single measurement device. Alternatively, the turbulent kinetic energy dissipation can be estimated using free-falling microstructure-profilers [Simpson et al., 1996; Peters and Bokhorst, 2000, 2001; Becherer et al., 2011]. An ADCP measures the fluctuating part of velocity within the inertial sub-range along the beam ray (O(1-10)m) over its beam width (O(1)m^2), whereas a microstructure-profiler measures the velocity variations within the viscous sub-range of turbulence (O(0.01-1)m). The combination of estimates of the turbulent kinetic energy production and the dissipation rate provides insight into the turbulence dynamics in natural systems such as estuaries and shallow seas.

Observations in the recent decade have shown that several feedback mechanisms are essential for the turbulence dynamics of an estuarine system [Stacey et al., 2011, and references therein]. Generally, a three-way interaction is present between turbulence, vertical shears in velocity and vertical stratification. Turbulence decreases vertical stratification and shears in velocity, while increased shears generate turbulence and thereby reduce the vertical stratific-

ation. On the other hand, vertical stratification dampens turbulence, but also increases the shears and thereby, potentially, produces turbulence. Furthermore, the interaction between the three actors depends on the type of estuary from a well-mixed [Lu and Lueck, 1999; Stacey et al., 1999a], weakly-, or periodically-stratified [Geyer et al., 2000; Stacey and Ralston, 2005; Stacey et al., 2008], or highly-stratified estuary [Kay and Jay, 2003; Geyer et al., 2008; Ralston et al., 2010; Scully et al., 2011]. In addition, Collignon and Stacey [2013] demonstrated that the timescale of the estuarine processes influencing the three actors is also important for their relative contribution to the stability of the water column.

In well-mixed and periodically-stratified estuaries, the main source of turbulence is generally assumed to originate from the shears in velocity near the seabed, which are generated by bed friction: the bed-generated turbulence [Peters and Bokhorst, 2001; Rippeth et al., 2001; Becherer et al., 2011]. Furthermore, the interaction between the tidal currents and the horizontal density gradient creates different dynamics during ebb and flood. Stacey and Ralston [2005] observed a difference in bottom boundary layer dynamics due to the stabilizing and de-stabilizing effect of the strain-induced buoyancy flux during the respective ebb and flood phase. They showed that the buoyancy flux is an important contributor to the turbulent kinetic energy budget, acting as a source or sink of turbulent energy during flood and ebb, respectively. Chant et al. [2007] observed that the relative contribution of the buoyancy term to the energy budget depends on the ratio between the strain-driven buoyancy flux and tidal amplitude, where greater tidal amplitudes reduce the contribution of the buoyancy term. Self-transport of turbulence over the water column is another important characteristic of turbulence. For example, Stacey et al. [1999a] observed vertical transport of turbulence from the bed upwards.

Opposing the classical model of predominant bed-generated turbulence, Collignon and Stacey [2013] and Arnott [2013] showed that the sources of turbulence production are more abundant than previously thought. They observed elevated turbulence production near the surface during late ebb generated by internal shears in cross-stream velocity. These observations were conducted over the slope of a channel, where cross-stream currents were only important during late ebb. Cross-stream currents are highly temporally-variable, thereby illustrating their complex contribution to estuarine dynamics. In addition, the spatial variability in mixing complicates the estuarine dynamics even further. Scully and Friedrichs [2007] and Arnott [2013] observed spatial variations in mixing, which influence the estuarine circulation. Generally, the deeper channel is characterized by greater tidal asymmetries in mixing due to the effect of classical tidal straining, whereas the shallower shoals display smaller asymmetries because of the predominantly well-mixed state of the water column. Classical tidal straining produces well-mixed conditions during flood and in-

creasingly vertically-stratified conditions during ebb due to the stabilizing and de-stabilizing effect of the along-stream density gradient on the water column stability during ebb and flood, respectively [Simpson et al., 1990].

Turbulent motions, or eddies, are present over a wide range of length scales. Large eddies transfer their energy to smaller scales: a processes called the energy cascade [Tennekes and Lumley, 1972]. At the smallest eddy scales, the molecular viscosity converts turbulent motions into heat. In periodically-stratified estuaries, as the Marsdiep basin, the maximum size of eddies is either limited by the distance from a boundary or by vertical stratification [Scully et al., 2011]. The vertical stratification in these type of estuaries, which is generated by classical tidal straining, reduces turbulence during ebb and enhances the estuarine circulation [Stacey et al., 2001; Souza et al., 2008; Burchard and Hetland, 2010; Becherer et al., 2011]. Recently, several studies have shown that vertical stratification can also occur during flood, which might alter the dynamics of turbulence and residual circulation in an estuary [Scully and Geyer, 2012; Aristizábal and Chant, 2014; de Vries et al., 2014]. The effect of flood stratification on the turbulence characteristics has, to our knowledge, not yet been investigated. Model simulations by Burchard et al. [2011] and Burchard and Schuttelaars [2012] show that the estuarine circulation is determined by the covariance between the eddy viscosity and the vertical shear in velocity, which implies a direct dependency on the turbulence characteristics. Generally, the estuarine circulation is driven by the baroclinic pressure gradient, i.e. the gravitational circulation, and by all processes that modify the shape of the vertical profile of velocity through intra-tidal asymmetries in vertical mixing and stratification, i.e. the tidal straining circulation [Geyer and MacCready, 2013, and references therein]. Therefore, the ebb-flood asymmetries in vertical stratification and turbulence are essential for the strength of the estuarine circulation. Furthermore, Geyer et al. [2000] observed for an approximately constant along-stream salinity gradient that the increase in tidal mixing from neap to spring tide decreases the strength of the vertical stratification and estuarine circulation in the weakly-stratified Hudson estuary, illustrating the great fortnightly variability in mixing and residual circulation that can be present in estuaries.

The recent advances in measuring turbulence provide the possibility to study turbulence dynamics in a variety of estuaries under a wide range of conditions. The present study area, the tidal inlet of the estuarine Marsdiep basin, is characterized by strong tidal currents, small density gradients and a complex bathymetry. Vertical stratification has been observed during flood [de Vries et al., 2014, Chapter 2], which modifies the vertical structure of along-stream velocity significantly [de Vries et al., 2015, Chapter 3]. To better understand the complex estuarine dynamics of the Marsdiep, it is essential to investigate the turbulence characteristics. Therefore, the objective of this chapter is to describe

the turbulence characteristics in the Marsdiep basin during neap and spring tide conditions.

This chapter is organized as follows. Section 5.2 discusses the characteristics of the study site and data collection as well as the data processing and data analysis. In section 5.3, the turbulence characteristics and their relation to estuarine dynamics is discussed. Section 5.4 provides a discussion and section 5.5 consists of a presentation of the main conclusions.

5.2 STUDY SITE, MATERIAL AND METHODS

5.2.1 *Study site*

The Marsdiep basin together with the Vlie basin delineates the Western Dutch Wadden Sea (Figure 5.1). The main sources of freshwater are the outlet sluices at Den Oever (DO) and Kornwerderzand (KWZ) which distribute their discharge over the Vlie and Marsdiep basins. The freshwater from KWZ is discharged through the Vlie and Texelstroom channels, whereas all the freshwater from DO is assumed to be discharged through the Marsdiep inlet [Zimmerman, 1976a]. Duran-Matute et al. [2014] showed with model simulations that the different pathways of freshwater transport are primarily determined by the wind forcing. In the Marsdiep inlet, salinity gradients are in the order of 10^{-4} psu/m in along- and cross-stream direction [de Vries et al., 2014, Chapter 2].

The water column is well-mixed during peak ebb and flood due to the high current speed, which varies between 1.5 and 2 m/s. The water column becomes periodically-stratified with salinity differences up to 6 psu during late flood and slack tides [de Vries et al., 2015, Chapter 3]. A great spatial variability in strength and duration of ebb and flood is present along the Marsdiep inlet with the currents being flood(ebb)-dominant in the southern (northern) part of the inlet [Buijsman and Ridderinkhof, 2007a]. Also, the northern part is deeper than the southern part which might have implications for the turbulence characteristics [de Vries et al., 2015, Chapter 3]. van Haren [2012] found, based on 3 days of pressure and velocity data, that turbulent motions in the center of the Marsdiep inlet are characterized by a 50(±20) s period, which originates from turbulence and high-frequency internal waves.

At the study site (Figure 5.1b), the large ebb current produces a well-mixed water column during almost the entire ebb phase and prevents classical tidal straining to generate vertical stratification during the ebb phase. On the contrary, the long duration of small currents during late flood (3 to 4 hours) facilitates the generation of vertical stratification by differential advection and cross-stream tidal straining during this phase of the tide [de Vries et al., 2015, Chapter 3]. Strong cross-stream currents (0.3 to 0.4 m/s) are present during

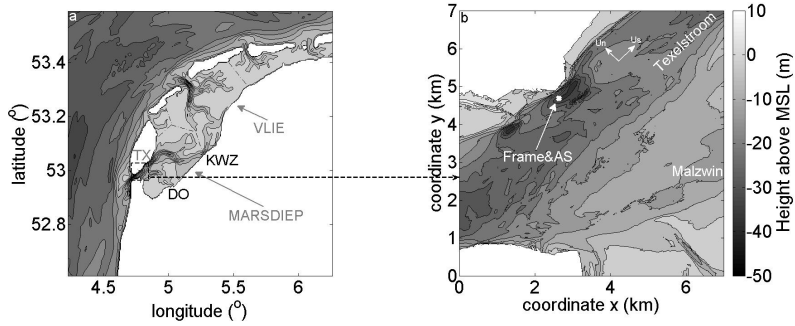

Figure 5.1: a) bathymetric map of the Western Dutch Wadden Sea (data source: Rijkswaterstaat, reference mean sea level, MSL) and, in detail, b) the study site with the location of the bottom frame and the anchor stations (AS). The northern (southern) channel is the Texelstroom (Malzwin). DO and KWZ indicate the location of the freshwater sluices at Den Oever and Kornwerderzand, respectively. The reference frame in the zoom-in (b) is a Cartesian coordinate reference frame with the origin in the southwest corner. The resolution of the zoom-in map of the study area is 20 m. The direction of the along-stream (Us) and cross-stream (Un) velocity components are indicated by the white arrows.

late flood and peak ebb, which are driven by centrifugal and Coriolis accelerations, and by density forcing [Buijsman and Ridderinkhof, 2008c]. In addition, an estuarine circulation of a magnitude up to 0.4 m/s is superimposed on a seaward-directed depth-averaged residual current [Chaper 4]. Furthermore, an asymmetry in drag coefficients is observed with higher values during ebb than during flood, which might influence the turbulence production [de Vries et al., 2015, Chapter 3].

5.2.2 *Data collection*

A 1.25m-high bottom frame equipped with an upward-looking ADCP and a conductivity, temperature, depth sensor (microCAT) is deployed at the north side of the Texelstroom channel on two occasions in Spring of 2012 (Figure 5.1b, Table 5.1). In March, the data is collected during spring tide conditions, whereas May is characterized by neap tide conditions. In the following text and captions

Bottom frame				**Anchor station**	
Start	End	Days	Conditions	Date	FLY
March 8	March 12	5	spring tide	March 10	no
April 28	May 4	7	neap tide	May 1	yes

Table 5.1: Overview of measurements in March and May, 2012.

these different deployments will be identified as spring and neap (tide), respectively. The along-stream salinity gradients are similar for both deployments, i.e. $2.8{*}10^{-4}$ psu/m (Figure 5.2).

Each deployment period is complemented with 13-hours measurements from the anchored NIOZ R.V. Navicula, named anchor stations (Table 5.1). The current velocity is measured with a downward-looking Rio Grande ADCP, the vertical structure of salinity and temperature is measured with a seabird CTD system and the turbulent kinetic energy dissipation is measured with a freefalling microstructure-profiler (FLY). The CTD and FLY casts are performed every 20 minutes. Due to technical problems, the majority of the FLY measurements during the spring tide conditions in March failed and these FLY data are therefore excluded.

5.2.3 *Instrumentation*

The bottom frame is equipped with a four-beam upward-looking 1.2MHz RDI Workhorse Monitor ADCP (hereafter $ADCP_{frame}$) with a beam angle of 20 degrees with the vertical, and measures the beam velocities with a bin size of 0.5 m in mode 1. The $ADCP_{frame}$ transmits eight pings per ensemble of 2.5 seconds. Multi-ping ensembles have the advantage that the reliability and accuracy of the measured velocity is greater, but on the other hand have the disadvantage of potentially underestimating the variance [Williams and Simpson, 2004]. A multi-ping approach is used in order to improve the accuracy of the measurements. The underestimation is considered minor, because the variance is averaged over 300 ensembles. Furthermore, the $ADCP_{frame}$ contains a pressure sensor to estimate the water depth and a calibrated compass. The SBE 37-SM MicroCAT is mounted 30 cm below the $ADCP_{frame}$ and records the conductivity, temperature and depth every 30 seconds.

The R.V. Navicula is equipped with a four-beam downward looking 1.2 MHz RDI Rio Grande ADCP (hereafter $ADCP_{nav}$), which records the east-west and north-south velocity with a bin size of 0.5 m in ensembles of 2 seconds, each including 2 pings. Per ensemble one bottom ping is transmitted to determine the water depth. The $ADCP_{nav}$ is attached to a pole at the starboard side of the

ship at 1 m below the sea surface. The $ADCP_{nav}$ signal is corrected for the ship's pitch, roll and heading in real-time. The ship's velocity is measured by means of bottom tracking or by means of the ship's differential GPS (dGPS), if the former is unavailable. Also, a SeaBird SBE 911 plus CTD system is operated to collect vertical profiles of conductivity, temperature and depth every 20 minutes. This system measures at 24 Hz.

Freefalling microprofiler casts are taken using the FLY profiler [Dewey and Crawford, 1988], which measures the small-scale velocity fluctuations using aerofoil shear probes and enables a direct computation of the turbulent kinetic energy dissipation rate, as discussed in section 5.2.5. The two shear sensors are calibrated and measure the velocity at 282 Hz.

5.2.4 *Data processing*

The upper 15 percent of the $ADCP_{frame}$ data below the sea surface are removed to exclude any side-lobe interference. Then, the Reynolds stresses are computed in beam direction, as discussed in section 5.2.5. Additionally, the velocity field is rotated from beam velocities into the direction of most explained variance of the depth-averaged current (along-stream current) and the axis perpendicular to it (cross-stream current).

Ideally, the bottom frame should be levelled to prevent any bias in computation of the velocity variance. However, due to the large water depth (30 m) and strong currents (2 m/s) it is impossible to send divers to level the frame. The pitch and roll are greater than 6 degrees during the beginning of the neap tide (May) deployment and these data are therefore excluded from further analysis. The frame levelled itself within pitch and roll angle smaller than 6 degrees and remained stable throughout the deployment. Lohrmann et al. [1990] showed that, for isotropic turbulence, the variance technique is reliable for tilt angles smaller than 8 degrees. The pitch and roll angles of the spring tide deployment are stable and smaller than 6 degrees. The bias due to pitch and roll is therefore minor. Only complete tidal cycles are used to provide consistent values of the turbulence characteristics for entire ebb and flood phases.

The data output of the microCAT are already given in temperature (ITS-90, °C), practical salinity (psu), potential density anomaly ($\sigma - \theta$, kg/m^3) and depth (m), which is computed internally with the standard Seabird software.

All $ADCP_{nav}$ data below the seabed, which originate from side-lobe interference, and the first bin above the seabed are removed. Then, the velocity field is rotated into an along-stream component, corresponding with the channels' orientation, and a cross-stream component, perpendicular to the dominant velocity axis. An average vertical profile of the along-stream and cross-stream velocity is computed every 20 minutes based on 60 ensembles (2 minutes). Fi-

nally, the reference frame of the vertical profiles of velocity is shifted from the sea surface towards height above the bed (Z, hab).

The CTD data are processed with the manufacturer's SBE Data Processing software (`http://www.seabird.com/software/`) in order to derive temperature (ITS-90, °C), practical salinity (psu), potential density anomaly ($\sigma - \theta$, kg/m^3) and depth (m). This software removes outliers and low-pass filters the data. Afterwards, the data are averaged in bins of 0.5 m.

All FLY data in the upper 2.5 m of the water column as well as all the data collected after the FLY reached the seabed are removed. The depth profile of each FLY cast is inspected visually to verify that the FLY was free-falling through the water column. The turbulent kinetic energy dissipation is computed in 2 directions using equation 5.13 below. The values of the turbulent kinetic energy dissipation rates in both directions correspond well with each other. In the results section, an average of both is used, which is depth-averaged over 1 m intervals.

5.2.5 *Data analysis*

5.2.5.1 *Hydrodynamics*

The along- and cross-stream salinity gradients are responsible for the main baroclinic pressure gradients in the area. A tidally-averaged estimate of the along-stream salinity gradient, $\langle \frac{\partial s}{\partial x} \rangle$, is obtained by assuming a frozen field approximation [Stacey et al., 2010]

$$\langle \frac{\partial s}{\partial x} \rangle = 2\pi \frac{S_{rms}}{L}, \tag{5.1}$$

where S_{rms} is the root-mean-square of salinity and L ($= u_{rms} * T$) is the tidal excursion length based on the root-mean-square of the depth-averaged along-stream velocity, u_{rms}, and the tidal period, T. The salinity is obtained from the microCAT data. The $\langle \frac{\partial s}{\partial x} \rangle$ lacks any information on the direction of the gradient, but estimates of $\langle \frac{\partial s}{\partial x} \rangle$ correspond well with the magnitude of the measured values by de Vries et al. [2014, Chapter 2].

The buoyancy frequency and potential energy anomaly are representative for the strength of the vertical stratification and the energy required to mix the entire water column, respectively. The square of the buoyancy frequency, N^2, is defined as

$$N^2 = -\frac{1}{\rho_0} \frac{\partial \rho}{\partial z} g, \tag{5.2}$$

where ρ_0 is a reference density and $\frac{\partial \rho}{\partial z}$ is the vertical derivative of density, ρ, obtained from the CTD casts during the 13-hours anchor stations. The potential energy anomaly (density), Φ, [Simpson and Nunes, 1981] is

$$\Phi = \frac{1}{H}\int_{-H}^{\eta} gz(\bar{\rho}-\rho)dz, \tag{5.3}$$

where η is the sea surface elevation and the overbar indicates a vertical average. Both parameters, N^2 and Φ, illustrate the intra-tidal variability in vertical stratification during the 13-hours anchor stations.

To obtain a better insight into the methods commonly used to determine the friction velocities and bed stress, important for the production of turbulence, three different techniques are compared. The friction velocity, $u_{*,log}$, defined as the velocity near the bed, is obtained from an extrapolation of the best-fit of the logarithmic velocity profile

$$u(z) = \frac{u_*}{\kappa} ln(\frac{z}{z_0}), \tag{5.4}$$

where u is the along-stream velocity (m/s), z_0 is a roughness length (m), z is the height above the bottom (m) and κ is the von Karman constant (0.41). The lowest 10 m above the bottom are used to obtain the friction velocity.

The estimate of $u_{*,log}$ is compared to an extrapolation of the along-stream Reynolds stresses, $u_{*,u'w'}$, and the turbulent kinetic energy dissipation, $u_{*,\epsilon}$, to the seabed following Perlin et al. [2005]

$$u_{*,u'w'} = \sqrt{\overline{u'w'}_{z=bed}}, \tag{5.5}$$

and

$$u_{*,\epsilon} = (\kappa \epsilon_{z=bed})^{1/3}. \tag{5.6}$$

where $\overline{u'w'}_{z=bed}$ and $\epsilon_{z=bed}$ are the extrapolated along-stream Reynolds stress and extrapolated turbulent kinetic energy dissipation near the seabed, respectively. Perlin et al. [2005] found the logarithmic fit to overestimate relative to the other two methods.

5.2.5.2 *Turbulence*

Several turbulence parameters are computed from the $ADCP_{frame}$ data. First, the Reynolds stresses are computed using the variance method described in Lohrmann et al. [1990] and van Haren et al. [1994]. The Reynolds stresses along the two planes formed by the beams are

$$\overline{(u'w')}_b = \frac{\overline{\hat{b}_3'^2} - \overline{\hat{b}_4'^2}}{4sin\theta cos\theta} = \overline{\hat{u}'(\hat{w}'-\hat{e}')}, \tag{5.7}$$

and

$$\overline{(v'w')}_b = \frac{\overline{\hat{b}_1'^2} - \overline{\hat{b}_2'^2}}{4sin\theta cos\theta} = \overline{\hat{v}'(\hat{w}' - \hat{e}')}, \tag{5.8}$$

where u and v are the horizontal velocities in the plane formed by beams 3 and 4, and by beams 1 and 2, respectively, w and e are the vertical and error velocity, b is the beam velocity and θ is the beam angle with respect to the vertical axis. The hat, prime and overbar indicate a measured quantity, a fluctuating part of velocity and a temporal average, respectively. The variance of each individual beam is computed over an area of O(1)m^2, and therefore no direct covariance between the beams can be computed, which is O(100)m^2. Inclusion of the error velocity in equations 5.7 and 5.8 relaxes the assumption of spatial homogeneity and enables a computation of the Reynolds stresses based on the variance of the fluctuating part of velocity, assuming the velocity fluctuations are homogeneous over the beam spread, as indicated by the subscript b [van Haren et al., 1994].

To provide the most reliable estimate of the Reynolds stresses, while fulfilling the requirement of approximate stationarity of the mean, the variance is averaged per 12.5 minutes, i.e. 300 samples, which is within the reliable averaging interval [Stacey et al., 1999a]. Afterwards, the along-beam estimates of the Reynolds stresses are rotated into along-stream and cross-stream component with positive values directed up-estuary (flood) and towards Texel (northwestern direction), respectively, for simplicity named $\overline{(u'w')}$ and $\overline{(v'w')}$.

Second, the mean turbulent kinetic energy shear production (W/kg) in along-stream, P_{long}, and cross-stream, P_{cross}, is computed by

$$P_{long} = \overline{(u'w')}\frac{\partial \overline{u}}{\partial z}, \tag{5.9}$$

and

$$P_{cross} = \overline{(v'w')}\frac{\partial \overline{v}}{\partial z}, \tag{5.10}$$

where $\overline{(u'w')}$ and $\overline{(v'w')}$ are the Reynolds stresses in along- and cross-stream direction. The vertical shear in along-stream, u, and cross-stream, v, velocity is given by $\frac{\partial u}{\partial z}$ and $\frac{\partial v}{\partial z}$, where z is the height above the bottom. The total turbulent kinetic energy production, P_{tot}, is then

$$P_{tot} = P_{long} + P_{cross}. \tag{5.11}$$

Third, the turbulent kinetic energy dissipation rate, ϵ, is obtained from the $ADCP_{frame}$ data through the structure function method described and validated by Wiles et al. [2006]. The structure function method is based on the

turbulent cascade theory of Kolmogorov, which links spatial variations in the fluctuating part of velocity within the inertial sub-range to turbulent kinetic energy dissipation. The turbulent kinetic energy dissipation rate is based on the following relationship following Taylor's theory of frozen turbulence in the inertial sub-range

$$D(z,r) = F + C_v^2 \epsilon^{2/3} r^{2/3}, \tag{5.12}$$

where $D(z,r)$ is the difference in the fluctuating part of velocity between two points separated along each beam by the distance r (1 to 5 m), F is an offset caused by uncertainties in the ADCP velocity estimate, ϵ is the turbulent kinetic energy dissipation (W/kg) and C_v is a constant (2.1). The difference in turbulent velocity fluctuations between two points along the beams is mainly determined by the size of the eddies as a function of r. A best-fit between the turbulent length scales for varying r and the fluctuating part of velocity in equation 5.12 produces an estimate of ϵ with the smallest offset F. The best-fit values of ϵ for each individual beam are averaged to produce one single estimate of dissipation. More detailed information on this method can be found in Wiles et al. [2006].

The 40 vertical profiles of ϵ collected with the FLY are used to validate the structure function method for the study site. The turbulent kinetic energy dissipation, ϵ_{FLY}, from the FLY casts is given by

$$\epsilon_{FLY} = 7.5\,\nu(\frac{\partial u}{\partial z})^2, \tag{5.13}$$

where ν is the kinematic viscosity based on a simple temperature approximation. The FLY measures the velocity fluctuations within the viscous sub-range and ϵ can therefore be estimated directly without spectrally fitting the data.

Fourth, several turbulent length scales are computed to evaluate the size range of the eddies. The strain-based Froude number, Fr_y, provides a measure of the influence of stratification on the size of the eddies [Valle-Levinson, 2010]

$$Fr_y = \frac{L_O}{L_K}^{4/3}, \tag{5.14}$$

where L_O is the Ozmidov length scale, which represents the largest turbulent length scale in stratified waters and L_K is the Kolmogorov length scale, which represents the smallest scale of turbulence

$$L_O = \frac{\epsilon^{1/2}}{N^{3/2}}, \tag{5.15}$$

and

$$L_K = (\frac{\nu^3}{\epsilon})^{1/4}, \tag{5.16}$$

where the kinematic viscosity, ν, is kept constant (10^{-6} m^2/s). Values of $Fr_y >$ 200 indicate turbulence is unaffected by stratification, between 15 and 200 signifies that stratification impacts small-scale turbulence, and $Fr_y < 15$ indicates stratification dampens turbulence at all scales [Gargett et al., 1984].

Fifth, the contribution of the different terms in the turbulent kinetic energy (TKE) balance is evaluated by comparing the production and dissipation of turbulence [Valle-Levinson, 2010]

$$\frac{D}{Dt}(TKE) = T + P + B - \epsilon, \tag{5.17}$$

where the temporal evolution, $D(TKE)/Dt$, depends on the magnitude of the transport (T), production (P), buoyancy production (B) and dissipation rate (ϵ) of turbulent kinetic energy. Buoyancy effects can either serve as a source or sink of turbulent energy. In a steady state, the terms on the right hand side sum up to zero. Generally in a well-mixed water column, a balance between P and ϵ is assumed.

Sixth, an important parameter for mixing is the eddy viscosity A_z, which is computed based on [e.g. van Haren et al., 1994; Scully et al., 2011]

$$A_z = \frac{-\overline{u'w'}}{\frac{\partial \overline{u}}{\partial z}}. \tag{5.18}$$

The intra-tidal variability of A_z is investigated and related to estuarine dynamics.

5.3 RESULTS

5.3.1 *Overview of hydrodynamic conditions*

Several features of the hydrodynamic conditions at the study site are illustrated by the bottom frame data (Figure 5.2). An ebb-dominant asymmetry in current magnitude is present, where the peak ebb current is generally larger than the peak flood current. Also, the semi-diurnal tide is distorted and is characterized by a long period (3 to 4 hours) of weak currents during late flood, a long duration (1 hr) of slack before ebb and a short duration (10 min) of slack before flood. Furthermore, cross-stream circulation cells occur during different phases of the tide, as discussed in more detail below. The salinity excursion is greater during spring than neap tide, but the larger tidal excursion during spring tide

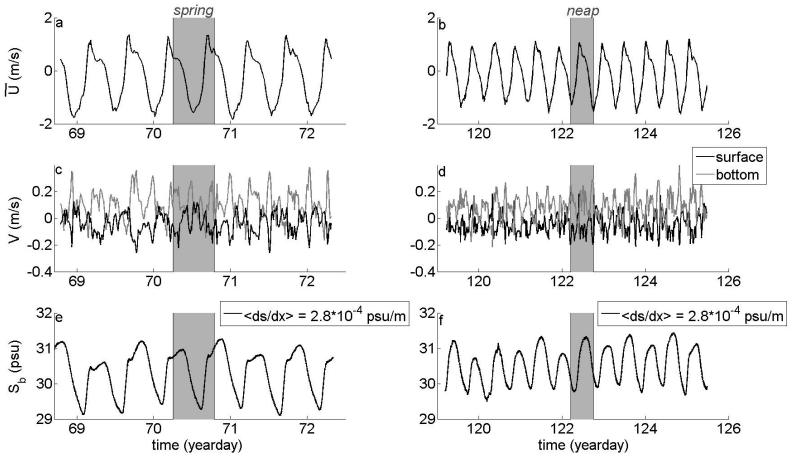

Figure 5.2: The depth-averaged along-stream current, $\bar{U}$, the surface (average of 4 bins around 26.5 m hab) and bottom (average of 4 bins around 3 m hab) cross-stream currents, V, and the bottom salinity, S_b, during the spring and neap tide deployments in March and May, 2012 (left and right column, respectively). The average salinity gradients of both deployments, $\langle \frac{\partial s}{\partial x} \rangle$, are indicated in the legends of the lowest row and are based on equation 5.1. The gray areas indicate the time span of the two 13-hours anchor stations next to the bottom frame.

results in similar along-stream salinity gradients for both deployments (Figure 5.2e,f).

A comparison of the average ebb and flood profiles of along-stream velocity, $< U_E >$ and $< U_F >$, shows a great intra-tidal and fortnightly variation (Figure 5.3a,d). The $< U_F >$ is characterized by a maximum current velocity at approximately 10 m above the seabed, whereas the ebb profile of along-stream velocity displays a near-logarithmic profile. The flood profile is similar for the spring and neap tide deployments, while the ebb profile varies considerably in magnitude between neap and spring tide. The tidally-averaged profiles of along- and cross-stream velocity, $< U >$ and $< V >$, are greater during spring than neap tide despite a similar magnitude of the along-stream salinity gradient, contrary to the general observation in estuaries [e.g. Jay and Smith, 1990a; Ralston et al., 2008] that an increase in tidal amplitude reduces the strength of the estuarine circulation.

The anchor station data illustrate the vertical dynamics of the currents and density over one spring and neap tidal cycle. The classical logarithmic profile of

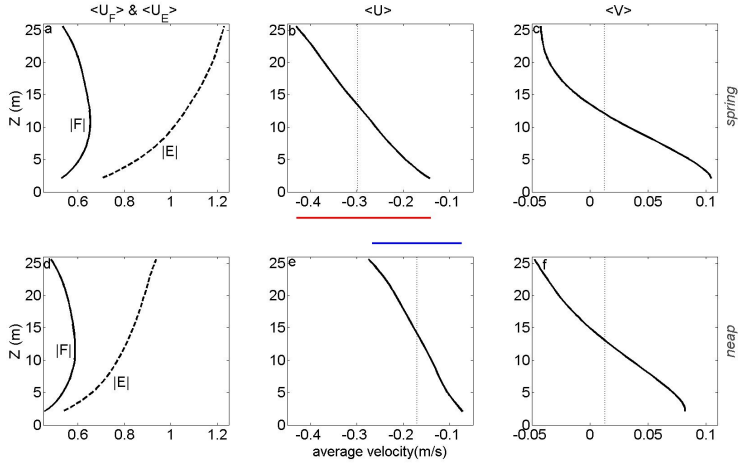

Figure 5.3: Vertical profiles of along- (U) and cross-stream (V) velocity averaged over several phases of the tide. The left column shows the flood- (F, solid line) and ebb- averaged vertical profiles (E, dashed line). The middle and right columns illustrate the tidally-averaged (angled brackets) vertical profiles of U and V, respectively. The upper and lower rows indicate the spring and neap tide conditions, respectively. The dotted vertical lines represent the depth-averaged mean of the profiles depicted in the related panels. The red and blue solid lines in the center indicate the strength of the estuarine circulation, i.e. the surface-bottom difference in $<U>$, during spring and neap tide conditions, respectively.

velocity during ebb is alternated by a mid-depth velocity maximum during late flood (Figures 5.4a and 5.5a), which is described in more detail in Chapter 3. The mid-depth velocity maximum is accompanied by a cross-stream circulation cell and the occurrence of mid-depth vertical stratification (Figures 5.4b,c and 5.5b,c). The cross-stream tidal straining of the density field generates vertical stratification during late flood and facilitates the occurrence of a mid-depth velocity maximum.

Cross-stream circulation cells are present during late flood and peak ebb (Figures 5.2c,d; 5.4b; 5.5b). The high velocities during ebb appear to prohibit the formation of vertical stratification, whereas the low current velocities during late flood facilitate the occurrence of vertical stratification. The buoyancy frequency and potential energy anomaly both reach their maximum values during late flood and their minimum during ebb (Figures 5.4d,e and 5.5d,e). The strength of the vertical stratification is smaller during neap than during spring tide, despite the equal along-stream salinity gradients, altering the strength of

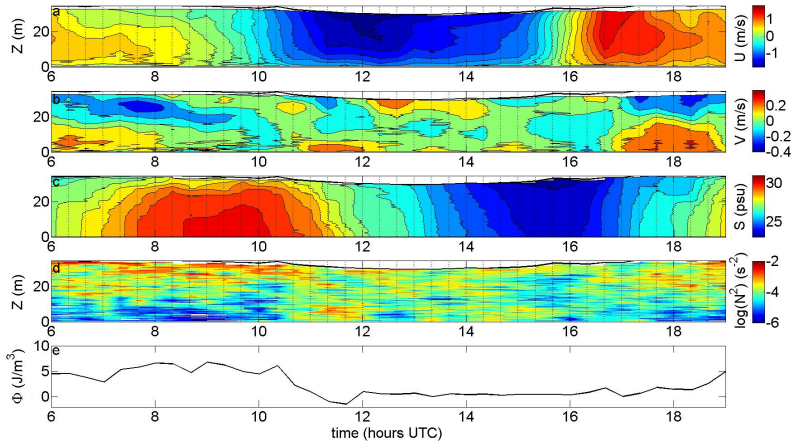

Figure 5.4: Anchor station measurements during spring tide in March. a), b) and c) show the vertical profiles of along-stream velocity (U), cross-stream velocity (V) and salinity (S). The buoyancy frequency squared, N^2 in equation 5.2, and the potential energy anomaly, Φ in equation 5.3, are given in d) and e). The height above the bed is indicated by Z and the time axis is given in hours UTC.

the estuarine circulation. The increase in cross-stream shears in along-stream velocity from neap to spring tide, as described in Chapter 2, is suggested to enhance differential advection during late flood, which generates additional vertical stratification through cross-stream straining, and explains the increase in vertical stratification.

5.3.2 *Reynolds stresses and friction velocities*

The tidal asymmetries and shape of the vertical profiles of velocity, described in the previous section, are also reflected in the shape of the Reynolds stress profiles: they are greater during ebb than during flood, and are accompanied by a related intra-tidal variation in height of the bottom boundary layer. The vertical profiles of the magnitude of the Reynolds stresses are depicted in Figure 5.6. The flood-averaged along-stream Reynolds stresses, $\overline{(u'w')}$, linearly decrease with height above the bed in the lower 8 and 12 m of the water column for neap and spring tide, respectively (Figure 5.6a,d). Above this height, the flood-averaged stresses remain constant throughout the water column. The ebb-averaged $\overline{(u'w')}$ are greater than the flood-averaged values by a factor of 1.5

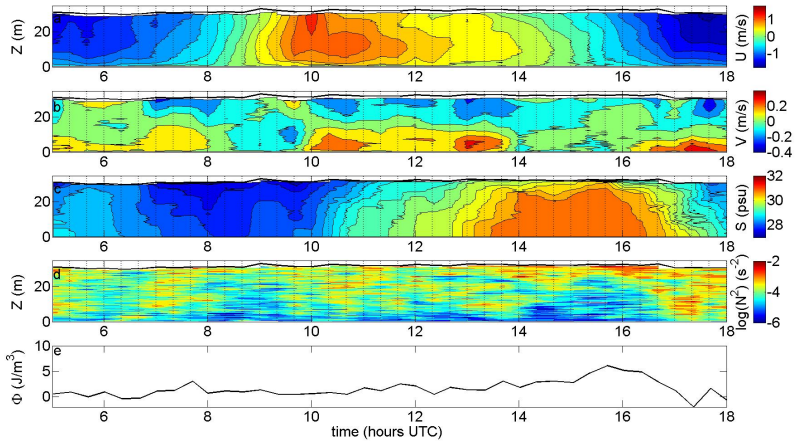

Figure 5.5: Same as in Figure 5.4, but then for the neap tide deployment in May.

to 3 for neap and spring tide, respectively. The ebb-averaged $\overline{(u'w')}$ decreases linearly up to 18 and 25 m above the bed. These parts of the water column, where $\overline{(u'w')}$ decreases linearly with height above the bed, are assumed to represent the bottom boundary layer [Stacey and Ralston, 2005]. The height of the bottom boundary layer, therefore, extends on average 2 times higher into the water column during ebb than during flood (ebb: entire water column, flood: half of the water column). Furthermore, the stress profiles indicate a greater fortnightly variation in $\overline{(u'w')}$ for the ebb than the flood phase (Figures 5.6a,d), corresponding with the fortnightly variation in tidal current magnitude.

In cross-stream direction, the ebb and flood Reynolds stresses, $\overline{(v'w')}$, show a similar fortnightly modulation (Figure 5.6b,e). Only a small difference between ebb and flood $\overline{(v'w')}$ is present during neap tide, which increases during spring tide, mainly because ebb $\overline{(v'w')}$ increases. During neap tide, the ebb and flood $\overline{(v'w')}$ are small relative to $\overline{(u'w')}$, while the maximum ebb $\overline{(v'w')}$ become increasingly important during spring tide, being greater than the flood $\overline{(u'w')}$.

A clear distinction in height of the bottom boundary layer is observed for peak tidal currents relative to its weaker tidal phases (Figures 5.6c,f). The bottom boundary layer almost covers the entire water column during peak ebb and flood, i.e. for velocities greater than 1 m/s, whereas it only covers the lower part of the water column for velocities smaller than approximately 1 m/s (Figure 5.6c,f). The long period of weak currents ($<$ 1 m/s) during late flood explains

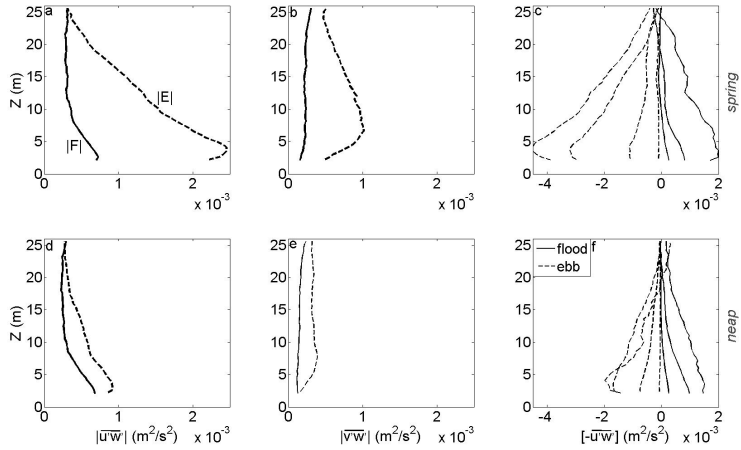

Figure 5.6: Flood- and ebb-averaged profiles, $|F|$ and $|E|$, of the Reynolds stresses in along- and cross-stream direction ($\overline{(u'w')}$ and $\overline{(v'w')}$ in the left and middle column, resp.) for the spring and neap tide deployments. The right column shows the averaged along-stream Reynolds stresses, $[\overline{(u'w')}]$, as a function of the depth-averaged along-stream current, binned in 0.5 m/s intervals, indicated by the brackets.

the restriction of the bottom boundary layer to the lower 10 m for the flood phase.

Generally, vertical profiles of $\overline{(u'w')}$ are expected to increase linearly towards the bed, reaching maximum values near the bed. For the higher current velocities ($>$ 1 m/s), the maximum $\overline{(u'w')}$ is reached 3 to 4 m above the bed, and $\overline{(u'w')}$ decreases again below this height (Figure 5.6c,f). The question arises what the effect is of the deviating $\overline{(u'w')}$ profiles on the estimation of the bed shear stress and the production and dissipation of turbulence.

The friction velocity obtained from the logarithmic law-of-the wall ($u_{*,log}$), the Reynolds stress ($u_{*,u'w'}$) and turbulence kinetic energy dissipation ($u_{*,\epsilon}$) profiles are compared in Figure 5.7. The friction velocity based on the logarithmic fit overestimates up to a factor 2 relative to the other two methods, especially for the peak current speeds when the maximum $\overline{(u'w')}$ are observed several meters above the seabed. The magnitude of $u_{*,u'w'}$ and $u_{*,\epsilon}$ correspond well with each other. The friction velocities computed with these two techniques are approximately 2 times smaller than the values previously computed for this basin using the common logarithmic law-of-the-wall fit [Buijsman and Ridderinkhof, 2007a; de Vries et al., 2015].

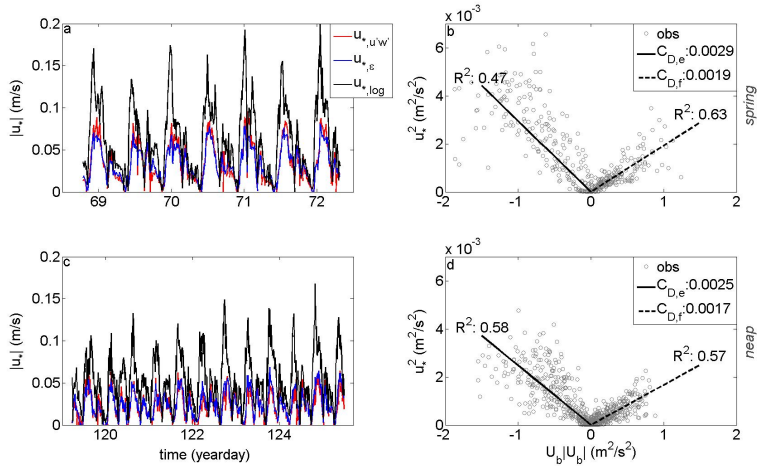

Figure 5.7: Comparison between three different techniques to compute the friction velocity, u_* (left column). Three methods are compared, as described in section 5.2.5. In the right column, an estimate of the ebb (e) and flood (f) drag coefficient, C_D, based on the squared friction velocity, $u^2_{*,\epsilon}$, and the near-bottom (2 m hab) current squared, described in Chapter 3, is given in the right column for spring and neap tide conditions (upper and lower row, respectively).

An ebb-flood asymmetry in drag coefficient is observed in Chapter 3 based on the logarithmic law-of-the-wall fit, which is contributed to the surrounding complex bathymetry but might be a consequence of the non-linear Reynolds stress profiles in the lower part of the water column (Figure 5.6). The relationship between $u_{*,\epsilon}$ squared and u_b squared provides an estimate of the drag coefficient and shows that an asymmetry in drag coefficient remains between ebb and flood (Figures 5.7b,d). The drag coefficient is persistently larger during ebb than during flood for both deployments. However, the drag coefficient is smaller when obtained from $u_{*,\epsilon}$, illustrating that the assumption of a constant flux layer is not valid anymore at the measured height of 2 m above the bed.

5.3.3 *Turbulence characteristics*

Figures 5.8 and 5.9 show that turbulence in the Marsdiep is not only generated by bed friction but also by internal shears in along- and cross-stream velocity. The extent of the bed-generated turbulence corresponds with the height of the bottom boundary layer: it affects the entire water column during spring tidal

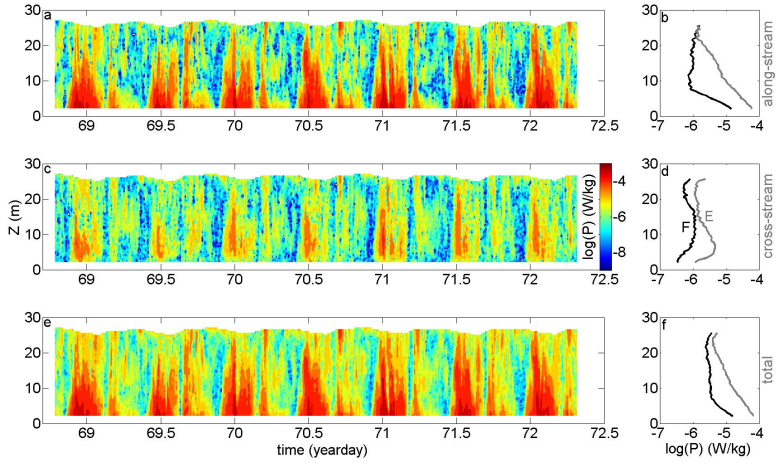

Figure 5.8: Turbulent kinetic energy production, P, during spring tide conditions. The along-stream, cross-stream and total production is given in the upper, middle and lower row, respectively. The left column shows the production per ensemble of 12.5 minutes, whereas the right column shows ebb-(E) and flood(F)-averaged profiles of P.

ebb conditions, whereas it is limited to the lower 8 to 12 m of the water column during flood (Figures 5.8a,b and 5.9a,b). Interestingly, elevated values of P_{long} are present at mid-depth during the late floods of spring tide, e.g. around Day 70.25 of March (Figure 5.8a), which are not created by bed-generated turbulence but rather by along-stream internal shears in velocity. This phenomenon corresponds with the occurrence of a mid-depth velocity maximum during late flood, which is more developed during spring tide than during neap tide. Turbulence is also generated in the upper part of the water column during neap tide conditions, which is also evident in the flood- and ebb-averaged vertical profiles of along-stream turbulence production (Figures 5.9a,b). The different fortnightly modulation of the flood and ebb currents results in a relatively minor change in the average flood profile of along-stream turbulence production from neap to spring tide, whereas the average ebb profile increases notably (Figure 5.8a, 5.9a). As a result, the average ebb and flood profiles are similar in shape and magnitude during neap tide, whereas they differ markedly during spring tide conditons.

In cross-stream direction, turbulence is primarily generated by internal shears (Figures 5.8c,d and 5.9c,d). Close to the seabed, production is an order of magnitude smaller than 5 m above the bed. Internal shears generate turbulence

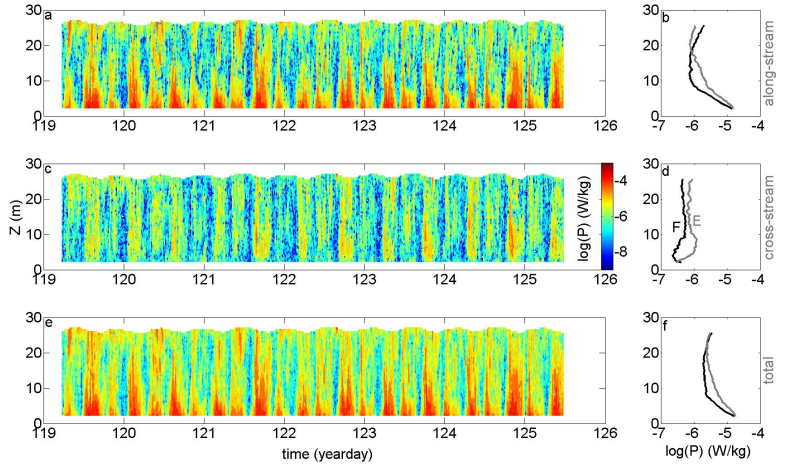

Figure 5.9: Same as Figure 5.8, but then for neap tide conditions.

particularly during late flood and peak ebb (Figures 5.8c and 5.9c). Ebb and flood P_{cross} are similar during neap tide, but differ from one other during spring tide, mainly because the increase of P_{cross} during the ebb phase (Figures 5.8d and 5.9d).

The total production of the depth-averaged turbulent kinetic energy as a function of the depth-averaged current is depicted in Figure 5.10, thereby separating the early and late ebb and flood phases from one another. Large differences are present between the early and late phases, resembling a hysteresis curve. The magnitude of P_{tot} differs up to an order of magnitude between the early and late tidal phases for currents smaller than 1 m/s. The greatest P_{tot} difference is observed between early and late ebb during spring tide conditions, but discrepancies are present in all panels. Furthermore, the late flood values are persistently lower than early flood values. The hysteresis curve in Figure 5.10, indicated by the arrows, shows that the vertical stratification during late flood and slack before ebb (Figures 5.4c and 5.5c) dampens the turbulence production during these phases of the tide, whereas the well-mixed conditions during late ebb and early flood facilitates higher values of P_{tot}.

The effect of vertical stratification on turbulence characteristics is further investigated through the turbulent length scale analysis, described in section 5.2.5, which requires an estimate of the turbulent kinetic energy dissipation. Therefore, the structure function method by Wiles et al. [2006] is validated with the FLY data. A comparison between ϵ from the $ADCP_{frame}$ and the FLY

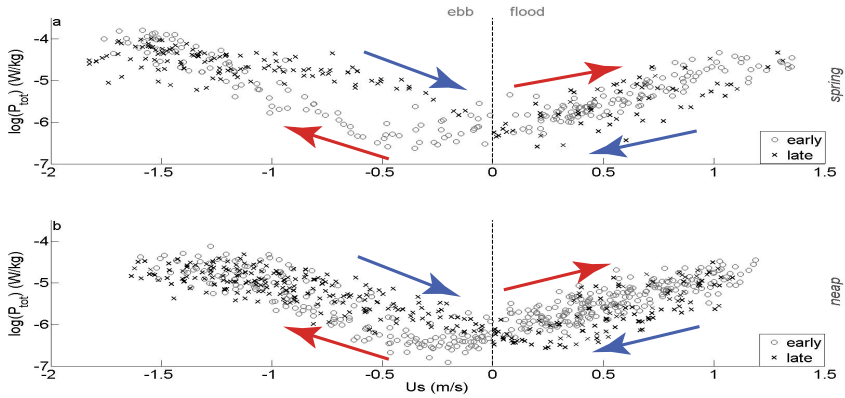

Figure 5.10: Comparison between depth-averaged production of turbulence, P_{tot}, during the early and late phases (gray circles and black crosses, respectively) of the ebb and flood tide as a function of the depth-averaged current, Us. The upper and lower row indicate spring and neap tide conditions, respectively. The arrows indicate the 'direction' of the tidal propagation for early and late phases of the ebb and flood tide (blue and red arrows, respectively) with the height of the arrow representing the relative magnitude of P_{tot}. The dashed vertical line indicates slack tide, i.e. the transition between ebb and flood.

during the 13-hours neap tide anchor station shows good agreement (Figure 5.11). The turbulent kinetic energy dissipation rate is of the same order of magnitude throughout the observational period and displays the same vertical structure. The tidally- and depth-averaged values of the FLY and ADCP estimates are 7.5* and 7.6*10^{-6} W/kg, respectively. The dissipation is characterized by the greatest values during peak ebb and the smallest values during slack before ebb. The duration of the slack tides differs, because the time period of slack before ebb is longer than slack before flood. The higher values of ϵ during the latter suggest that turbulence production is not in instant equilibrium with dissipation. The good agreement between the two techniques, despite measuring different ranges of the turbulence spectrum, gives confidence that ϵ from

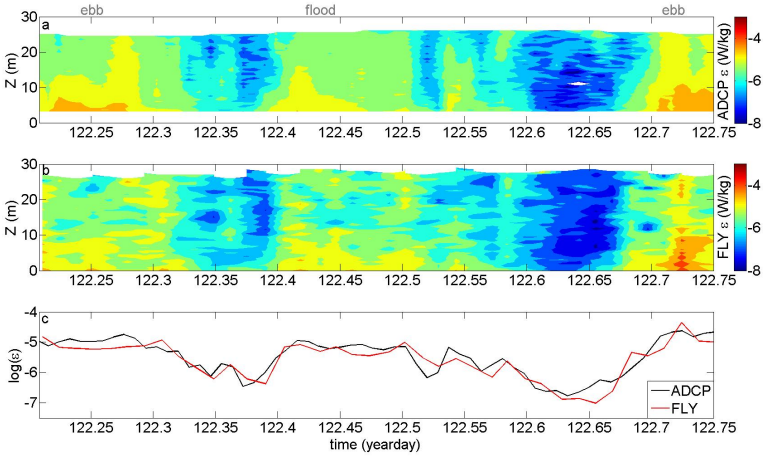

Figure 5.11: Comparison between the logarithmic of turbulent kinetic energy dissipation, ϵ, obtained from the ADCP (a) and FLY (b) measurements during the neap tide conditions. The lowest panel (c) shows a comparison between the depth-averaged values of ϵ from the ADCP and FLY.

the $ADCP_{frame}$ is reliable for investigating the production and dissipation of turbulence and their respective length scales.

The intra-tidal variation in turbulent eddy size is indicated by the Ozmidov and Kolmogorov length scales in Figure 5.12. The largest turbulent length scale, the Ozmidov length scale L_O, is generally in the order of 10^1 m during most of the tidal cycle, which is large for a water depth of 30 m, suggesting that the distance to the boundary is the limiting factor instead of the presence of vertical stratification. However during late flood and slack before ebb, the Ozmidov length scale decreases to a magnitude of 10^{-1} to $10^{-1.5}$ m, implying that vertical stratification dampens large-scale turbulence. This decrease in L_O is most pronounced during spring tide when the vertical stratification is greatest. The variation in Kolmogorov dissipation length scale, L_K, is mainly explained by variations in ϵ over the tidal cycle. Slack tides are characterized by smaller ϵ, which result in an increase in L_K. It indicates that dissipation occurs at greater turbulent length scales. The increase in L_K is most pronounced during slack before ebb, because the long duration facilitates the dissipation of background, or ambient, turbulence.

The ratio between the Ozmidov and Kolmogorov length scales as incorporated in the strain-induced Froude numbers, Fr_y, enables us to evaluate the impact of vertical stratification on the size of the turbulent eddies. Generally, Fr_y is in the order of 10^4 to 10^6, which evidences that overall small-scale tur-

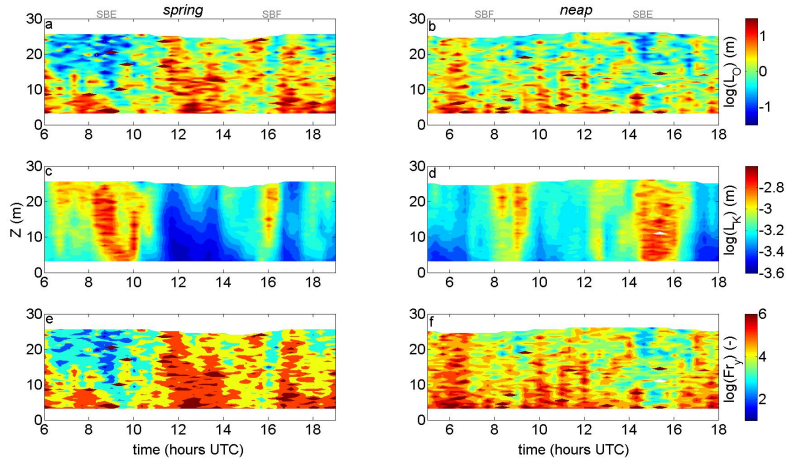

Figure 5.12: Ozmidov, L_O, and Kolmogorov, L_K, length scales (upper and middle rows, respectively) and the strain-induced Froude number, Fr_y, (lower row) for spring tide and neap tide anchor stations (left and right column, respectively), as described in section 5.2.5. The slack before ebb, SBE, and slack before flood, SBF, are indicated at the top. The data is plotted on a logarithmic scale.

bulence is not influenced by vertical stratification. However, Fr_y decreases to values of $10^{1.5}$ between late flood and slack before ebb, implying that then small-scale turbulence is affected by vertical stratification.

5.3.4 *The turbulent kinetic energy budget*

An investigation of the balance between the production and dissipation of turbulence provides indications of the location of the sources and sinks in the water column. The ratio between the log of ϵ and P_{tot}, as depicted in Figure 5.13 with values greater (smaller) than 1 indicating an excess in turbulent production (dissipation), shows intra-tidal and fortnightly variations in turbulence dynamics. The ratio varies between 1.1 and 1.3 near the bed during spring tidal ebb conditions, implying that more turbulence is generated than dissipated (Figure 5.13a). In the upper part of the water column, the ratio is between 0.6 and 1, suggesting a sink for turbulent energy. Generally, the greatest shears in velocity are present near the seabed, which result in the production of turbulence. Turbulence is transported vertically and reaches the upper part of the water column, where vertical shears and turbulence production are generally smal-

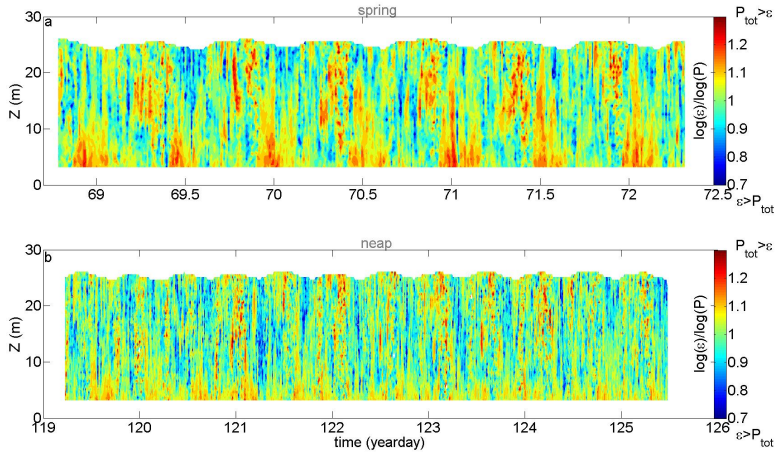

Figure 5.13: Ratio between the logarithmic of turbulent kinetic energy dissipation and total production for spring and neap tide (upper and lower panel, respectively). Values greater (smaller) than 1 indicate an excess of turbulent kinetic energy production (dissipation), because the ratio is based on the logarithms of two values smaller than 1, e.g. $\log(10^{-4})$ divided by $\log(10^{-2})$ is 2.

ler, enabling a net dissipation of turbulence. However, several exceptions are observed over the tidal cycle.

A surplus of P_{tot} is observed at mid-depth during late flood, especially during spring tide, while equilibrium values with a ratio of 1 are present up and below the mid-depth P_{tot} maximum (Figure 5.13a). The occurrence of vertical stratification during this time interval suggests an influence of the buoyancy term (Figure 5.4c). During neap tide conditions, the ratio is closer to 1 over the entire water column, implying that, over the largest part of the water column during neap tide, turbulent production and dissipation are in equilibrium (Figure 5.13b). The differences illustrate the hydrodynamic changes that occur from neap to spring tide. Deviations from this equilibrium only occur close to the seabed and near the sea surface during neap tide. The increasing deviations towards spring tide conditions are explained by the increase in vertical shears in along-stream and cross-stream currents, which enhance the turbulence production, as described in section 5.3.1 and 5.3.3.

It is noteworthy to mention that turbulent kinetic energy production is of the same order of magnitude as turbulence dissipation, only if the cross-stream production is included. Average profiles of flood-, ebb- and tidally-averaged P_{tot} and ϵ demonstrate the good correspondence between the magnitude of turbu-

lence production and dissipation (Figure 5.14). Without the inclusion of the cross-stream turbulence production, the vertical profiles of P_{long} and ϵ differ from one another with the latter being structurally larger than the former (not depicted). If the cross-stream production is included, the profiles of P_{tot} and ϵ resemble each other fairly well (Figure 5.14a-f), implying that P_{cross} is an important source of turbulence production. The ebb-, flood- and tidally-averaged cross-stream contribution to the total turbulence production are all characterized by a similar pattern. In the lower 10 m of the water column, the cross-stream contribution increases from 2 to 4 percent near the bed to approximately 30 percent at 10 m above the bed. Between 10 and 25 m, the cross-stream contribution fluctuates between 30 and 50 percent with a slightly upward increasing trend.

During spring tide, the tidally-averaged profiles show a surplus of turbulence production over the water column (Figure 5.14c). The discrepancies in the lower and upper part of the water column are determined by the ebb and flood phases, respectively (Figures 5.14a-c). During ebb, bottom-generated turbulence is either advected in along- or cross-stream direction or is dampened during early ebb by the vertical stratification originating from the late flood phase. An excess in turbulence production is primarily observed during peak ebb when the water column is well-mixed (Figures 5.4c and 5.13a), thereby excluding the buoyancy term as a sink. Therefore, advection of turbulence is the most likely mechanism that explains the difference between the production and dissipation. During flood, a surplus of turbulence production is observed in the upper part of the water column for both neap and spring tide conditions, related to turbulence production by internal along- and cross-stream shears. The presence of vertical stratification during late flood suggests that buoyancy serves as a sink in the upper part of the water column, which explains the surplus of turbulence production. In May, the tidally-averaged vertical profiles of P_{tot} and ϵ are nearly identical, suggesting a balance between turbulence production and dissipation during neap tide conditions. Only in the lower part of the water column, bed-generated turbulence is greater than the dissipation. The turbulence is most likely advected horizontally or vertically.

5.3.5 *Eddy viscosity*

Figure 5.15 displays the median profiles of the eddy viscosity per 0.1 m/s bin of the depth-averaged along-stream velocity, Us. The left (right) column shows the average profiles from peak flood (ebb) to peak ebb (flood), named FtoE (EtoF). The x-axis of FtoE is reversed, which corresponds with the temporal propagation of the tide from late flood to early ebb.

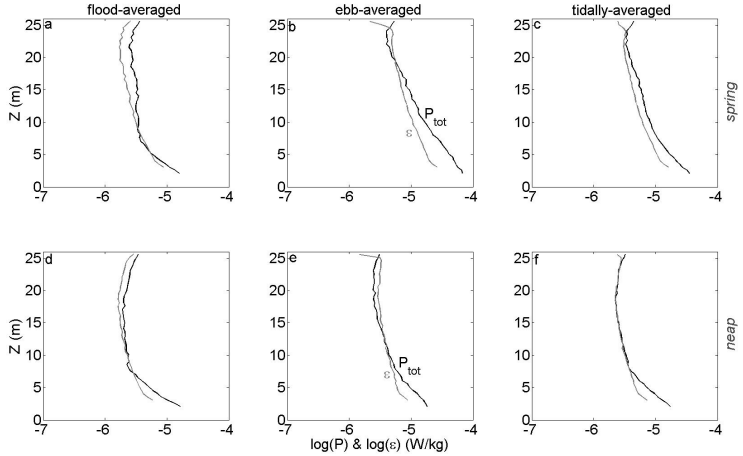

Figure 5.14: Comparison of the flood-, ebb- and tidally-averaged profiles of total turbulent kinetic energy production, P_{tot}, and dissipation, ϵ, for spring (upper row) and neap tide conditions (lower row).

Different vertical distributions of the eddy viscosity are observed depending on the phase of the tide. A parabolic shape of the eddy viscosity profile is present when the currents are greater than a threshold velocity, which lies between 0.5 and 1 m/s. The parabolic profile is characterized by maximum values in the middle of the water column, because the size of the eddies that generate vertical mixing decreases towards the boundaries, viz. the sea surface and seabed. Below this threshold velocity, the shape is not characterized by maximum values in the middle, but by maximum values in the lower part of the water column.

The strength of the eddy viscosity varies over several orders of magnitude during the tidal cycle. Maximum and mean values are in the order of 10^{-1} and 10^{-2} m^2/s, respectively. The tidally-averaged values of A_z vary over a fortnightly timescale with the largest values occurring during the ebb phase of spring tide. The greatest fortnightly variation is observed during the ebb phase of the tide, whereas the eddy viscosity magnitude and shape remains similar from neap to spring tide. Estimates of A_z by Buijsman and Ridderinkhof [2008c] based on the Munk and Anderson relation are at least one order of magnitude smaller than the values presented here.

A discrepancy is present between FtoE and EtoF for currents smaller than 0.5 m/s. During neap and spring tide conditions, vertical stratification during the long period of small currents in the late flood phase is accompanied by a lowering of the maximum eddy viscosity, whereas it is absent for EtoF. Furthermore, the magnitude of A_z is greater for the same current magnitude during

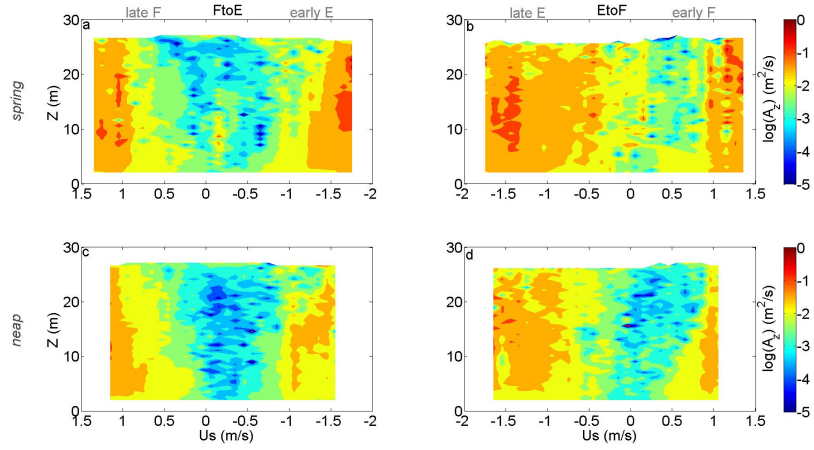

Figure 5.15: Median eddy viscosity profiles from peak flood to peak ebb (FtoE, left column) and vice versa (EtoF, right column) for spring and neap tide conditions (upper and lower row, respectively) as a function of the depth-averaged along-stream current, Us. A median profile is computed per 0.1 m/s bin of the depth-averaged current. The x-axis in the left column is reversed to reflect the temporal propagation of the tide from late flood to early ebb.

late ebb and flood than during the early tidal phases. The same is observed for EtoF (Figure 5.15b,d): early flood is characterized by a gradual increase of the bottom boundary layer, where the lowered A_z maximum gradually transforms into a parabolic shape. Both aspects illustrate that a certain amount of time is required for the eddy viscosity profile to fully develop, suggesting that the eddy viscosity profile is subject to tidal asymmetries in current magnitude.

5.4 DISCUSSION

5.4.1 *Vertical structure of turbulence*

The observations in the ebb-dominant Texelstroom channel display a great intra- and inter-tidal variability in along-stream currents as a result of the tidal asymmetries present in the region,impacting the turbulence characteristics. The ebb phase is characterized by the largest currents, producing a well-mixed water column. The smaller peak flood current also generates well-mixed conditions, but is followed by a long period of small currents (0.5 to 1 m/s), which is characterized by a weakly-stratified water column. Vertical stratification during late

flood generates a mid-depth maximum in along-stream velocity, a phenomenon investigated in Chapter 3. The observations presented in this study show that the along-stream current remains relatively constant from neap to spring tide conditions for the flood phase, whereas a great variation is observed over the fortnightly timescale for the ebb phase. Cross-stream circulation cells are prevalent during late flood and peak ebb, and increase from neap to spring tide. A similar increase in cross-stream current magnitude towards spring tide is observed by Chant [2002] and Seim et al. [2009] in a curved channel of two weakly-stratified estuaries. However in these estuaries, the increase in tidal amplitude is accompanied by a decrease in strength of the estuarine circulation, suggesting different dynamics than in the periodically-stratified Marsdiep basin. In the former, the dynamics of vertical stratification more adequately correspond to the pattern of classical tidal straining estuaries.

The observations show that the commonly-assumed dominant near-bed, or near-boundary, generated along-stream turbulence [Peters and Bokhorst, 2001; Rippeth et al., 2001; Becherer et al., 2011] scales well with the magnitude of the tidal current, resembling the intra- and inter-tidal variability described above. However, the vertical profiles of turbulence are modified by a variety of factors. Several deviations from the classical vertical structure of primarily bed-generated turbulence in estuaries are observed.

Generally, Reynolds stresses increase downwards and reach their maximum near the seafloor, which corresponds with previous studies [Stacey et al., 1999a; Geyer et al., 2000; Rippeth et al., 2002; Williams and Simpson, 2004]. However for greater ebb and flood velocities, a maximum is observed several meters above the seabed. A modification of the hydrodynamic conditions as a result of the presence of bedforms, near-bed tidal straining or cross-stream currents [Seim et al., 2002; Fong et al., 2009; van Haren, 2010] can enhance the shears at a certain height above the seafloor. The complex bathymetry produces an asymmetry in drag coefficient [de Vries et al., 2015, Chapter 3] and sandwaves are an ubiquitous feature in the Marsdiep inlet [Buijsman and Ridderinkhof, 2008a]. The presence of this elevated maximum during peak flood, when no strong cross-stream circulation cell is present, and its relationship with the current speed suggest that near-bed tidal straining and cross-stream circulation are not likely to contribute to this maximum. Therefore, the complex bathymetry and bedforms are the most likely mechanisms that explain the occurrence of maximum Reynolds stresses at several meters above the bed.

Additionally, an estimation of the drag coefficient based on several methods shows that the logarithmic fit method overestimates with respect to the methods based on the Reynolds stress and turbulent dissipation rate profiles, as already discussed in Perlin et al. [2005]. However, the asymmetry in drag coefficient between ebb and flood, as described in Chapter 3, is persistent for all methods, providing more evidence for the observed asymmetry in drag coef-

ficient as a result of the complex bathymetry, which modifies the vertical shears in velocity in the lower part of the water column.

The bottom boundary layer dynamics in the Marsdiep are characterized by large intra- and inter-tidal variations which have a profound impact on the hydrodynamic structure of the water column. Generally, the bottom boundary layer is greater during ebb than during flood, which contrasts with e.g. Geyer et al. [2000] and Li and Zhong [2009]. The absence of the vertical stratification during ebb, commonly generated by tidal straining, partly explains the disparity. Furthermore, the tidal asymmetry in drag coefficient and the tidal distortion both impact the extent of the bottom boundary layer.

The limited bottom boundary layer during late flood facilitates the generation of vertical stratification by cross-stream straining and by advection of salinity, which in turn leads to dampening of turbulence. With the available data it is impossible to compute the buoyancy term. However, evidence of dampening of turbulent length scales is provided by the length scales analysis. Furthermore, the shape of the vertical profiles of turbulence production and dissipation indicates that the buoyancy term acts as a sink during late flood (and early ebb). It contrasts with the study by e.g. Stacey and Ralston [2005] and Chant et al. [2007] who observed the buoyancy term to act as a source during flood. The vertical stratification is generated during late flood, persists until early ebb, and creates a hysteresis between different phases of the tide: the depth-averaged production of turbulence is greater during late ebb and early flood than during late flood and early ebb.

The principal deviation from the classical profile of turbulence is explained by the role of the cross-stream component of the tidal flow. In the Marsdiep basin, the total production of turbulence approximately balances the turbulence dissipation rate, but only when the cross-stream production of turbulence is taken into account. The cross-stream production contributes between 0.3 to 0.5 to the total production, and is especially important during late flood and peak ebb. This finding corresponds with Collignon and Stacey [2013] and Arnott [2013] who observed elevated cross-stream internal shear production of turbulence on the slope of a channel during late ebb. The observations in the Texelstroom channel show that internal shears in cross-stream currents can also contribute in a (curved) tidal channel with large lateral variations in water depth. Furthermore, the mid-depth maximum in along-stream velocity during late flood creates internal shears in along-stream velocity, which also act as a source of turbulence production in the upper part of the water column. The mid-depth along- and cross-stream internal shears are generated by laterally-driven flood stratification [Chapters 2 and 3] and curvature, cross-stream density gradients and Coriolis [Buijsman and Ridderinkhof, 2008c]. So, vertical stratification during late flood acts in two ways: it is a sink of turbulence, but indirectly also generates turbulence by increasing the vertical shears in along-stream velocity.

5.4.2 *Turbulence in relation to estuarine dynamics*

Several aspects of the observed turbulence in the Marsdiep basin can have implications for the estuarine dynamics in the region. The intra-tidal variation in height of the bottom boundary layer implies that the friction velocity, taken as a measure for vertical mixing, is not affecting the current structure of the entire water column during the entire tidal period. Geyer et al. [2000] already noted that the presence of a limited bottom boundary layer produces a discrepancy in shape of the tidally-averaged shear and stress. Therefore, Seim et al. [2002] and Ralston et al. [2008] proposed an effective tidally-averaged bottom boundary layer height in order to close the depth-averaged along-stream momentum balance. However, the observations in the Marsdiep show that the intra-tidal variations are large, which raises the question whether the dynamics are similar over different phases of the tide. In addition, sources of turbulent kinetic energy production originate from internal shears which might modify the areas of vertical mixing.

The shape of the eddy viscosity profiles of ebb and flood displays two important features relevant for the estuarine dynamics. Firstly, the greater part of the flood phase is characterized by maximum values in the lower part of the water column, whereas the ebb phase is characterized by a parabolic profile with the maximum values at mid-depth, implying that the assumption of a temporally-constant shape of the eddy viscosity profile is not valid. Geyer et al. [2000] observed eddy viscosity profiles with their maximum values located in the lower part of the water column during both peak ebb and flood conditions. They found the magnitude to be structurally a factor 2 greater during flood for both spring and neap tide. The profiles in the Marsdiep basin show a greater variation in shape over the tidal cycle, stressing the importance of considering all phases of the tidal cycle. In addition, the magnitudes are larger during late ebb and flood than during the early tidal phases, illustrating the time lag that accompanies the development of turbulence.

These variations suggest that model formulations of the eddy viscosity are required which not only consider changes in magnitude, but also in temporal decay and in shape of the eddy viscosity profiles. Zitman and Schuttelaars [2012] demonstrated that different algebraically-prescribed eddy viscosity parameterizations produce markedly different modelled residual circulation patterns. Numerical models such as Delft3D and GOTM generally provide a wide range of turbulence closure models. The observations presented in this study illustrate the importance of using a two-equations turbulence closure model, which includes transport and temporal decay of turbulence. For an assessment of different two-equation closure models is referred to Warner [2005].

Secondly, the magnitude of the eddy viscosity is greater during ebb than during flood, which is the opposite asymmetry as expected from the tidal straining

dynamics [Simpson et al., 1990; Rippeth et al., 2001; Burchard and Hetland, 2010]. An ebb-dominant asymmetry in eddy viscosity and mixing is expected to create a reversed estuarine straining circulation [Cheng et al., 2010; Burchard and Schuttelaars, 2012; Basdurak et al., 2013]. However, Chapter 4 shows that a classical estuarine circulation is present at the study site with a magnitude up to 0.4 m/s, which scales well with the baroclinic pressure gradient. Thus, asymmetries in peak mixing appear not to markedly modify the total magnitude of the estuarine circulation.

In Chapter 4, we observe that the estuarine circulation is mainly generated during late flood and slack before ebb during a long period of weak currents (3 to 4 hours), which this study has shown is characterized by weak vertical mixing. Therefore the mixing asymmetry, which is primarily determined by the peak values of ebb and flood, appears not to be of importance in the Marsdiep. The increase in strength of the estuarine circulation from neap to spring tide for a constant along-stream salinity gradient is explained by the increase in vertical stratification during late flood generated by cross-stream tidal straining and advection of salinity, highlighting the three-dimensional dynamics of the Marsdiep basin. Model simulations by Stacey et al. [2008], neglecting the effect of the baroclinic pressure gradient, show that late flood stratification is expected to produce a reversed estuarine circulation. No decrease or reversal is observed in the Marsdiep with increasing vertical stratification towards spring tide, because the increased vertical stratification during late flood modifies the vertical structure of along-stream velocity, creating a mid-depth velocity maximum, which enhances the estuarine circulation. The observations presented in this study suggest that the time interval of small vertical mixing, when the estuarine circulation develops, is determined by the ratio between water depth and vertical mixing, and by the tidal distortion.

5.5 CONCLUSIONS

The observations of turbulent kinetic energy production and dissipation during neap and spring tide conditions elucidate the complex turbulence dynamics in the periodically-stratified Marsdiep basin. The tidal asymmetry in strength and shape between ebb and flood, and their evolution over the spring-neap tidal cycle, considerably impact the turbulence characteristics.

Tidal currents and turbulence production are greater during ebb than during flood with the disparity increasing towards spring tide. As a result, the bottom boundary layer covers almost the entire water column during most of ebb, whereas this is only the case during the peak current of flood. The bottom boundary layer during the remainder of flood is restricted to the lower 8 to 12 m of the water column. This pattern deviates from the classical tidal straining in

(periodically- and weakly-stratified) estuaries. The small bottom boundary layer during late flood facilitates the generation of flood vertical stratification due to cross-stream tidal straining and produces a mid-depth maximum in along-stream velocity. The vertical stratification impacts turbulence production and results in a hysteresis curve with greater production during late ebb and early flood versus the opposite phases of the tide.

The observations show that an approximate balance between turbulence production and dissipation is present under most conditions, but only when the contribution of the cross-stream production is taken into account. Besides the classical bed-generated turbulence, vertical shears in along- and cross-stream velocity produce turbulence during late flood and peak ebb, especially during spring tide conditions. The cross-stream production can contribute up to 30 and 50 percent to the total production, illustrating its importance. The buoyancy term appears important during late flood, when vertical stratification stabilizes the water column and acts as a sink for turbulent energy, contrasting the classical tidal straining estuary. Furthermore, the profiles of the production and dissipation of turbulent kinetic energy suggest an upward transport of turbulence during ebb, increasing towards spring tide. In addition, a time lag and decay of turbulence is observed, which varies between succeeding slack tides.

The main finding of this chapter is the observation that the cross-stream contribution is essential for the turbulent kinetic energy budget. Furthermore, internal vertical shears in along-stream velocity contribute to the production of turbulence during late flood of spring tide. Interestingly, no reversed estuarine circulation is observed despite the opposite asymmetry in mixing. The estuarine circulation appears primarily generated during late flood and slack before ebb during a long period of weak mixing, which is facilitated by the tidal distortion and by the presence of flood vertical stratification. As a result, the estuarine circulation increases from neap to spring tide conditions.

6

CONCLUSIONS AND RECOMMENDATIONS

This thesis aims at increasing our understanding of the local estuarine hydrodynamics in the periodically-stratified Marsdiep basin, focusing on the vertical structure of currents, density and turbulence. A wide range of observations and some numerical model results have been combined to reach this objective. The main findings of the thesis are discussed per individual research question. Furthermore, recommendations for further research are provided at the end.

6.1 CONCLUSIONS

1) What is the spatial and temporal variability of the vertical structure of instantaneous along-stream currents and density?

Tidal currents in the Marsdiep basin are characterized by a large spatial and temporal variability, created partly by the complex bathymetry of the basin. In the ebb-dominant Texelstroom channel, ebb-flood asymmetries in magnitude and duration favor the ebb phase. The peak flood current is smaller than the ebb current. Furthermore, peak flood is followed by a long period of small currents, which is absent during late ebb. The duration of slack before ebb is longer than slack before flood, being 52 versus 14 minutes, respectively. The tidal asymmetry in magnitude fluctuates on a fortnightly timescale: the peak ebb current increases considerably from neap to spring tide, whereas the flood current remains relatively constant. The disparity is related to a temporal modulation of the horizontal residual circulation cell, originating from tide-bathymetry interaction.

The spatial variability of the (depth-averaged) current is also reflected in the correlation between tidal current amplitude and water depth. The amplitude is segregated into two regimes based on water depths smaller and greater than approximately 15 m. The tidal amplitude is proportional to water depth when smaller than 15 m, with only minor fortnightly variations along this depth range. The opposite is observed for water depths greater than 15 m: there the tidal amplitude remains relatively uniform, while it changes markedly over

the spring neap tidal cycle. The differential fortnightly modulation, described above, produces variations in lateral shears of the along-stream velocity, which explains the increase in differential advection from neap to spring tide, as discussed in Chapter 2 and further substantiated in the succeeding chapters.

The two observed regimes correspond with the impact of bed friction on the vertical structure of velocity, through the presence of a limited bottom boundary layer. Generally, the height of the bottom boundary layer in the Marsdiep basin is characterized by a great intra-tidal variability: the layer covers almost the entire water column during peak current conditions and most of ebb, but only the lower part (10-15 m) of the water column during other phases of the tide, especially late flood. The limited bottom boundary layer indirectly enables a modification of the vertical structure of along-stream velocity during late flood.

The vertical structure of the along-stream currents in the Marsdiep basin deviates from the standard estuarine profiles in a variety of ways. Generally, the superposition of the baroclinic and barotropic pressure gradients produces the greatest near-bed (near-surface) shears in along-stream velocity during flood (ebb) [MacCready and Geyer, 2010; Geyer and MacCready, 2013]. However, the observed ebb-flood asymmetry in drag coefficient modifies the near-bed vertical shears, resulting in greater near-bed shears during ebb than flood. Thus, the vertical profiles are opposite to typical profiles of velocity in estuaries. The asymmetry in drag coefficient appears to be a spatially variable phenomenon. Therefore, the near-bed shears of velocity are expected to vary spatially, depending on the spatial variations in water depth and bedform characteristics.

Higher up in the water column, other deviations from standard vertical profiles are observed. Interestingly, the classical tidal straining mechanism is not important in the ebb-dominant Texelstroom channel because the large currents during ebb inhibit vertical stratification to form and vertical shears to increase in the upper part of the water column. However, vertical stratification has a considerable effect on the vertical structure of velocity during flood. The small currents and weak mixing during late flood facilitate the generation of vertical stratification during late flood by cross-stream tidal straining and advection. Vertical stratification during flood inhibits the vertical exchange of momentum, which enables the generation of a mid-depth maximum in along-stream velocity by the superposition of the barotropic and baroclinic pressure gradients. The increase in cross-stream currents towards spring tide enhances cross-stream straining and advection, which results in more pronounced mid-depth velocity maxima towards spring tide.

This thesis shows that the cross-stream density gradient is at least equally important for the estuarine hydrodynamics as the along-stream gradient. However, the magnitude of both gradients are connected to each other and the tidal current itself through e.g. differential advection.

2) What determines the vertical structure of the residual currents, thereby focusing on the dynamics of the estuarine circulation?

This thesis conclusively shows that an estuarine circulation is present in the Marsdiep basin, characterized by a great seasonal variability. In Summer, the estuarine circulation is negligible due to the low freshwater discharge from the IJsselmeer, whereas in Autumn and Spring an estuarine circulation up to 0.4 m/s is observed. The estuarine circulation is superimposed on a depth-averaged residual current, which is forced by bathymetrically-induced residual currents and by remote wind effects. The estuarine circulation scales well with the solution proposed by Geyer et al. [2000], but lacks a typical fortnightly modulation characterized by an increase in magnitude towards neap tide, as is common in most estuaries. Furthermore, the presence of vertical stratification during flood, and its absence during ebb, are opposite to the classical tidal straining mechanism, but produce no observed changes in magnitude or direction of the estuarine circulation. An ebb-dominant asymmetry in lateral advection becomes increasingly important for along-stream salinity gradients greater than $2.5*10^{-4}$ psu/m and creates a reduction in estuarine circulation. The asymmetry in lateral advection in the Marsdiep basin is ebb-dominant as a result of the presence of the largest cross-stream currents during peak ebb and the timing of vertical stratification. The observed asymmetry in lateral advection is contrary to studies in literature, which found a flood-dominant asymmetry and an increase in estuarine circulation for estuaries where tidal straining is important.

The scaling of the estuarine circulation usually depends on an approximation of vertical mixing by the tidal currents either through the friction velocity or the product of the drag coefficient and tidal amplitude. Generally, the peak current and peak vertical mixing are assumed to determine the strength of the estuarine circulation. However, the observations in the Marsdiep basin show that well-mixed conditions are already reached during the less energetic phases of the tide. So, any additional increase in current speed and related vertical mixing will therefore not change the well-mixed conditions towards peak ebb and flood. Under predominantly well-mixed conditions, the strength of peak vertical mixing is less important. Rather the duration of the period of weak vertical mixing determines the strength of the estuarine circulation. This period of weak mixing is mainly governed by the tidal distortion and the ratio between water depth and the tidal amplitude (the Unsteadiness number).

The long period of weak vertical mixing during late flood explains the generation of a classical estuarine circulation by the gravitational and tidal straining circulation during late flood, facilitated by the tidal distortion and the flood stratification. Furthermore, the increase in vertical stratification and the more pronounced mid-depth velocity maximum towards spring tide (for a constant

along-stream salinity gradient) together explain the observed increase in estuarine circulation toward spring tide. The high currents during most of ebb reduce the classical tidal straining circulation during ebb, which generally produces the typical decrease in estuarine circulation towards spring tide, as described in literature.

This thesis highlights the non-steady behavior of the estuarine circulation in periodically-stratified estuaries and suggests that asymmetries in tidal currents can contribute to the strength of the estuarine circulation by modifying the time period of weak vertical mixing. Furthermore, vertical stratification during flood produces a mid-depth velocity maximum, which also impacts the strength of the estuarine circulation. Spatial variations in water depth and in tidal asymmetries show that the estuarine circulation is greatest in the ebb-dominant, deeper, northern part of the Marsdiep inlet, as illustrated by the GETM/GOTM model results.

3) What are the characteristics of turbulence during neap and spring tide conditions and how are these connected to the barotropic and baroclinic components of the tide?

Turbulence characteristics in the Marsdiep basin differ between ebb and flood and between neap and spring tide conditions due to a variety of factors and processes. The asymmetry in current magnitude is one of the principal forcing agents that explains the variability in turbulence dynamics. Turbulence during peak flood and ebb is produced by bed-generated turbulence, extending over the entire water column. However, the weak currents during late flood create a long period of small turbulence production, whereas the late ebb phase is characterized by high turbulence production. The fortnightly modulation of the ebb current creates a great fortnightly variation in turbulence production, whereas the relatively constant flood current consists of a relatively constant turbulence production over the spring-neap tidal cycle.

The classical bed-generated turbulence is a paramount source of turbulence in the periodically-stratified Marsdiep basin, consistent with other estuaries. However, internal shears in cross-stream (and along-stream) velocity are also important sources during distinct phases of the tide, which contradicts the paradigm of predominantly bed-generated turbulence. However, it agrees with recent observations of internal cross-stream turbulence production during late ebb by Collignon and Stacey [2013] and Arnott [2013] at the channel slope. In the Marsdiep basin, the cross-stream internal shears are especially important during peak ebb and late flood. Furthermore, along-stream shears during the late flood mid-depth velocity maximum also produce elevated mid-depth turbulence production. The additional sources can modify the vertical mixing dynamics over the water column.

The importance of cross-stream turbulence is further emphasized by the balance between turbulence production and dissipation. Total turbulence production only balances turbulence dissipation when the cross-stream production is included. Cross-stream turbulence production contributes between 30 and 50 percent to the total production.

The presence of vertical stratification during late flood acts as a sink of turbulent energy and produces a hysteresis in turbulence production. Total depth-averaged production of turbulence is greater during late ebb and early flood than during the opposite phases of the tide. However, the along-stream internal shears generated by the vertical stratification are also an additional source of turbulence.

The observations of turbulence in the main channel of the Marsdiep highlight the three-dimensional nature of turbulence and stress the importance of internally-generated turbulence in certain types of estuaries. Furthermore, the observed ebb-dominant asymmetry in vertical mixing contrasts the classical tidal straining estuaries. Despite the opposite mixing asymmetry, a classical estuarine circulation is still present at the study site, providing more evidence that not the strength of vertical mixing, but rather the duration of weak mixing is essential for the magnitude of the estuarine circulation in periodically-stratified estuaries.

Concluding remarks

The complexity of the Marsdiep basin provides a good study area to investigate a wide range of processes and mechanisms that are important for the estuarine dynamics. Furthermore, it highlights many of the factors that require consideration for the allocation of a tidal energy plant. An understanding of the tidal distortion and spatial variability of the tidal currents is required to optimize the tidal energy extraction strategy. Also, the vertical structure of velocity is altered considerably over the tidal cycle by the variable drag coefficient and the periodic stratification of the water column. Moreover, the turbulence characteristics are important for the forces acting on the structure of the tidal turbine and also partly determine the impact of the turbine on the ambient environment. This study shows that, for the benefit of optimal tidal energy extraction in estuaries, not only the vertical structure of along-stream velocity requires investigation, but also the vertical stratification and cross-stream current dynamics.

It is remarkable that despite the occurrence of many non-classical processes, a classical estuarine circulation is still observed in the Marsdiep basin. The vertical and cross-stream density gradients appear related to the strength of the along-stream density gradient and the tidal amplitude, which enables a simplification based on the latter two parameters, as already discussed by Scully

et al. [2009]. However, the cross-stream dynamics play a crucial role in the hydrodynamics of the Marsdiep basin because they distribute momentum, generate turbulence and modify the vertical structure of along-stream velocity. It is therefore essential to understand, and include, all the (cross-stream) processes that occur in an estuary in order to comprehend the three-dimensional circulation and transport patterns of suspended matter. This thesis demonstrates that a broad range of small-scale observations can aid in understanding the wide variety of processes that shape the hydrodynamics in the periodically-stratified Marsdiep basin.

6.2 RECOMMENDATIONS

As always, conducted research raises new questions that require further investigation. The same applies to this thesis. Several aspects of the Marsdiep system benefit from more investigation, as highlighted below:

- *Spatial dynamics of vertical stratification*: This thesis focused on the ebb-dominant part of the Marsdiep basin, where vertical stratification is shown to be essential for the vertical current structure. However, no long-term observations are available for other areas. The great spatial variability in water depth and tidal currents merits a comprehensive investigation into the timing and strength of vertical stratification by observations and/or model simulations and their effects on the vertical structure of velocity. For example, two bottom frames equipped with an ADCP and a minimum of 3 microCAT sensors in an ebb- and flood-dominant section of the Marsdiep inlet/basin would provide insight into the effects of different tidal asymmetries on the generation of vertical stratification. Furthermore, the spatial variability in turbulence dynamics can be investigated to complement the observations presented in this thesis, if the ADCP is set to a high-ping frequency.
- *Three-dimensional estuarine circulation*: Most studies in literature have focused on point and/or cross-stream variability of the estuarine circulation, similar to this thesis. However, the complex bathymetry in the Marsdiep basin invites for an investigation into the along-stream variability in estuarine circulation to assess the importance of changes in water depth on the circulation patterns. Additionally, this study could aid in better understanding the spatial variability in drag coefficient for distinct morphologic areas of the Marsdiep basin, and their effect on the vertical structure of velocity.
- *Frontal dynamics*: The Marsdiep basin is characterized by different water masses due to the large spatial differences in water depth. The interaction, exchange and dynamics between these fronts (e.g. channel-shoal exchange) require more research. Spatial surveys in spring are ideal, because the density gradients are generally large and weather conditions are favorable.

• *Sediment dynamics*: The exchange of suspended sediment between the North Sea and the Wadden Sea has been investigated using the ferry observations between Den Helder and Texel, which provide insight into the total flux of sediment. The long-term ADCP measurements from the bottom frame are fit for calibration to suspended sediment concentrations, thereby complementing the ferry observations. These bottom frame measurements provide a high-resolution long-term dataset, which can be used to obtain insight into the temporal variability of suspended sediment concentrations and, more importantly, into the processes that drive suspended sediment transport. A study on the suspended sediment transport at the study area can benefit from the detailed knowledge of the small-scale and local hydrodynamics presented in this thesis. Studies on bedload and bedform transport and on primary production in the water column might also benefit from the acquired knowledge on hydrodynamics.

• *Density gradients and estuarine dynamics in the entire Dutch Wadden Sea*: This thesis shows that the along- and cross-stream salinity gradients are important for the estuarine dynamics in the Marsdiep basin. However, the gradients are usually approximated, because no long-term measurements are available. The relevance of the density gradients to the Wadden Sea UNESCO world heritage site merits long-term monitoring of these parameters to better understand the entire Wadden Sea dynamics. The long-term salinity and temperature measurements at the NIOZ jetty provide a starting point for monitoring, but are not sufficient to understand and predict the importance of the density gradients for the rest of the Wadden Sea. Traffic buoys along the main channels of each basin can be equipped with cheap CTD sensors, collecting valuable information. Additional velocity measurements in the channels provide a comprehensive dataset, which can provide detailed knowledge on the variability of estuarine dynamics in the Wadden Sea basins, providing a better understanding of the system as a whole. Alternatively, the available GETM/GOTM model can complement the observations to provide a broad general overview of the variability.

BIBLIOGRAPHY

Aristizábal, M. and Chant, R. J. (2014). Mechanisms driving stratification in Delaware Bay estuary. *Ocean Dynamics*, 64(11):1615–1629.

Arnott, K. D. (2013). *Temporal variations of vertical mixing across a coastal plain estuary*. PhD thesis, University of Florida.

Aubrey, D. G. and Speer, P. (1985). A study of non-linear tidal propagation in shallow inlet/estuarine systems Part I: Observations. *Estuarine, Coastal and Shelf Science*, 21:185–205.

Basdurak, N. B. and Valle-Levinson, A. (2012). Influence of Advective Accelerations on Estuarine Exchange at a Chesapeake Bay Tributary. *Journal of Physical Oceanography*, 42(10):1617–1634.

Basdurak, N. B., Valle-Levinson, A., and Cheng, P. (2013). Lateral structure of tidal asymmetry in vertical mixing and its impact on exchange flow in a coastal plain estuary. *Continental Shelf Research*, 64:20–32.

Becherer, J., Burchard, H., Flöser, G., Mohrholz, V., and Umlauf, L. (2011). Evidence of tidal straining in well-mixed channel flow from micro-structure observations. *Geophysical Research Letters*, 38(17):2–6.

Blanton, J. O., Lin, G., and Elston, S. A. (2002). Tidal current asymmetry in shallow estuaries and tidal creeks. *Continental Shelf Research*, 22(11-13):1731–1743.

Boon, J. D. and Byrne, R. J. (1981). On basin hypsometry and the morphodynamic response of coastal inlet systems. *Marine Geology*, 40:27–48.

Buijsman, M. C. (2007). *Ferry-observed variability of currents and bedforms in the Marsdiep inlet*. PhD thesis, Netherlands Institute for Sea Research.

Buijsman, M. C. and Ridderinkhof, H. (2007a). Long-term ferry-ADCP observations of tidal currents in the Marsdiep inlet. *Journal of Sea Research*, 57(4):237–256.

Buijsman, M. C. and Ridderinkhof, H. (2007b). Water transport at subtidal frequencies in the Marsdiep inlet. *Journal of Sea Research*, 58(4):255–268.

Buijsman, M. C. and Ridderinkhof, H. (2008a). Long-term evolution of sand waves in the Marsdiep inlet. I: High-resolution observations. *Continental Shelf Research*, 28(9):1190–1201.

Buijsman, M. C. and Ridderinkhof, H. (2008b). Long-term evolution of sand waves in the Marsdiep inlet. II: Relation to hydrodynamics. *Continental Shelf Research*, 28(9):1202–1215.

Buijsman, M. C. and Ridderinkhof, H. (2008c). Variability of secondary currents in a weakly stratified tidal inlet with low curvature. *Continental Shelf Research*, 28(14):1711–1723.

Burchard, H. (1999). Recalculation of surface slopes as forcing for numerical water column models of tidal flow. *Applied Mathematical Modelling*, 23:737–755.

Burchard, H. (2009). Combined Effects of Wind, Tide, and Horizontal Density Gradients on Stratification in Estuaries and Coastal Seas. *Journal of Physical Oceanography*, 39(9):2117–2136.

Burchard, H. and Baumert, H. (1995). On the performance of a mixed-layer model based on the k-e turbulence closure. *Journal of Geophysical Research*, 100:8523–8540.

Burchard, H. and Bolding, K. (2001). Comparative Analysis of Four Second-Moment Turbulence Closure Models for the Oceanic Mixed Layer. *Journal of Physical Oceanography*, 31(8):1943–1968.

Burchard, H. and Hetland, R. D. (2010). Quantifying the Contributions of Tidal Straining and Gravitational Circulation to Residual Circulation in Periodically Stratified Tidal Estuaries. *Journal of Physical Oceanography*, 40(6):1243–1262.

Burchard, H., Hetland, R. D., Schulz, E., and Schuttelaars, H. M. (2011). Drivers of Residual Estuarine Circulation in Tidally Energetic Estuaries: Straight and Irrotational Channels with Parabolic Cross Section. *Journal of Physical Oceanography*, 41(3):548–570.

Burchard, H. and Hofmeister, R. (2008). A dynamic equation for the potential energy anomaly for analysing mixing and stratification in estuaries and coastal seas. *Estuarine, Coastal and Shelf Science*, 77:679–687.

Burchard, H., Lass, H. U., Mohrholz, V., Umlauf, L., Sellschopp, J., Fiekas, V., Bolding, K., and Arneborg, L. (2005). Dynamics of medium-intensity dense water plumes in the Arkona Basin, Western Baltic Sea. *Ocean Dynamics*, 55(5-6):391–402.

Burchard, H., Petersen, O., and Rippeth, T. P. (1998). Comparing the performance of the Mellor-Yamada the k-e two-equation turbulence models. *Journal of Geophysical Research*, 103:10,543–10,554.

Burchard, H. and Schuttelaars, H. M. (2012). Analysis of Tidal Straining as Driver for Estuarine Circulation in Well-Mixed Estuaries. *Journal of Physical Oceanography*, 42(2):261–271.

Canuto, V., Howard, A., Cheng, Y., and Dubovikov, M. (2001). Ocean Turbulence. Part I: One-Point Closure Model-Momentum and Heat Vertical Diffusivities. *Journal of Physical Oceanography*, 31:1413–1426.

Cartwright, D. E. (2000). *Tides: A scientific history*. Cambridge University Press.

Chant, R. J. (2002). Secondary circulation in a region of flow curvature: Relationship with tidal forcing and river discharge. *Journal of Geophysical Research*, 107(3131):1–14.

Chant, R. J., Geyer, W. R., Houghton, R., Hunter, E., and Lerczak, J. A. (2007). Estuarine Boundary Layer Mixing Processes: Insights from Dye Experiments. *Journal of Physical Oceanography*, 37(7):1859–1877.

Chen, S.-N. and Sanford, L. P. (2009). Axial Wind Effects on Stratification and Longitudinal Salt Transport in an Idealized, Partially Mixed Estuary. *Journal of Physical Oceanography*, 39(8):1905–1920.

Cheng, P. and Valle-Levinson, A. (2009). Influence of Lateral Advection on Residual Currents in Microtidal Estuaries. *Journal of Physical Oceanography*, 39(12):3177–3190.

Cheng, P., Valle-Levinson, A., and de Swart, H. E. (2010). Residual Currents Induced by Asymmetric Tidal Mixing in Weakly Stratified Narrow Estuaries. *Journal of Physical Oceanography*, 40(9):2135–2147.

Cheng, P., Valle-Levinson, A., and de Swart, H. E. (2011). A numerical study of residual circulation induced by asymmetric tidal mixing in tidally dominated estuaries. *Journal of Geophysical Research*, 116(C1):C01017.

Cheng, P., Wilson, R. E., Chant, R. J., Fugate, D. C., and Flood, R. D. (2009). Modeling Influence of Stratification on Lateral Circulation in a Stratified Estuary. *Journal of Physical Oceanography*, 39(9):2324–2337.

Chriss, T. M. and Caldwell, D. R. (1982). Evidence for the influence of form drag on bottom boundary layer flow. *Journal of Geophysical Research*, 87(C6):4148.

Collignon, A. G. and Stacey, M. T. (2012). Intratidal Dynamics of Fronts and Lateral Circulation at the Shoal-Channel Interface in a Partially Stratified Estuary. *Journal of Physical Oceanography*, 42(5):869–883.

Collignon, A. G. and Stacey, M. T. (2013). Turbulence Dynamics at the Shoal-Channel Interface in a Partially Stratified Estuary. *Journal of Physical Oceanography*, 43(5):970–989.

Cudaback, C. N. and Jay, D. A. (2000). Tidal asymmetry in an estuarine pycnocline: Depth and thickness. *Journal of Geophysical Research*, 105(Cll):26,237–26,251.

Cudaback, C. N. and Jay, D. A. (2001). Tidal asymmetry in an estuarine pycnocline: 2. Transport. *Journal of Geophysical Research*, 106(C2):2639.

Dastgheib, A., Roelvink, J., and Wang, Z. (2008). Long-term process-based morphological modeling of the Marsdiep Tidal Basin. *Marine Geology*, 256(1-4):90–100.

de Boer, G. J., Pietrzak, J. D., and Winterwerp, J. C. (2008). Using the potential energy anomaly equation to investigate tidal straining and advection of stratification in a region of freshwater influence. *Ocean Modelling*, 22(1-2):1–11.

de Ruijter, W. P. M. (1983). Effects of velocity shear in advective mixed-layer models. *Journal of Physical Oceanography*, 13:1589–1599.

de Vries, J. J., Nauw, J. J., Ridderinkhof, H., and van Aken, H. M. (2014). An exploratory study of the variability of currents and density in the Marsdiep. *Continental Shelf Research*, 84:70–83.

de Vries, J. J., Ridderinkhof, H., Maas, L. R. M., and van Aken, H. M. (2015). Intra- and inter-tidal variability of the vertical current structure in the Marsdiep basin. *Continental Shelf Research*, 93:39–57.

de Vries, J. J., van Aken, H. M., and Nauw, J. J. (2012). Variability of currents and vertical stratification in the Marsdiep. *NCK-days 2012 : Crossing borders in coastal research : jubilee conference proceedings*, 63:1–5.

Dewey, R. and Crawford, W. (1988). Bottom stress estimates from vertical dissipation rate profiles on the continental shelf. *Journal of Physical Oceanography*, 18:1167–1177.

Dronkers, J. (1986). Tidal asymmetry and estuarine morphology. *Netherlands Journal of Sea Research*, 20(2-3):117–131.

Dronkers, J. J. (1964). *Tidal computations in rivers and coastal waters*. Wiley & Sons, New York.

Duran-Matute, M., Gerkema, T., de Boer, G. J., Nauw, J. J., and Gräwe, U. (2014). Residual circulation and freshwater transport in the Dutch Wadden Sea: a numerical modelling study. *Ocean Science*, 10(4):611–632.

Edwards, K., MacCready, P., Moum, J., Pawlak, G., Klymak, J., and Perlin, A. (2004). Form Drag and Mixing Due to Tidal Flow past a Sharp Point. *Journal of Physical Oceanography*, 34:1297–1312.

Fisher, N. R., Simpson, J. H., and Howarth, M. J. (2002). Turbulent dissipation in the Rhine ROFI forced by tidal flow and wind stress. *Journal of Sea Research*, 48(4):249–258.

Flöser, G., Burchard, H., and Riethmüller, R. (2011). Observational evidence for estuarine circulation in the German Wadden Sea. *Continental Shelf Research*, 31(16):1633–1639.

Flöser, G., Riethmüller, R., Nauw, J. J., and Burchard, H. (2013). Observational evidence for the general presence of estuarine circulation in the Wadden Sea. *Journal of Coastal Research*, 65:1527–1532.

Fofonoff, N. P. (1985). Physical properties of seawater: A new salinity scale and equation of state for seawater. *Journal of Geophysical Research*, 90(C2):3332.

Fong, D. A., Monismith, S. G., Stacey, M. T., and Burau, J. R. (2009). Turbulent Stresses and Secondary Currents in a Tidal-Forced Channel with Significant Curvature and Asymmetric Bed Forms. *Journal of Hydraulic Engineering*, 135(3):198–208.

Friedrichs, C. and Aubrey, D. (1988). Non-linear Tidal Distortion in Shallow Estuaries : a Synthesis. *Estuarine, Coastal and Shelf Science*, 27:521–545.

Fugate, D. C. and Chant, R. J. (2005). Near-bottom shear stresses in a small, highly stratified estuary. *Journal of Geophysical Research*, 110(C3):C03022.

Gargett, A., Osborn, T. R., and Nasmyth, P. W. (1984). Local isotropy and the decay of turbulence in a stratified fluid. *Journal of Fluid Mechanics*, 144:231–280.

Geyer, W. R. (1993). Three-dimensional tidal flow around headlands. *Journal of Geophysical Research*, 98(1):955–966.

Geyer, W. R. (1997). Influence of Wind on Dynamics and Flushing of Shallow Estuaries. *Estuarine, Coastal and Shelf Science*, 44(6):713–722.

Geyer, W. R. and MacCready, P. (2013). The Estuarine Circulation. *Annual Review of Fluid Mechanics*, 46(1):175–197.

Geyer, W. R., Scully, M. E., and Ralston, D. K. (2008). Quantifying vertical mixing in estuaries. *Environmental Fluid Mechanics*, 8(5-6):495–509.

Geyer, W. R., Trowbridge, J. H., and Bowen, M. M. (2000). The Dynamics of a Partially Mixed Estuary. *Journal of Physical Oceanography*, 30:2035–2048.

Goodrich, D. M., Boicourt, W. C., Hamilton, P., and Pritchard, D. W. (1987). Wind-induced destratification in Chesapeake Bay. *Journal of Physical Oceanography*, 17:2232–2240.

Groeskamp, S. and Maas, L. R. M. (2012). Ship-borne contour integration for flux determination. *Journal of Sea Research*, 74:26–34.

Groeskamp, S., Nauw, J. J., and Maas, L. R. M. (2011). Observations of estuarine circulation and solitary internal waves in a highly energetic tidal channel. *Ocean Dynamics*, 61(11):1767–1782.

Guo, X. and Valle-Levinson, A. (2008). Wind effects on the lateral structure of density-driven circulation in Chesapeake Bay. *Continental Shelf Research*, 28(17):2450–2471.

Handler, R. A., Mied, R. P., Evans, T. E., and Donato, T. F. (2001). Convergence fronts in tidally forced rotating estuaries. *Journal of Geophysical Research*, 106:27,145–27,162.

Hansen, D. V. and Rattray, M. (1966). New dimensions in estuary classification. *Limnology and oceanography*, 11(3):319–326.

Jay, D. A. and Musiak, J. D. (1996). Internal Tidal Asymmetry in Channel Flows ' Origins and Consequences. *Coastal and Estuarine Studies*, 50:211–249.

Jay, D. A. and Smith, J. D. (1990a). Circulation , density distribution and neap-spring transitions in the Columbia River Estuary. *Progress in Oceanography*, 25:81–112.

Jay, D. A. and Smith, J. D. (1990b). Residual circulation in shallow estuaries 1. Highly Stratified, Narrow Estuaries. *Journal of Geophysical Research*, 95:711–731.

Jay, D. A. and Smith, J. D. (1990c). Residual circulation in shallow estuaries 2. Weakly Stratified and Partially Mixed, Narrow Estuaries. *Journal of Geophysical Research*, 95(89):733–748.

Jiang, C., Li, J., and de Swart, H. E. (2012). Effects of navigational works on morphological changes in the bar area of the Yangtze Estuary. *Geomorphology*, 139-140:205–219.

Kay, D. J. and Jay, D. A. (2003). Interfacial mixing in a highly stratified estuary 1. Characteristics of mixing. *Journal of Geophysical Research*, 108(C3):1–15.

Lacy, J. R. and Monismith, S. G. (2001). Secondary currents in a curved, stratified, estuarine channel. *Journal of Geophysical Research*, 106(2000):31283–31302.

Lacy, J. R., Stacey, M. T., Burau, J. R., and Monismith, S. G. (2003). Interaction of lateral baroclinic forcing and turbulence in an estuary. *Journal of Geophysical Research*, 108(C3):1–15.

Le Hir, P., Roberts, W., Cazaillet, O., Christie, M., Bassoullet, P., and Bacher, C. (2000). Characterization of intertidal flat hydrodynamics. *Continental Shelf Research*, 20(12-13):1433–1459.

Lerczak, J. A. and Geyer, W. R. (2004). Modeling the Lateral Circulation in Straight, Stratified Estuaries. *Journal of Physical Oceanography*, 34:1410–1428.

Li, C. (2002). Axial convergence fronts in a barotropic tidal inlet-sand shoal inlet, VA. *Continental Shelf Research*, 22(18-19):2633–2653.

Li, C., Armstrong, S., and Williams, D. (2006a). Residual Eddies in a Tidal Channel. *Estuaries and Coasts*, 29(1):147–158.

Li, C. and O'Donnell, J. (1997). Tidally driven residual circulation in shallow estuaries with lateral depth variation. *Journal of Geophysical Research*, 102:27,915–27,929.

Li, C. and O'Donnell, J. (2005). The Effect of Channel Length on the Residual Circulation in Tidally Dominated Channels. *Journal of Physical Oceanography*, 35:1826–1840.

Li, C. and Valle-Levinson, A. (1999). A two-dimensional analytic tidal model for a narrow estuary of arbitrary lateral depth variation: The intratidal motion. *Journal of Geophysical Research*, 104:23,525–23,543.

Li, C., Valle-Levinson, A., Atkinson, L. P., Wong, K.-C., and Lwiza, K. M. (2004). Estimation of drag coefficient in James River Estuary using tidal velocity data from a vessel-towed ADCP. *Journal of Geophysical Research*, 109(C3):C03034.

Li, M. and Zhong, L. (2009). Flood-ebb and spring-neap variations of mixing, stratification and circulation in Chesapeake Bay. *Continental Shelf Research*, 29(1):4–14.

Li, M., Zhong, L., Boicourt, W. C., Zhang, S., and Zhang, D.-L. (2006b). Hurricane-induced storm surges, currents and destratification in a semi-enclosed bay. *Geophysical Research Letters*, 33(2):L02604.

Lohrmann, A., Hackett, B., and Roed, L. P. (1990). High resolution measurements of turbulence, velocity and stress using a pulse-to-pulse coherent sonar. *Journal of Atmospheric and Oceanic Technology*, 7:19–37.

Lu, Y. and Lueck, R. G. (1999). Using a Broadband ADCP in a Tidal Channel. Part I: Mean Flow and Shear. *Journal of Atmospheric and Oceanic Technology*, 16:1556–1567.

Lu, Y., Lueck, R. G., and Huang, D. (2000). Turbulence Characteristics in a Tidal Channel. *Journal of Physical Oceanography*, 30:855–867.

Lueck, R. G. and Lu, Y. (1997). The logarithmic layer in a tidal channel. *Continental Shelf Research*, 17(14):1785–1801.

Maas, L. R. M. (1997). On the nonlinear Helmholtz response of almost-enclosed tidal basins with sloping bottoms. *Journal of Fluid Mechanics*, 349:361–380.

Maas, L. R. M. and van Haren, J. J. M. (1987). Observations on the vertical structure of tidal and inertial currents in the central North Sea. *Journal of Marine Research*, 45(2):293–318.

MacCready, P. and Geyer, W. R. (2010). Advances in Estuarine Physics. *Annual Review of Marine Science*, 2(1):35–58.

Martin, W. D. and MacCready, P. (2011). Influence of large-scale tidal asymmetry on subtidal dynamics in the western Strait of Juan de Fuca. *Journal of Geophysical Research*, 116(C2):C02009.

McLaughlin, J., Bilgili, A., and Lynch, D. (2003). Numerical modeling of tides in the Great Bay Estuarine System: dynamical balance and spring-neap residual modulation. *Estuarine, Coastal and Shelf Science*, 57(1-2):283–296.

Mied, R. P., Handler, R. A., and Evans, T. E. (2000). Longitudinal convergence fronts in homogeneous rotating channels. *Journal of Geophysical Research*, 105:8647–8658.

Moum, J. and Nash, J. (2000). Topographically Induced Drag and Mixing at a Small Bank on the Continental Shelf. *Journal of Physical Oceanography*, 30:2049–2054.

Murphy, P. L. and Valle-Levinson, A. (2008). Tidal and residual circulation in the St. Andrew Bay system, Florida. *Continental Shelf Research*, 28(19):2678–2688.

Nauw, J. J., Merckelbach, L. M., Ridderinkhof, H., and van Aken, H. M. (2014). Long-term ferry-based observations of the suspended sediment fluxes through the Marsdiep inlet using acoustic Doppler current profilers. *Journal of Sea Research*, 87:17–29.

Nunes, R. A. and Simpson, J. H. (1985). Axial Convergence Estuary in a Well-mixed. *Estuarine, Coastal and Shelf Science*, 20:637–649.

Nunes-Vaz, R., Lennon, G., and de Silva Samarasinghe, J. (1989). The Negative Role of Turbulence in Estuarine Mass Transport. *Estuarine, Coastal and Shelf Science*, 28:361–377.

Pawlowicz, R., Beardsley, B., and Lentz, S. (2002). Classical tidal harmonic analysis including error estimates in MATLAB using T_TIDE. *Computers & Geosciences*, 28(8):929–937.

Perlin, A., Moum, J., Klymak, J., Levine, M., Boyd, T., and Kosro, P. (2005). A modified law-of-the-wall applied to oceanic bottom boundary layers. *Journal of Geophysical Research*, 110(C10):C10S10.

Peters, H. and Bokhorst, R. (2000). Microstructure Observations of Turbulent Mixing in a Partially Mixed Estuary . Part I : Dissipation Rate. *Journal of Physical Oceanography*, 30:1232–1244.

Peters, H. and Bokhorst, R. (2001). Microstructure Observations of Turbulent Mixing in a Partially Mixed Estuary . Part II : Salt Flux and Stress. *Journal of Physical Oceanography*, 31:1105–1119.

Postma, H. (1954). *Hydrography of the Dutch Wadden Sea (PhD thesis)*. PhD thesis.

Pritchard, D. W. (1956). The dynamic structure of a coastal plain estuary. *Journal of Marine Research*, 15:33–42.

Ralston, D. K., Geyer, W. R., and Lerczak, J. A. (2008). Subtidal Salinity and Velocity in the Hudson River Estuary: Observations and Modeling. *Journal of Physical Oceanography*, 38(4):753–770.

Ralston, D. K., Geyer, W. R., Lerczak, J. A., and Scully, M. E. (2010). Turbulent mixing in a strongly forced salt wedge estuary. *Journal of Geophysical Research*, 115(C12):C12024.

Ridderinkhof, H. (1988). Tidal and residual flows in the Western Dutch Wadden Sea I: numerical model results. *Netherlands Journal of Sea Research*, 22(21):1–21.

Ridderinkhof, H. (1989). Tidal and residual flows in the Western Dutch Wadden Sea III: vorticity balances. *Netherlands Journal of Sea Research*, 24(32):9–26.

Rippeth, T. ., Fisher, N. R., and Simpson, J. H. (2001). The Cycle of Turbulent Dissipation in the Presence of Tidal Straining. *Journal of Physical Oceanography*, 31:2458–2471.

Rippeth, T. P., Simpson, J. H., and Williams, E. (2003). Measurement of the Rates of Production and Dissipation of Turbulent Kinetic Energy in an Energetic Tidal Flow: Red Wharf Bay Revisited. *Journal of Physical Oceanography*, 33:1889–1901.

Rippeth, T. P., Williams, E., and Simpson, J. H. (2002). Reynolds Stress and Turbulent Energy Production in a Tidal Channel. *Journal of Physical Oceanography*, 32:1242–1251.

Scully, M. E., Friedrichs, C., and Brubaker, J. (2005). Control of Estuarine Stratification and Mixing by Wind-induced Straining of the Estuarine Density Field. *Estuaries*, 28(3):321–326.

Scully, M. E. and Friedrichs, C. T. (2007). The Importance of Tidal and Lateral Asymmetries in Stratification to Residual Circulation in Partially Mixed Estuaries. *Journal of Physical Oceanography*, 37(6):1496–1511.

Scully, M. E. and Geyer, W. R. (2012). The Role of Advection, Straining, and Mixing on the Tidal Variability of Estuarine Stratification. *Journal of Physical Oceanography*, 42(5):855–868.

Scully, M. E., Geyer, W. R., and Lerczak, J. A. (2009). The Influence of Lateral Advection on the Residual Estuarine Circulation: A Numerical Modeling Study of the Hudson River Estuary. *Journal of Physical Oceanography*, 39(1):107–124.

Scully, M. E., Geyer, W. R., and Trowbridge, J. H. (2011). The Influence of Stratification and Nonlocal Turbulent Production on Estuarine Turbulence: An Assessment of Turbulence Closure with Field Observations. *Journal of Physical Oceanography*, 41(1):166–185.

Seim, H. E., Blanton, J. O., and Elston, S. A. (2009). The effect of secondary circulation on the salt distribution in a sinuous coastal plain estuary: Satilla River, GA, USA. *Continental Shelf Research*, 29(1):15–28.

Seim, H. E., Blanton, J. O., and Gross, T. (2002). Direct stress measurements in a shallow, sinuous estuary. *Continental Shelf Research*, 22(11-13):1565–1578.

Simpson, J. H., Brown, J., Matthews, J., and Allen, G. (1990). Tidal Straining, Density Currents, and Stirring in the Control of Estuarine Stratification. *Estuaries*, 13(2):125.

Simpson, J. H., Crawford, W., Rippeth, T., Campbell, A., and Cheok, J. (1996). The vertical structure of turbulent dissipation in shelf seas. *Journal of Physical Oceanography*, 26:1579–1590.

Simpson, J. H. and Nunes, R. A. (1981). The Tidal Intrusion Front: An Estuarine Convergence Zone. *Estuarine, Coastal and Shelf Science*, 13:257–266.

Simpson, J. H., Williams, E., Brasseur, L. H., and Brubaker, J. M. (2005). The impact of tidal straining on the cycle of turbulence in a partially stratified estuary. *Continental Shelf Research*, 25(1):51–64.

Souza, A. J., Fisher, N. R., Simpson, J. H., and Howarth, M. J. (2008). Effects of tidal straining on the semidiurnal cycle of dissipation in the Rhine region of freshwater influence: Comparison of model and measurements. *Journal of Geophysical Research*, 113(C1):1–10.

Speer, P. E. and Aubrey, D. G. (1985). A study of non-linear tidal propagation in shallow inlet/estuarine systems Part II: Theory. *Estuarine, Coastal and Shelf Science*, 21(5691):207–224.

Stacey, M. T. (2003). Estimation of Diffusive Transport of Turbulent Kinetic Energy from Acoustic Doppler Current Profiler Data. *Journal of Atmospheric and Oceanic Technology*, 20(6):927–935.

Stacey, M. T., Brennan, M. L., Burau, J. R., and Monismith, S. G. (2010). The Tidally Averaged Momentum Balance in a Partially and Periodically Stratified Estuary. *Journal of Physical Oceanography*, 40(11):2418–2434.

Stacey, M. T., Burau, J. R., and Monismith, S. G. (2001). Creation of residual flows in a partially stratified estuary. *Journal of Geophysical Research*, 106:13–17.

Stacey, M. T., Fram, J. P., and Chow, F. K. (2008). Role of tidally periodic density stratification in the creation of estuarine subtidal circulation. *Journal of Geophysical Research*, 113(C8):1–13.

Stacey, M. T., Monismith, G., and Burau, J. R. (1999a). Measurements of Reynolds stress profiles in unstratified tidal flow. *Journal of Geophysical Research*, 104:933–949.

Stacey, M. T., Monismith, S. G., and Burau, J. R. (1999b). Observations of Turbulence in a Partially Stratified Estuary. *Journal of Physical Oceanography*, 29:1950–1970.

Stacey, M. T. and Ralston, D. K. (2005). The Scaling and Structure of the Estuarine Bottom Boundary Layer. *Journal of Physical Oceanography*, 35(1):55–71.

Stacey, M. T., Rippeth, T. P., and Nash, J. (2011). Turbulence and Stratification in Estuaries and Coastal Seas. In *Treatise on Estuarine and Coastal Science*, volume 2, pages 9–36. Elsevier Inc.

Stanev, E. V. and Wolff, J. (2003). Tidal response shaped by nonlienar topographic control. *Terramare*, 12(12):112–117.

Tennekes, H. and Lumley, J. (1972). *A first course in turbulence*. the MIT press, Cambridge, MA.

Tropea, C. (1981). A note concerning the use of a one-component LDA to measure shear stress terms. *Exp. in Fluids*, 10:209–210.

Valle-Levinson, A. (2008). Density-driven exchange flow in terms of the Kelvin and Ekman numbers. *Journal of Geophysical Research*, 113(C4):C04001.

Valle-Levinson, A. (2010). *Contemporary Issues in Estuarien Physics*. Cambridge University Press.

Valle-Levinson, A., Caceres, M. A., and Pizarro, O. (2014). Variations of tidally driven three-layer residual circulation in fjords. *Ocean Dynamics*, 64(3):459–469.

Valle-Levinson, A., Li, C., Royer, T. C., and Atkinson, L. P. (1998). Flow patterns at the Chesapeake Bay entrance. *Continental Shelf Research*, 18(10):1157–1177.

Valle-Levinson, A., Li, C., Wong, K.-C., and Lwiza, K. M. (2000). Convergence of lateral flow along a coastal plain estuary. *Journal of Geophysical Research*, 105:17,045–17,061.

Valle-Levinson, A. and Wilson, E. (1994). Effects of sill processes and tidal forcing on exchange in eastern Long Island Sound Housatonic. *Journal of Geophysical Research*, 99.

van Aken, H. M. (1986). The onset of seasonal stratification in shelf seas due to differential advection in the presence of a salinity gradient. *Continental Shelf Research*, 5(4):475–485.

van Haren, H. (2010). Very near-bottom tidal straining in a sea strait. *Geophysical Research Letters*, 37(16):2–6.

van Haren, H. (2012). High-frequency bottom-pressure and acoustic variations in a sea strait: internal wave turbulence. *Ocean Dynamics*, 62(8):1123–1137.

van Haren, H., Oakey, N., and Garrett, C. (1994). Measurements of internal wave band eddy fluxes above a sloping bottom. *Journal of Marine Research*, 52(5):909–946.

van Rijn, L. (1993). *Principles of sediment transport in rivers, estuaries and coastal seas Part 1*. Aqua Publications.

van Rijn, L. (2011). *Principles of fluid flow and surface waves in rivers, estuaries, seas and oceans*. Aqua Publications.

Verney, R., Deloffre, J., Brun-Cottan, J.-C., and Lafite, R. (2007). The effect of wave-induced turbulence on intertidal mudflats: Impact of boat traffic and wind. *Continental Shelf Research*, 27(5):594–612.

Verspecht, F., Rippeth, T. P., Howarth, M. J., Souza, A. J., Simpson, J. H., and Burchard, H. (2009). Processes impacting on stratification in a region of freshwater influence: Application to Liverpool Bay. *Journal of Geophysical Research*, 114(C11):C11022.

Visser, A. W. and Souza, A. J. (1994). The effect of stratification on tidal current profiles in a region of fresh-water influence. *Oceanologica Acta*, 17:369–381.

Warner, J. C. (2005). Numerical modeling of an estuary: A comprehensive skill assessment. *Journal of Geophysical Research*, 110(C5):1–13.

Warner, S. J., MacCready, P., Moum, J. N., and Nash, J. D. (2013). Measurement of Tidal Form Drag Using Seafloor Pressure Sensors. *Journal of Physical Oceanography*, 43(6):1150–1172.

Wiles, P. J., Rippeth, T. P., Simpson, J. H., and Hendricks, P. J. (2006). A novel technique for measuring the rate of turbulent dissipation in the marine environment. *Geophysical Research Letters*, 33(21):L21608.

Williams, E. and Simpson, J. H. (2004). Uncertainties in Estimates of Reynolds Stress and TKE Production Rate Using the ADCP Variance Method. *Journal of Atmospheric and Oceanic Technology*, 21:347–357.

Winant, C. and Gutierrez de Velosco, G. (2003). Tidal Dynamics and Residual Circulation in a Well-Mixed Inverse Estuary. *Journal of Physical Oceanography*, 33:1365–1379.

Winterwerp, J. C. and Wang, Z. B. (2013). Man-induced regime shifts in small estuaries - I: theory. *Ocean Dynamics*, 63(11-12):1279–1292.

Winterwerp, J. C., Wang, Z. B., van Braeckel, A., van Holland, G., and Kösters, F. (2013). Man-induced regime shifts in small estuaries - II: a comparison of rivers. *Ocean Dynamics*, 63(11-12):1293–1306.

Wong, K.-C. (1994). On the nature of transverse variability in a coastal plain estuary. *Journal of Geophysical Research*, 99(94):14,209–14,222.

Wong, K.-C. and Moses-Hall, J. E. (1998). On the relative importance of the remote and local wind effects to the subtidal variability in a coastal plain estuary. *Journal of Geophysical Research*, 103(C9):18393.

Wong, K.-C. and Valle-Levinson, A. (2002). On the relative importance of the remote and local wind effects on the subtidal exchange at the entrance to the Chesapeake Bay. *Journal of Marine Research*, 60(3):477–498.

Zimmerman, J. T. F. (1976a). Mixing and flushing of tidal embayments in the western Dutch Wadden Sea part I: Distribution of salinity and calcutation of mixing time scales. *Netherlands Journal of Sea Research*, 10 (2):149–191.

Zimmerman, J. T. F. (1976b). Mixing and flushing of tidal embayments in the Western Dutch Wadden Sea, part II: analysis of mixing processes. *Netherlands Journal of Sea Research*, 10 (4):397–439.

Zimmerman, J. T. F. (1986). The tidal whirlpool: A review of horizontal dispersion by tidal and residual currents. *Netherlands Journal of Sea Research*, 20:133–154.

Zitman, T. J. and Schuttelaars, H. M. (2012). Importance of cross-channel bathymetry and eddy viscosity parameterisation in modelling estuarine flow. *Ocean Dynamics*, 62(4):603–631.

ACKNOWLEDGEMENTS

I would like to thank Hendrik van Aken for his guidance over the last four years and his willingness to keep on supervising me after his retirement. I would like to thank Herman Ridderinkhof for the additional supervision and help, especially towards the end of the project. Our meetings kept me on track and were good for the in-between evaluations. I really appreciate the time Herman was willing to put in. Furthermore, I'd like to thank Leo Maas for his help and guidance through the last phases of the PhD process. Of course, this thesis would not have been possible without the help of many more people.

The captain and crew of the Navicula, consisting of Bram Fey, Tony van der Vis, Wim-Jan Boon, Hein de Vries and Klaas-Jan Daalder are thanked for all their help with succesfully executing the cruises, ranging from in-situ and instant troubleshooting and some crazy measurement campaigns to nice talks, lunches, dinners and beers in between science. The volunteers are too many to mention, but were of course invaluable for the cruises. A double thanks to you all! For the technical, support I would like to thank Roald van der Heide, Jack Schilling and Co, Frans Eigenraam, Eric Wagemaakers, Ruud Groenewegen, Martin van der Laan and Sven Ober who helped with the moorings, instrumentation and data availability. Cees Veth is thanked for his help with the FLY.

I'd like to thank Janine Nauw for teaching me the ins-and-outs of doing measurements with the Navicula and for her help during the last four years. Thank you, Leo Maas (again) and Theo Gerkema, for always having your doors open for any questions that I had and for the motivating talks, showing that science is all about curiosity. And thank you, Hans van Haren, for your useful feedback on the turbulence chapter. Joeri, thank you for the great design of the cover! I really enjoyed our brainstorming sessions with good salsa music.

I'd also like to thank the NIOZ for being a great work place. I really had a good time. Thank you, everyone, for the great talks about everything and nothing, in particular my office mates Matias and Maxi, Meinard, Carola, Femke, Sjoerd, Jenny, Laura, Anna, Sander, Borja, Leandro, Ruud, Andrea, Fred, Stefani, Paolo and everyone else I forgot to mention. Also, our little lunch running club (Janine, Meinard and Roland) was a great break between the days spent behind the computer.

My parents, Coby en Nico, showed me the beauty of being interested in a wide range of topics and stimulated me during my studies and PhD project. Thank you for all your interest and support. My big little brother, Paul, was

also continuously interested in my work and contributed to ideas in his own original way. Last but definitely not least, I'd like to thank my girlfriend Ronja for sharing this adventure with me. Thank you for de-stressing me so many times, cheerleading/coaching me and most importantly just simply being there.

This document was typeset using `classicthesis` developed by André Miede.

Final Version as of 13th July 2015 (`classicthesis` draft).

LIST OF PUBLICATIONS

1. de Vries, J. J., Ridderinkhof, H., Maas, L. R. M., and van Aken, H. M. (2015). Intra- and inter-tidal variability of the vertical current structure in the Marsdiep basin, *Cont. Shelf. Res.*, 93:39-57.
2. Hoekendijk, J. P. A., de Vries, J. J., van der Bolt, K., Greinert, J., Brasseur, S., Camphuysen K. C. J. and Aarts, G. (2015). Estimating the spatial position of marine mammals based on digital camera recordings, *Ecology and Evolution*, 5:578-589.
3. de Vries, J. J., Nauw, J. J., Ridderinkhof, H., and van Aken, H. M. (2014). An exploratory study of the variability of currents and density in the Marsdiep, *Cont. Shelf. Res.*, 84:70-83.
4. de Vries, J. J., van Aken, H. M. and Nauw, J. J. (2012). Variability of currents and vertical stratification in the Marsdiep, *NCK-days 2012 : Crossing borders in coastal research : jubilee conference proceedings*, 119-123.
5. de Vries, J. J., Ridderinkhof, H., Duran-Matute, M., and van Aken, H. M. (under review). On the vertical structure of the residual current in the periodically-stratified Marsdiep basin, *Cont. Shelf. Res.*
6. de Vries, J. J., Ridderinkhof, H., and van Aken, H. M. (under review). Observations of turbulence in the periodically-stratified Marsdiep basin *J. Geophys. Res.*

CURRICULUM VITAE

Jurre de Vries was born on September 22, 1986 in the beautiful city of Groningen. After graduating from the Praedinius Gymnasium (high school) in 2004, he decided to broaden his horizon and go on a cultural exchange. He went a year to Panamá to live with a host family and to get to know the Latin-American culture and language. This great experience made him even more interested in discovering the world in all of its aspects. Therefore, he decided to study Earth Sciences at Utrecht University in 2005. Quickly it became clear to him that he was most interested in the Earth's surface and, particularly, in coastal processes. He completed his Bachelor in 2008 by specializing in *Physical Geography* and by writing his thesis on 'Dune formation and dune development on the Wadden Islands' under the supervision of prof. dr. Piet Hoekstra. Focusing more on coastal research, he started the Master programme Physical Geography at Utrecht University in 2008, specializing in *Coastal Dynamics, Fluvial Systems and Global Change*. His Master's fieldwork was conducted on the (Wadden) Island of Texel, which resulted in the thesis 'The infragravity wave behaviour at a secondary tidal inlet, the Slufter', supervised by prof. dr. Gerben Ruessink. Having the urge to know more about how research is conducted at other institutes, he did his half-year (Masters') internship at the Franklin and Marshall College in Lancaster, Pennsylvania on the analysis of megaripple data and on the development of a self-organisation bedform model, under the supervision of dr. Eddie Gallagher. Furthermore, he had the opportunity to participate in a fieldwork on studying the dynamics of rip-currents and the intra-tidal grain size distribution in Monterey Bay, California. Jurre had the feeling he was not done yet studying and decided to explore the possiblity to do a PhD. After completing his Masters cum laude, he started his PhD at the NIOZ on March 1, 2011, which nicely combined his affinity for the (Wadden) Sea with a new vibrant work atmosphere, many exciting field campaigns and the opportunity to learn something new every day.